Characterization of the viral replicase of hepatitis E virus

Karoline Metzger

Doctoral Thesis

Characterization of the Hepatitis E Virus Replicase

Karoline Metzger

January 31, 2022

Center for Infection and Immunity of Lille
Molecular and Cellular Virology
Dr. Jean Dubuisson
Supervisor: Dr. Cécile–Marie Aliouat–Denis

Jury:
Pr. Anne Muhr–Tailleux, President
Dr. Jérôme Gouttenoire, Reviewer
Dr. François Helle, Reviewer
Dr. Annette Martin, Examiner
Pr. Philip Meuleman, Examiner
Dr. Cécile–Marie Aliouat–Denis, Supervisor

Acknowledgments

First, I want to thank Jean for accepting me in his lab all the way back during my Master 2 and then welcoming me back for my PhD. I still remember how excited I was when my application for my Master 2 project was accepted and how this whole process went so smoothly.
Next, I am thanking Cécile–Marie for tutoring me starting from my Master's project until the very end of my PhD thesis. I have learned everything from experiments in the lab to how to write a good paper and a proper dissertation to just name a few examples. I am so glad I came back for my PhD, because I knew that I was going to be in such good hands!
I am thanking Laurence to have co–tutored me during this whole time and for always coming in with some good advice on how to proceed. It really would not have been the same experience without you.
I am very grateful to have had Anne Muhr–Tailleux and Annette Martin in the jury of my CSI. Our discussions and their comments helped tremendously shaping my project and progress. Likewise, I want to thank all the members of my PhD jury: Philip Meuleman, Jérôme Gouttenoire and François Helle for accepting to be part of this journey and for evaluating my PhD thesis.
Very importantly, thank you, Cyrine, for being my partner in the ORF1 project, my first person to share my results with, my temporary roommate and my friend during this more–than–3–year adventure.
Of course I want to thank the whole HEV and MCV lab for all kinds of help during my time spent there. The HEV lab meetings and also other discussions with its members have been a big help during the course of my thesis, since fruitful conversations and constructive criticism are the core of good scientific work. So, thank you, Claire for always having an open ear, for your words of encouragement and especially for all your help with this ever so ungrateful mass spectrometry.
Speaking of mass spectrometry, I want to thank our collaboration partner Jean–Michel Saliou for all the analyses he did for us and the hours of evaluation and discussions spent on this subject.
On that note, I would like to thank also Philippe Roingeard for his collaboration on the elctron–microscopy experiments and for his valuable suggestions concerning our projects.

Now, I would like to thank Virginie and Charline for helping out with experiments, and let's be honest, for making all our lives much easier by that. My RT qPCR and IPs would not have been as pretty without your help. But I am also grateful for our discussions around these experiments and everything far beyond that.
Moving on to team ORF2, a big thank you goes to Kevin for being my bench partner and my French teacher. Two of my biggest successes were managing to understand you when you talk at a normal speed and recognizing French expressions that only exist in your head.
Also, I am thanking Martin for being part of the HEV PhD student crew, our team would not have been complete without you.
The last member of our "HEV team" is of course Esther, who we gladly welcomed as she is a real asset to our team. I want to thank you for your professional input, but especially for all the quality time that we spent in– and outside of the lab watching anime, exploring the Bretagne and baking delicious cookies.
On that matter, I want to include also Imelda and Fethi in this thank you, since we shared so many great times together. My Totoro plushie and the ducky cookie (and the Fethi–cotta) will always and forever be appreciated by me.
I do not want to forget thanking Yoan and Marine, that were interns under the supervision of Cécile–Marie and I. Both of them managed to advance our project and were really good, hard–working students.
I am really grateful to the rest of the MCV lab as well. I want to thank all of you for being invested in my work, for listening to my presentations, asking critical questions and offering help or insight when needed. This includes of course past PhD students and members as well, who were working here during my Master's or the beginning of my PhD.
Last but not least, I want to thank my friends and family for their moral support. A special thank you goes to my mother, her husband and my brother for always lending an open ear and for visiting me here in France as often as possible. And of course, this chapter would not be complete without thanking my baby bird who supported me during the ups and downs of this PhD endeavor.

Contents

Acronyms

BSA Bovine serum albumin

CRE *Cis*–reactive element

DMEM Dulbecco's Modified Eagle Medium

dsRNA Double stranded RNA

GMP Guanosinemonophosphate

Grp78 78–kDa glucose–regulated protein

GTase Guanylyltransferase

HAV Hepatitis A virus

HBV Hepatitis B Virus

Hel Helicase

HEV Hepatitis E virus

HLC Hepatocyte like cell

HSP70 Heat shock cognate protein 70

HSP90 Heat shock protein 90

HSPG Heparan sulfate proteoglycan

HVR Hypervariable region

IFN Interferon

Ig Immunoglobulin

IRF Interferon regulatory factor

ISG Interferon stimulated gene

ISL Internal stem loop

JAK–STAT Janus–kinase signal transducer and activator of transcription protein

JR Junction region

m7G 7–methylguanosine

MAPK Mitogen–activated protein kinase

Met Methyltransferase

MS Mass spectrometry

MVB Multi vesicular bodies

NA Neuralgic Amytrophy

NHP Non human primate

NTP Nucleotide triphosphate

NTPase Nucleoside triphosphatase

ORF Open reading frame

PBS Phosphate buffer

PCP Papain–like cystein protease

PHH Primary Human Hepatocytes

RBV Ribavirin

RdRp RNA dependent RNA polymerase

RIG–I Retinoic acid–inducible gene I

RUBV Rubella Virus

SFV Semliki Forest virus

sgP Subgenomic promoter

SINV Sindbis virus

SOT Solid Organ Transplantation

TBK–I Tank binding kinase I

VLP Virus like particle

List of Figures

List of Tables

Abstract

Hepatitis E virus (HEV) is the major cause of acute hepatitis worldwide. Currently, no effective anti–viral treatment against HEV is available and an HEV vaccine is restricted to China. HEV is a positive–sense RNA virus expressing 3 open reading frames (ORFs). ORF1 encodes the ORF1 non–structural polyprotein, the viral replicase which transcribes the full–length genome and a subgenomic RNA that encodes the structural ORF2 and ORF3 proteins. Our aim is to better characterize ORF1: to determine whether it is processed during the HEV lifecycle and to identify the compartment of replication. As no commercial antibody recognizes ORF1 in HEV–replicating cells, we aimed at inserting epitope tags within the ORF1 sequence of the cell–culture selected genotype 3 p6 strain. First, a HEV replicon where the Gaussia luciferase reporter gene lies under the control of ORF1 was used to assess the replication efficacy of the tagged genome by luminometry. The insertion of the 2 V5 tags in the hypervariable region did not significantly impact the replication of genomic and production of subgenomic RNA, whereas the insertion of an HA tag at the C–terminus of the RNA–dependent RNA polymerase reduced the production of subgenomic RNA. Tags were next inserted both into the infectious full–length p6 HEV genome and into ORF1 heterologously expressed. Western–blot and immunoprecipitation analyses of tagged ORF1 expressed in the 3 systems showed a high molecular weight protein ($>$180kDa) that likely corresponds to the unprocessed form of ORF1 and that can be detected up to 25 days after electroporation of the p6 infectious RNA in PLC3 cells. Additionally, lower molecular weight proteins (90–180kDa) were detected in lower abundance, suggesting that ORF1 might be processed. Mass spectrometry analyses were performed to identify the sequence of the potential cleavage products observed by western blot and colloidal blue staining. It appears that the N–terminus of all V5–tagged proteins of lower molecular weight is stable and corresponds to the N–terminus of the full length ORF1 protein. However, the C–terminus was not yet identified. Interestingly, western blot analysis of subcellular fractions as well as confocal microscopy revealed cytoplasmic and nuclear localization of the tagged ORF1, indicating that the ORF1 might pass through the nucleus during infection.

Finally, we used the RNAscope technique to visualize the intracellular HEV RNA. Probes were designed against positive and negative–stranded HEV RNA. Genomic and subgenomic RNA were found in close proximity to each other and to viral proteins in perinuclear substructures that may correspond to replication complexes.

Résumé

Le virus de l'hépatite E (VHE) est la principale cause d'hépatite aiguë dans le monde. Actuellement, aucun traitement antiviral efficace contre le VHE n'est disponible et un vaccin contre le VHE n'est disponible qu'en Chine. Le VHE est un virus à ARN simple brin de polarité positive exprimant 3 cadres de lecture ouverts (ORF). L'ORF1 code pour la polyprotéine non structurale ORF1, ou réplicase virale, qui transcrit le génome complet et un ARN sous–génomique qui code pour les protéines structurales ORF2 et ORF3. Notre objectif est de mieux caractériser l'ORF1 : déterminer si cette protéine subit une maturation au cours du cycle viral et identifier le compartiment de réplication du VHE.

Comme aucun anticorps commercial ne reconnaît l'ORF1 en système réplicatif, nous avons cherché à insérer des épitopes dans la séquence ORF1 de la souche p6 de génotype 3 qui a été sélectionnée en culture cellulaire.

Tout d'abord, un réplicon du VHE où le gène rapporteur Gaussia luciférase se trouve sous le contrôle de l'ORF1 a été utilisé pour évaluer l'efficacité de réplication du génome étiqueté. L'insertion de 2 étiquettes V5 dans la région hypervariable n'a pas eu d'impact significatif ni sur la réplication du génome ni sur la production d'ARN sous-génomique, alors que l'insertion d'un épitope HA à l'extrémité C–terminale de l'ARN polymérase ARN–dépendante a réduit la production d'ARN sous–génomique. Des étiquettes ont ensuite été insérées à la fois dans le génome infectieux p6 HEV complet et dans l'ORF1 exprimée de manière hétérologue. Des analyses en Western–blot et par immunoprécipitation de l'ORF1 étiquetée et exprimée dans les 3 systèmes ont révélé la présence d'une protéine de poids moléculaire élevé ($>$180kDa) qui correspond probablement à la forme ORF1 de pleine longueur. Celle–ci a pu être détectée jusqu'à 25 jours après électroporation de l'ARN infectieux p6 dans les cellules PLC3.

En outre, les protéines de poids moléculaires inférieurs (90–180kDa) ont été détectées en plus faible abondance, ce qui suggère que l'ORF1 est clivée. Des analyses par spectrométrie de masse ont été réalisées pour identifier la séquence des produits de clivage potentiels. Il apparaît que l'extrémité N–terminale de toutes les protéines étiquetées V5 de faible poids moléculaire est stable et correspond à l'extrémité N–terminale de la protéine entière.

Cependant, l'extrémité C–terminale n'a pas encore été identifiée. De façon intéressante, l'analyse par western blot des fractions subcellulaires ainsi que la microscopie confocale ont révélé une localisation cytoplasmique et nucléaire de l'ORF1 étiquetée, indiquant que l'ORF1 pourrait être transloquée dans le noyau pendant l'infection.
Enfin, nous avons utilisé la technique RNAscope pour localiser l'ARN du VHE à l'intérieur de la cellule hôte. Les sondes ont été conçues pour s'hybrider spécifiquement aux brins positif et négatif de l'ARN du VHE. L'ARN génomique et subgénomique ont été localisés à proximité les uns des autres ainsi que des protéines virales dans des structures périnucléaires qui pourraient représenter les complexes de réplication du VHE.

1. Introduction

1.1. Discovery of HEV

Hepatitis E virus (HEV) was first described in 1983 by Balayan *et al.* using electron microscopy [3]. The study showed virus like particles of a size of 27 nm derived from stool samples of a volunteer that ingested the previously unknown virus (Fig. 1). There was no evidence of an infection with Hepatitis A virus (HAV) despite the similarity of symptoms that were observed after the ingestion of the virus.
Therefore, previous epidemics that were thought to be caused by HAV were explained or re–investigated concerning the involvement of HEV.
The first reported HEV cases were the Kashmir epidemic of 1978 by Khuroo *et al.* (1980) [4]. At the time, there was an outbreak of jaundice with 52,000 cases and 1700 deaths in this region, which could not be attributed to HAV. However, due to the lack of basic health care and research facilities, the discovery of HEV, as the real causative agent, did not occur until 1983.
In 1993, Purcell *et al.* re–analyzed samples from an epidemic that occurred in Delhi in 1955–56 and confirmed the presence of HEV [5]. In this period, 35,000 cases of jaundice were reported and at the time wrongly attributed to HAV.
Finally, in 1990, the HEV genome was partially cloned by Reyes *et al.* and fully sequenced by Tam *et al.* in 1991 [6] [7].

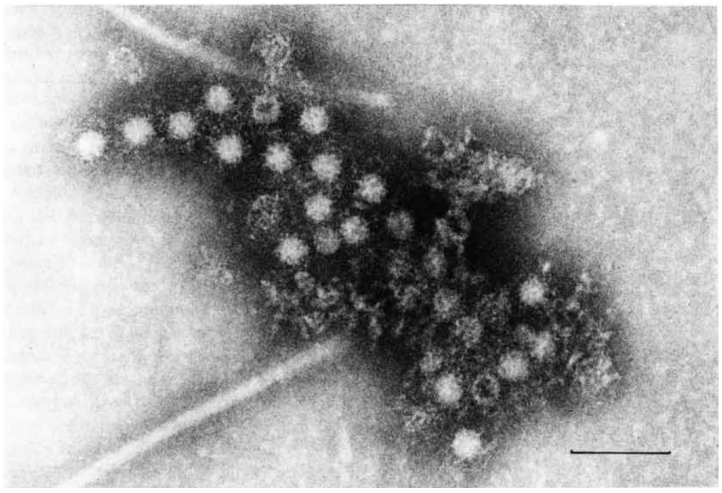

Figure 1: Immune aggregate of virus like particles recovered from the stool of an experimentally infected volunteer, [3].

1.2. Classification of HEV

HEV belongs to the family of *Hepeviridae*, which is currently divided into *Orthohepevirus* and *Piscihepevirus* (Fig. 2a) [8].
The *Orthohepevirus* genus is further classified into the species *Orthohepevirus* A, that infects humans, swine, boar, deer, rabbits, camels and mongooses, *Orthohepevirus* B infecting birds, *Orthohepevirus* C, which infects rodents and ferrets and *Orthohepevirus* D, that infects bats. The *Piscihepevirus* genus consists of one species (Piscihepevirus A) that includes the cutthroat trout virus (CTV) [8].
HEV has been misclassified numerous times due to sequence similarities to different other positive–stranded RNA viruses before it was finally given a separate family [9].
In 2004, HEV was accorded its own genus of *Hepevirus* and in 2009 its own family of *Hepeviridae*, because more sequences were available that showed genetic distance to other families [10]).
HEV has a very wide host range (Fig. 2b). Out of 8 recognized *Orthohepevirus* A genotypes, at least 4 are able to infect humans amongst other animals (genotypes 1–4). Genotypes 1 and 2 infect only human, while animal reservoirs have been found for genotypes 3 and 4 mainly in swine, deer and wild boar. HEV RNA (genotype 3) has been found in other animals such as rabbits and bottleneck dolphins, which was most likely caused by spillover infections or spillover hosts. Spillover infections occur when livestock is raised together and is caused by close contacts among animals or between humans and animals. Evidence for this is the low seroprevalence of HEV in those animals despite the presence of HEV RNA [11]. Interestingly, also a member of the *Orthohepevirus C* species was able to cause infection in humans, which was transmitted by rats [12, 13].
However, with the dramatic increase in the number of HEV strains identified within the past decade, many strains remain unclassified at present, underscoring the marked genomic variability among HEV strains [11].

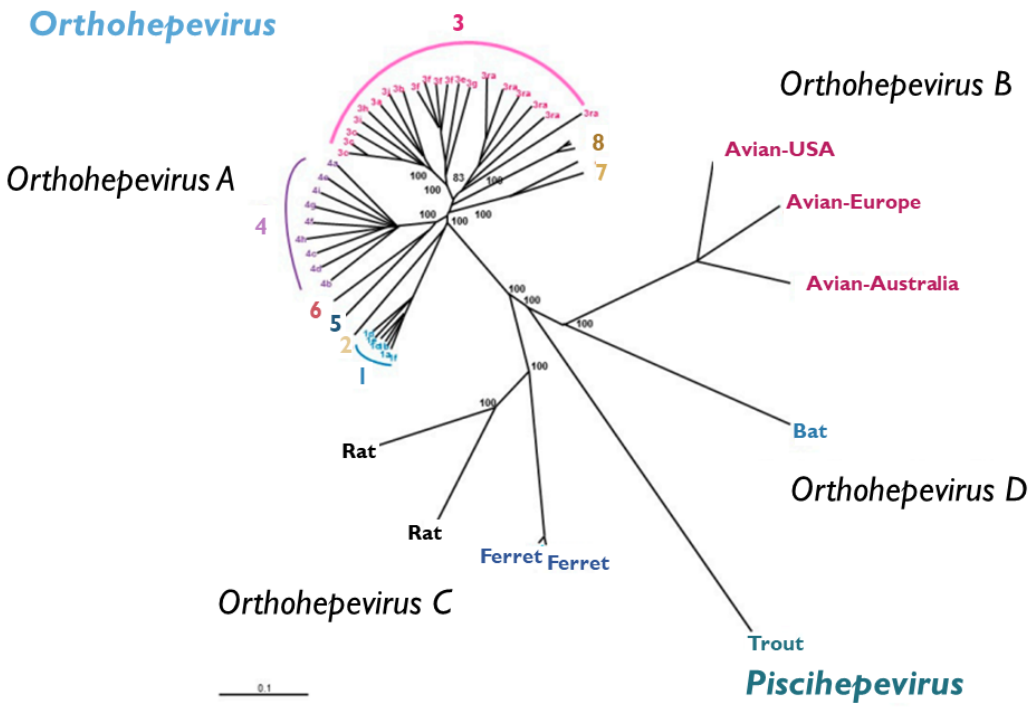

(a)

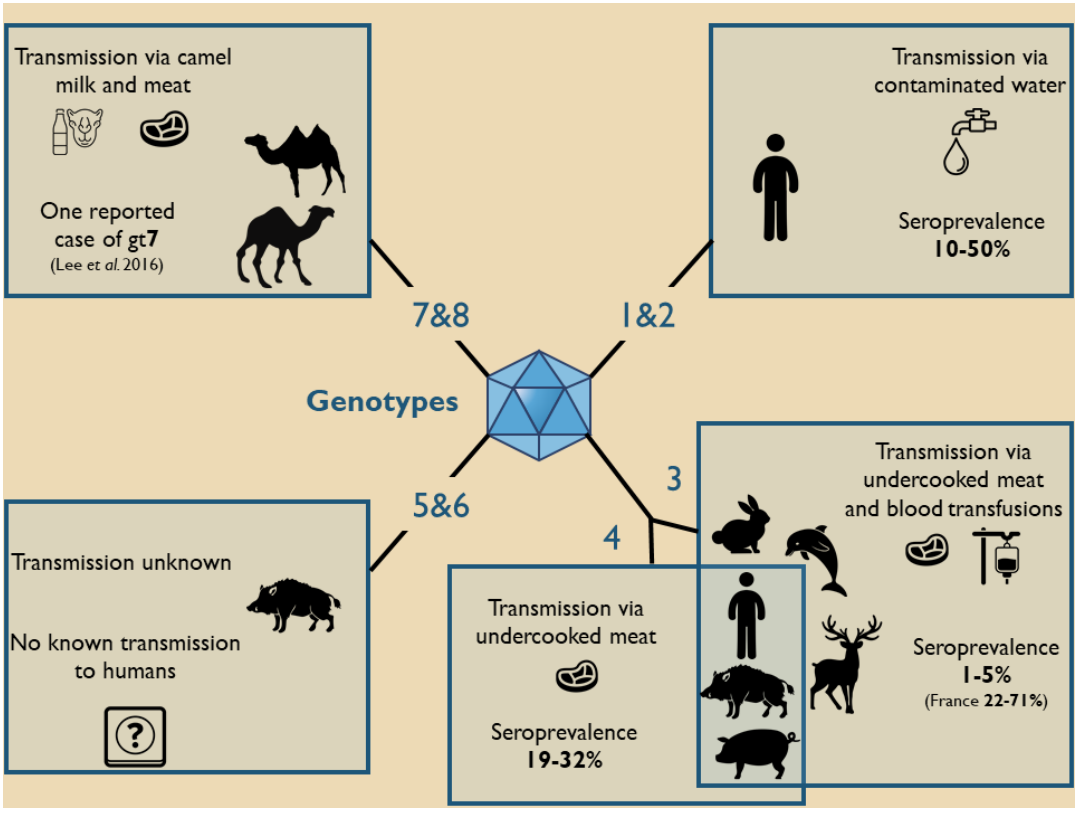

(b)

Figure 2: Taxonomy and transmission of genotypes of Hepatitis E Virus. (a) Classification of Hepatitis E Virus, adapted from [14]. The sequence alignment was done based on full–length sequences of HEV strains by using ClustalW and BioEdit (version 7.0). The neighbor–joining method was implemented with a bootstrap of 100 replicates. (b) Genotypes of Hepatitis E Virus (*Orthohepevirus* A) and their transmission.

1.3. Epidemiology

HEV is the causative agent of hepatitis E and one of the most common causes of acute hepatitis worldwide. Of 20 million cases, 3.3 million are symptomatic. 60,000 deaths can be attributed to genotype 1 and 2 each year [15].
Between 2005 and 2015 the cases of HEV due to genotype 3 have risen by 10–fold [16]. In 2015, 5,500 cases were reported in EU/EEA countries where this genotype is prevalent. Five of 12 EU/EEA countries reported 28 deaths between 2005 and 2015, that were all attributed to genotype 3 [17, 18].
Hepatitis E is widely distributed and considered to have emerged from developing countries, where the prevalence has augmented during the last years [19–21].
There are currently 8 genotypes of a single serotype and 4 of them can infect humans (Fig. 2b and 3) [22].
Genotypes 1 and 2 infect only humans and circulate predominantly in low–income countries (Asia and Africa). They are transmitted via the fecal–oral and the anthroponotic route through contaminated water resulting in sporadic cases of hepatitis E, but sometimes also in large epidemics. Between 1988 and 2013, 17 large scale outbreaks were reported in Africa [23–25].
Hepatitis E is highly endemic in East and South Asia and accounts for 20–50% of acute hepatitis cases in this region. The seroprevalence of anti–HEV antibodies ranges between 10–50% [15].
Usually, genotypes 1 and 2 are self–limiting and do not cause chronic hepatitis [21]. In the immunocompetent population, mortality rates lie between 1–2%. Yet, the fatality for pregnant women raises up to 25% due to unknown reasons possibly related to changes in the immune system during pregnancy [26–28]. Hormonal changes and a high viral load might play a role in the disease progression as well. Also, cytokine gene polymorphisms is associated with an adverse outcome of the pregnancy [29]. A meta–study by Ahmad in 2020 found out that the seroprevalence of HEV in pregnant women lies at 16.51%, yet displaying a large heterogeneity according to the geographical region and detection methods used in the study. An acute HEV infection in the third trimester is one of the leading causes of fetal and maternal deaths, therefore pregnant women belong to a high risk group of HEV infections [30].
On the other hand, genotypes 3 and 4 can infect human and have a reservoir in animals as well. They are prevalent in high income countries and are transmitted through direct contact with animals and through the consumption of animal products. HEV is able to cross the species–barrier as demonstrated by experimental infections

of primates with swine HEV [31]. Conversely, pigs [31], rabbits [32] and non–human primates [33] were infected with human HEV (Fig. 20).The ability of HEV to cross species–barriers especially puts animal workers at risk.
Primary reservoirs are swine, deer and boar with swine being the biggest [33–35]. Since the virus can be killed by incubation at $71\,^{\circ}C$ for 20 minutes, it is supposed that the transmission occurs primarily via undercooked meat [36]. However, HEV RNA can be detected in fruits and vegetables through contact with water that was contaminated by an infected animal [37].
This transmission route results in sporadic cases and rarely in small epidemics that can be attributed to a common source of aliment [20, 21]. Another route of transmission is the transfusion of blood products [38]. Nowadays, blood transfusions are routinely screened for HEV in Ireland, the UK and the Netherlands, while in France and Germany, screens are only performed in high–risk patients such as organ transplant patients. In other countries (Greece, Portugal, Spain, Italy) the screening process is still under evaluation [39].
The seroprevalence varies greatly among different countries owing to the different diagnostic methods being used. In France it ranges between 21.9–71.3% depending on the region, whereas the average seroprevalence in the healthy population of industrialized countries ranges from 1–5% [40, 41].
Between 2005 and 2015 the number of cases in France rose from 20/year to 2,200/year, which can be attributed to more frequent testing and better clinical awareness [42].
Phylogenetic analysis showed that in Europe/France, the predominantly circulating type of HEV is genotype 3f, which accounts for 59% of the genotype 3 infections [42]. The strain that will be characterized in this study belongs to this genotype as well.
For genotypes 3 and 4, the infection is usually self–limiting similar to genotypes 1 and 2, however, immunocompromised patients can develop a chronic infection [8].
Also, patients with a pre–existing chronic liver condition are at higher risk to suffer from acute liver failure when infected with HEV [43].
Nowadays, hepatitis E is not longer considered a travel sickness and it is important to observe the circulation of the virus in humans and animals in Europe to pinpoint the sources of contamination [16, 19].

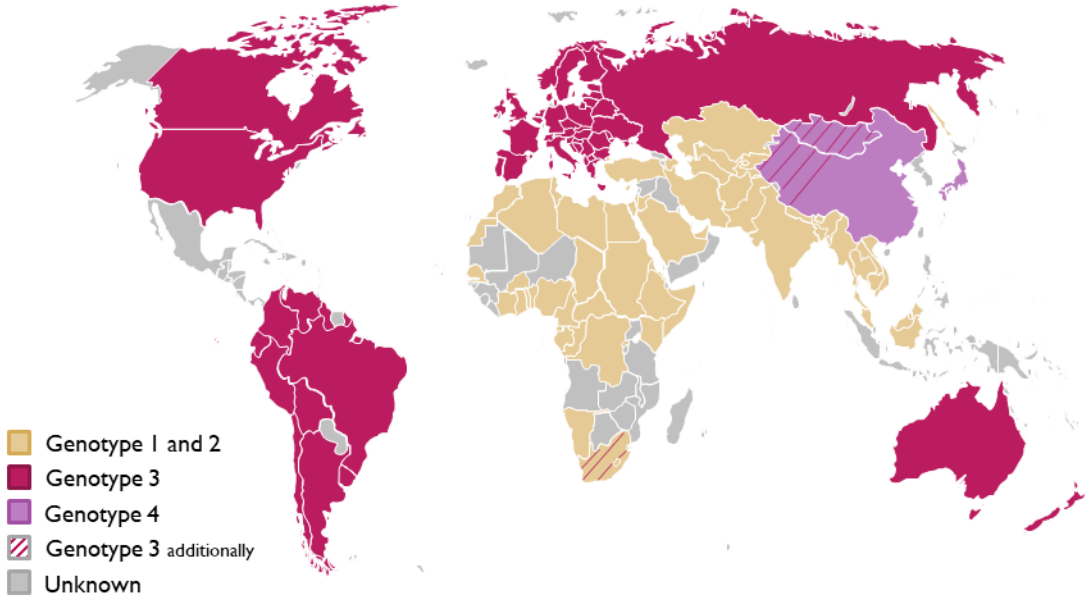

Figure 3: World wide repartition of HEV, adapted from [44].

1.4. Clinical Manifestations

The majority of HEV infections are asymptomatic and if the patient develops symptoms, the illness is usually self–limiting and resolves within a few weeks [45].
Nevertheless, icteric hepatitis occurs in 5–30% of infected patients. In these cases, the prodromal phase is characterized by fever, nausea, vomiting, anorexia, abdominal pain [46] and malaise. The following icteric phase is defined by symptoms such as jaundice and dark urine. Usually, the symptoms resolve after one week, yet the mortality ranges from 0.5–4% in immunocompetent patients [45].
Clinically HEV is similar to HAV, explaining why several HEV epidemics were mistaken for HAV outbreaks early on (Chapter 1.1) [46]. The clinical course differs depending on the HEV genotypes.
HEV1 and 2 mainly infect young males between the ages of 15–30 years in low–income countries. Symptoms range from asymptomatic or a mild systemic illness to icteric hepatitis and acute liver failure. Pregnant women belong to a high risk group, since the mortality rises up until 25% upon infection. Symptoms include hemorrhage, eclampsia and acute liver failure. Also, stillbirths are more common due to the vertical transmission of the virus. The reason for this increase in mortality is unknown,

but it might be related to the immune status during pregnancy, that is characterized by reduced T–cell activity and cytokine production, a predominant T–helper 2 cell response and a down–regulation of antigen presentation. These modifications go along with hormonal changes in pregnant women [47].
On the other hand, HEV3 and 4 circulating in high–income countries induce a different clinical course. These genotypes infect primarily middle aged and elderly men above the age of 55 years that mostly resolve asymptomatically. In Europe 5–33% of the infected patients develop symptoms and high risk groups include patients with underlying diseases [48–50].
Chronic infections have been observed for patients infected with HEV3 and 4. A chronic infection is marked by HEV replication that persists for more than 3 months. It occurs in immunocompromised patients such as solid organ transplant (SOT) recipients [51–53] and HIV–infected individuals [54–56], patients undergoing chemotherapy [57], and stem cell transplant recipients [58]. In 10% of chronic cases, a rapid progress to cirrhosis was observed [51–53]. As opposed to HEV1 and 2, genotypes 3 and 4 do not increase mortality or the risk of stillbirths in pregnant women.
Therefore it is crucial to find an efficient and specific treatment especially for patients that are part of high–risk groups.

1.4.1. Extrahepatic Manifestations

Evidence suggests that HEV not only replicates in the liver, but additionally in extrahepatic tissues such as the peripheral nervous system, the pancreas, renal tissue, hematoma cells and potentially further unknown sites. These manifestations occur during or after acute or chronic hepatitis through a yet unknown viral mediated direct or an immune mediated indirect mechanism [59].
While many details are unknown, the ability of HEV to cloak itself with the host cell membrane while circulating in the blood stream (Chapter 1.5.1) might explain the ability of the virus to reach a broad cell range [60, 61].
All reported disorders that occurred in 2 patients or more according to Rawla *et al.* 2020 can be found in Fig. 4 divided into 3 groups of manifestations [62].
Among these, neurological manifestations are the most frequently observed [19].
Indeed, a study from France found that 16.5% of patients infected with HEV suffered from neurological symptoms [63]. This could not be confirmed in a study conducted in

China, where no correlation between HEV infection and neurological symptoms was found. Hence this might indicate that genotype 3 (prevalent in France) is associated with neurological symptoms whereas genotype 4 (prevalent in China) is not [64].
Several cohort case studies showed that 2.4–10.6% of patients suffering from Neuralgic Amytrophy (NA) were infected with HEV. Also, a multicenter European study found that HEV–NA shows a distinct clinical phenotype: patients predominantly show bilateral asymmetrical involvement more often and more extensive damage to the brachial plexus ($p<0.001$). Involvement of areas outside the brachial plexus was further more common in HEV–NA patients ($p<0.01$) [65]. However, since neurological symptoms appear several months after infection and due to a possible cross–reactivity when co–infected with other viruses such as cytomegalovirus or varizella zoster virus, HEV serology needs to be interpreted with caution [66, 67].
The pathophysiology of the described disorders remains unknown, but it was observed that neurological injuries appear more frequently in immunocompetent people [63]. This might suggest that immunological processes play a critical role. According to Kamar *et al.* 2010, HEV replication in the central nervous system might be possible and it was found that HEV can replicate in several neuronal cell lines [68, 69]. Furthermore, it was shown in a gerbil model that HEV damages the blood–brain–barrier [70, 71].
Renal manifestations occur in both acute and chronic infections. It was suggested by Del Bello *et al.* (2015) that the underlying mechanisms might be similar to manifestations that are seen upon HCV infection, where immune complexes form between HCV antigen, IgG antibodies and a rheumatoid factor in the glomeruli [72].
Hematological and cardiovascular manifestations mainly consist of anemia and thrombocytopenia. Both conditions have been observed for several viruses (HAV, hepatitis B virus (HBV) and Cytomegalovirus) [69]. The cardiovascular manifestations include myocarditis [73, 74], cardiac arrythmias [75], long QT syndrome and Torsade's de pointes [76].
Furthermore, an association has been found between pancreatitis and HEV infection as it has been established for HAV, HBV and HCV previously [77, 78]. This condition may even lead to life–threatening consequences.
Lastly, other manifestations have been reported, but further research needs to be done. Among the observed injuries are: thyroid diseases, myasthenia gravis, Henloch–Schönlein purpura and acute polyarthritis [62].

Neurological Manifestations

Disorder	Reference	Number of Patients
Neuralgic Amytrophy	9-24	102
Guillain-Barré Syndrome	24-40; 10;54	36
Mononeuritis multiplex	10	6
Meningo-radiculitis	10, 44	5
Cerebral ischemia	11, 39	5
Encephalitits	11, 13, 41, 39	5
Facial nerve palsy	11, 46, 47	3
Peripheral Neuropathy	50, 39, 24	3
Epilepsy	11	2
Polyneuromyopathy	24, 43	2

Cardiovascular & Hematological Manifestations

Disorder	Reference	Number of Patients
Cryoglobulinemia	55	51
Monoclonal gammopathy	24	17
Lymphocytosis	24	14
Thrombocytopenia	58, 24	13
Lymphopenia	24	8
Myocarditis	56, 57	2
Malignancies (Acute myeloid leukemia, plasmacytoma)	24	2

Gastro-Intestinal and Renal Manifestations

Disorder	System	Reference	Number of Patients
Pancreatitis	Gastro-Intestinal	60; 62-67	22
Acute Kidney Injury	Renal	60, 61	2
Cryoglobulinemic membranoproliferative glomerulonephritis	Renal	72, 73	2

Figure 4: Extrahepatic Manifestations of HEV, according to [62].

1.5. Molecular Biology of HEV

1.5.1. Viral Particle

HEV particles measure between 32 nm–34 nm in diameter and possess an icosahedral capsid [3]. It consists of 180 copies of the capsid protein producing a *T=3* symmetrical structure [79, 80]. Its crystal structure was obtained by producing virus like particles (VLP) from the truncated capsid protein in insect cells. Successively, 3 different domains were identified: the S (shell)–, the M (middle)– and the P (protruding)–domain (Fig. 10) [81]. The S–domain is most conserved among HEV genotypes and it is responsible for forming the icosahedron as a jelly–roll which is the most common structure for RNA viruses [82]. The M–domain interacts with the S– and the P–domain and it is involved in virion stability [80]. Studies suggest that the amino–terminal region is involved in forming the correct *T=3* symmetry and the carboxy–terminus is important for RNA encapsidation [83]. The P–domain is hypothesized to be the binding site for the cellular receptor and is a target for neutralizing antibodies [84]. This domain folds into β–barrels and its polysaccharide–binding sites likely help receptor binding and/or capsid disassembly.

Even though HEV is classified as a non–enveloped virus, particles isolated from blood have been found to be enveloped in the host cell membrane. Additionally, the ORF3 protein has been detected on the surface of the viral particle [85]. On the other hand, particles isolated from bile and feces have not been found to be enveloped, since the bile salts might strip lipids from the virus [86, 87]. On the surface of the naked virus however, the ORF3 protein is not detectable [85]. It was hypothesized that the host–membrane could protect the viral particle in the blood stream from the host's immune system and therefore increases viral infectivity. Whereas, this protection is not necessary any more in bile where the virus will be shed into stool [14].

1.5.2. Genomic Organization

The HEV genome is a postive–sense single–stranded RNA, which is divided into 3 open reading frames (ORF) containing a 7–methylguanine cap (m7G) at the 5' end and a poly(A)–stretch at the 3' end [7, 88]. These two features allow the translation of HEV genome by the host's ribosomes [7, 88].
The ORF1, ORF2 and ORF3 have been identified by Tam *et al.* in 1991, but recently sequence analysis revealed an ORF4 for genotype 1 only [7, 89].
During replication 2 distinct RNAs are transcribed. The genomic RNA has a size of 7,2 kb and contains the complete genome, whereas the subgenomic RNA of 2,2 kb serves as template for ORF2 and ORF3 translation (Fig. 5) [90].
The non–structural protein consists of the ORF1 protein and the structural proteins of the ORF2 and the ORF3. The ORF1 is the largest ORF and it encodes a polyprotein with several domains that are all implicated in viral replication (Fig. 5). It will be further described in chapter 1.5.4.
ORF3 overlaps with the N–terminal region of ORF2 (330 nucleotide overlap), but it does not overlap with ORF1 [91].
The ORF4 is overlapping with the X– and the helicase–domain of the ORF1 (Fig. 5) and is controlled by an Internal ribosome entry side (IRES) structure initiating its translation under ER stress [90, 92]. Antibodies against ORF4 have been detected in patient sera as well [89].

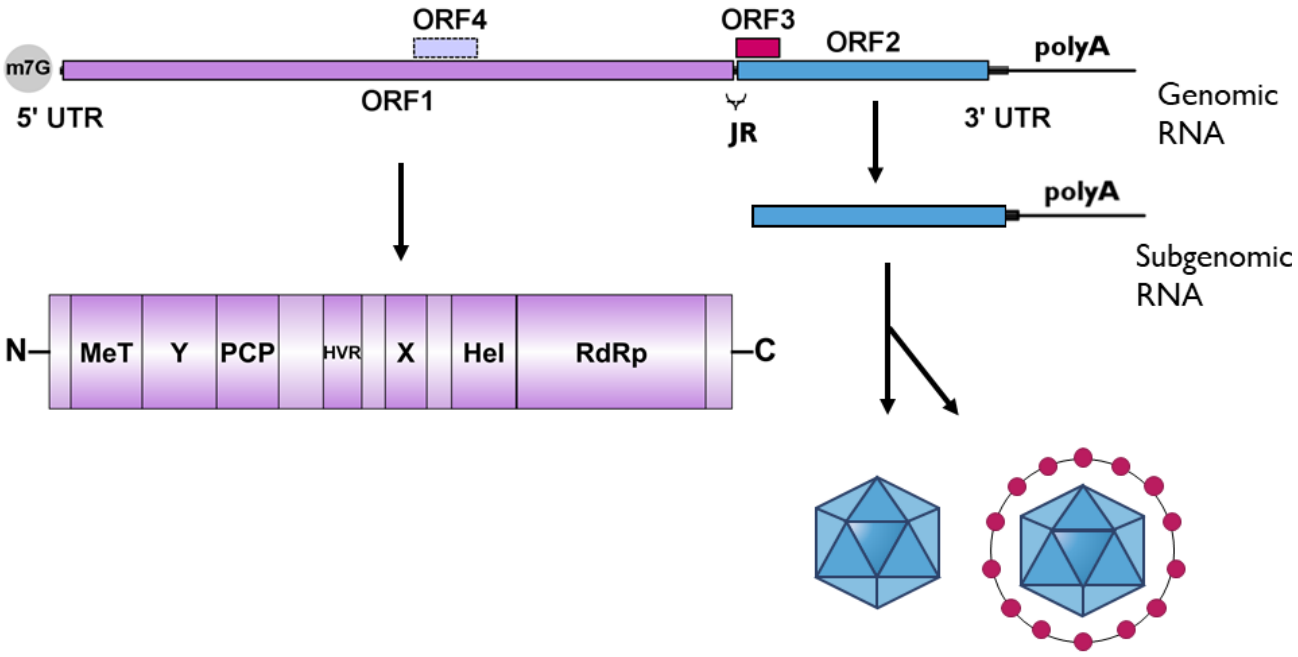

Figure 5: Genome organization of HEV gt3 Kernow C1/p6. m7G: 5'-methylguanosine cap, UTR: untranslated regions, JR: junction region, polyA: poly–adenosine–tail. The ORF4 is only present in gt1. The ORF1 consists of 1761aa.

1.5.3. *Cis*–reactive Elements

Several *cis*–reactive elements (CREs) have been identified in the HEV genome (Fig. 6).

Following the m7G, the 5' UTR spans over 26 nucleotides before ORF1 begins [93]. This region forms a stable hairpin loop that is required to bind ORF2 and is involved in encapsidation of the viral genome [94, 95].

The start codon for ORF3–RNA transcription lies at position 5122 and thereby 15 bp downstream of the stop codon of ORF1. Overlapping with the last 27 nt of ORF1 until the transcription start site of ORF3 lies the junction region (JR) that forms a stable hairpin loop as a RNA secondary structure. This region is acting as a subgenomic promoter for the subgenomic RNA and is therefore required during the HEV life cycle[96, 97]. Additionally, the JR contains a highly conserved CRE, that overlaps with the stable hairpin loop and is crucial for viral replication and infectivity [98, 99].

Another RNA secondary structure element lies at the 3' poly(A)–tail of the HEV genome which also overlaps with the C–terminus of the ORF2. It forms 2 stem loops that bind the RNA dependent RNA polymerase (RdRp) of the ORF1 protein and is thus involved in viral replication [100].
In the central region of ORF2 lie two RNA elements that form internal stem loops (ISLs) that are called ISL1 and ISL2. Silent mutations that disrupt these ISL lead to a reduction of capsid synthesis and single mutations of a *Gaussia* luciferase replicon reduce luciferase expression suggesting these ISL are important for replication efficacy [43].
Ju *et al.* in 2020 reported 2 additional CREs that are located in the MeT–domain of ORF1 (nucleotides 102–131) and the C–terminus of ORF2 (nucleotides 7311–7340). Both of them are crucial for viral replication and viral particle production and they are able to recruit ORF1 to the replication complex [101].

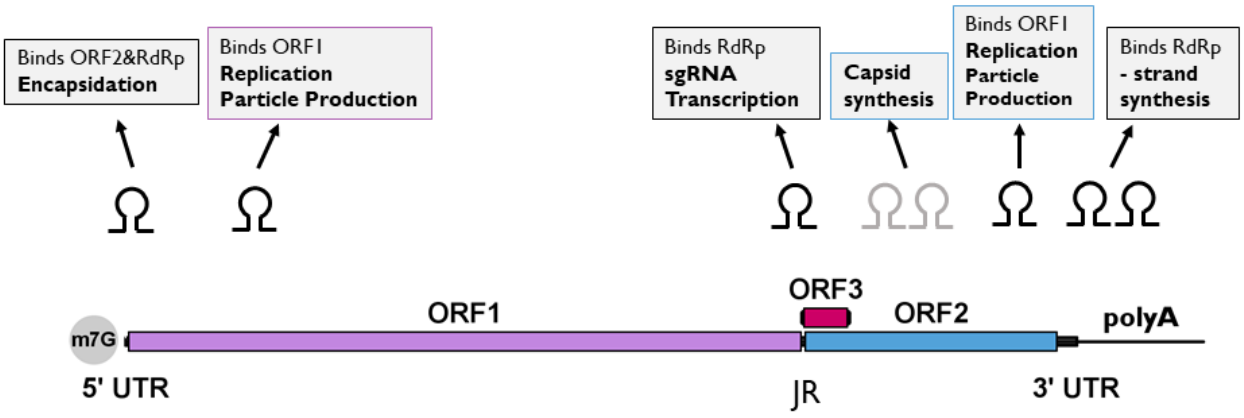

Figure 6: *Cis* reactive elements with binding partners and their functions in the HEV genome. UTR: untranslated region, JR: junction region.

1.5.4. The Non–structural Protein ORF1

The ORF1 is a polyprotein with a mass of 186 kDa (HEV genotype 1, strain Sar55) – 194 kDa (HEV genotype 3 Kernow–C1/p6 [102], calculated with ExPASy [103]) and is also known as replicase due to its functioning in virus replication [22].
The domains have been computationally assigned as can be seen in Fig. 7 based on sequence homology to other viruses [104].

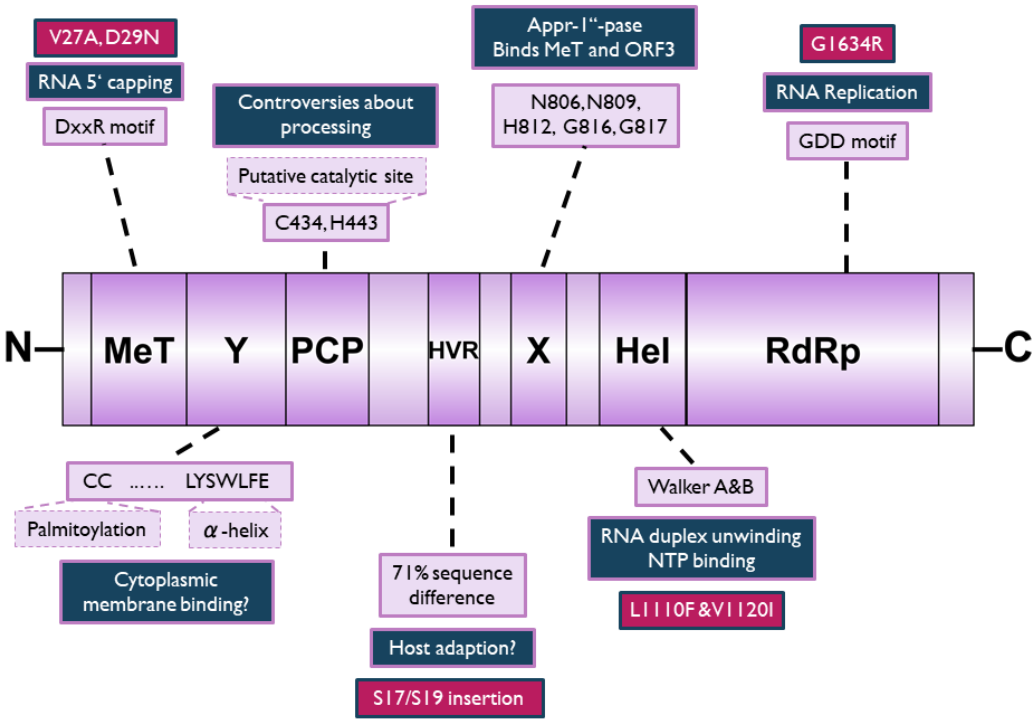

Figure 7: The polyprotein ORF1. MeT: methyltransferase domain, Y: Y domain, PCP: papain–like cystein protease domain, HVR: hypervariable region, X: X/macro domain, Hel: helicase domain, RdRp: RNA dependent RNA polymerase domain. Purple: Sequence motifs that are implicated in the function of the domain (unless specified otherwise), Dark blue: Function of the domain, Raspberry: Mutations that lead to higher viral load in cell culture or patients or are associated with a more severe disease outcome.

It appears to be most closely related to the family of Rubivirus, Betateravirus and Benyvirus [105].
The methyltransferase (Met)–, the helicase (Hel)–, the papain–like cysteine protease (PCP)– and the RNA dependent RNA polymerase (RdRp)–domain have been functionally studied by themselves or in combination, whereas the functions of the X–domain, the Y–domain and the hypervariable region (HVR) remain widely uncertain

[104].
Furthermore, it still remains unknown whether the polyprotein is cleaved into individually active proteins or acts as a single polyprotein with multiple functions. This will be further discussed in chapter 1.6.2.

The MeT–domain The 7–methylguanosine (m7G) capping at the 5'–end confers stability to eukaryotic or prokaryotic mRNAs and it allows efficient translation in eukaryotic cells. It can also avoid the recognition of viral RNAs and their degradation during the innate immunity response. In eukaryotic cells, the capping reaction typically consists of three distinct enzymatic reactions: At first, the 5' γ–phosphate is cleaved by an RNA 5'–triphosphatase (RTPase), next the guanylyltransferase (GTase) hydrolyses a guanosinetriphosphate (GTP) molecule and transfers the resulting guanosinemonophosphate (GMP) to the 5'–end of the RNA and at last, a methylgroup gets transferred to the GMP by the methyltransferase (MTase).
These reactions can be carried out by different enzymes (MTase and GTase) or by multifunctional enzymes [106].
A bioinformatic analysis in 1992 revealed a methyltransferase at the N–terminus of the ORF1 protein [104]. The ORF1 domain organization of HEV resembles that of viruses belonging to the Alpha–like super–group. Other well known members of this super–group are Sindbis virus (SINV), Semliki Forest virus (SFV), Chikungunya virus (CHIKV) and Rubella virus (RUBV) (ICTV). The RNA molecules of its members are 5' capped and one of the hallmarks of this group is the presence of a unique type of capping enzyme, since it possesses the combined activity of the MTase and GTase [107, 108]. The MTase–GTase of the alphavirus–like super–group first methylates GTP and subsequently transfers it to the 5' end of the viral mRNA (Fig. 9) [108–110], which differs from the cellular pathway where the transfer occurs before the methylation [106]. This makes the MeT an attractive target for antiviral drug design. Prior to this step, a RNA triphosphate reaction occurs, which is carried out by the HEV helicase domain using its NTPase active site, which is explained later (chapter 1.5.4) [111–115].
The 5'–end of the HEV mRNA has indeed been found to be capped [88].
Magden *et al.* expressed a combined construct of MeT–Y–PCP domain in baculovirus and it has combined MTase–GTase activity (Fig. 9). The MeT–domain alone has a size of approximately 200 amino acids that is considered the core region [108].

However, in baculovirus, capping only occured when a MeT–, Y–, PCP–domain comprising construct was expressed. Thus, the MTase activity can not be attributed to the MeT core domain exclusively [110, 116].
As in other MeT domains of other Alphavirus–like supergroup members, a conserved H (H64), followed by a DxxR (D34xxR37) motif and a conserved Y (Y20) was found in HEV [107].
HEV is infectious in primates only when its RNA is capped, since the 5'–triphosphate, that is formed during RNA synthesis, is a trigger for interferon response of the innate immune system [116, 117]. Therefore the viral RNA is protected by capping at the 5'–end.
Furthermore, the MeT domain is also believed to interact with cytoplasmic membranes [110, 118].
In patients it has been found that the mutations V27A and D29N increase viral load, while the H105R mutation results in a decrease in viremia [119, 120].
A clinical study found that the mutation of F179S in genotype 1 was associated with the development of fulminant hepatitis [110, 120].

The Y–domain As opposed to the MeT–domain, very few details about the Y–domain are known.
In members of the alpha–like supergroup it was suggested that the Y–domain which lies downstream of the MeT core region is the minimal entity which is required for its enzymatic activity [121, 122]. Among the alpha–like supergroup, the Y–domain is conserved in secondary structure, but not in sequence. RNA secondary structure prediction has demonstrated stable hairpin formations, that affect RNA replication and virus infectivity when mutated [118].
Recently, it was attributed the term "iceberg region", since this region is longer than the MeT core domain itself thereby resembling an iceberg. In Sindbis virus and Semliki Forest virus it was found that internal deletions and certain mutations reduce or abrogate MTase–GTase enzymatic activity [122, 123]. In case of HEV, it was shown that fragments with the length of 470 and 527 residues had no enzymatic activity, suggesting the necessity of a rather large translational product for enzymatic activity [110].
The Y–domain is essential for capping activity, but is has other putative functions as well. A highly conserved cystein dyad (C_{336}–C_{337}) was identified as a potential palmitoylation site in the Y–domain [118] , that is needed for cytoplasmic membrane–

binding and that may be essential to establish replication complexes, as a crucial part of viral replication [124]. Indeed, a mutation of the cysteine dyad resulted in the abolishment of RNA replication [118].
Furthermore, a conserved hydrophobic sequence was found, that forms an α–helix (LYSWLFE) and might be implicated in membrane binding, as it is the case in bromo mosaic virus (BMV) and cucumber mosaic virus (CMV–1a) [118].
Also, RNA secondary structure prediction has demonstrated stable hairpin formations, that affect RNA replication and virus infectivity when mutated [118].
All in all, a critical role for the Y–domain in RNA replication is suggested, possibly through RNA capping activity or membrane binding.

The PCP–domain Proteases are enzymes that hydrolyze amide bonds of peptides and proteins. In eukaryotes they play important roles in many physiological processes and in viruses, proteases can process the viral polyprotein(s) [125]. Importantly, many viral proteases have been potent targets for antiviral therapy, for example against HIV [126].
The HEV PCP–domain shows a moderate sequence similarity to the protease domain of Rubella virus, however, sequence similarity between this region and other viral or cellular papain–like cysteine proteases has not been found [104]. On the other hand, the conservation of a short stretch around the putative catalytical cysteine (Cys 481) and 2 additional cysteine (Cys 434 and Cys 457) residues suggest that the HEV PCP is a papain–like cysteine protease [104].
Despite the low to moderate sequence similarity between the RUBV and the HEV protease, their structural similarity appears higher according to *in silico* modeling of the HEV PCP. In this report a catalytical dyad (Cys 434 and His 443) was identified, which occurs in other viruses too (Foot–and–mouth disease virus, coronavirus 229E and RUBV) [127]. These findings point towards the presence of a papain–like cysteine protease.
Furthermore, mutation of several residues in this region His (H443L, H497L, H590L) and Cys (C457A, C459A,C471A, C472A, C481A, C483A) residues abolished HEV RNA replication. These amino acids might be putative catalytical residues of the PCP domain [127].
In contrast to the previous observations, a study by Paliwal *et al.* found that the HEV protease exhibits characteristics of a chymotrypsin protease. When expressing and purifying the protease domain (aa 440–610 of the gt1 Indian strain) an inhibition was

found by inhibitors of chymotrypsin proteases (PMSF and chymostatin). Moreover, the HEV protease was able to efficiently digest chymotrypsin specific fluorogenic peptide substrates [128].
This difference to the previous results was explained in another report by Saraswat *et al.* in 2020 who showed evidence for the existence of a papain–like cysteine protease. According to them, the use of the Indian strain that contains 9 additional amino acids at the C–terminus of the protein and shows considerable variations explains the different observations [129].
Furthermore, 12 inhibitors of various proteases were tested on the HEV protease that was expressed and purified in the baculovirus in native conditions. It was found that the protease of HEV was resistant to serine, aspartic and metalloprotease inhibitors, but it was inhibited by cysteine protease inhibitors. Additionally, *in silico* modeling showed structural similarity to papain–like cysteine proteases [129].
Nevertheless, since the HEV PCP position predictions were based on a low to moderate sequence similarity to the RUBV protease domain, new evidence even suggests a different region for the putative protease domain (Fig. 8). The resulting protein (residue 510–691aa) showed high structural similarity to fatty acid binding domains and a potential zinc coordination site was found as well [130].
Furthermore, different studies show controversial results for the processing of ORF1 questioning the protease activity of the PCP domain (Chapter 1.6.2) [131–134].
On a different note, the PCP might be implicated in immune evasion strategies. When expressed as a fusion protein with the MeT domain, it shows deubiquitinase activity that limits the activation of retionic acid–inducible gene I (RIG–I) and tank binding kinase I (TBK–I), which in turn reduces the activation of the interferonβ (IFNβ) promoter (Fig. 16). Consequently, interferon stimulated genes (ISGs) i.e. ISG15 are less expressed [135].

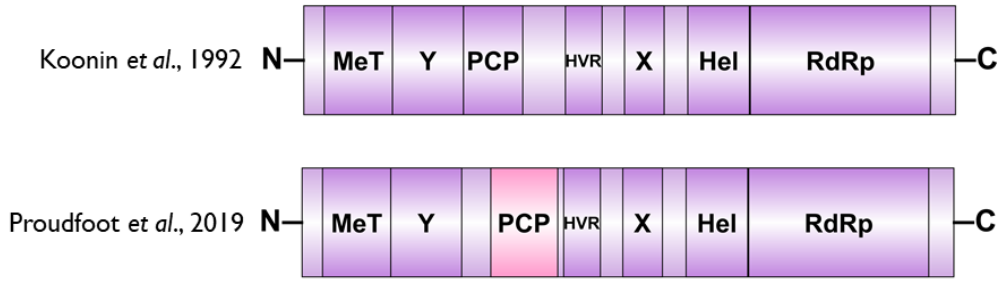

Figure 8: Annotation of domains in the ORF1 according to Koonin *et al.* 1992 [104] and Proudfoot *et al.* 2019 [130]

The HVR The HVR is considered hypervariable since it contains the greatest divergence out of all ORF1 domains [136]. It is rich in proline residues, thus it is also referred to as polyprolin region (PPR) [136–138]. The HEV HVR is considered an intrinsically disordered region, which means that it does not form a compact 3–D structure [136].
Length and sequence of both regions are highly variable among strains. The HVR sequence difference between HEV genotypes mounts up to 71%. The HVRs of HEV genotypes 1 and 2, that infect only humans, are more conserved (31% sequence difference for gt1) than those of genotypes 3 and 4 (41% difference for gt 3) infecting humans and certain animal species. This might indicate that the HVR is a modulator of infectivity and involved in host tropism [88, 139, 140].
It is believed that the HVR serves as a hinge between the X–domain and the upstream regions due to its flexibility. The high amount of structure–breaking amino acids (Pro and Gly) leads to unstable tertiary structures and increases flexibility [104, 141, 142]. This flexibility can mediate conformational changes that are involved in protein–protein interactions [136].
The HVR sequences are functionally interchangeable between different genotypes. Although genotype specific differences have been observed, since replicons with swapped HVRs replicated at lower efficacy than the wt replicons. This indicates that the composition of the HVR may influence replication efficacy [137]. Furthermore, the HVR might interact with viral and/or host factors to modulate replication efficacy [22]. Additionally, the HVR can tolerate small deletions, as the amino acid residues are dispensable regarding virus infectivity. Yet, a complete deletion of the HVR resulted in virus attenuation [139]. Furthermore, it was observed that deletions at the N–terminus and the center of the HVR resulted in more drastic reductions of replication compared to deletions at the C–terminus [137].
In turn, certain insertions can enhance viral replication. The most prominent example is the HEV genotype 3 Kernow–C1 strain that was isolated from a patient co–infected with HEV and HIV that revealed an insertion of the human ribosomal gene S17 (174nt) in its HVR. After 6 passages in HepG2/3CA cells, this species appeared to be the most abundant variant present. It was found that viruses possessing this insertion replicate 500 times more efficiently in cell culture, therefore the S17 is favorable for cell culture adaptation [102]. Furthermore, it replicates not only in human hepatoma cell lines, but also in mice, cat, dog and hamster cell lines (Chapter 1.11) [143]. This implies that the insertion of host gene fragments could expand host range

[144].
It appears that the HVR can tolerate insertions of host genes, as two other genes (S19 and GTPase activating protein) have been identified in isolates (LBPR strain and Kernow strain) [102, 145]. Moreover, a duplication of a region of the HVR and an insertion of the RdRp have been observed in a chronically infected patient, that enhanced the viral replication capacity [146].
Taken together, the HVR is a hotspot of genetic recombination and a key factor in evolution and adaptation [136, 139].

The X domain The X domain is located downstream of the prolin–rich region, but its function in the HEV life cycle is still unknown.
The adjacent helicase domain might even interact with the X domain in order to function as described in the following processes [147].
The X domain is also known as macrodomain due to its similarity to the macroH2A protein [148]. Macrodomains are evolutionary conserved domains that can bind ADP–ribose and some of them are even able to hydrolyse ADP–ribose–1'phosphate to yield ADP ribose [149–151].
ADP–ribose is covalently attached to target proteins by poly–ADP–ribose–polymerases (PARP) and has a variety of effects such as alteration of enzyme activity, protein–protein interactions, and protein stability. This post–translational modification is necessary for many cellular processes: DNA repair, transcription, chromatin biology and long–term memory formation [150, 152, 153]. Furthermore, ADP–ribosylation is induced by IFNs to resist a viral infection. Macrodomains can therefore counter the innate immune system by removing ADP–ribosylation from proteins [148].
Also, the domain is involved in the tRNA splicing pathway by catalyzing the conversion of ADP–ribose 1'monophosphate to ADP ribose [96].
Macrodomains are encoded by many cellular proteins, but also by RNA viruses such as Coronaviridae, Togaviridae and Matonaviridae [104, 154]. Sequence homology of the HEV macrodomain has indeed been found with cellular ADP–ribose–1'– monophosphatase (Appr–1'–pase) [96, 155].
The putative active site might be constituted of the amino acids N806, N809, H812, G816 and G817 and in fact the mutation of the latter 3 amino acids results in a decrease of HEV replication [96]. The active site potentially connects a β–stand and a α–helix and is required for HEV replication on a post–translational level [96].
Furthermore, the X domain inhibits type I IFN induction by preventing interferon reg-

ulatroy factor 3 (IRF3) phosphorylation and thereby blocking the induction of IFNβ transcription (Fig. 16) [156].
The C–terminal region of the X domain interacts with the MeT and ORF3 through the amino acids I66–I67 and L101–L102 and therefore could play a role in different stages of the viral life cycle [157].
It was also found that its interaction with the light chain subunit of human ferritin suppresses ferritin secretion in cells, which subsequently attenuates the host's immune response [158].
Additionally, an inhibition of apoptosis is suggested, since the domain is functionally related to PARP–1 and viruses are known to show an effect on apoptosis of infected cells [155, 159]. However, this has not been experimentally demonstrated yet.

The Hel domain Helicases are nucleic acid separating enzymes that are involved in a number of cellular processes. They separate either DNA–DNA, DNA–RNA or RNA–RNA NAs via nucleotide triphosphate (NTP), usually ATP, hydrolysis [160]. The RNA Helicase of HEV is able to unwind double stranded RNA in a 5'–3'–direction [161]. Indeed, in *E. coli* the Hel domain was shown to possess nucleotide triphosphatase (NTPase) and 5'–3' duplex unwinding activities. It shows hydrolysis of all rNTPs and all dNTPs, but with relatively low efficacy for dNTPs compared to rNTPs [115].
The HEV helicase domain belongs to the superfamily I (of 6 superfamilies) according to sequence similarity and conserved motifs to other helicase proteins. Superfamily I includes also helicases of alphaviruses, arteriviruses, coronaviruses and rubiviruses [161].
In this domain, 7 conserved motifs (I, Ia, II, III, IV, V, VI) are present in a co–linear fashion. All superfamilies share 2 motifs: the Walker A (motif I) and Walker B (Motif II) sites that are involved in NTP binding. The Walker A site is characterized by hydrophobic acids followed by a GxxxxGKS/T motif and is binding to β– and γ–phosphates of NTP, while the Walker B site (DEAP) chelates the Mg^{2+} of the Mg–NTP complex [162]. Mutating motif A (GKS to GAS) results in 70% loss of ATPase activity, mutation in motif B (DEAP to AAAP) in 50% loss and mutations in both motifs cause 100% loss of RNA replication [163]. Thus both motifs are equally important for ATP hydrolysis, since both mutants lost their ability to unwind RNA duplexes. This implies that the unwinding ability of the Hel domain is dependent on the energy provided by ATP hydrolysis

[161].
In a follow–up study it was found that motifs Ia, II and II are indispensable for ATP hydrolysis and RNA duplex unwinding. When motif Ia was deleted, unwinding ability was completely abolished while ATPase activity shrunk by approx. 50%. Upon deletion of motif III, ATPase and unwinding activity was significantly reduced and the deletion of motif II resulted in a loss of ATPase activity, whereas unwinding activity was not reduced [164].
The region from 960–1204 is likely involved in the NTPase activity of the mRNA cap formation, as it presents NTP hydrolysis activity that is required for the first step of the capping process (Fig. 9) [115].
In HEV gt 1 infected patients, the mutations L1110F and V1120I (between motif IV and V) are associated with a higher incidence of fulminant hepatic failure. This mutations lead to a slight decrease in ATPase activity, but no effect on RNA duplex unwinding activity [163].

The RdRp–domain The RdRp is essential for RNA virus replication and therefore found in every RNA virus (except for retroviruses). It synthesizes positive sense and negative sense RNA transcripts from negative sense and positive sense viral RNA (Fig. 9).
The RdRps can be divided into 3 supergroups based on sequence similarity. The HEV RdRp belongs to supergroup III together with alphaviruses, rubiviruses and plant viruses such as beet necrotic yellow vein virus (BNYVV) [104]. So far no structure is available for any member of this superfamily [138].
The HEV RdRp contains 8 conserved motifs (motifs I–VIII) similar to RdRps of other positive–stranded RNA viruses [100].The GDD motif represents the catalytic triad of the enzyme and binds Mg^{2+}. Mutation of this motif abolishes viral replication, thus it is essential for replicase activity [10].
The RdRp from an Indian HEV isolate has been successfully expressed *in vitro* in *E. coli* as a 63 kDa protein and it was shown to bind specifically to the 3'–terminus of the HEV genome sense strand to produce the antisense strand [100]. Furthermore, it binds to the subgenomic promoter (sgP) to transcribe the subgenomic RNA [165].
However, it was shown that the RdRp has the highest affinity for the 3'UTR, then the 5' UTR and then the sgP, but it is unknown how the binding to the different regions is regulated. The RdRp likely binds cooperatively the 3' UTR and the sgP to initiate

sgRNA synthesis [165].
Also, the recombinant RdRp is localized at the ER of the host cells, indicating that this could be the site of replicase localization [166]. The subcellular localization will be further discussed in Chapter 1.6.4
Viral RdRps often interact with viral or host proteins to complement RdRps activity, establish a scaffold for the replicase or modulate its activity. It was observed that the HEV RdRp interacts with the PCP and likely with the MeT and Hel as well to complement the RNA transcription activity [167]. Additionally, it interacts with several host immune factors. One example is the IFN produced protein IFIT1 which inhibits translation of virus proteins. The RdRp of HEV is able to interact with IFIT1 and counter its translation inhibition [168] (Fig. 16). Yet another example is the microRNA miR–122 that appears as a pro–viral factor enhancing viral replication *in vitro*. It was found that the HEV gt1 RdRp harbors a binding site for miR–122, however, its specific role is unknown [169, 170]. The role of miR–122 has been more extensively studied within the HCV life cycle, where it also enhances the virus replication at several stages. Evidence suggests that miR–122 promotes viral genome stabilization, protein translation, genome amplification and protein recruitment [171–176].
Several mutations and some insertions in the RdRp are associated with ribavirin treatment failure in chronically infected patients. A well characterized mutation is the G1634R substitution that increases viremia [177] and enhances HEV replication and infectivity in cell culture [177–179].
Taken together, the RdRp is an attractive therapeutic target. Indeed, zinc salts and RNAi showed promising effects on viral replication inhibition, but a specific treatment targeting the RdRp has not been approved yet [138].

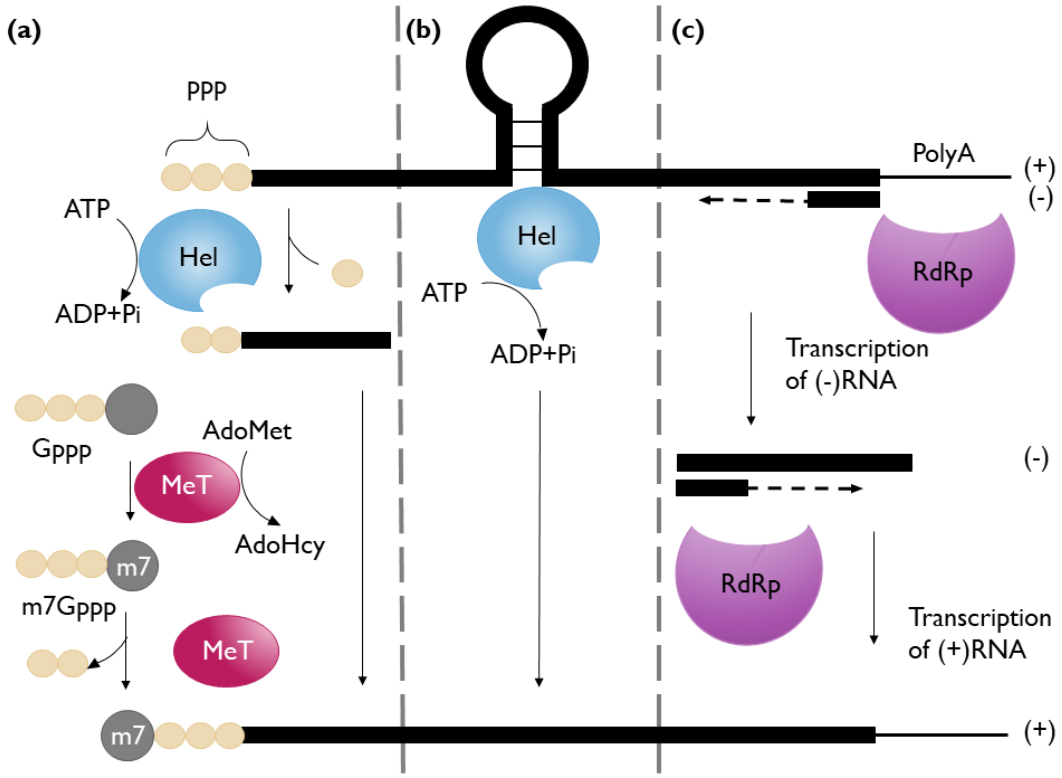

Figure 9: Functions and mechanisms of selected ORF1 domains. (a) Capping of mRNA, (b) Unwinding of RNA, (c) Transcription of antisense and sense RNA. ppp: triphosphate, Pi: phosphate, AdoMet: S–adenosyl–l–methionine, AdoHcy: S–adenosyl–l–homocysteine

.

1.5.5. The Structural Proteins

The capsid protein ORF2 The ORF2 protein consists of 660aa and makes up the capsid protecting the viral RNA by binding to the 5' end of the HEV genome [94, 180]. Crystal structure experiments suggest a division of the capsid protein into three subunits: the S (shell)–, the M (middle)– and the P (protruding)–domain (Fig. 10) [81]. When expressed in an animal cell culture system, proteins of 72 kDa and 84 kDa in size were found that represent the nonglycosylated and the glycosylated forms of the ORF2 [181].

At the N–terminus, a signal sequence potentially enables the capsid protein to be translocated into the ER to be further glycosylated [181]. ORF2 contains 3 potential glycosylation sites displaying a conserved motif (N–X–S/T) [182–184], but only two of them are glycosylated in infected cells [185]. Furthermore, it was found that gly-

cosylation occurs only on ORF2 proteins that are not involved in infection, but which are nevertheless secreted in large amounts by infected cells [186]. These ORF2 forms are called ORF2g (glycosylated) and ORF2c (cleaved) and they are the most abundant forms in patient sera. On the other hand, the ORF2i (infectious) is not glycosylated and is associated with infectious particles. The different glycosylation status implies different pathways for the production of the capsid protein (Fig. 11) [185, 186]. The different forms of ORF2 vary not only in their post–translational modifications, but also concerning their translation start site, ORF2i being the shortest of all three forms. The capsid protein can bind genomic RNA at the 5'–end of HEV RNA genome and its C–terminus is required for RNA encapsidation and particle stabilization [83, 94].
So far, very little is known about the interaction of the ORF2 protein with cellular factors, however, capsid proteins of non–enveloped viruses play an important role in virus entry, intracellular trafficking and signaling [187]. It may interact with heparan sulfate proteoglycans (HSPGs) in an initial attachment step of the viral particle to the cell surface [188]. Furthermore, it binds to heat shock protein 90 (HSP90) and 78–kDa glucose–regulated protein (Grp78) that are involved in intracellular trafficking [181, 189].
Besides that, ORF2 modulates the host cell transcription by interacting with elongation initiation factor 2A (eIF2A), activating transcription factor 4A (ATF–4), heat shock protein 72 (HSP72), nuclear factor κB (NFκB)and of the C/Ebp–homologous protein (CHOP) promoter [190, 191].
Even though HEV is a non–enveloped virus, a lipid component was shown in cell culture produced viral particles and led some authors to consider HEV to be quasi–enveloped [192]. The impact of glycosylation on the quasi–envelope yet remains to be identified.

The phosphoprotein ORF3 The other structural protein of HEV is the ORF3 that encodes the smallest protein with 112–115 aa and 12–13kDa in size (VP13) [7, 193]. At its 3'–end, it overlaps partially with the ORF2, but not with the ORF1 [90]. Sequence analysis has indicated two hydrophobic regions D1 and D2 at the N–terminus and two Proline–rich regions P1 and P2 at the C–terminus (Fig. 10). A homodimerization of the ORF3 protein by the C–terminal prolin–rich regions was suggested and recently confirmed in mammalian cells [194, 195].
The D1 region is rich in cysteine residues, which ensure cytoskeleton association

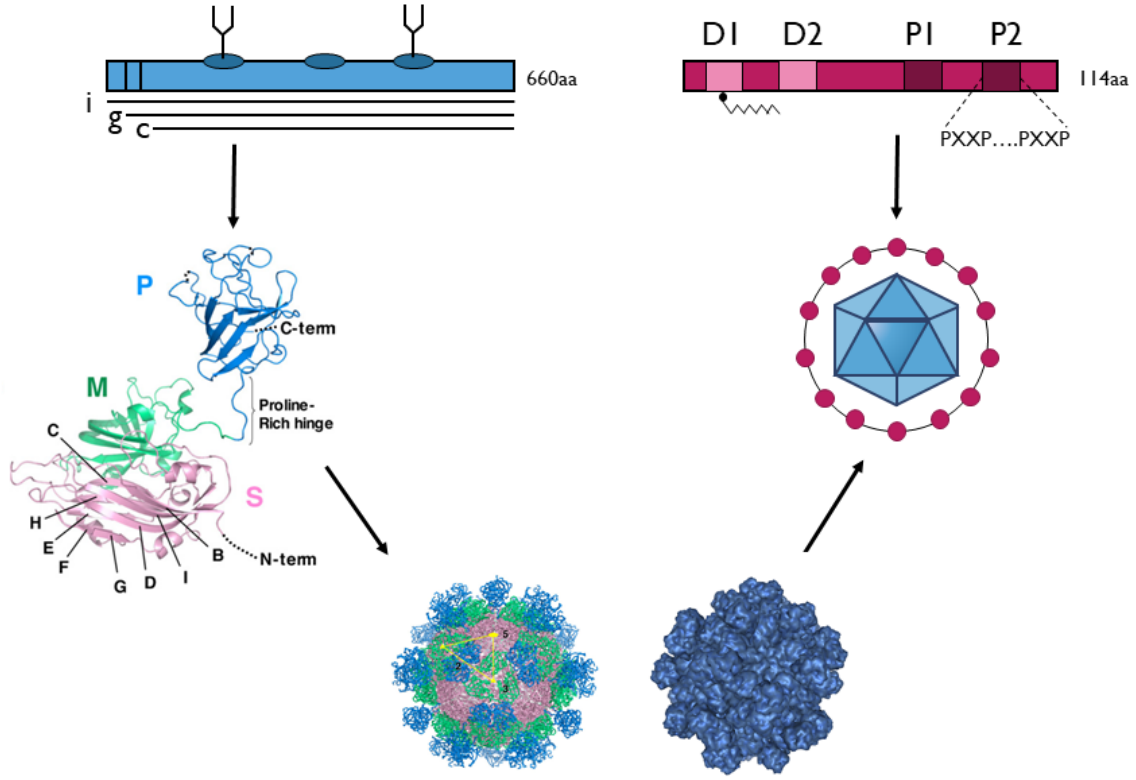

Figure 10: Schematic and structural overview of the structural proteins of HEV. Blue=ORF2 showing three potential glycosylation sites of which 2 are glycosylated; g=glycosylated, i=infectious, c= cleaved. Red=ORF3; D1 contains a palmitoylation site and P2 2 PXXP motifs. Crystal structure by [81].

through the binding of microtubules [193, 196]. Additionally, the palmitoylation of the cysteine rich segment is important for membrane association, subcellular localization and stability of the protein [197].

The D2 domain contains a binding site for hemopexin, a plasma protein with a high binding affinity to heme and which is mainly expressed in the liver [198, 199].

The P1 domain possesses two overlapping phosphorylation kinase sites at S70. It can be phosphorylated by the mitogen–activate protein kinase (MAPK) and by the cyclin dependent kinase [200]. The phosphorylated ORF3 interacts with the capsid protein and cellular proteins such as the cytoskeleton, al–micoglobulin/bikunin precursor, tumor susceptibility gene 101 (TSG101) and src–homology domains [201–203].

The P2 region has two PXXP motifs (Fig. 10) that allow binding of the sarc–homology 3 domain (SH3) and is associated with the signal transduction of cellular proteins related to cell growth, differentiation and other regulatory functions [204]. It also inter-

acts with tumor suppressor gene 101 (TSG101) that is part of the endosomal sorting complex required for transport–pathway (ESCRT–pathway) and facilitates virion release in association with a lipid quasi–envelope [105].
Additionally, studies show that the ORF3 protein is inserted within the quasi–envelope that surrounds HEV particles circulating in the patient sera and in the supernatants of HEV producing cells and it is inside the exosomes that constitute the quasi–envelope [197]. Even though the ORF3 protein is not necessary for viral replication in cell culture, it is crucial for infectivity, indicating its role in viral release [205]. A study by Nagashima *et al*. 2011, suggests that the PSAP motif within the P2 domain is essential for the formation of membrane associated HEV particles with the ORF3 protein on their surface [206].
Moreover, ORF3 proteins were found on HEV virions in sera and cell culture supernatants, but not in bile or feces [85].
Another study by Ding *et al*. in 2017, suggested that ORF3 functions as a viroporin. It forms multimeric complexes within ER–derived membranes that create an ion channel, thereby classifying it as a class I viroporin. As a result, ion flux across membranes is facilitated and the electrochemical gradient across the plasma membrane is disrupted, which in turn stimulates viral budding [195].

1.6. Cellular Biology of HEV

1.6.1. HEV Life Cycle

Until recently, it lacked an efficient cell culture system for HEV, hence the replication cycle remains largely unknown. Nevertheless, a model that has been proposed can be found in Fig. 11.
A receptor for virus entry has not been identified yet, but HEV VLP studies have shown that aspecific attachment involves HSPGs (Fig. 11 (1.)) [188].
Furthermore, the ORF2 capsid protein of the naked virus might bind to heat shock cognate protein 70 (HSP70) and Grp78 on the cell surface to mediate virus entry. It was found that these interactions are essential for intracellular transport but not essential as a receptor [188, 207]. Also, integrin α3 is potentially involved in the entry of non–enveloped HEV [208].
A potential sugar binding site within the M domain of the capsid is conserved among the different mammalian HEV genotypes implying a functional role in binding to the

cellular receptor [209].
It is furthermore suggested that the entry mechanisms of the non–enveloped HEV particle and quasi–enveloped HEV differ from each other. The naked virus is internalized through clathrin– and dynamin–2 mediated endocytosis, that requires cholesterol and is possibly transported via HSP90 in an unknown manner [94, 210–212].
On the other hand, the uptake of the quasi–enveloped virus requires Rab5 and Rab7, and the quasi–envelope is degraded in the lysosome [213]. It was reported that the quasi–enveloped HEV entry is slower, which might explain the lower infectivity of the quasi–enveloped virus compared to naked virions [214].
After genome uncoating and release into the cytoplasm, first, the viral replicase has to be translated by the cellular machinery to ensure viral replication (Fig. 11 (3.+ 4.)). The translation of the non–structural protein involved the eukaryotic translation initiation factors 4A, 4G, 4E (belonging to the eIF4F complex) that are critical for viral replication [215]. After that, an intermediary negative–sense RNA is produced by the RdRp that serves as a template for the transcription of genomic and subgenomic RNA (Fig. 11 (5.)). The unwinding of the RNA strand might be executed by the viral helicase domain of the ORF1 (Fig. 9) [115].
An additional task of the viral helicase might be the initiation of RNA capping by its 5' triphosphatase activity. Subsequently, the 7–methylguanosine is transferred to the 5'–end of the RNA by the MeT to confer stability to the mRNA (Fig. 9) [110, 161]. For these processes it is unclear whether the ORF1 acts as a polyprotein or if it is cleaved into several domains.
The subcellular compartment of the viral replication has not been identified yet. However, an association between ORF1 and perinuclear membranes has been confirmed as well as a localization between the ER and the Golgi compartment [216]. Exact subcellular locations have to be further investigated.
Next, subgenomic RNA containing ORF2 and ORF3 is synthesized following the attachment of the RdRp to the subgenomic promoter (Fig. 11 (6.)). The ORF2 and ORF3 are translated by leaky ribosome scanning, where the ribosomes bypassing the ORF3 AUG start codon continues to scan downstream to initiate protein synthesis at the ORF2 AUG start codon located in close proximity [90].
From here, 2 different ways of exiting the host cell are possible for HEV (Fig. 11 (7.)). As it can be found in Fig. 11 under 8., ORF2 does not get assembled into viral particles and exits the cell via the ER and the Golgi apparatus. In this case, two forms of the ORF2 have been observed: ORF2g and ORF2c [186].

The other possibility is the assembly of the newly synthesized capsid and the genomic RNA into viral particles (Fig. 11 (9.)). The form of the ORF2 protein that is associated with viral particles is the ORF2i. Here, the genomic RNA binds to the C–terminus of the capsid which results in capsid dimers. The packaging of the viral genome likely occurs due to a putative RNA packaging signal near the 5' terminus of the HEV genome [94]. While data are lacking for mammalian cells, in insect cells, a spontaneous self–assembly is suggested [80]. This could mean, that the capsid protein and the newly synthesized RNA need to be in close proximity to each other, which is also supported by protein–protein interaction studies [167].
Lastly, viral egress possibly involves ORF3. The unglycosylated form of ORF2 interacts with the phosphorylated ORF3 [201]. Furthermore, the PSAP motif of ORF3 is able to interact with Tsg101, that is also involved in ESCRT [217]. Indeed, it was observed that HEV release is inhibited when the ESCRT pathway was knocked out through mutational studies and the deletion of ORF3 expression inhibited HEV secretion in an infectious system [205, 206].
The ORF3 interacts with several other cellular components too (cytoskeleton, alpha–microglobulin/bikunin precursor) via their SH3–domains [200, 202].
The enveloped HEV was detected in multivesicular bodies (MVBs) in association with TGN protein 2 and CD63, implying that the capsid buds into intracellular vesicles to form MVBs. These structures are part of an exosome like release pathway (Fig. 11 (10.)) [218].
Furthermore, ORF3 acts as a viroporin that facilitates ion permeability at the plasma membrane [195]. Also, cell polarity plays an important role in directing the ORF3 localization. HEV is mostly released at the apical membrane [219] [86]. The apical site faces the bile duct, where the released virus is not enveloped. In this case, ORF3 was not detected on the surface of HEV. However, it was detectable on particles that are released at the basolateral side of the cell into the blood–stream. It is speculated that the necessity for an envelope in the blood–stream is due to the protection it confers against the host's immune response since the envelope masks epitopes from neutralizing antibodies targeting the capsid protein. On the other hand, in the bile duct, where the bile salts disorganize the lipid layer, this protection is not necessary any more.

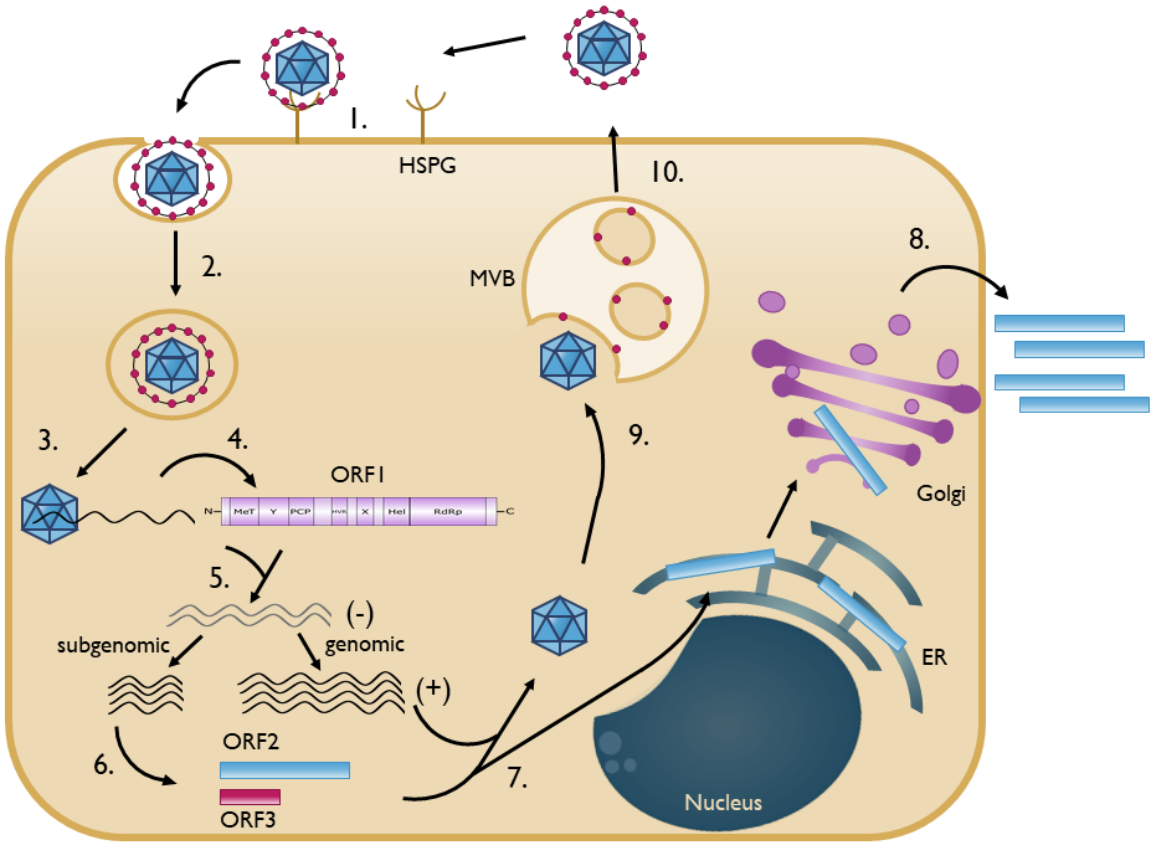

Figure 11: Life cycle of HEV. 1. Entry, 2. Uptake, 3. Release into cytoplasm, 4. Translation of the nonstructural protein, 5. Genome replication, 6. Translation of the structural proteins, 7./8. Release of ORF2g/c, 9. Assembly of infectious particles, 10. Release of enveloped virus. Inspired by [185]

1.6.2. Processing of the Non–structural Protein

In the life cycle of positive–sense RNA viruses the nonstructural protein generally gets cleaved by either viral or by cellular proteases to start replication of the viral genome. Proteases are enzymes that cleave polypeptide bonds. They can be classified within 5 major groups: serine, cysteine, aspartic, threonine and metallo–proteases [220]. Papain–like cysteine proteases are the largest subfamily among cysteine proteases and occur in animals, plants, bacteria and viruses. Most members of this group possess a catalytical triad (C–H–D), but some members are functional with a catalytical dyad (C–H) [127]. The catalytical dyad has been observed in other viruses such as Rubella virus and Coronavirus 229E [127].
In those examples, the viral non structural protein gets cleaved by the viral PCP, how-

ever, the same has not been shown for HEV yet. In fact, there has been a large amount of controversy about the functionality of the PCP domain of HEV. On the one hand, studies report no cleavage for the polyprotein and on the other hand, studies found putative cleavage products, but cannot prove it with certainty.
An overview of the cleavage products reported can be found in Tab. 1.
In several studies, ORF1 cleavage was not observed or was deemed not convincing due to inconsistent results.
In the study published by Ansari *et al.* (2000), no cleavage was observed neither following *in vitro* translation of ORF1, nor after its transfection in HepG2 cells or when expressed in *E. coli* [131]. In the same year, Ropp *et al.* showed the appearance of inferior products when ORF1 was expressed by vaccinia virus (Tab. 1). However, mutation of the catalytical dyad did not abrogate the cleavage, therefore the HEV PCP was likely not responsible for it [132].
In 2013, Pertillä *et al.* observed cleavage of tagged ORF1 after *in vitro* translation, nevertheless cleavage was also observed in absence of the HEV PCP or any other proteases [216].
Altogether, these findings do not suggest polyprotein cleavage by the HEV PCP. Yet, the presented expression systems and assays do not represent physiologically relevant conditions. Also, the involvement of cellular proteases or other cellular factors that can activate the viral protease cannot be ruled out.
Among the studies observing possible cleavage, is the report by Sehgal *et al.* (2006) that expressed a N– and C–terminally tagged ORF1 by baculovirus. Upon cell lysis and western blot against the tags, several smaller products were observed in a time–dependent manner. Mass spectrometry even revealed peptide sequences of the MeT domain in the 35 kDa fragment. The inhibition of cysteine proteases by E–64d abolished most cleavage, however, it could not be ruled out that processing might involve other non–cysteine proteases [133].
In 2013, Parvez confirmed the occurrence of potential cleavage products (Tab. 1) upon transfection of a tagged ORF1 protein in HuhS10–3 cells. The size of the smaller tagged proteins is in concordance with previous reports [127].
Another study attempts to prove the protease activity of the HEV protease by performing a digestion assay of *in vitro* transcribed and translated truncated ORF1 (Met–PCP and Hel–RdRp). Indeed, cleavage occurs and reveals smaller products that are in line with protein sizes discussed before [128].
Kanade *et al.* showed in 2018 that cysteine proteases might not be the sole pro-

teases involved in the replication of HEV. They identified cleavage site of thrombin and factor Xa (serine proteases) that are conserved among HEV genotypes. Indeed, mutation of these cleavage sites abrogated HEV replicon replication in Huh 7 S10–3 cells. Furthermore, thrombin was able to cleave truncated ORF1 protein *in vitro*. It was additionally demonstrated that thrombin and factor Xa were crucial for HEV replication in transfected cells. Thus, these results open up a new perspective of the proteases involved suggesting even a serine protease activity [221].
In one approach the HEV genotype 3 genome was tagged with an HA–epitope and electroporated in Hep293TT cells, however no potential cleavage products were detected [222]. Another study that was conducted in a cell culture system by Ju *et al.* in 2020 did not observe any minor bands in addition to the full length ORF1 protein either. In this approach, an antibody to the ORF1 X–domain was engineered and HepG2C3A cells transfected with ORF1 cDNA were analyzed [101].
Lastly, the most recent study by Proudfoot *et al.* suggests the existence of a zinc metalloprotease in the ORF1 that is located in a slightly different position than previously predicted (510–691aa) (Fig. 8). Initially, the boundaries of the HEV PCP were based on alignments with homologs in other viruses, but the sequence similarity was low (below 20%) and the PCP could not be extensively characterized. In this study, the newly identified region yielded a stable soluble protein, suitable for crystallization that also coordinated a zinc ion. The domain is structurally homologous to fatty acid binding domains, but no specific ligands have been identified yet [130]. Further studies are required to confirm its relevance in a cell culture system.
Yet, the reports in favor of processing do not include biologically relevant systems and are not completely consistent concerning the HEV PCP activity. In conclusion, the controversy of the ORF1 processing is largely due to the absence of a relevant cell culture system and the lack of knowledge of the PCP domain of the ORF1.

Table 1: Processing of ORF1 as described in the literature

Expression System	Cell Line	Construct	Cleavage Products	Reference
Baculovirus	*T.ni* insect cells	Tagged ORF1	N–terminal: 122, 106, 93, 59, 26 C–teminal: 98, 47, 35, 22	[133]
HEV Sar55 replicon	Huh S10–3	Tagged ORF1	N–terminal: 35 C–terminal: 78	[127]
In vitro translation	*E.coli* C43	MeT–PCP Hel–RdRP	35kDa 55, 35 kDa	[128]
In vitro purification	Bacteria	X–Hel Hel–RdRp	25kDa 25kDa	[221]
In vitro translation Transfection Prokarytic Expression	 HepG2 *E.coli* JM109	Tagged ORF1	None	[131]
Vaccinia Virus	HeLa, Vero, HepG2, Chang liver cell lines	Tagged ORF1	107, 78 kDa	[132]
Plasmid vector	293T	Tagged ORF1	None	[134]
In vitro translation		Tagged ORF1	130, 57 kDa	[216]
HEV replicon	Hep293TT cells	Tagged ORF1	None	[222]
HEV RNA transfection	HepG2C3A cells	ORF1	None	[101]

1.6.3. Membrane Rearrangement Induced by HEV

Cellular membranes are required for replication, assembly and/or release of viruses and all positive–sense RNA viruses synthesize RNA in association with internal cellular membranes [223, 224]. They likely increase efficacy of virus production by providing a physical platform, that provides a protected environment for viral replication and assembly [225]. The reorganization of cellular cytoskeleton and membrane compartments thus leads to changes in cellular morphology that were already described in the 1950s [226, 227].

Positive sense RNA viruses generally replicate in the cytoplasm, therefore membranes can provide a replication complex encompassing cellular and viral components. Additionally, these membranes can contribute to evade host defense mecha-

nisms that detect double stranded RNA (dsRNA)[228].
Different virus families use different membrane organization strategies (Fig. 12). Positive–stranded RNA viruses use a wide variety of membranes ranging from the outer ER membranes, compartments of the secretory pathway, endosomes, mitochondria or other organelles (Fig. 12) [229–235] . HCV for examples creates a membranous web consisting of single double membrane vesicles (DMVs) mainly derived from the ER [236]. Similarly, Coronaviridae and Arteriviridae build ER–derived DMVs as well, where they produce a dsRNA intermediate during replication [237, 238]. Togaviridae on the other hand create spherules of 50–400nm on endosomes for RNA replication [239]. These isolated compartments help to hide from innate immune responses to dsRNA.
Rubella Virus and Alphaviruses have a relatively similar ORF structure compared to HEV even though their sequence similarity is low. Alphaviruses produce membrane invagination and spherules in infected cells. The vesicular structures or ”cytopathic vacuoles” (CPVs) have a diameter of 600–2000nm. These vacuoles contain the non structural proteins and lysosomal enzymes [225]. The sites of viral replication are derived from endosomes and lysosomes and are in many cases connected to the rough ER. While the NSPs are synthesized in the cytoplasm, they bind to endosomes and lysosomes to form the replication complex.
Also, the Rubella Virus (RUBV) induces vacuoles containing spherules that are connected to the ER [240, 241]. These replication complexes are membrane–bound cytoplasmic vacuoles that are lined internally with vesicles measuring $60\,\mathrm{nm}$ in diameter. However, RUBV virions have not been detected in the vacuoles where the vesicles were found [240].
In HEV, membrane rearrangement has not been studied yet due to the absence of a relevant cell culture system. Additionally, the role of ORF1 in this process would be difficult to determine since there is no commercial antibody available against this protein.

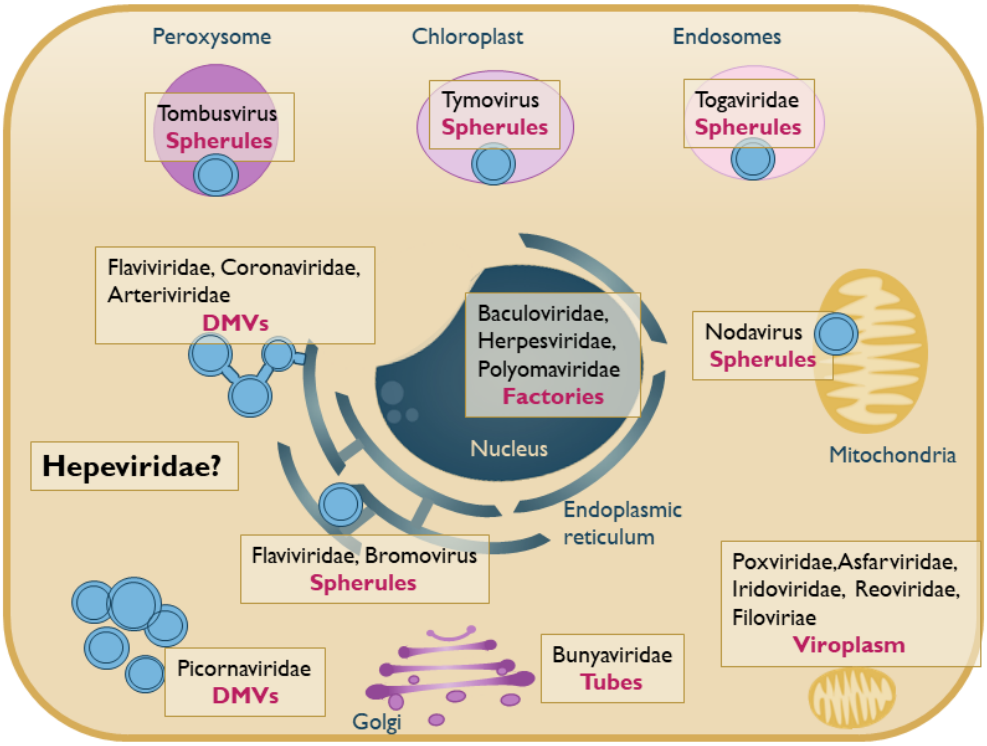

Figure 12: Membrane rearrangement and viral factories induced by other viruses and virus families. The red text indicates the structure that is induced next to the organelle that is affected. Adapted from Expasy: [242]

1.6.4. Subcellular Localization of ORF1

As mentioned in the previous chapter, the association of HEV with host membranes remains unknown to this day and attempts to locate the ORF1 have been difficult for a long time due to a lack of an efficient cell culture system. However, several recent reports have described the localization of ORF1 in different cell culture systems.
In 2017, Lenggenhager *et al.* published 2 antibodies recognizing the RdRp– and the MeT–region of ORF1 [243]. They reported a cytoplasmic staining when ORF1 (Genotype 3, Kernow C1 strain) was expressed in Huh7 cells *via* an expression vector. However, ORF1 could not be detected in HEV infected patient tissue using the same antibodies. In contrast, ORF2 was detectable both in Huh7 cells and in patient tissues. Compared to ORF2, ORF1 is likely less abundant in patient tissues and is

therefore more difficult to detect. Moreover, there might be a spatial and temporal restriction of the non–structural protein.
Using the BacMam expression system Kumar *et al.* reported the detection of ORF1 domains (pSHEV–3) in Huh7 cells using specific antibodies against the MeT–, PCP– and RdRp–domain (Fig. 13) [244]. The Met– and PCP– staining showed a nuclear and perinuclear localization of ORF1, while the RdRp–staining reveals a predominantly perinuclear localization.

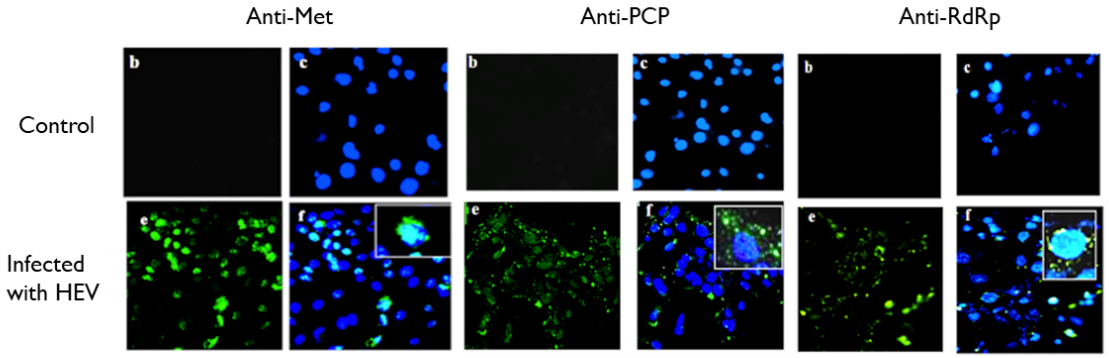

Figure 13: Staining of MeT, PCP and RdRp domain of the ORF1 protein expressed in Huh7 cells, [244]

.

Another study by Szkolnicka *et al.* in 2019 reported the visualization of a HA–tagged HEV replicon (HEV83–2–27) in HepG2/C3A cells [222]. The staining appeared in the cytoplasm as well and showed a dot–like structure. On the other hand, the ORF1 could not be identified using the anti–RdRp or anti–Hel antibody that were published by Lenggenhager *et al.*. Furthermore, a partial colocalization between ORF1 and ORF2/ORF3 was found in the cytoplasm. This might imply that the replication and assembly sites are located in close proximity. Co–staining of ORF1 with CD–63 and CD–151 showed a moderate degree of colocalization (Pearson coefficient of 0.61 and 0.6 respectively) and a partial overlap was found with markers of the ERGIC and Golgi as well (Pearson coefficient of 0.51 in both cases)(Fig. 14). This suggests that HEV uses modified early secretory pathway membranes for replication.

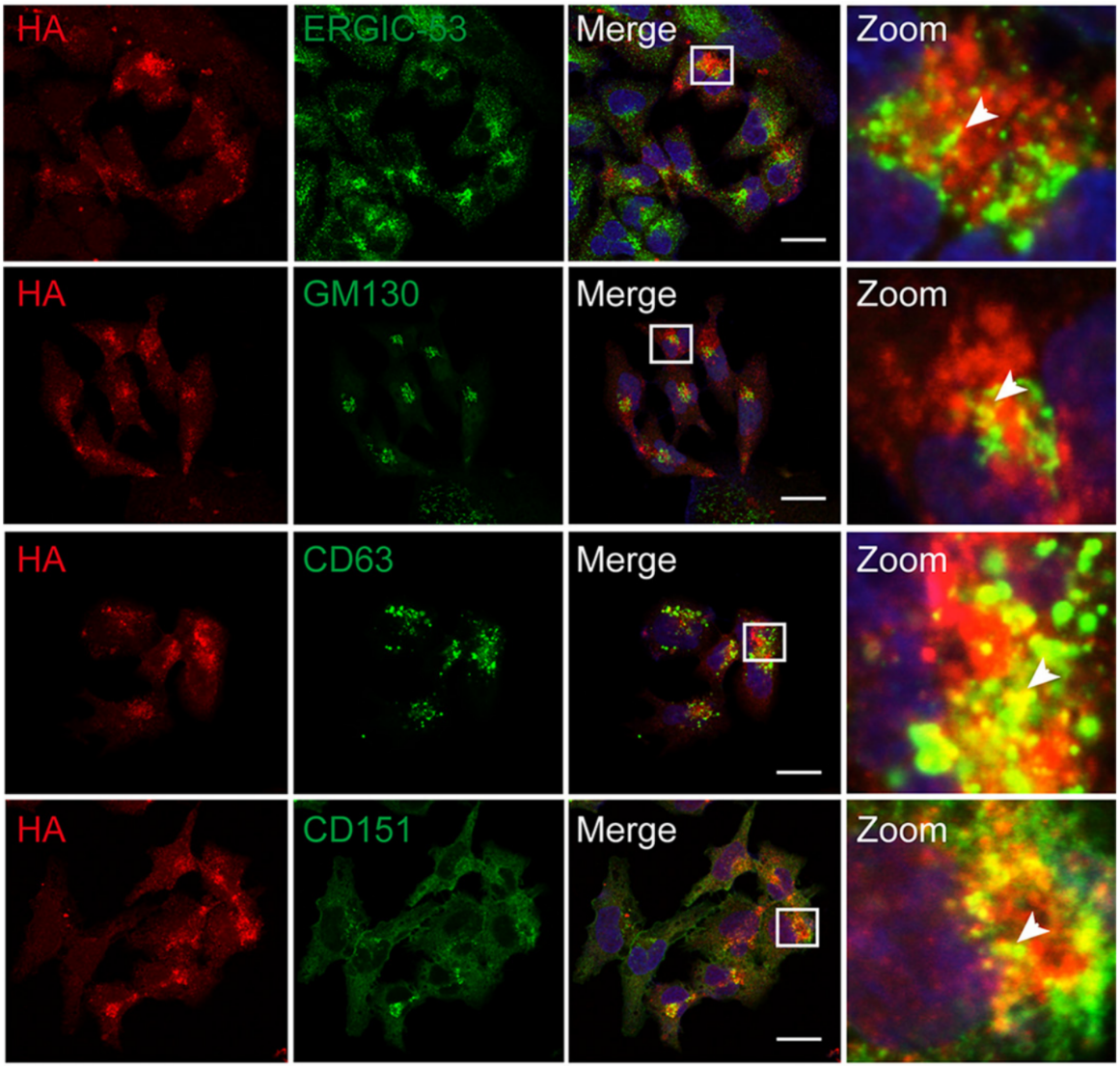

Figure 14: Co–staining of HA–tagged ORF1 protein and different exosomal markers in Hep293TT cells at 5 days post transfection. ERGIC–53 is a marker for the ERGIC compartment, GM130 for the golgi apparatus, CD63 and CD151 are tetraspanins in exosomes. The white bar marks 20 µm. [222]

To study the subcellular localization of viral replication, it is possible to not only study the localization of viral proteins, but also viral RNA. During the replication of a positive–stranded RNA virus, the postive strand serves as a template for the negative –strand. The negative strand in turn serves as an intermediate from which new +strand RNA is synthesized. Therefore it is interesting to stain both positive and negative–stranded RNA. There are several techniques available to visualize RNA in cells and the RNAscope®technique (ACD Bio) was employed by for example Liu *et al.* in 2019 to target HCV RNA in Huh7.5.1 cells (Fig. 15). The positive and negative–

stranded RNA appears in a dot like structure throughout the cell and in proximity to the non–structural protein NS5A and the core viral protein.

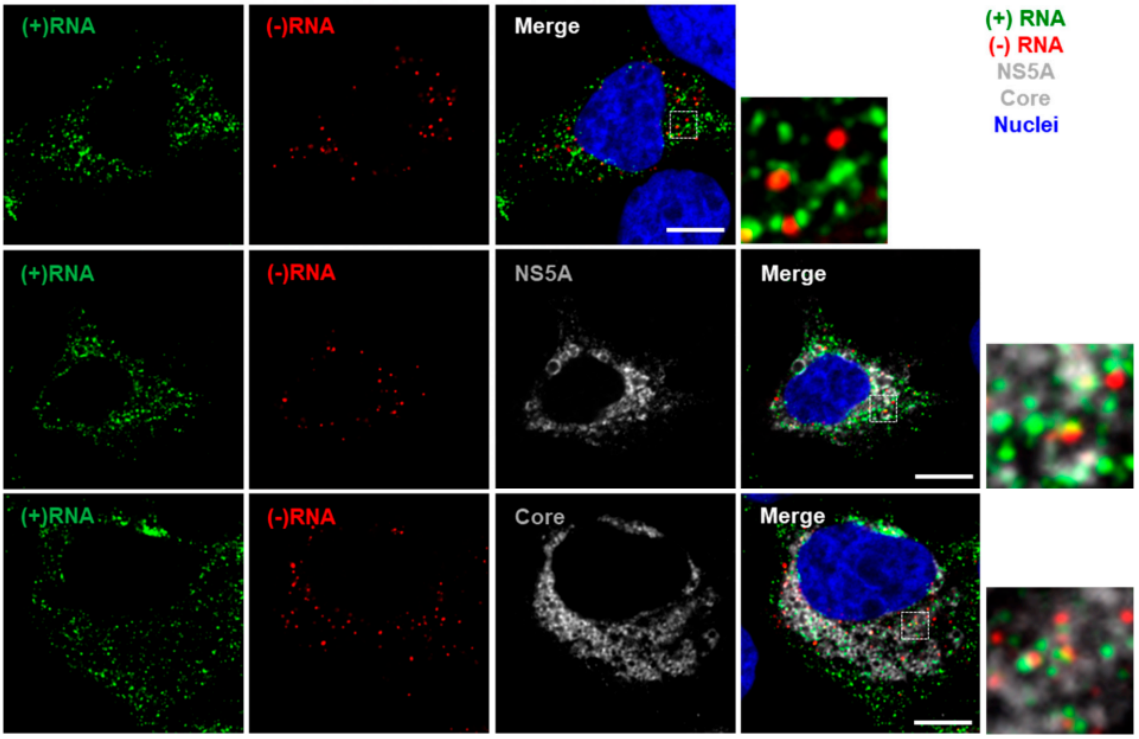

Figure 15: RNAscope staining of HCV RNA in Huh7.5.1 cells. The white bar marks 10 µm, [245].

1.7. Pathogenesis

To this date, the pathogenesis of HEV remains poorly understood. It is still unclear how the viral particles reach the liver as it is transmitted *via* the fecal–oral or the zoonotic route. It has been shown that HEV can replicate in intestinal cell lines and moreover, the ORF2 has been detected by *in situ* hybridization in the intestinal crypt of chronic patients. Therefore, it can be hypothesized that the virus first replicates in the intestinal tract and reaches the liver over the bloodstream in its quasi–enveloped form [86, 87].
Next, HEV replicates in the hepatocytes where it can be released as a quasi–enveloped particle into blood or bile [61]. However, most particles are released at the apical membrane, which leads to the bile tract [86]. There, the bile salts likely strip away the quasi–envelope leaving the virus to be shed into stool or urine naked [44].
HEV itself has no cytopathic effect, implying that HEV–induced pathogenesis is a consequence of the host immune response. Indeed, natural killer cells and cytotoxic T–cells are major players in the immune response against HEV.

1.7.1. Innate Immune Response

The innate immune system is a major host defense mechanism triggered by viral infections, although its response to HEV during an acute or chronic infection remains poorly understood to this date.
One prominent characteristic is the rapid and effective detection of invading pathogens by recognition of their pathogen associated molecular patterns (PAMPS) by the host's pattern recognition receptors (PRRs) [246]. Foreign RNA sensors comprise RIG–I–like receptors (RLRs) and Toll–like–receptors (TLRs) that sense viral RNA in the cytoplasm or the endosomal compartment respectively. Among members of the RLR family are RIG–I and melanoma differentiation associated gene (MDA5) (Fig. 16) [247]. Viral recognition by for example RIG–I activates a signaling cascade including the TBK and IRF3, which leads ultimately to the production of proinflammatory cytokines and IFNs [247, 248].
Next, IFNs transcriptionally stimulate a variety of ISGs through the janus–kinase signal transducer and activator of transcription protein (JAK–STAT) pathway, thus creating an antiviral state.
ISG15 for example is an ISG that targets a broad range of newly translated proteins.

The mechanism of their inhibition is unclear, but it likely disrupts its function by conjugation of the ISG15 to the newly synthesized protein [249].
Another ISG is the 2',5'–oligoadenylate synthetase (OAS), that targets mRNAs and ribosomal RNAs. It polymerizes ATP into 2'5' oligo (A) chains, which then activate the RNase L that degrades both cellular and viral mRNAs and ribosomal RNAs, which as a result inhibits viral replication [250, 251].
The Protein Kinase R (PKR) as well recognizes RNA molecules, but contrary to the 2',5'OAS, it targets dsRNA that occur especially during viral replication. The kinase binds the dsRNA through its 2 RNA–binding motifs resulting in PKR activation and autophosphorylation, thereby inhibiting translation [252].
IFNs, and especially IFN–α, have been used for decades to treat viral infections, such as chronic HBV and HCV infections. IFN–α has also been used as an off–label drug for treatment of chronic HEV [19].
Many viruses including HEV have adapted to subvert IFN–α induction and also IFN activated JAK–STAT signaling.
Firstly, the subversion of IFN–α can happen at several instances and is induced by different HEV proteins. The PCP domain of the ORF1 protein of HEV can inhibit the activation of RIG–I and the TBK–I *via* its deubiquitinase activity thus blocking the activity of IRF3, a molecule that is activated downstream of this signal cascade (Fig. 16) [156]. Recently, it was discovered that the MeT and the X domain of the ORF1 downregulate IRF3 activity by inhibiting its phosphorylation [253]. Thus the inhibition of IFN activation in turn might block or reduce the inductions of ISG expression.
On the other hand, ORF3 increases protein levels of RIG–I and its activation [254]. The exact role of this is unclear, but it suggests that HEV tightly controls the balance between activation and inhibition of IFNs at different stages of its life cycle.
Secondly, HEV has adapted to subvert IFN activated JAK–STAT signaling by inhibiting ISG signaling. Bagdassarian *et al.* found that a truncated version of ORF1 containing the MeT–, Y– and PCP–domain inhibited the activation of ISGs through an unknown mechanism. It was speculated that the protein might inhibit STAT1 phosphorylation or the recruitment of STAT to the IFN receptor [255].
Furthermore, the HEV polymerase is binding to the ISG IFIT1 to protect the viral RNA from IFIT1–mediated translation inhibition [168].
Also, the interferon–induced phosphorylation of STAT1 is inhibited by ORF3. Consequently the synthesis of 2 antiviral proteins, dsRNA activated PKR and 2',5'–OAS, is abrogated [14].

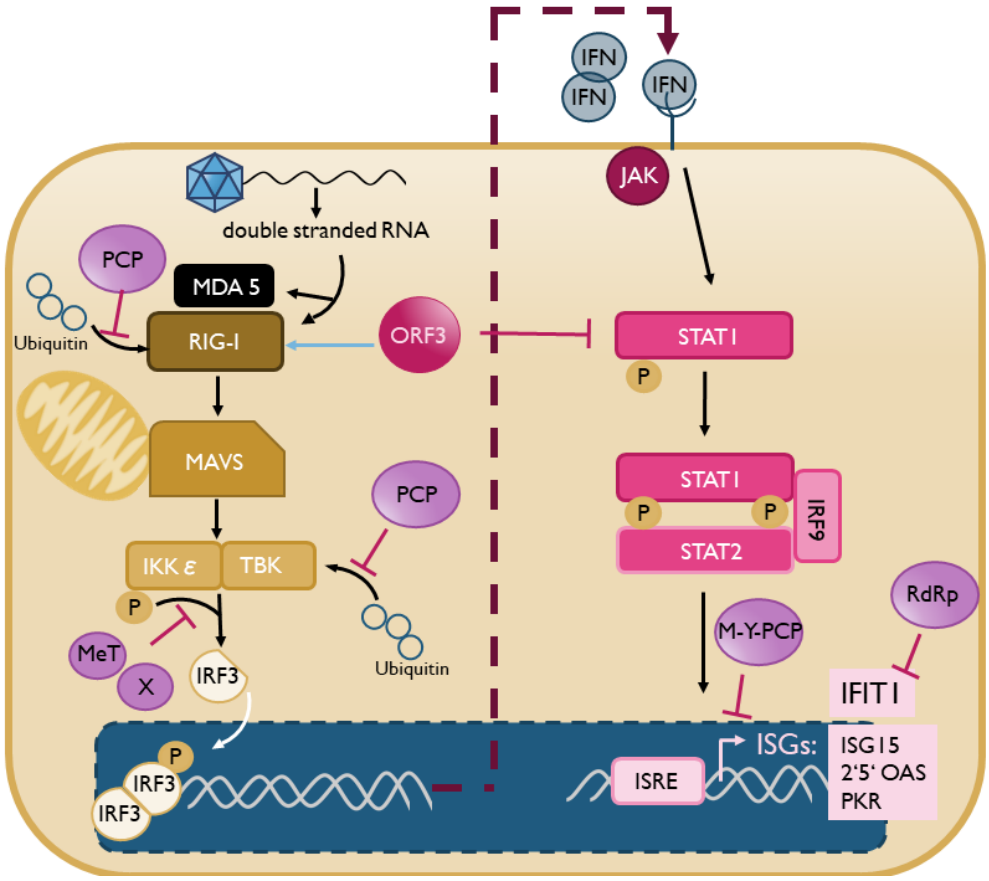

Figure 16: Innate immunity signaling cascade, inspired by [14]. RIG–I:retionic acid inducible gene–I , MAVS: Mitochondrial Antiviral Signaling Protein , IKKϵ: I–kappa–B kinase epsilon , TBK: tank–binding kinase, IRF3: Interferon Regulatory Factor 3, IFN: interferon, JAK: Janus Kinase , STAT: Signal Transducer and Activator of Transcription, IRF9: Interferon Regulatory Factor 9 , ISRE: Interferon–Stimulated Response Element, ISG: Interferon Stimulated Gene, IFIT1: Interferon Induced Protein with Tetratricopeptide Repeats 1, 2'5'OAS:2',5'–oligoadenylate synthetase, PKR: Protein Kinase R.

1.7.2. Adaptive Immune Response

HEV induces specific antibodies early after infection. Studies in non–human primates showed that HEV specific antibodies protected them from subsequent infections [256–258].

In humans, the HEV specific IgM level reaches its peak at 6–8 weeks after infection and is undetectable 5–6 months later (Fig.17). Contrarily, the IgG levels gradually increase during the acute and convalescent phase and last several years to protect the host (Fig.17) [21]. A protective role of naturally acquired antibodies has been doc-

umented in outbreak and non–outbreak settings [259].
The ORF2 protein is the main target for neutralizing antibodies (Zhang 2012, Tang 2015) as it is exposed when the particle is naked [260, 261]. In its quasi–enveloped form, HEV is more resistant to antibodies implying an evasion from a humoral response by sheltering the capsid protein [262].
Similarly, HEV elicits a specific CD8+ and CD4+ T cell response during acute infections. *In vitro* the functionality of T cells was characterized by proliferation and the release of cytokines. The durability of HEV specific T cells after acute infection is not exactly known. It was suggested that the T cell response decreases in the early months after infection, however a longitudinal study showed a rapid decline in HEV specific T cells after the first week of infection [263, 264]. Nevertheless, long lived memory T cells are produced successfully after the infection [263, 265–267].
The infiltration of T cells may lead to liver damage due to cytotoxic activity. CD8+ T cells have been found in liver biopsies of patients suffering from HEV induced acute liver failure and fulminant hepatic failure [268, 269]. Also, it was found that genes associated with cytotoxic activity were overexpressed in these patients [269]. On the contrary, less IFNγ and TNFα and fewer CD4+ cells were present compared to patients where HEV could be resolved. While it is unclear whether this is the cause or the consequence of the disease progression, it can be concluded that the T cell response is associated with the immune pathogenesis in the liver [270].
Furthermore, T cells target specific epitopes of ORF2, which are mostly conserved among several strains [263]. Even T cells recognizing epitopes of ORF1 have been observed [271].
In a chronic infection, a continuously high antigen stimulation will lead to T cell exhaustion resulting in impaired proliferation, cytokine production or cytotoxic activity. This effect has already been demonstrated in HBV, HCV and HIV [272].
Additionally, high antigen levels may lead to a dysfunctional T cells response. Contributing factors to T cell exhaustion and dysfunction are a negative regulation of regulatory T cells and interleukin 10 (IL10) as well as the upregulation of inhibitory receptors such as programmed cell death protein 1 (PD–1) and cytotoxic T–lymphocyte–associated antigen 4 (CTLA–4). While on the one hand, both limit the immunopathology by regulating the proliferation of T cells, on the other hand, it facilitates HEV replication. However it is unsure whether the dysregulation stems from the chronicity of HEV or the immunosuppressive therapy administered prior or during the infection [267, 271].

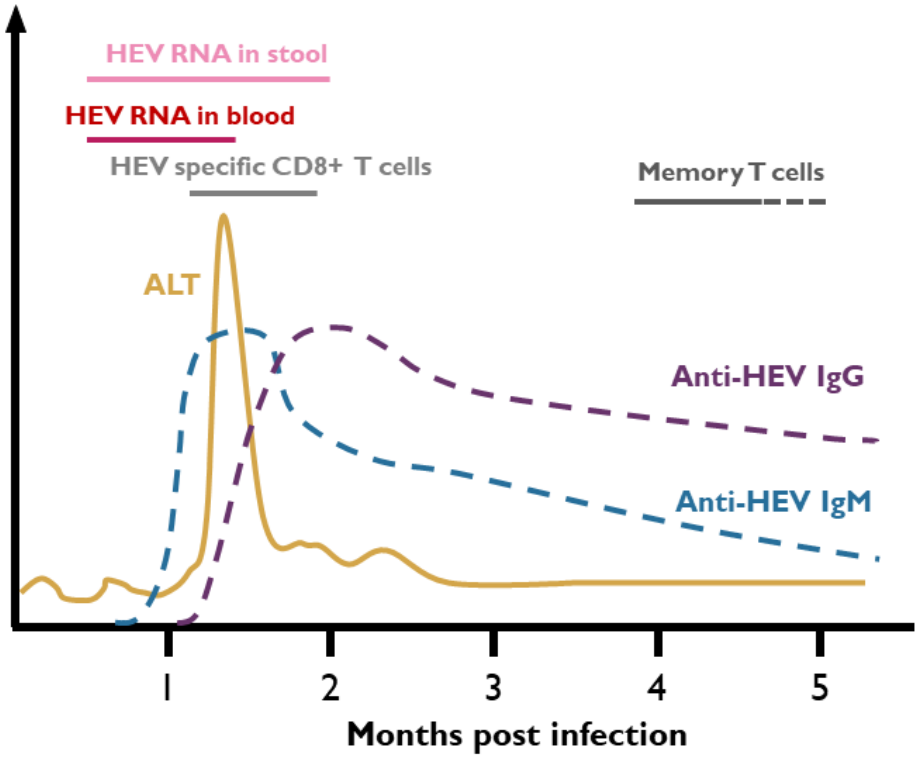

Figure 17: HEV specific antibody levels in patient sera, CD8+ T cells and Alanine aminotransferase (ALT) over the course of an infection, [14]

1.8. Diagnosis

In most cases, HEV is self–limiting, thus a diagnosis is usually not performed. However, in case of an infection of immunocompromised patients or pregnant women, it is important to detect HEV RNA or antibodies according to clinical standards.
HEV infection can be diagnosed either indirectly by detection of anti–HEV antibodies or directly by detecting HEV RNA or capsid antigen in blood or other bodily fluids [44]. Indirect diagnosis relies on the detection of anti–HEV immunoglobulinss (Igs) IgG and IgM. The production of IgM antibodies is induced by all 4 genotypes of HEV in a similar manner during the acute phase of illness and last until 4–5 months after infection, thereby indicating an acute or recent infection (Fig. 17). IgG antibodies can be detected just after IgM levels rise and they increase further until the convalescent phase.

Some studies suggest that IgG antibodies remain for years after infection, however the exact duration has not been determined yet [273, 274].
In clinical settings, ELISA and immune–chromatographic assays are used routinely to detect HEV antibodies. Several anti–HEV antibody ELISA assays are available for detection of IgM and IgG [275].
The Wantai test from China has been reported to have a good sensitivity and specificity and is favored by many laboratories worldwide [276]. This test detects the HEV antigen, but it can show false positive results since it detects the ORF2g and ORF2c that remain detectable in patient sera even after the hepatitis has resolved.
The difference of seroprevalence in different countries can partly be attributed to the usage of different detection assays [275].
In some studies, IgM immunochromatographic assays showed higher sensitivity than certain ELISA assays [277, 278]. However it is noteworthy that there is not a single Food and Drug Administration (FDA) approved serological assay that can be used for clinical HEV diagnosis. The available assays can only aid HEV diagnosis and can be used in epidemiological studies [279].
Importantly also, the detection of HEV antibodies in immunocompromised people could fail in establishing an accurate diagnosis due to delayed seroconversion and low antibody titers. Thus, confirmation of HEV infection increasingly relies on molecular or direct methods [279].
The detection and quantification of HEV RNA in blood, feces or other bodily fluids is considered the gold standard to diagnose an active HEV infection [44]. In 2011, the WHO has released a standard of HEV RNA that permits comparison of qualitative and quantitative PCRs assays worldwide [280].
Direct diagnostic methods detect viral RNA by amplification of the overlapping region of ORF2/ORF3 that is conserved among genotypes [281].The viral RNA is detectable in feces and blood as of one week before clinical symptoms (Fig. 17).
Furthermore, the HEV genotypes or subgenotypes can be characterized by sequencing different regions of the genome such as ORF2 or the RdRp of ORF1. This information helps to determine the molecular epidemiology of the virus or the potential occurrence of mutations in the RdRp that are associated with ribavirin treatment failure [146, 177].
Usually, HEV is diagnosed via the indirect method by measuring anti–HEV IgM levels. In case of positive results, the HEV RNA gets analysed to characterize its molecular features and the strain is sent to the national reference center. If no anti–HEV IgM are

detected, no recent infection is indicated for immunocompetent patients. However, immunocompromised patients might be infected without displaying specific antibodies, therefore HEV RNA levels are measured to determine their status (Fig. 18) [282].

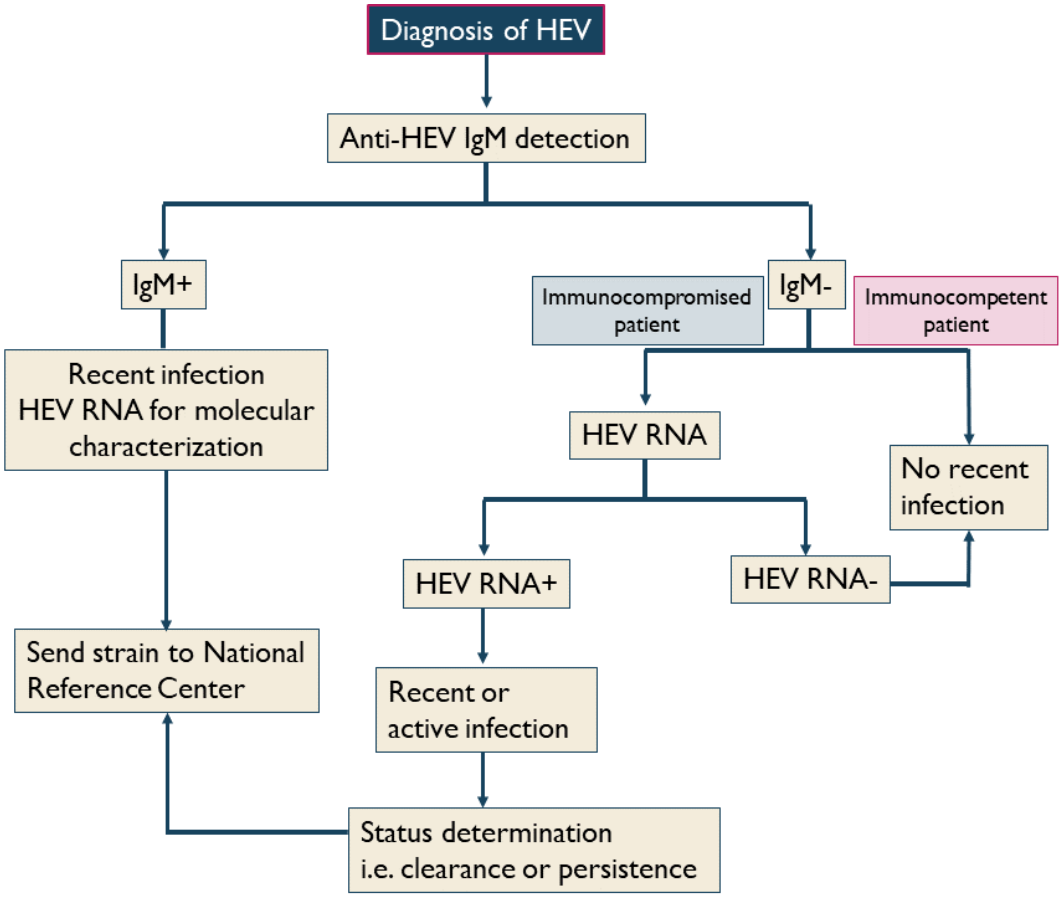

Figure 18: Flow diagram of HEV diagnosis, adapted from [282]

1.9. Treatment

Usually, HEV infection is self–limited in the immunocompetent population and viral clearance occurs spontaneously, therefore a specific treatment is not required. However, in industrialized countries with a growing population of immunocompromised patients (for example solid organ transplant (SOT) patients), HEV poses a real public health problem. Nevertheless, a recommended treatment is not yet available.

To date, chronically infected patients are treated as follows: first, their immunosuppression will be reduced, next, PEGylated IFNα is administered and at last ribavirin

therapy is started (Fig. 19)[45, 146].
The reduction of immunosuppressants in SOT patients needs to be carefully evaluated as the risk of allograft rejection may increase. In 1/3 of HEV infected patients, dosage reduction leads to viral clearance, therefore the remaining part is treated with PEGylated IFNα for 3–12 months which results in viral clearance in 80% of cases [283, 284]. Although, this treatment cannot be administered to SOT patients, since it increases the risk of allograft rejection due to the stimulation of the immune system [14]. As opposed to that, liver transplant recipients and a hemodialysis patient have successfully cleared HEV infection upon PEGylated IFN treatment [283, 285]. Most commonly, ribavirin (RBV) is used as off–label drug either as monotherapy or in combination with PEGylated IFNα if that is possible [286–288]. While RBV is safe to use in immunocompromised patients, it cannot be given to pregnant women due to a possible feto–toxicity and hemolytic anemia [275]. In 90% of cases, RBV therapy leads to viral clearance, but RBV treatment failure has been reported in patients.
RBV is an inhibitor of a cellular enzyme inosine monophosphate dehydrogenase (IMPDH). It depletes the intracellular GTP pool which impedes RNA replication by inhibiting the IMPDH, since it shares important structural features with guanosine [289]. This in turn induces mutagenesis of the HEV genome which can lead to an error catastrophe, which means that the majority of genomes of a virus population are nonfunctional [290, 291]. Additional mechanisms of action are the immunomodulation of T helper cells and the potentation of induction of ISGs [292].
The exact mechanism *in vivo* is unclear, but it was found that more heterogenous intra–host HEV populations were more likely to induce chronicity [293, 294]. Certain HEV intra–host populations showed modifications (single nucleotide variants (SNVs) and mutations or insertions in the HVR) that could be associated with RBV monotherapy failure. Especially the G1634R mutation in the RdRp has been observed in a number of patients and is associated with increased replication fitness in tissue culture and *in vivo* [295, 296].
So far, no other antiviral therapy has been shown to be effective against HEV. Sofosbuvir, a nucleoside analogue that is an effective antiviral against HCV, inhibits HEV *in vitro*, but has received mixed reports in patients [297–300]. The natural compound silvestrol, which proved effective against Ebola, blocks HEV replication *in vitro*, but results from clinical trials are still missing [301]. The nucleoside analogue NITD008 and the non–nucleoside inhibitor GPC–N114 also block HEV replication *in vitro* while the two compounds exhibit a synergistic effect. They have not been tested in clinical

trials yet [302].

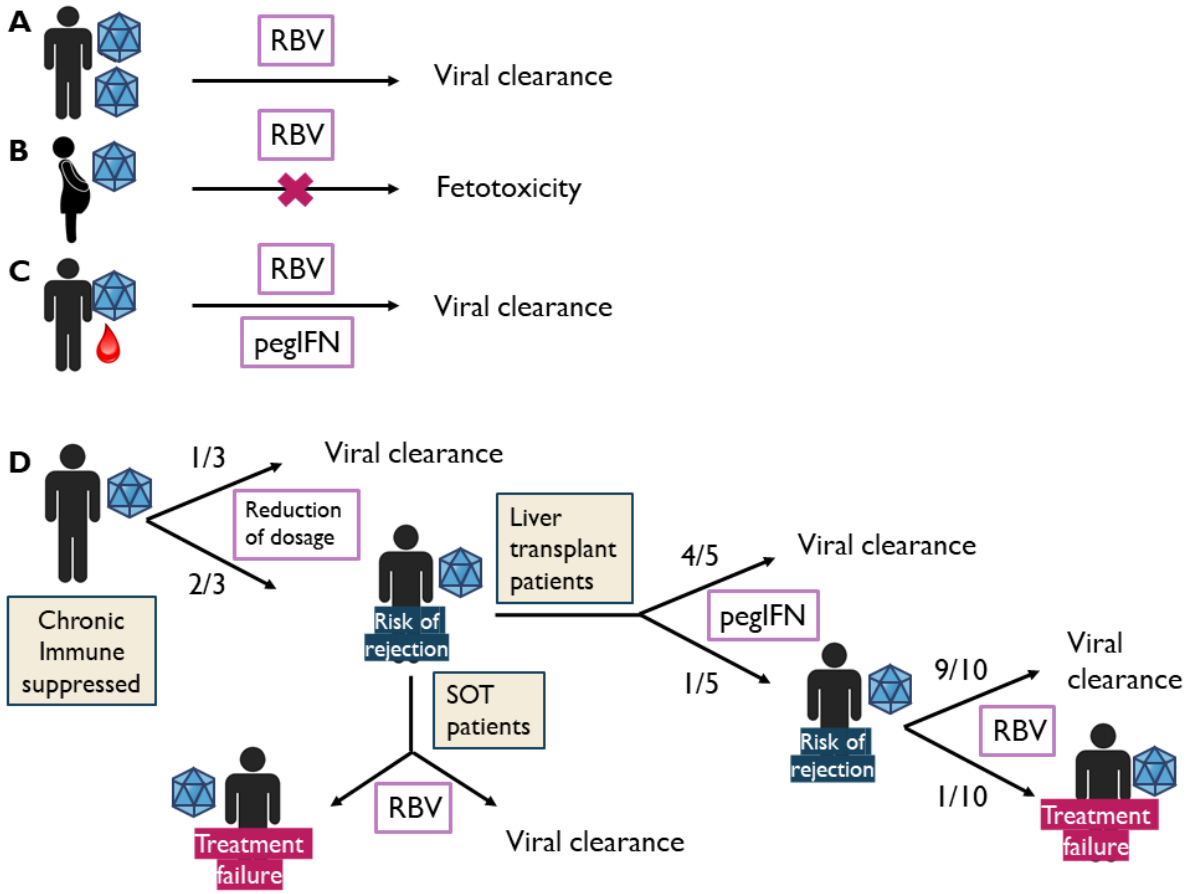

Figure 19: Treatment of HEV infection. A: people with a high viral load; B: Pregnant women; C: People suffering from a hematological disease; D: chronically immune suppressed people.

1.10. HEV Vaccine

Currently, there is no vaccine available worldwide that confers protection against more than two genotypes of HEV.

Most vaccines or vaccine candidates that have been tested are based on the HEV capsid protein (Tab. 2). GlaxoSmithKline conducted a study on a recombinant HEV vaccine that ended in phase II. A recombinant HEV VLP vaccine finished phase III clinical trials that were performed by Xiamen Innovax Biotech. However, the vaccine that was commercialized under the name Hecolin® is only available in China (Tab.

2) [303]. The vaccine is based on 239 amino acids of ORF2 (aa368–aa606) and it self–assembles in VLPs that are structurally similar to the capsid protein in an *E. coli* expression system [304–306]. It shows a good immunoreactivity in patient serum samples and exhibits an efficient protection of 96% and 86% after 5 years [307]. Three doses are given at 0, 1 and 6 months and 200,000 doses are provided per year [15]. The vaccine shows protection to hepatitis caused by HEV genotype 1. Limited data are available for genotype 4 and no data are available concerning genotypes 2 and 3 [308–310].

However, several drawbacks were encountered. Firstly, the cases of HEV infection dropped by only 7.58% and the state of clinical data is inadequate (Chinese Center for Disease Control and Prevention). Next, there is an insufficient public awareness since the infection mostly occurs in endemic regions. Lastly, there is no data available on under 16 and over 65 year old patients as well as pregnant women. Therefore, it is necessary to further improve the vaccination strategy. For example, currently, clinical trials are performed on the safety of Hecolin® in pregnant women in Bangladesh (NCT02759991). Another approach would be examination of HEV specific T cell responses in Hecolin® vaccinated individuals, since the vaccine is thought to elicit a predominantly humoral response [259]. One immune based therapeutic strategy includes the restoration of HEV specific T cells by blocking PD–1 and CTLA–4, which could lead to T cell immunity. However, the patient specific responses to the inhibition of this pathway create a challenge for the development of personalized immunotherapy [267]. Yet another strategy could be the development of a T cell based vaccine. The peptide based vaccine could target CD8 cytotoxic T cells or CD4 helper T cells [311, 312]. The identification of the target epitope remains essential for designing peptide based T cell vaccines [263, 266, 271]. While this approach could be useful for chronically infected HEV patients, the main drawback is the limited understanding of the T cell response against HEV.

One major problem for the implementation of a vaccine program based on the existing vaccine or vaccine candidates is the different transmission of genotypes 1 and 2 versus genotypes 3 and 4. WHO does not recommend the vaccines in populations without outbreaks posing low risk of mortality. Consequently, outbreaks of genotypes 3 and 4 would not be part of the immunization program. Therefore it could be useful to instead vaccinate animal reservoirs, especially swine, instead of humans [313]. However, considering that HEV infections in pigs are asymptomatic and self–limited, a vaccine protecting from HEV only might be uninteresting for farmers since the cost

benefit ratio is low. Thus, the vaccine could possess a double protection from HEV and for example foot and mouth disease virus (FMDV). Behloul *et al.* reported a computational approach of the combination of the two epitopes for neutralizing antibodies of both viruses. The chimeric protein was stable, antigenetic and immunogenetic, but has not been studied *in vivo* yet [313].

Table 2: Vaccine candidates of HEV, [314]

Expression System	ORF2 Amino Acids	Genotype &Strain	Remarks	Reference
E. coli	221–660	GT1, Burma	No protection in macaques	[180]
	394–607	China	Poorly immunogenic in mice	[315]
	368–606	China, GT1	Phase III clinical trials, Hecolin	[308]
	439–660	GT 4 NJ–703	Computational Simulation	[313]
Baculovirus	112–607	GT1, Sar–55	Phase II clinical trials	[316]
	112–577	GT1, Burma	[93]	
	112-660	GT1, Burma	Breakthrough infection in macaques	[317]
	112–534	GT1, Burma	Oral route	
Yeast *Pichia pastoris*	551-607	China		[318]
Transgenic tomato plants	394–607	China		[319]
DNA vaccines	1–660	Burma	Stability	
	1–660	GT1, India	Protection in macaques	[320]
	1–660	GT1, Burma	Protection using gene gun	[321]
	1–660	GT1, India	Additional protein	

1.11. Cell Culture Systems

For a long time, an efficient cell culture system was not available to study HEV. While the most recent developed tools still present limits, great progress has been made.
Culturing of HEV began in 1987 when Pillot *et al.*, inoculated liver cells with HEV isolated from fecal specimen. In 1990, a molecular clone was created by Reyes *et al.* through PCR [322]. A first break–through was achieved when in 2007 Okamoto *et al.* isolated the virus from a Japanese patient with high viral load and infected 21 cell lines. They observed an efficient replication in hepatoma cell lines and a lung cancer cell line [323].
While previous studies used mainly HEV genotype 1, in 2007 Tanaka *et al.* developed a cell culture system in the hepatocarcinoma cell line PLC/PRF/5 for HEV genotype 3 [324].
In 2011 Shukla *et al.* successfully adapted the genotype 3 Kernow–C1 strain, which was isolated from a patient co–infected with HIV and HEV presenting a high viral load, to cell culture after 6 passages. The strain was therefore called Kernow–C1/p6 and it contains an insertion from a ribosomal protein S17 in the HVR. This insertion was found in a minority of viral populations in the patients as well, thus it is not a cell culture artifact [102].
While patient isolates are a relevant biological system to study HEV, they are inefficient in spreading and present a variability between and within patients risking inconsistency between experiments [2, 219, 325]. The use of cDNA clones can overcome low replication efficacy and the reproducibility problem. Also, genetic modifications can be performed. The cDNAs were created from subgenomic PCR amplification and assembly through restriction enzymes [2, 326]. In certain strains reporter genes were inserted as for example the *Gaussia* luciferase or a green fluorescent protein (GFP) that substitutes the majority of the ORF2 and ORF3 gene in the Kernow–C1/p6 strain, which is used in this study as well [10].
Other cDNA clones include a Kernow–C1/p6 strain that contains a S19 ribosomal protein in the same region as the S17 insertion previously mentioned [145]. When A549 cells persistently infected with HEV genotype 3, cell culture adaptive mutations and insertions have been found derived from of other parts of the ORF1 and adjacent regions [327]. The insertions could be a tool to enhance viral replication since they are associated with increased viral fitness.
Moreover, it is important to pair the desired HEV strain with the correct cell line, since there is no universal cell culture system available. HEV has a broad host and tissue

tropism, thus it replicates in various cancer cell lines (Selection of cell lines supporting the Kernow–C1/p6 strain found in Tab. 3). Therefore not only infection of the liver but also extrahepatic manifestations can be studied in humans and animals. In 2018 Montpellier *et al.* reported an efficient cell culture system for the production of HEV Kernow–C1/p6 in PLC3 cells, a subclone of the PLC/PRF/5 cell line. Viral titres reach up to 3.3×10^7 FFU/mL . In this study, most experiments were undertaken in PLC3 cells together with Huh7.5 cells [186].

The advantage of cancer cell lines are easy handling, robustness and availability. Drawbacks are slow virus replication and unsuccessful propagation of HEV from low titre samples. Additionally, hepatoma cell lines have a defective immune system and other cellular pathways are less faithfully represented [1].

To overcome those drawbacks primary human hepatocytes (PHH) and induced pluri–potent stem cells (iPSC) can be used. PHH and mouse embryonic fibroblasts (MEF) support the infection with Kernow–C1/p6, but their availability is limited and their life span is rather short. Also, the variability of PHHs is high depending on the donor's health status, the isolation protocol and culture conditions [2]. Hepatocyte like cellss (HLCs) which are derived from iPSC or embryionic stem cells (ESC) on the other hand have the advantage of self–renewal and generation of patient–specific disease models [328]. This system has similar characteristics to known cell culture systems, but it can be infected by non–adapted HEV isolates. In fact, clones that have been adapted replicate less efficiently than non–adapted strains. This could be the reason why the S17 insertion of the Kernow–C1 strain remained a minority in patients [1]. Furthermore, these cells possess phase I, II and III drug metabolizing enzymes and are thus suitable for metabolism and drug disposition studies [329].

Another useful tool to study HEV is the polarized cell culture model. In a study by Capelli *et al.* a subclone of HepG2/C3A cells were used that presented an apical (oriented towards the bile) and a basolateral side (oriented towards the blood). It was found that while HEV particles are released from both sides, the vast majority was secreted at the apical side (94–99%). Furthermore, apically released HEV genotypes 1 and 3 were 6 and 9 times more infectious, respectively. This model mimics physiological conditions thereby presenting an advantage over classic cell culture systems [86].

Table 3: Cell lines that support Kernow–C1/p6 replication, table from [1] and [2]

Cell line	Origin	Reference
Caco–2	Colon	[144]
Hepa–RG	Liver	[330]
HepG2/3CA	Liver	[144]
Huh–7 S10–3	Liver	[331]
Huh7.5	Liver	[144]
PLC/PRF/5	Liver	[144]
PLC3	Liver	[186]
A549	Lung	[144]
M03.13, DBRTG, SK–N–MC, DAOY	Neuron	[332]
U87	Neuron	[333]
JEG–3, BeWo	Placenta	[334]
FRhK–4 (rhesus macaque)	Kidney	[331]
LLC–PK1 (pig)	Kidney	[144]
OHH1.Li (deer)	Liver	[144]
MDCK (dog)	Kidney	[144]
CRFK (cat)	Kidney	[144]
LLC–RK1 (rabbit)	Kidney	[144]
Hepa 1–6 (mouse)	Liver	[144]
PHH	Liver	[335]
HLCs	Liver	[336]

1.12. Animal Models

Several animal models are currently in use to complement the research done in cell culture (Fig. 20).

Non human primates (NHPs) susceptible to HEV infections include: Chimpanzees, rhesus macaques, pig–tailed macaques, ferrets, owl monkeys, squirrel monkeys, tamarins and patas monkeys. Most susceptible were Chimpanzees, rhesus macaques and cynomolgus monkeys, thus they are the most suitable models to study HEV infection [33, 337]. An infection of rhesus macaques with HEV genotypes 1 and 3 led to elevated serum levels of the liver enzymes ALT and AST, viremia, seroconversion, liver lesions and viral shedding in stool [338–340].The acute infection was very similar to humans.

NHPs are not only susceptible to human HEV but also to other species derived HEV (swine derived HEV3, rabbit derived HEV3, cow derived HEV4 and camel derived HEV7) making them a good tool to study cross–species transmission [339, 341, 342].

A chronic infection could be achieved when infecting rhesus macaques with swine derived HEV4 [341, 342].
However, pathogenesis in pregnant animals could not be studied as no vertical transmission and increase of mortality was observed [340]. Nevertheless, recently, an ex–vivo model was set up to study the replication of HEV genotypes 1 and 3 at the maternal–foetal interface using the decidua basalis and fetal placenta [343].
Rhesus macaques and cynomolgus monkeys show protective immunity against HEV therefore they can be used to identify vaccine candidates [307, 315, 344]. Since NHP are not a natural host for HEV, this presents a drawback in this model. Also, financial and ethical reasons limit the use of NHP in HEV research [345].
Pigs on the other hand, are a natural host for HEV and they are one of the primary reservoirs for genotypes 3 and 4 [346–348]. The progress of infection is subclinical with mild to moderate histopathological lesions and no elevation of liver transaminases [349]. Viral shedding has been recorded for up to 28 days [350]. It was the first model to show extrahepatic manifestation sites in small intestine, colon, spleen and kidney [351]. Pigs can be infected with human derived HEV3 and HEV4, rabbit derived HEV3 and wildboar derived HEV3 making cross–species studies possible [347, 349, 352]. Furthermore, pigs can be infected chronically and their immune response can be studied. Vaccine candidates can be evaluated as well, as it was shown that the truncated recombinant of capsid antigens derived from swine, rat, and avian HEV strains induce anti–HEV IgG resulting in partial cross-protection against HEV genotype 3 [353, 354]. However, drawbacks include the limited presentation of clinical disease and the inability to study human derived HEV genotypes 1 and 2 [355].
HEV infection in rabbits was first identified in 2009 by Zhao *et al.* Rabbit derived genotypes 3 and 4 lead to a subclinical infection with microscopic lesions characterized by local hepatocellular necrosis [356]. Elevated liver transaminases indicate acute liver damage. The infection can become chronic and extrahepatic replication sites have been found in the salvary gland, tonsil, spleen, thymus gland, lymph nodes, heart, lung, intestine and kidney [325, 357, 358]. Moreover, rabbits can be infected by human derived HEV4 [32] and swine derived HEV4 [359], thus making it a good model to study HEV infection. Additionally, high mortality in pregnant rabbits and vertical transmission has been observed making it the only mammalian animal model to study pregnancy related conditions [360]. Yet, this model is limited due to its inability to study human HEV1 and HEV3, since it is only susceptible to human derived HEV4.
Even though rodents are a well–characterized model bearing many advantages due

to their small size and ease of manipulation, they only provide limited success as models for HEV infection. Especially in mice, discrepancies are observed upon HEV infection. While C57BL/6 mice are not susceptible to infection with human derived HEV GT1, swine derived HEV3 and wild boar derived HEV GT4 by intravenous injection [361], reports using Balb/c mice showed successful infection with swine derived HEV4 [362]. The discrepancy might be due to differences in viral isolates and the source of the virus and/or species tropism [355].

Humanized mouse models consist of three week old homozygous uPA/SCID(beige (USB) mice injected intrasplenically with human hepatocytes [363, 364]. The *in situ* infection with human derived HEV genotypes 1 and 3 is successful and results in viremia, fecal viral shedding and detection of HEV antigens, whereas liver enzymes were not elevated [355, 365–367]. A chronic infection could be established and HEV RNA in serum and stool could be detected up to 4 months after infection. Viral RNA was detected in liver and spleen, but not in brain and kidney deeming this model not suitable for studying extrahepatic manifestations [366]. Cross–species transmission has not been studied in detail. In humanized mice, the adaptive immune system is lacking, therefore the effect of HEV on the innate immune system can be studied. On the other hand, the lack of the adaptive immune system can be an inconvenience in other studies [355, 367, 368]. Furthermore, the lack of clinical representation and the high cost are a drawback for further studies [355].

Similar to C57BL/6, Wistar rats are not susceptible to the mentioned HEV strains, neither could other cross-species transmissions be established [369]. Nude rats can be infected with rat derived HEV–C1 and develop a persistent infection, where HEV RNA is detectable in liver and intestine, but not in other organs [369]. Due to the limited clinical presentation and the inability to be infected by human derived HEV, this model is not preferable to use [355].

Ferrets develop, subclinical, acute or persistent hepatitis upon infection with ferret derived HEV and viral RNA can be detected in stool and sera [370]. They may be potential candidates for studies of pathogenesis and immunological responses of HEV [371]. Cross–species transmission has not been evaluated yet. Ferret derived HEV can be propagated in PLC/PRF/5 cells [371]. This model has not been well characterized yet, this is why further development would be necessary.

The mongolian gerbil was successfully infected with swine derived HEV4 where viremia, fecal viral shedding and a clinical progression was observed including extrahepatic detection of HEV RNA [372, 373]. This was similar for the infection with human de-

rived HEV1 [374]. So far however, this model has not yet been characterized well.
Only limited data are provided for the tree shrew, since there is currently only one report by Yu *et al.* available. Inoculation with swine derived HEV4 resulted in seroconversion of IgG, RNA detection is serum, stool, liver, bile, spleen, kidney and detection of capsid in spleen and kidney. Liver lesions were observed as well [375].
In chicken, HEV causes hepatitis–splenomegaly syndrome [376]. It could be a useful model for clinical and pathological aspects, as a clinical progression such as gross and microscopic liver lesions are observed. Extrahepatic manifestations could be observed as well [377]. Also, chicken are a suitable model for vaccine studies [378]. Overall though, this model is limited since an infection with human derived HEV is not possible. Additionally, the clinical course of HEV in chicken and humans differs significantly [355].
The family of *Hepeviridae* contains not only the *Orthohepevirus*, but also *Piscihepevirus* including its sole member the cutthroat trout virus. When infected, fish cell lines generate large amounts of infectious virus. The genomic divergence to human derived HEV may permit compare–and–contrast studies. However, due to the physiological differences, this model is only of limited use [379].

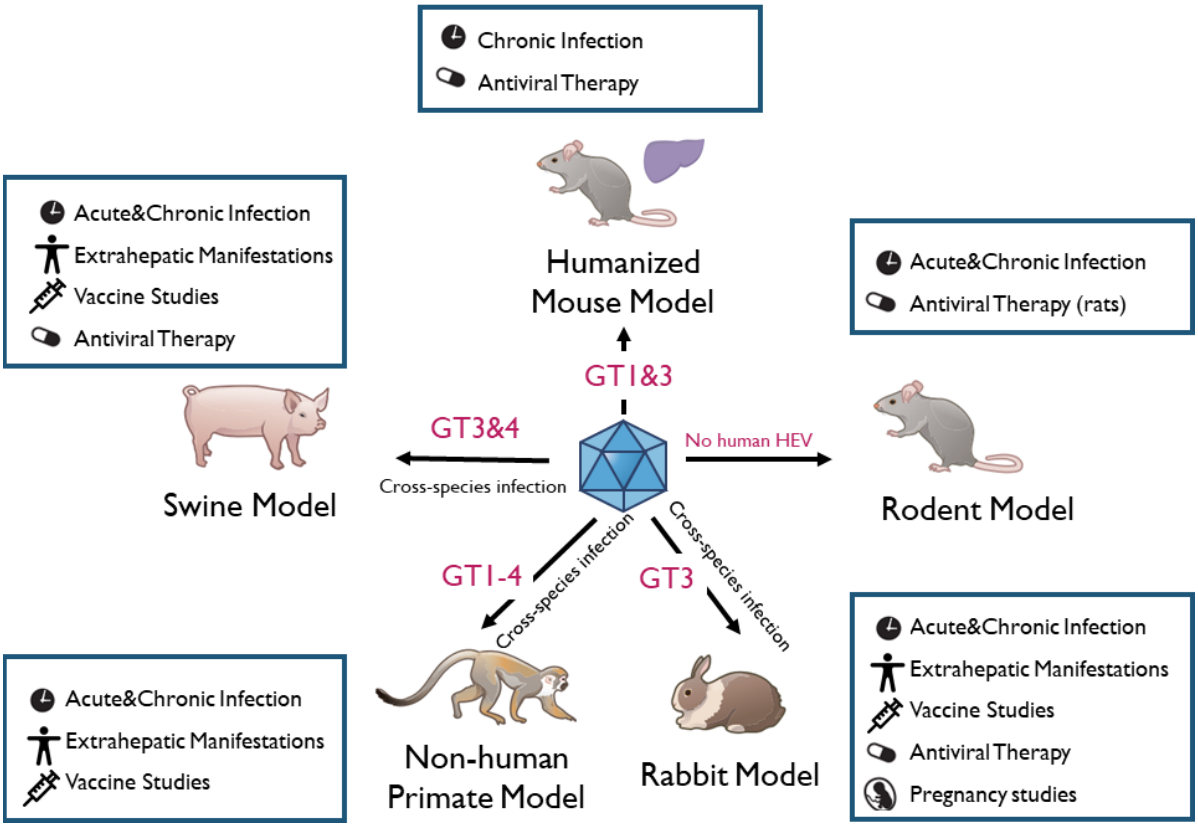

Figure 20: Mostly used animal models for HEV infection adapted from [345]

2. Material

2.1. Buffers and Culture Media

Table 4: Commercially available Buffers, Cell Culture Media & Molecular Weight Markers

Buffers	Company
10x Phosphate buffer (PBS)	Euromedex
1x PBS	Thermo Fisher Scientific
6x DNA Gel Loading Dye	Thermo Fisher Scientific
1x Medium 199	Thermo Fisher Scientific
1x Dulbecco's Modified Eagle Medium (DMEM)	Thermo Fisher Scientific
Fetal Calf Serum	Thermo Fisher Scientific
LB broth	Sigma–Aldrich
100x Non–essential amino acids	Thermo Fisher Scientific
Opti–MEM I Reduced Serum Media	Thermo Fisher Scientific
5x Passive Lysis Buffer	Promega
Page Ruler™Prestained Protein Ladder (10–180 kDa)	Thermo Fisher Scientific
10x Tris Buffer	Euromedex
1x Trypsin	Thermo Fisher Scientific
100x Ampicillin	
2–Log DNA ladder (0,1 kb–10 kb)	New England Biolabs Inc.
100bp DNA ladder	New England Biolabs Inc.

Table 5: Home made buffers & media

Buffer	Chemical	Final Concentration
TAE Buffer 1x	Tris	40 mM
	Acetic Acid	20 mM
	EDTA	1 mM
B1 Buffer	Tris–HCl (pH 7.5)	50 mM
	NaCl	100 mM
	EDTA	2 mM
	Triton–X	1 %
	SDS	0,1 %
Laemmli Buffer 4x	Tris-HCl (pH 6.8)	277,8 mM
	Glycerol	44,4 % (v/v%)
	SDS	4,4 %
	Bromphenol blue	0,02 %
	DTT	200 mM
Migration Buffer 1x for SDS–PAGE (pH 8.3 without adjustment)	Tris base	25 mM
	Glycine	192 mM
	SDS	1 %
Transfer Buffer 1x for SDS–PAGE (pH 8.3 without adjustment)	Tris	25 mM
	Glycine	190 mM
	Ethanol	20 %
	SDS	0,04 %
Blocking Solution for western blot	PBS	1x
	Fat–free milk	5 %
	Tween	0,2 %
Washing Buffer 1x for Western Blot	PBS	1x
	Tween–20	0,2 %
Fixation Solution for Colloidal Blue Staining	Ethanol	50%
	Phosphoric Acid	3%
	Water	47%
Colloidal Blue Solution	Water	60%
	Phosphoric Acid	10%
	Ammoniumsulfate	10%
	Brilliant Blue G250	0.12%
	Methanol	20%
DMEM complete	DMEM	89%
	Fetal Calf Serum	10%
	Non essential amino acids	1%
HEV medium	DMEM	45%
	Albumax (in PBS)	1 mg mL^{-1}, 2%
	Sodium Pyruvate	1%
	Non essential amino acids	1%
	Medium 199 1x	45%
Fixation Buffer for EM pH 7.3	Monosodiumphosphate	100 mM
	Sodiumhydroxide	675 mM
	Paraformaldehyde	4%
	Glutaraldehyde	2.5%
Immunogold Fixation Buffer pH 7.2	Phosphate Buffer	100 mM
	PFA	4%
	Glutaraldehyde	0.05%

2.2. Cell lines, Vectors and Primers

Table 6: Cell lines

Cell line	Details	Reference
PLC3 Cells	A cellular clone of the human hepatic cell line PLC/PRF/5	[186]
Huh7.5 Cells	A cellular clone derived from a hepatocytic human cell line permissive to HCV replication	[380]
H7–T7–IZ	Huh 7.5 cells that constitutively express the T7 polymerase	[236]

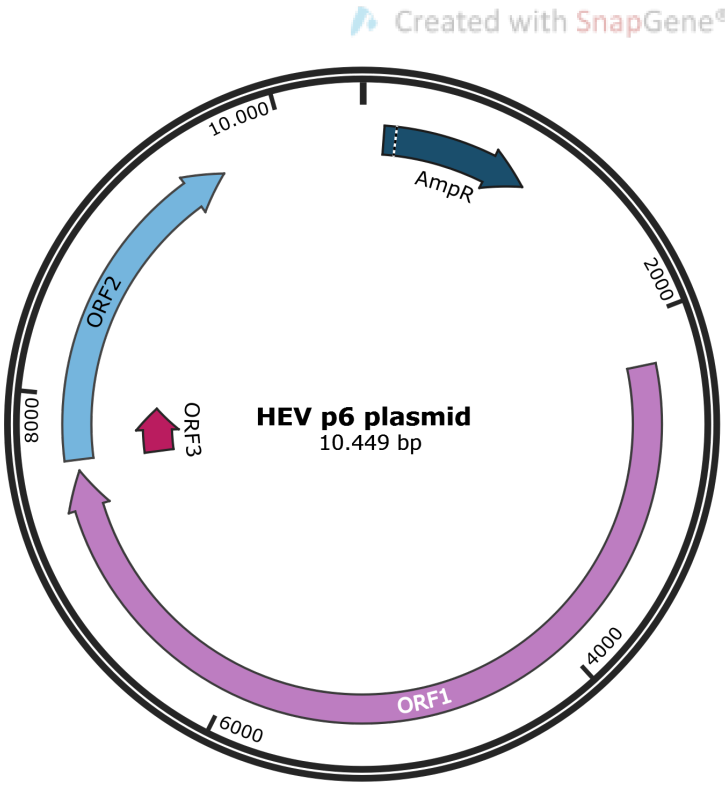

(a) HEV Kernow–C1/p6 plasmid. Accsession number:JQ679013, kindly provided by Sue Emerson.

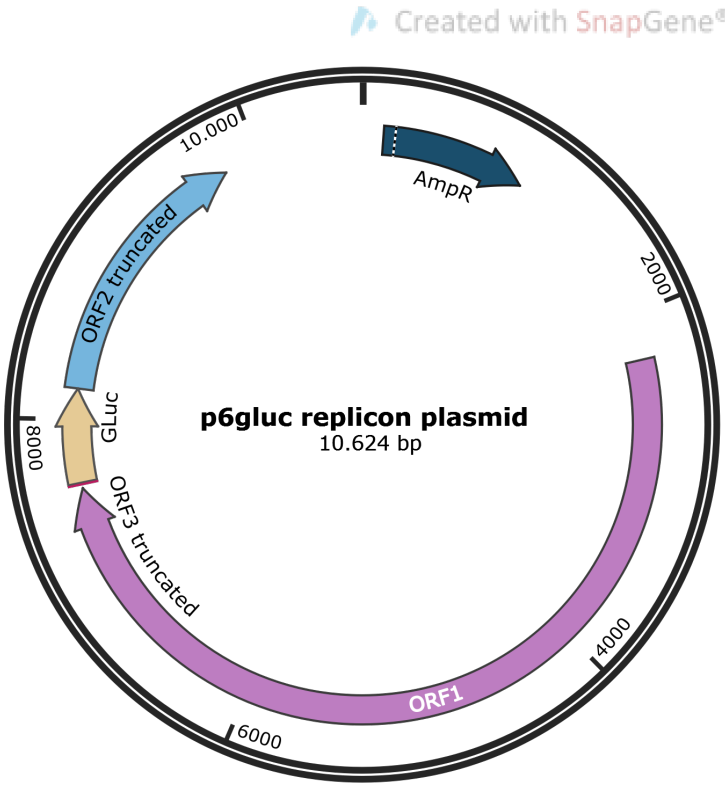

(b) HEV Kernow–C1/p6 replicon harboring the *Gaussia* luciferase [43, 102]. ORF2 and ORF3 are truncated.

Figure 21: HEV Kernow–C1/p6 derived plasmids

Table 7: Primer sequences used in the fusion PCR to target the different inserted fragments US: upstream fragment, DS: downstream fragment. All primers have been ordered at Sigma–Aldrich Life Science

Insert Name	Primer	Sequence
H2 US	1194(+) EcoRV	5'-GC GAT ATC CAA GGG CAT GCG CCG GTT G-3'
	2222(–) HA	5'-GGCGTAGTCGGGCACGTCGTAGGGGTAATCACT AGCAGGCGGGGTAGGG-3'
H2 DS	2244(+) HA	5'-TACCCCTACGACGTGCCCGACTACGCCATTTGG GCGT-TACCACCGCCCTCCG -3'
	3351(–) NdeI	5'-TGCATATGTAGCAGCAACAGGTG-3'
H3 US	1194(+) EcoRV	see above
	2248(–) HA	5'-GGCGTAGTCGGGCACGTCGTAGGGGTACTCCT CGGAGGGCGGTGGTAACGCCC-3'
H3 DS	2247(+) HA	5'-TACCCCTACGACGTGCCCGACTACGCCTGCTAC ACGCGCCTGGGCAACGAC-3'
	3351(–) NdeI	see above
H4 US	2179(+) NotI	5'-AGGCGGCCGCCCCTGC-3'
	2423(–) HA	5'-GGCGTAGTCGGGCACGTCGTAGGGGTAAGCCT CCTCCTGCAGCTTGATGGAG-3'
H4 DS	2448(+) HA	5'-TACCCCTACGACGTGCCCGACTACGCCCAGGT CGATGCAGCATCTGTGCCCC-3'
	3351(–) NdeI	
H5 US	2179(+) NotI	see above
	2457(–) HA	5'-GGCGTAGTCGGGCACGTCGTAGGGGTAGAGG GTAAGGGGCACAGATGCTGC-3'
H5 DS	2502(+) HA	5'-TACCCCTACGACGTGCCCGACTACGCCCCTGTT GTGTCACCTTCCCCACC-3'
	3351(–) NdeI	
H6 US	2179(+) NotI	
	2476(–) HA	5'-GGCGTAGTCGGGCACGTCGTAGGGGTAGGGC GACCCAGCAGGCACGAGGG-3'
H6 DS	2520(+) HA	5'-TACCCCTACGACGTGCCCGACTACGCCCCACC ACCACCTCCACCCGTGCG-3'
	3351(–) NdeI	

Table 7: Primer sequences used in the fusion PCR to target the different inserted fragments US: upstream fragment, DS: downstream fragment. All primers have been ordered at Sigma–Aldrich Life Science

Insert Name	Primer	Sequence
V1	2178(+) V5-NotI	5'-GAGGCGGCCGCCCCTGCTTCGGCTGCTGCCCC GGGGAAGCCCATCCCTAACCCGCTCCTCGGTCT CGATTCTACGCCTGCTAGTGATATTTGGGCG-3'
	3351(–) NdeI	
V2 US	2244(+)V5	5'-GGTAAGCCTATCCCTAACCCTCTCCTCGGTCTCG ATTCTACGATTTGGGCGTTACCACCGCCCTCCG-3'
	3351(–) NdeI	
V2 DS	2222(–)V5	3'-CCCTACCCCGCCTGCTAGTGATGGTAAGCCTA TCCCTAACCCTCTCCTCGGTCTCGATTCTACG-5'
	2179(+) NotI	
H1 US	5322(+) HA	5'-TACCCCTACGACGTGCCCGACTACGCCTGAATA ACATGTTTGTTGCATCGCCC-3'
H1 DS	5442(–) NruI	5'-TGGTCGCGAAGTTGCTGGCCACGGCC-3'
	5296(–) HA	5'-GGCGTAGTCGGGCACGTCGTAGGGGTATTCTA CCCGCTGTATGATGGAATTTG-3'
	4598(+) NsiI	5'-GTCATGCATGGTATTTGAAAATGACTTTTCGG-3'
V3 US	5322(+) V5	5'-GGTAAGCCTATCCCTAACCCTCTCCTCGGTCTC GATTCTACGTGAATAACATGTTTGTTGCATCGCCC-3'
	5442(–) NruI	
V3 DS	5296(–) V5	5'-CGTAGAATCGAGACCGAGGAGAGGGTTAGGGA TAGGCTTACCTTCTACCCGCTGTATGATGGAATTTG-3'
	4598(+) NsiI	

Table 8: Primers and Probes designed for qPCR of HEV, Supplier: Life technologies

Name	Nucleotide	Sequence	Reference
Upstream ORF1	Primer	TGACTCCTCATAAGCATCGC	[335]
Downstream ORF1	Primer	AAGACATTCTGCGCTTTGTT	[335]
Upstream ORF2	Primer	GGTGGTTTCTGGGGTGAC	[381]
Downstream ORF2	Primer	AGGGGTTGGTTGGATGAA	[381]
Upstream GLuc	Primer	TGGATCTTGCTGGCAAAGGT	[97]
Downstream GLuc	Primer	TCTGTGTGTGGACTGCACAA	[97]
Probe ORF1	Probe	CCGTGGTTCCGTGCCATTGA	[335]
Probe ORF2	Probe	TgATTCTCAgCCCTTCgC	[381]
Probe GLuc	Probe	GGCTTGCCAACGTGCAGTGT	[97]

Table 9: Probes designed for RNAscope of HEV, Supplier: ACDBio

Name	Target	Catalogue Number
A	ORF1 RdRp sense	579841–C3
B	ORF1 RdRp antisense	1030631–C2
C	ORF2 sense	586651
D	ORF2 antisense	1030641–C4
E	ORF1 PCP sense	579831

2.3. Enzymes, Kits and Antibodies

Table 10: Used Kits

Kit	Company
Nucleospin (R) gel and PCR Purification	MACHEREY–Nagel
Nucleospin (R) Plasmid	MACHEREY–Nagel
Nucleospin (R) Xtra Midi	MACHEREY–Nagel
Q5–HF PrimeSTAR Master Mix 2x	Clontech
RNA Transcription mMESSAGE mMACHINE T7	Invitrogen Thermo Fisher
Renilla Luciferase Assay	Promega
Subcellular Protein Fractionation for cultured cells	Thermo Fisher Scientific
Pierce™ECL Western Blot Substrate	Thermo Fisher Scientific
SuperSignal™West Pico Chemiluminescent Substrate	Thermo Fisher Scientific
Nucleospin RNA Plus for RNA extraction	MACHEREY–Nagel
RNeasy Mini Kit for RNA extraction	Qiagen
Affinity Script Multiple Temperature cDNA Synthesis Kit	Agilent
TaqMan Universal PCR Master Mix	Applied Biosystems
Dynabeads™Antibody Coupling kit	ThermoFischer Scientific
Protein G Sepharose 4 Fast Flow	GE Healthcare
RNAscope® Multiplex Fluorescent Reagent Kit v2	ACDBio
RNAscope® 4–Plex Ancillary Kit for Multiplex Fluorescent Kit v2	ACDBio
RNAscope® Wash Buffer Reagents	ACDBio
RNAscope® H_2O_2 and Protease Reagents	ACDBio

Table 11: Used Enzymes & their Buffers

Enzymes and Buffers	Concentration	Company
EcoRV–HF	100.000U/mL	New England Biolabs Inc.
NotI–HF	20.000U/mL	New England Biolabs Inc.
NdeI	20.000U/mL	New England Biolabs Inc.
NruI–HF	10.000U/mL	New England Biolabs Inc.
NsiI–HF	20.000U/mL	New England Biolabs Inc.
MluI–HF	20.000U/mL	New England Biolabs Inc.
Cutsmart Buffer 10x		New England Biolabs Inc
T4 Ligase	400.000U/mL	New England Biolabs Inc.
T4 Ligase Buffer 10x		New England Biolabs Inc.
Antarctic Phosphatase	5.000U/mL	New England Biolabs Inc.
Antarctic Phosphatase Buffer 10x		New England Biolabs Inc.

Table 12: Antibodies. Secondary Antibodies used in IF are bound to a fluorophore. Secodary Antibodies for WB were linked to horse radish peroxidase (HRP)

Antibody	Host	Clonality	Company	Dilution
anti–HA (clone 3F10)	Rat	monoclonal	Roche	1:250
anti–V5	Mouse IgG2a	monoclonal	Invitrogen	1:1000
anti–V5	Mouse IgG2a	monoclonal	Abcam	1:500
anti–V5	Goat	polyclonal	Abcam	IP
anti–ORF2	Mouse IgG2a	monoclonal	Millipore	1:800
anti–ORF3	Rabbit	polyclonal	S. Emerson Lab	1:1000
anti–CD63	Mouse IgG1	monoclonal	BD Pharmingen	1:100
anti–CD71	Mouse IgG1	monoclonal	Santa Cruz	1:100
anti–CD81	Mouse IgG1	monoclonal	Santa Cruz	1:100
anti–Rab11	Rabbit	monoclonal	Cell Signaling	1:100
anti–EHD1	Rabbit	polyclonal	Abcam	1:1000
anti–Pacsin2	Rabbit	polyclonal	MyBiosource	1:1000
anti–α lamin	Rabbit	polyclonal	Abcam	1:1000
anti–γ tubulin	Mouse IgG1	monoclonal	Sigma–Aldrich	1:4000
anti–Calnexin	Rabbit	polyclonal	Abcam	1:1000
anti–SP1	Rabbit	polyclonal	Abcam	1:1000
anti–Mouse (Cy3, Alexa 488)	Goat		Jackson	1:500
anti–Rat (Alexa 555)	Goat		Invitrogen	1:500
anti–Rabbit (Alexa 488)	Goat		Invitrogen	1:500
anti–Rat–HRP	Goat		Invitrogen	1:20000
anti–Mouse–HRP	Goat		Invitrogen	1:20000
anti–Rabbit–HRP	Goat		Invitrogen	1:20000

3. Methods

3.1. Cloning

3.1.1. PCR

In total, 2 different tags were inserted into 7 different positions of the HVR and at the C–terminus of the RdRp of the HEV p6gLuc replicon. Therefore, 11 corresponding primer pairs have been designed for each upstream and downstream direction containing the tag and thereby inserting it at the respective position (Tab. 7). A fusion PCR was set up as shown in Fig. 22. At first, the upstream and downstream fragments were amplified separately (PCR 1 and PCR 2) using conditions that can be found in Fig. 22.

Table 13: Component quantities for a 50 µL total volume PCR

Component	Volume [µL]
Primer (10 µM)	2
Template (10 ng)	5
Q5–HF PrimeSTAR Master Mix 2x	25
Milli Q sterile water	ad 50

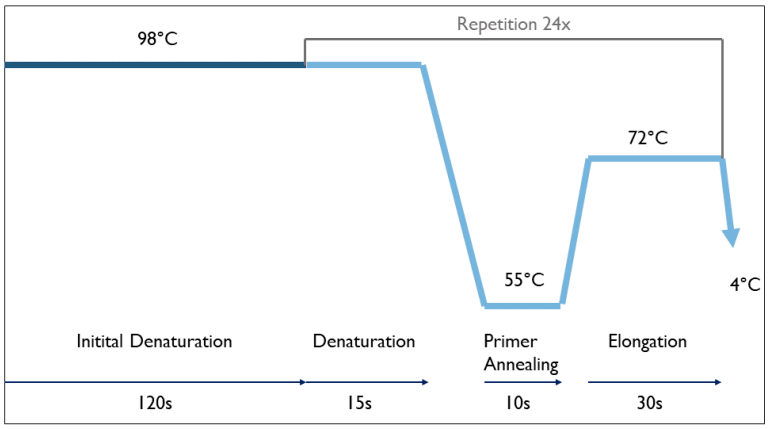

Figure 22: PCR scheme

To amplify DNA, one cycle of initial denaturation (120 s at 98 °C) was followed by 24 cycles of denaturation – primer annealing – elongation (Fig. 22) thus, leading to exponentional amplification of the starting DNA matrix. The denaturation step allows the two strands of the DNA to separate. The annealing step enables the hybridization of the primers to the DNA template. Finally, the last step allows the DNA polymerase to elongate the DNA. The samples were then

kept at 4 °C or −20 °C until used.
To ligate the upstream and the downstream fragment, a fusion consisting of a single cycle was set up (Tab. 14). In this case, the elongation step required 7 min while all other settings remain the same as in Fig. 22.

Table 14: Component quantities for a 50 µL total volume PCR

Component	Volume [µL]
Upstream Fragment (approx. 10 ng)	5
Downstream Fragment (approx. 10 ng)	5
Q5–HF PrimeSTAR Master Mix 2x	25
Milli Q sterile water	ad 50

Furthermore, primers were not needed and the amount of template could be adjusted depending on the concentration obtained through the previous PCR and purification. The total reaction volume remained 50 µL.
Finally, the fused fragment was amplified following the conditions, which can be found in Tab. 13 and Fig. 22 by using the upstream and downstream primer of the respective insert.
The PCR products were separated by gel electrophoresis (section and purified as described in section using the Nucleospin (R) gel and PCR Purification (Tab. 10).

3.1.2. Agarose Gel Electrophoresis

An agarose gel electrophoresis was used to separate DNA fragments based on their size and their charge. The agarose concentration amounted 1 % in 1x TAE buffer and was heated up several minutes in a microwave. After the agarose had cooled down for several minutes, two drops of ethidiumbromide were added per 40 mL melted gel and it was poured into a gel chamber. The gel needed to set 30 min before use.
The electrophoresis samples were mixed with 6x loading buffer, that contained a dye that ensures visibility of the migration front during the run.
Afterwards, the samples were loaded into the wells of the gel and a voltage (100–135V) was applied to the electroporation chamber letting the negatively charged DNA travel to the anode (approx. 30–45 minutes).
At last, the gel was exposed to UV light to visualize the DNA. The size of these products were compared to size molecular weight marker (2–Log DNA ladder or 100bp marker).

3.1.3. Gel Purification

After separation by agarose gel electrophoresis, the DNA fragments of interest were purified by using the Nucleospin(R) gel extraction kit (see Tab. 10).
The DNA fragment of expected size was cut from the gel under UV light and weighted in a 2mL Eppendorf tube. Afterwards, the kit instructions were followed. The amplified DNA fragment was finally eluted in 40 µL RNase free water.

3.1.4. Vector and Insert Restriction Digests

Vector and insert DNA have to be digested by the same restriction enzymes to allow their ends to overlap and to be ligated during the next step (Tab. 15).

Table 15: Restriction Digestion in 50 µL

Component	Volume [µL]
Amplified insert DNA/Vector DNA (approx 5 µg)	40
Cutsmart 10x Buffer	5
Restriction Enzyme 1 (10000U/µL)	2.5
Restriction Enzyme 2 (10000U/µL)	2.5
Milli Q sterile water	ad 50 if needed

The restriction digestion took place in a 37 °C waterbath for 3 h. If necessary, the vector was dephosphorylated (subsection 3.1.5). To purify the digested inserts and the vector, the fragments were separated by agarose gel electrophoresis (subsection 3.1.2). Afterwards, the DNA was retrieved by DNA purification (subsection 3.1.3).

3.1.5. Vector Dephosphorylation

To prevent re–ligation of the plasmid without the insert, 5'–ends of the restricted vector were dephosphorylated by the antarctic phosphatase. This reaction takes place after at least 2 hours of incubation of the restriction digestion.
The mixture was incubated for another 30 minutes, then the enzyme was heat inactivated by incubation at 70 °C for 5 min. Then the purification takes place as detailed before (subsection 3.1.3).

Table 16: Dephosphorylation of vector DNA by the Antarctic Posphatase

Component	Volume [µL]
Vector DNA Restriction Digest	50
10x Antarctic Phosphatase Buffer	5.5
Antarctic Phosphatase (5000 U/mL)	1

3.1.6. Vector and Insert Ligation

Vector and insert were ligated in a ratio of 1:3, which was calculated using the NEBioCalculator.
It was incubated at RT for 2 h and 10 min for the ligation of blunt ends or sticky ends, respectively.

Table 17: Vector and Insert Ligation in 20 µL

Component	Volume [µL]
Vector DNA (1:3)	approx 2
Insert DNA (3:1)	approx 5
T4 Ligase 10x Buffer	2
T4 Ligase (40 000 U/mL)	1
Milli Q sterile water	ad 20

3.1.7. Transformation and Culture of Bacteria

50 µL of competent *E.coli* (strain TOP10) were mixed with 10 µL of ligated plasmid and were further incubated on ice for 30 min. Next, a heat shock was performed for 2 min at 37 °C. After cooling the bacteria down on ice, 150 µL of LB medium was added and at least 50 µL were plated on an ampicillin LB plate, that was subsequently incubated at 37 °C overnight.
The following day, 6 colonies per plate were picked, placed into 3,5 mL of LB Medium with a concentration of 0,3 µg mL^{-1} of ampicillin and were shaken at 150 rpm for 12 h–16 h at 37 °C.

3.1.8. Plasmid Purification and Sequencing

3.1.8.1. Miniprep

After the transformation, the plasmid was purified from bacterial chromosomal DNA and cell wall by using the Nucleospin(R) plasmid kit (Tab. 10). This kit allows to purify relatively small quantities of plasmid DNA in order to screen many clones for successful cloning.

The kit instructions were followed to purify the plasmids from the bacterial culture.
To check for the insertion of the fragment of the expected size, the plasmid was digested with the restriction enzymes bordering the insert. 2 µL of eluted plasmid were mixed with 2 µL of 10X cutsmart buffer, 0,1 µL of each of the respective restriction enzymes (Tab. 15) and 18 µL MilliQ sterile water. The restriction reaction was incubated at 37 °C for 2 h. Next, the results of the digest were visualized on an agarose gel.

3.1.8.2. Sequencing

The sequencing of the insert was outsourced to Genoscreen (Lille Pasteur Institute), that uses the Sanger sequencing method and 100 ng of each plasmid sample. One primer is needed to sequence 500 bp approximately. Thus, the primers (5 mM), that cover the entire insert, were chosen according to each construct.
An alignment of the sequences of the constructs with the wildtype DNA was performed by using VectorNTI® software.

3.1.8.3. Midiprep

Once the construct has been confirmed to be correct by sequencing, the plasmid DNA preparation can be scaled up by using the Nucleobond(R) Xtra Midi kit that also allows to get DNA of higher quality (Tab. 10).
At first, a pre–culture of 4 mL LB medium with 0,3 mg mL^{-1} ampicillin was incubated for 16 h at 37 °C at 150 rpm. 500 µL of this culture were used to inoculate the main culture of 100 mL, which was then grown under the same conditions as the pre–culture.
The following day, plasmid were purified by following the instruction of the kit.

3.1.9. Plasmid Linearization and RNA Transcription

To transcribe RNA from the plasmid DNA, the circular plasmid was linearized and precipitated. Therefore it is cut with an unique–site enzyme (MluI–HF) that is located downstream of the poly A tail of the HEV genome (Fig. 21b).
25 µg of DNA were mixed with 25 µL of 10X cutsmart buffer, 70 IU of the restriction enzyme and water up to 250 µL. It was incubated for 2 h at 37 °C.
Afterwards, 800 µL chloroform/isoamylalcohol (96:4 v/v) were added to purify the plasmid DNA from the restriction enzyme. It was shaken for 10 min and afterwards centrifuged for 15 min at 14 000 rpm, so that the proteins gather in the organic phase and the DNA in the aqueous phase.
The upper aqueous phase was carefully abstracted from the organic phase and placed into a

fresh tube. 1.2 times the volume of the aqueous phase of pure ethanol and 100 µL of sodiumacetate (3M, pH 5.5) was added, mixed and stored at −20 °C overnight to allow precipitation of the plasmid DNA.
The next day, the precipitated DNA is centrifuged for 15 min at 4 °C and 14 000 rpm. The ethanol–containing supernatant was carefully removed and the DNA was left to dry at RT.
Next, it was resuspended in 20 µL nuclease free water and the OD was measured to determine the plasmid concentration and purity.
To synthesize capped RNA, an *in vitro* transcription was conducted for 2h at 37 °C using a RNA transcription kit (Tab. 10). Following a treatment with DNase, the transcribed RNA was precipitated by following the LiCl method as indicated in the kit. After the precipitation solution was added, the RNA was vortexed and frozen for 30 min and thawed 2 times to increase precipitation efficacy.
Next, it was centrifuged at 14 000 rpm for 5 min, so the supernatant could be carefully removed. The pellet was washed 3 times with 70 % ethanol and left to dry until the ethanol was completely evaporated. Finally, the pellet was resuspended in an appropiate amount of nuclease free water and the OD was measured.

3.2. Cell Culture

3.2.1. Electroporation of PLC3 and Huh7.5 Cells

For one electroporation, 6x10^6 PLC3 or Huh7.5 cells are mixed with 20 µg of RNA.
The subconfluent cells were washed once with 2 mL of PBS and incubated with the same quantity of trypsin at 37 °C for approximately 5 min. The trypsinized cells were resuspended in 10 mL of DMEM medium and alltogether dispatched into a falcon tube that was centrifuged at 800 rpm for 6 min. Afterwards, they were washed twice with 10 mL Opti–MEM medium and centrifuged under the same conditions as before. Finally, the pellet was resuspended in nx400 µL of Opti–MEM medium, where n stands for the number of electroporations, and dispatched into 5 mL tubes. Each tube contained 6x10^6 cells. 20 µg of RNA were added to each cell suspension and the RNA–cells mixture was quickly transferred to a 2 mm electroporation cuvette.
The electroporation was conducted at the following conditions:

Table 18: Electroporation Conditions

Condition	Unit
Voltage	150 V
Capacity	1000 µF
Resistance	∞
Cuvette	2 mm

Afterwards, 300 µL of the electroporated cell suspension were added to 12 mL DMEM medium and resuspended. The cells were further diluted and plated according to the following assay. Lastly, the cells were incubated at 37 °C and 5% CO_2.

3.2.2. Production of HEVcc

To produce and concentrate viral particles in the supernatant of PLC3 cells, the growing conditions were optimized [186].
After electroporation, PLC3 cells were taken up in 12 mL DMEM complete. Next, 3 mL were transfered in a T–75 flask and 9 mL of DMEM complete were added. The cells were incubated at 37 °C and 5% CO_2 for 24 hours. The next day, the medium was replaced by HEV medium (Tab. 5) and the cells were transferred at 32 °C and 5% CO_2. The incubation time varied between 10–14 days depending on the level of confluency. The supernatants were collected, aliquoted and stored at −80 °C. The cells were lysed and the lysate was stored at −20 °C.

3.2.3. Infectivity Assay

Infectious titers and percentage of infection of particles that were produced in PLC3 cells were measured (Chapter 3.2.2).
First, Huh7.5 cells were seeded in collagen coated 96 well plates (clear bottom) 24 hours before infection. 3000 cells were seeded in each well in 100 µL of DMEM complete medium. The cells were incubated overnight at 37 °C.
The next day, dilutions of the infectious particles were prepared in a 96 well dilution plate. Each sample was tested as a triplicate. The first samples were the undiluted PLC3 supernatants and each dilution was carried out in a 1/10 manner in DMEM medium without serum.
Afterward, the supernatant of the Huh7.5 cells was aspirated. Quickly, but gently 100 µL of the diluted infectious supernatant was transferred to the Huh7.5 cells. It was incubated for 8 hours at 37 °C, then the infectious supernatant was replaced by 100 µL of complete DMEM. The cells were grown for 3 more days. After 3 days, the cells were fixed and subjected to immunofluorescence (Section 3.5.1). For measuring infectious titers the ORF2 protein was stained with the antibody anti–1E6 (Tab. 12).
The calculation of the infectious titer was done manually at the fluorescence microscope. Positive cells were counted in the wells of the 1/10 or 1/100 dilution and three wells per chosen dilution were counted. The formula that measures the number of fluorescence forming units

(FFU) is shown below.

$$FFU/\mathrm{mL} = positivecells \times dilutionfactor \times 10$$

Additionally, the percentage of infection was calculated by evaluating images taken from the whole well infected by non diluted supernatant. The number of positive cells were counted automatically in ImageJ.

3.3. Kinetic measurements

3.3.1. Luciferase Assay

The principle of the luciferase assay relies on the conversion of a substrate molecule into a chemoluminescent product due to the presence of a reporter protein. In this case, the reporter gene *Gaussia* luciferase, that is secreted into the cell supernatant, can convert the substrate luciferin together with coelenterazine into coelenteramide and light.
After electroporation, the replication fold of the epitope–tagged HEV replicons was measured over the course of 5 days. Therefore, 4x10^4 cells per well were plated in a 24 well plate in a volume of 500 µL. A triplicated of each sample was prepared to ensure technical repeatability. Since the *Gaussia* luciferase is secreted into the supernatant, a small quantity of supernatant was sampled every day and was stored at $-20\,^{\circ}\mathrm{C}$.
The supernatant was thawed and centrifuged for 5 min at 14 000 rpm at RT. The samples were diluted 1:100 with 1x renilla lysis buffer in a total volume of 100 µL. 5 µL of the dilution were transferred into a white 96 well plate suitable for reading the bioluminescent signal using the Centro–Luminometer (Berthold).
Therefore, 20 µL of a 1x luciferin substrate solution were added by the machine within the reading process, allowing the measurement to be conducted directly after the conversion to coelenteramide and light for 10 s in each well. The luminescence quantity is indicated in arbitrary units.

3.3.2. RNA extraction and RT qPCR

Following electroporation the cells were plated in 6 well plates or T–25 flasks between 4 hours and 7 days.
The total RNA was extracted from cell lysates with the Nucleospin RNA Plus kit and from cell supernatant with the RNeasy Mini kit (Tab. 10). After cell lysis and before extraction, the lysates and supernatants were stored at $-80\,^{\circ}\mathrm{C}$ so that extraction could be performed at the same time. The extraction was done according to the supplier's protocol.
Next, RNA concentration was measured and adjusted to $100\,\mu\mathrm{g}\,\mu\mathrm{L}^{-1}$.In order to quantify the

HEV genome, a standard curve was prepared by diluting *in vitro* transcribed HEV p6 plasmid in 7 different dilutions ranging from 2.6x10^8 to 2.6x 10^2 RNA copies. The standard curve was mixed with total RNA extracted from mock electroporated PLC3 cells to resemble the unknown sample as much as possible. For each reverse transcription (RT) and following qPCR the standard curve was included next to the samples. The RT takes place in two steps, since the second step contains heat sensitive reagents. At first, the RNA samples, the nuclease free water and the polydT primer were incubated for 10 minutes at $65\,^{\circ}\mathrm{C}$. After that, the other reagents were added to the mix.
The reaction mix for the cDNA synthesis can be found in Tab. 19 and the program is displayed in Tab. 20.

Table 19: Reverse Transcription, AffinityScript cDNA Synthesis

Reagent	Volume [µL]
Nuclease free water	9.7
RNA sample [$100\,\mathrm{ng}\,\mu\mathrm{L}^{-1}$]	5
PolydT primer ($0{,}5\,\mu\mathrm{g}\,\mu\mathrm{L}^{-1}$)	1
10x Reverse Transcriptase Buffer	2
dNTPs ($100\,\mathrm{mM}$)	0.8
Reverse Transcriptase	1
RNase block ribonuclease (40IUµL)	0.5

Table 20: RT program

Step	Temperature [°C]	Duration [min]
Initiation	42	5
RT	55	60
	70	15
Hold	4	∞

The cDNA can be safely stored at $-20\,^{\circ}\mathrm{C}$.
Upon completion of the RT, the qPCR was undertaken. Probes were designed against the ORF1, the ORF2/3 and the GLuc that can be found in Tab. 8 . The reaction mix is shown in Tab. 21 and the program in Tab. 22. Finally, the data can be analyzed in the ThermoFisher scientific cloud.

Table 21: qPCR, TaqMan Universal PCR Master Mix

Reagent	Volume [µL]
TaqMan universal Master Mix 2x	5
Forward Primer	0.375
Reverse Primer	0.375
Probe	0.375
RNase free water	1.8
cDNA sample	4

Table 22: qPCR program

Step	Temperature [°C]	Duration [min]
Initiation (1 cycle)	95	10
Amplification (40 cycles)	95	0.25
	60	1

3.4. Protease Inhibition

It is currently not known whether or not the protease of HEV is functional, therefore several protease inhibitors were tested.
After electroporation of PLC3 cells with tagged and wildtype p6 RNA, the cells were seeded into 96 well plates in a volume of 150 µL. Each well contained 50000 cells and each testing condition was performed as a triplicate. Directly, the protease inhibitors were added to the PLC3 cells (Tab. 23). The cells were incubated for 5 days and each day starting from 1dpe, 10 µL of supernatant was sampled.
Subsequently, the replication efficacy was analyzed by doing a luciferase assay (see Chapter 3.3.1).
At day 5, an MTS assay was performed to ensure cell viability.

3.4.1. MTS Assay

The MTS assay is used to determine cell viability of cells that were exposed to protease inhibitors. The assay was performed following the protease inhibition experiment described in the chapter above (Chapter 3.4).
Therefore, 20^4 cells were seeded per well and it was incubated at 37 °C at 5% CO_2. On day 5 post electroporation 20 µL were added to each well and it was incubated for 1 hour at 37 °C at 5% CO_2. Afterwards, the absorbance was recorded immediately at 490 nm.

Table 23: Protease Inhibitors

Protease Inhibitor	Target Protease/ Chelator	Working concentrations 1/2/3 [µM]	Supplier
E–64d	Cysteine	1/10/50	Sigma Aldrich
Antipain	Cysteine and serine	10/100/200	Sigma ALdrich
Leupeptin	Cysteine	10/100/500	Sigma Aldrich
EDTA	Metallochelator	2000/10000/50000	Sigma Aldrich
EGTA	Metallochelator	2000	Sigma Aldrich
TPEN	Zn^{2+} chelator	2/10	Sigma Aldrich
Velpatasvir	NS5A Inhibitor	0.005/0.01/0.05	Selleckchem

3.5. Imaging of cells

3.5.1. Immunofluorescence

Following the electroporation of PLC3 and Huh7.5 with the different constructs, the cells were seeded in 24 well plates on top of round cover slips that had been previously deposited at the bottom of the wells. The cells were grown between 4 hours and 15 days at 37 °C in 5 % CO_2. It was aimed to grow 1x10^5 cells in one well at the time of fixation.

Following 2 gentle washings with PBS the cells were fixed by incubating with 300 µL 3% PFA for 20 minutes. They were washed thrice with PBS and incubated with 500 µL ice cold Methanol for 5 minutes. After washing three times with PBS the fixed cells could be stored for up to one week at 4 °C or immunofluorescence could be performed directly.

Next, the cells were permeabilized with 500 µL PBS containing 0,5 % Triton X–100 for 10 min. Blocking was performed with 500 µL 10 % goat serum diluted in PBS to saturate all unspecific binding sites. It was incubated for 30 min at RT.

The primary antibody was diluted in blocking solution according to its respective optimized conditions (Tab. 12). 50 µL per coverslip of the antibody solution were incubated on a parafilm layer in a wet chamber for 30 min at RT. The cover slips were re–transfered into their wells and washed 3 times with PBS.

The secondary antibody and DAPI were diluted in blocking solution in a 1:500 manner. The cover slips were placed onto the secondary antibody solution and it was incubated for 20 min in a dark, humid chamber. The cover slips were then retransferred into their wells and washed three times with PBS.

At last, the cover slips holding the cell monolayer were then fixed on a glass slide with 7 µL of Mowiol, an anti–fading agent. The slides were kept in a dark chamber at RT overnight and were later stored at 4 °C.

3.5.2. Detection of HEV RNA

The RNAscope® is a technique that specifically and sensitively detects RNA. The specificity is ensured by designing a pool of probes against a mRNA sequence of at least 18 nucleotides each. The probe is made up of 3 parts: the target–specific binding site, a spacer and the pre–amplifier binding site (Fig. 23). The target specific binding site encompasses 18–25 bases per probe. Two of those oligo probes need to align next to each other in order to bind the pre–amplifier that recognizes the upper part of 20 bases for each probe. In total, a pool of 20 oligo pairs can bind to the RNA of interest.
Next, the amplifier binds to the pre–amplifiers, which can then bind to the label dyes. These amplification steps are the reason for the high sensitivity of this technique, while the hybridization with approximately 50 bases of the probe allow a high specificity.
At first, probes were designed against two different regions in the HEV genome: the genomic and the subgenomic RNA (Fig. 24). Probe A targets the RdRp region (sense RNA), probe B covers the RdRp and the Hel domain (anti–sense RNA) and probe E hybridizes the PCP domain (sense RNA). The probes that are targeting the subgenomic RNA are C (sense) and D (anti–sense).
Next, 10^5 cells were fixed at 3 dpe on coverslips (Chapter 3.5.1). Afterwards, the instructions of the kit (Tab. 10) were followed.
For the pre–treatment, the cells were incubated with 4–6 drops of hydrogen peroxide for 10 minutes at RT followed by a protease III (diluted 1:15 in PBS, 150 µLper sample) treatment for 15 minutes at RT. The cover slips were then mounted onto a glass slide with nail polish and a hydrophobic barrier was created by using a hydrophobic pen. Next, the probes were added to the cells to hybridize with their target at 40 °C for 2 hours. After this step, the cells can be stored in 5x SSC buffer overnight or it can be continued with the assay.
Then, sequentially 4–6 drops of pre–amplifiers 1, 2 and 3 were added to the cells and it was incubated for 30 minutes in case of pre–amplifier 1 and 2 and 15 minutes for pre–amplifier 3 at 40 °C. Afterwards, the amplifiers bound to the HRP were added (4–6 drops) to the cells and it was incubated for 15 minutes at 40 °C. The signal was then developed by adding the Opal dye diluted 1:1500 in TSA buffer (150µLper sample). It was incubated at 40 °C for 30 minutes. After each incubation with the Opal dye, the HRP was blocked with the HRP blockers for 15 minutes at 40 °C.
If only RNA was labeled, the last step consisted of an incubation with 4–6 drops of DAPI for 30 seconds at RT before the cover slips were mounted onto a glass slide using mowiol.
If an IF is performed after the labeling of HEV RNA, the cover slips were detached from the glass slide and put back into a 24 well plate. After that, the IF is performed as described in section 3.5.1.

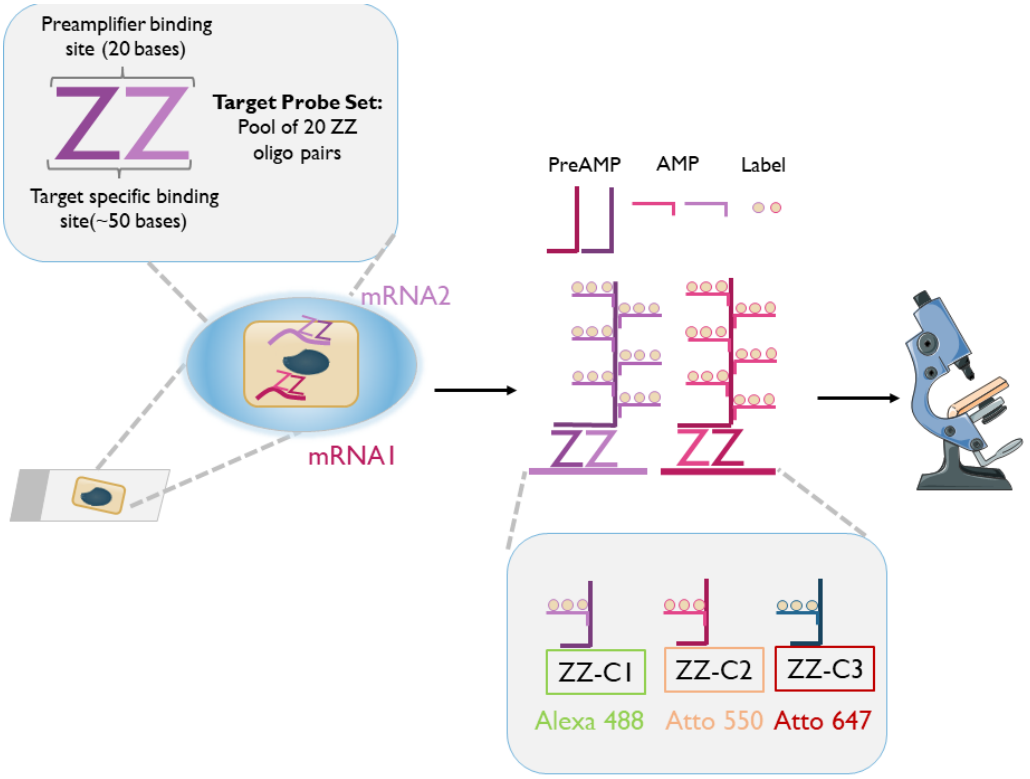

Figure 23: Overview of the RNAscope procedure. PreAMP: pre–amplifier, AMP: amplifier, ZZ–C: channel. Alexa 488, Atto 550 and Atto 647 are the fluorophores. Adapted from ACDBio.

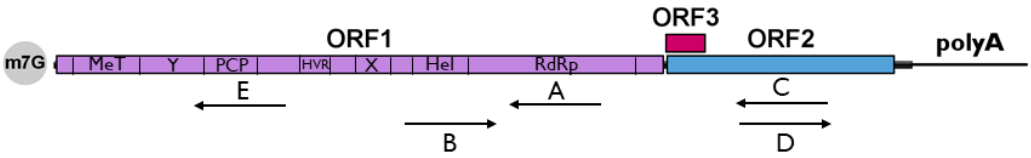

Figure 24: Probe design of probes A–E against the HEV genome. Probes accessible on acdbio.com.

3.5.3. Electron Microscopy

Transmission Electron Microscopy The transmission electron microscopy makes ultrastructures of cells visible (Chapter 3.6.3).

For this technique, approximately 6x10^6 cells are needed. The cells were trypsinized and resuspended in DMEM complete medium. After pelleting (800 rpm, 6 min) they were rinsed with PBS and resuspended in 10 mL cold fixation buffer (Tab. 2.1). The cells were incubated

at 4 °C for 24–48 hours. After that time, the cells can stay at RT.
The visualization by EM was performed by our collaboration partner (Pr Philippe Roingeard, Julien Gaillard, Inserm U966, Univ. François Rabelais, Tours, France).

Immune Gold Electron Microscopy The immune gold staining allows a specific labeling of proteins while making the ultrastructure of cells visible. In this setting, the secondary antibodies are coupled to gold beads that appear as electron dense round particles under the microscope. Different proteins can be co–labeled with different antibodies that are coupled to beads of different sizes. (Chapter 3.6.3).
As for TEM, 6x10^6 cells were fixated per experiment. The cells were trypsinized and resuspended in DMEM complete medium. After pelleting (800 rpm, 6 min) the cells were rinsed twice with PBS and the supernatant was removed. Next, the cells were fixed with 10 mL of fixation buffer (Tab. 5) at RT for 1 hour. From time to time, they were mixed gently by inversion. Finally, the cells were pelleted again and resuspended in 150 µL of the same fixation solution. 1 mL of PBS was added to avoid over fixation.
The microscopy of the fixed cells was performed by Cyrine Bentaleb and our collaboration partners (Pr Philippe Roingeard, Julien Gaillard, Inserm U966, Univ. François Rabelais, Tours, France).

3.6. Microscopes

3.6.1. Fluorescence Microscope

Fluorescence microscopes consist of 3 basic filters: an excitation filter, a dichroic beam splitter and an emission filter. The excitation filter selects the wavelength to excite the specimen, while the emission filter only lets the wavelength of interest pass. The dichroic beam splitter is set at 45° angle, thereby reflecting shorter wavelength deriving from the excitation and allowing longer wavelengths to transmit.
A Zeiss fluorescence microscope and a Mercury Illumination System were used to visualize the labeling.

3.6.2. Confocal Microscope

All immunofluorescence images shown (Chapter 5.9) were taken by the Zeiss LSM 880 confocal microscope that possesses an Airyscan detection unit.

The confocal microscope as the fluorescence micrscope consists of a Laser that excites the fluorophore, beam splitters and an emission filter, however the resolution of the image is significantly enhanced.
The resolution of a conventional microscope is dependent on the diffraction nature of light. This means that infinitesimally small points are imaged as blurred objects, which are called Airy discs.
For two fluorophores, the Rayleigh criterion defines the minimal distance between the self–emitters for them to be visible separately.
The confocal microscope achieves a better resolution due to the integration of a pinhole between the beam splitters, that rejects out–of–focus light (Fig. 25). Narrowing the aperture of the pinhole increases the resolution, but decreases detection efficiency at the same time. This problem is solved by imaging the Airy disk onto a concentrically–arranged hexagonal detector array. The Airyscan detector is combined with the Zeiss LSM 880 and consists of 32 detector elements (GaAsP detector elements), that are arranged in a compound–eye–fashion. These elements themselves act as small pinholes, while the pinhole itself remains open, thereby collecting all the light. In the next step, the pixels will be reassigned to their original location, thus increasing the signal to noise ratio.

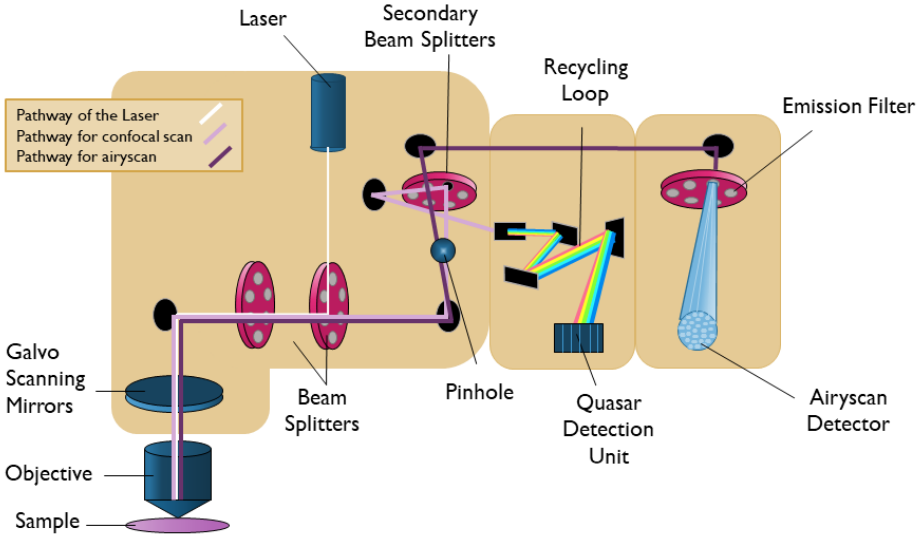

Figure 25: Schematic presentation of the LSM 880 confocal micrscope with Airyscan detector. Adapted from Zeiss Manual.

3.6.3. Electron Microscope

Through EM organic macromolecules can be observed in multiple states in their native environment. The size of the molecules can range from several tens of kilo daltons to mega daltons and whole cells or tissue sections. This technique requires a much smaller sample amount than nuclear magnentic resonance (NMR) spectroscopy of crystallization and the maximum oberservable onject size is only limited by the specimen thickness than can be penetrated by an electron beam [382].
An electron microscope consists of 3 principle systems: an electron gun and condenser system, an image producing system and an image recording system. Additionally, a vacuum system containing pumps and a power supply are required.
The electron gun produces the electron beam and a condenser system focuses this beam onto the object. The electrons leave the negatively charged cathode and are accelerated towards the anode, where they pass through the central aperture at constant energy. The intensity and angular aperture of the beam are controlled by a condenser lens system between then gun and the specimen.
The image producting system consists of an objective lens, a movable specimen stage and intermediate and projector lenses. The objective lens produces a real intermediate image that is further magnified by the projector lens (Fig. 26).
Lastly, the image recording system is necessary to convert the electron image into a reproduction that is perceptible to the human eye. This is achieved by allowing the electrons to fall on a fluorescent screen or by capturing the image digitally to display it on a computer monitor [383].
Two recent innovations have contributed to the rapid progress of this technique. The first one is the development of the direct electron detector (DED): it detects the electrons directly and reads them at a high frame rate without a mechanical shutter. The use of monolithic active pixel sensors (MAPS) greatly improves the signal to noise ration in EMs.
The second improvement concerned that image processing. Most samples contain more than one unique 3D structure which caused the image to be blurry. However, a breakthrough came from the development of statistical algorithms that were based on maximum likelihood procedures that eventually lead to a reduction of noise [384] [385] [386].
The specimen is generated by plunging the sample into a cryogen, which is usually liquid ethane. Then it is loaded into the column of an EM operating at high vacuum and low temperatures to keep the ice amorphous, which reduces the effect of radiated damage, since the electrons could scatter on crystalline ice [382].

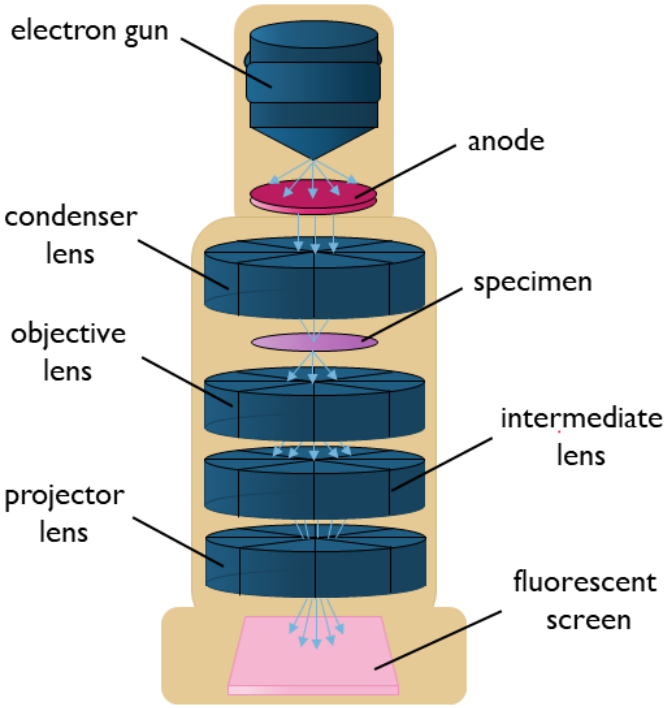

Figure 26: Schematic presentation of an electron microscope. Adapted from [383]

3.7. Protein Analysis

3.7.1. Cell Lysis

Cell lysates of the electroporated PLC3 and Huh7.5 cells were analyzed by SDS–PAGE followed by western blotting at different time points.
The electroporated cells were seeded in 6 well plates ($1x10^6$) or 10cm dishes ($6x10^6$) at the point of cell lysis. The lysis buffer was B1 buffer containing protease inhibitors (Tab. 5). First, the cells were washed three times with PBS and were lysed in cold lysis buffer (10cm dish: 200 µL, 6 well plate: 60 µL). The lysate was then collected immediately in Eppdendrof tubes and incubated for 20 minutes on a turning wheel at 4 °C. Next, the samples were centrifuged at 14 000 rpm at 4 °C for 15 min. All cell membrane debris was pelleted during the spin, whereas the soluble proteins remain in the supernatant.
At last, the supernatant was collected and stored at −20 °C.

3.7.2. Bicinchoninic Acid Protein Assay

After cell lysis, protein concentration of the cell lysates need to be measured to load equivalent amounts of proteins onto SDS–PAGE gels to be able to make comparisons.
First, a Bovine serum albumin (BSA) standard curve was prepared by serial dilution with the

following concentrations:

- 5000 µg mL^{-1}
- 2500 µg mL^{-1}
- 1250 µg mL^{-1}
- 625 µg mL^{-1}
- 312,5 µg mL^{-1}
- 156,25 µg mL^{-1}
- 0 µg mL^{-1}

A solution of bicinchoninic acid and Cu(II)SO_4 was prepared in a 50:1 ratio.
10 µL of each BSA standard sample, which was measured as a duplicate to ensure accuracy of the measurement, and of each cell lysate sample were mixed with the bicinchoninic acid solution and incubated for 30 min at 37 °C.
Finally, the OD was measured at 562 nm.

3.7.3. Subcellular Fractionation

The fractionation of subcellular compartments was used to characterize the distribution of viral proteins in the cell.
Subcellular fractionation was performed using the subcellular protein fractionation kit for cultured cells following the supplier instructions (Tab. 10).
Next, the fractioned lysate was analyzed by SDS–PAGE gel electropohoresis and western blot (chapters 3.7.4&3.7.6).

3.7.4. SDS–PAGE gel electrophoresis

The SDS–PAGE acrylamide gel electrophoresis was used to separate proteins collected from cell lysates.
The acrylamide concentration of the gel depends on the size of the protein that needs to be detected.
The gel was divided into the separation gel below and the stacking gel above containing the wells, which were filled with protein samples. The volumes for the different kind of gels can be found in Tab. 24 and 25.
The samples were mixed with 4x Laemmli buffer (containing DTT, Tab. 5) and heated up

to 70 °C for 10 min to denature the proteins. Next, they were applied onto the SDS gel in a tank surrounded by 1 L migration buffer. A constant voltage of 80 V was applied to the samples when they cross the stacking gel. The voltage was then increased to 150 V when they reached the separation gel.

Table 24: Components of a 10% acrylamide separation gel for gel electrophoresis

Chemical	Volume [mL]
Water	4.8
Acrylamide 40% (37:5:1)	2.5
Tris HCl 1.5 M (pH 8.8)	2.5
SDS 20%	0.1
APS 10%	0.1
TEMED	0.012

Table 25: Components of one stacking gel for gel electrophoresis

Chemical	Volume [mL]
Water	3.2
Acrylamide 40% (37:5:1)	0.5
Tris HCl 1.5 M (pH 6.8)	1.25
SDS 20%	0.03
APS 10%	0.03
TEMED	0.006

3.7.5. Colloidal Blue Staining

The colloidal blue stains proteins on a SDS–gel.
After the migration was finished the gel was incubated in fixation solution (Tab. 5) for 2 hours at RT under constant shaking. Next, the gel was washed 3 times with MilliQ water for 10 minutes each time under constant shaking. The staining was carried out with colloidal blue staining solution for 2 days (at least one day) under constant shaking.

3.7.6. Western Blot

After the migration was finished the proteins were transferred to a nitrocellulose blotting membrane. Therefore, the gel and the membrane were placed in a cassette surrounded on both

sides by whatman paper and a fiber pad, which had previously been soaked in transfer buffer (Tab. 5). The chamber was placed back into the tank, while the gel side of the cassette holder is facing the cathode (–) and the membrane side is facing the anode (+) and filled with 1 L of transfer buffer. An electric field of 100 V was applied for 90 min at 4 °C.
To block unspecific binding sites, the membrane was further incubated with 10 mL blocking solution (Tab. 5) at RT for 1 h while shaking.
Next, the primary antibody (12) was added in 10 mL of a 1x PBS containing 0.2% Tween and 2% BSA solution. The nitrocellulose membrane was incubated overnight at 4 °C while shaking.
The next day, the membrane was washed 3 times with washing solution (Tab. 5) for 10 min each at RT.
The HRP–conjugated secondary antibody was diluted 1:20000 in 10 mL of blocking solution was added to the membrane for 45 min at RT. The membrane was washed 3 times with washing solution.
To reveal the specific bands, the membrane was incubated with 1,5 mL of a substrate solution (Tab. 10) for 1 min or 5 min at RT that produces a chemoluminescent signal which can be detected after exposure on an X–ray film. The image is then revealed using a film developer.

3.7.7. Immunoprecipitation

An immunoprecipitation was performed to increase the ORF1 concentration to ease the detection by western blot and to purify the protein for mass spectrometry.
After electroporation the cells were seeded in at least one 10cm dish and grown between 4h and 3 days. Then, the cells were lysed in a larger amount (400 µL–1 mL) of lysis buffer and IP was either performed directly or lysates were stored at −20 °C.
Next, protein G sepharose beads were equilibrated with lysis buffer by washing and centrifuging them 3 times at 6000 rpm at 4 °C. To remove proteins binding unspecifically to the beads, the cell lysate (500 µg) was first pre–cleared with 40 µL of beads for 30 min at 4 °C on a spinning wheel. Afterwards, the pre–cleared cell lysate was incubated with the tag directed antibody (Tab. 12) for 2 h at 4 °C on a spinning wheel. Now, 40 µL of beads were added to the cell lysate antibody mixture and incubated for another 2 h in the same conditions. After this, the beads were washed 6 times with 500 µL PBS NP–40 0.5%.
Finally, the proteins attached to the beads were eluted in 50 µL of 4x Laemmli Buffer by heating them for 10 min at 70 °C.
Afterwards, the immunoprecipitates can be analyzed by SDS–PAGE followed by western blotting or mass spectrometry (section 3.7.6 or section 3.7.8).

3.7.8. Mass Spectrometry

Mass spectrometry (MS) is a technique used to detect, sequence and quantify molecules based on their mass to charge (m/z) ratio.
To be measured by the spectrometer, the molecules are ionized in the gas phase by electronic ionization. Thus the molecules undergo fragmentation and are separated by the mass spectrometer according to their m/z ratio. A magnetic field then deflects the path of the individual ions based on their m/z ratio and subsequently they hit the ion detector. The produced result displays the m/z ratio of the ions versus their abundance.
The spectrometer consists of 3 principal components. An ion source that ionizes the molecules and produces the gas phase, an analyzer that sorts ions according to their m/z ratio and a detector that records the abundance for each resolved ion species.
Proteins are very big molecules that cannot be resolved by a mass spectrometer, therefore they need to be digested into smaller peptides. The most commonly used enzyme is trypsin, but other enzymes can be used as well.
The sample preparation for analysis by mass spectrometry can be found in previous sections (Chapter 3.7.7, 3.7.4 and 3.7.5). To sum it up, after electroporation of the tagged HEV p6 genome in PLC3 cells, the cells were lysed and the tagged ORF1 protein was immunoprecipitated. Next, the eluate ($40\,\mu L + 20\,\mu L$) was separated in 2 fractions on a SDS gel. One half of the SDS gel was subjected to western blot and the other half was stained with colloidal blue. With the help of the revealed film, the desired bands were cut from the SDS gel. Finally, the proteins from the band were analyzed by the mass spectrometer.
NanoLC–MSMS analyses of the protein digests were performed on a UltiMate–3000 RSLC-nano System coupled to a Q–Exactive instrument (Thermo Fisher Scientific). Collected raw data were processed and converted into *.mgf peak list format with Proteome Discoverer 1.4 (Thermo Fisher Scientific). MS/MS data were interpreted using search engine Mascot (version 2.4.0, Matrix Science) with a tolerance on mass measurement of 0.2 Da for precursor and 0.2 Da for fragment ions, against a composite targetdecoy database (40584 total entries) built with Swissprot *Homo sapiens* database (TaxID=9606, 20 May 2016, 20209 entries) fused with the sequences of ORF2 (H9E9C9-HEV) and a list of classical contaminants (119 entries). Carbamidomethylation of cysteine residues, oxidation of methionine residues, protein N–terminal acetylation and propionamidation of cysteine residues were searched as variable modifications. Up to one trypsin or three Asp–N missed cleavage were allowed. Semi–specific cleavage was also authorized. Peptides were filtered out according to the cutoff ion score $>$ 25 and a minimal size of 7 amino acid residues. The MS experiments were carried out by our collaborator Jean–Michel Saliou (Proteomics and modified peptides platform, Institut Pasteur de Lille).

4. Objectives

The objective of this study is the characterization of the HEV replicase and thereby the replication step during the life cycle of the virus. This main goal can be divided into three different subgoals.

The first objective is the identification of the subcellular localization of HEV replication. The second subgoal consists of the analysis of cleavage of the ORF1 protein, since it is currently unknown whether or not the protein is processed. Thirdly, we investigated whether or not the ORF1 protein induces membrane rearrangement in host cells.

All subgoals require the use of antibodies to detect the ORF1 protein (Immunofluorescence and Western Blot). However, there is no commercial or functional antibody against the ORF1 protein available, therefore we inserted tags into the non–structural protein genome. The very first part of this thesis serves to validate the tagged constructs in different assays to ensure viral replication and infectivity of HEV are preserved and legitimate the epitope–tag strategy.

Then, the ORF1 expression and processing were studied overtime by Western blotting by using either the *Gaussia* luciferase replicon system, the heterologous expression system and an HEV cell culture system.

Furthermore, the characterization of potential cleavage products was undertaken by mass spectrometry analysis to identify their sequences.

Not only the HEV replicase was studied but also its subcellular localization and colocalization with host cellular markers as well as with viral RNA. This was carried out by *in situ* hybridization with probes using the RNAscope® technique.

The identification of membrane rearrangement by the ORF1 protein was studied by transmission electron microscopy and immuno–gold staining.

5. Results

5.1. HEV constructs

In this study, three different systems were used to characterize the HEV replicase (Fig. 27). The HEV p6 contains all three viral genes in full length and is therefore infectious. The productive cell lines for HEV are PLC3 cells (Tab. 6), a cell culture system that was developed in the HEV lab [186]. The HEV p6 allows the most accurate interpretation of the viral life cycle as all three phases (entry, replication and egress) are represented.
The HEV p6–GLuc replicon contains the full length ORF1 gene and a *Gaussia* luciferase reporter gene that substitutes the majority of the ORF3 and the ORF2 protein. This substitution allows to quantitatively analyze the replication step in isolation. The p6–GLuc replicon can be manipulated in a BSL–2 facility since it is not infectious.
The heterologously expressed HEV pTM plasmid contains the full length ORF1 gene as well. It does not contain the other viral proteins, but they can be expressed by transfection of a separate plasmid. The advantage of this plasmid is the T7–controlled expression of the ORF1 protein in H7–T7–IZ cells that constitutively express the T7 polymerase. Furthermore, a separate expression of the ORF1 protein alone allows us to study effects that may be induced by the ORF1 protein only.
In this report, the main focus lies on the HEV p6 and the HEV p6–GLuc replicon. Results concerning the heterologously expressed ORF1 can be found in more detail in the PhD thesis of Cyrine Bentaleb.

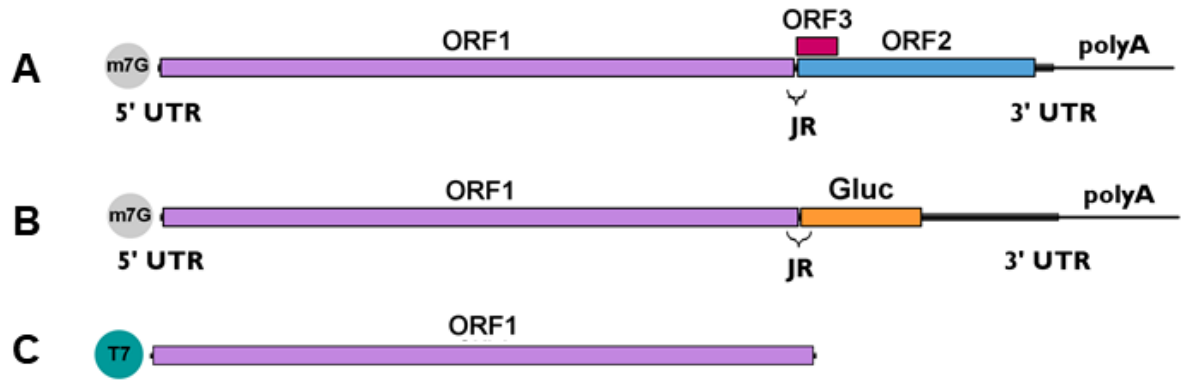

Figure 27: HEV constructs that were used in this study. **(A)**: Full length HEV p6 genome that contains ORF1, ORF2 and ORF3. JR= junction region, UTR= untranslated region. **(B)**: HEV p6–GLuc replicon that contains the full length ORF1 protein and truncated ORF2 and ORF3 protein. The majority of the ORF2 and the totality of the ORF3 was replaced by a *Gaussia* luciferase reporter gene. (**C**): The HEV pTM ORF1 plasmid contains the full length ORF1 gene that lies under the control of the T7 promoter.

5.2. Insertion of Tags into the ORF1

As there is no commercial and functional antibody available against the ORF1 protein, 2 different epitopes were inserted in 7 locations of the orf1 sequence (Fig. 28). All location sites starting with an H represent the insertion of an HA tag while all sites starting by V indicate a V5 epitope insertion.

The goal when choosing a location for inserting a tag was to not impact the replication efficacy of the p6–wt–GLuc replicon or the p6 HEV.

The H1 location lies at the C–terminus of ORF1 in front of the stop codon, so that the tag would not disturb the integrity of the polyprotein.

All the other epitopes were inserted into the HVR of ORF1, since this region can tolerate small insertions and deletions without compromising the replication ability of the polyprotein. Some insertions have even led to an increase of the adaption of the virus to cell culture, notably the insertion of the human ribosomal S17 protein [102].

The H2 and V2 positions were chosen based on an insertion that has been found in a different HEV strain. In this case, the S19 ribosomal protein insertion was found in this position while the virus was still replicating (Fig. 28 (A) [102]). Therefore, this position appeared to be a promising epitope insertion site.

The H3 and H4 epitopes are located at the beginning and the end of the S17 insertion respectively. And the H5 and H6 are inserted into the proline rich region of the HVR while conserving the position of the proline residues (Fig. 28 (C)).
Finally, the V1 insertion site was chosen based on a sequence alignment between the V5 epitope and the HVR amino acid sequence. A position was found, where four amino acids could remain unchanged, whereas three amino acids were mutated and seven were inserted (Fig. 28 (B)).
Other tags (HA and c–myc) in 6 different positions were previously tested as well, however, they did not replicate efficiently or the ORF1 protein was not detectable in immunofluorescence or western blot experiments (data not shown).
At first, all tags were inserted into the p6–wt–GLuc replicon genome to test their replication efficacy. If the tagged constructs showed a similar replication capacity as the p6–wt–GLuc, the tags were further inserted into the infectious p6 genome.

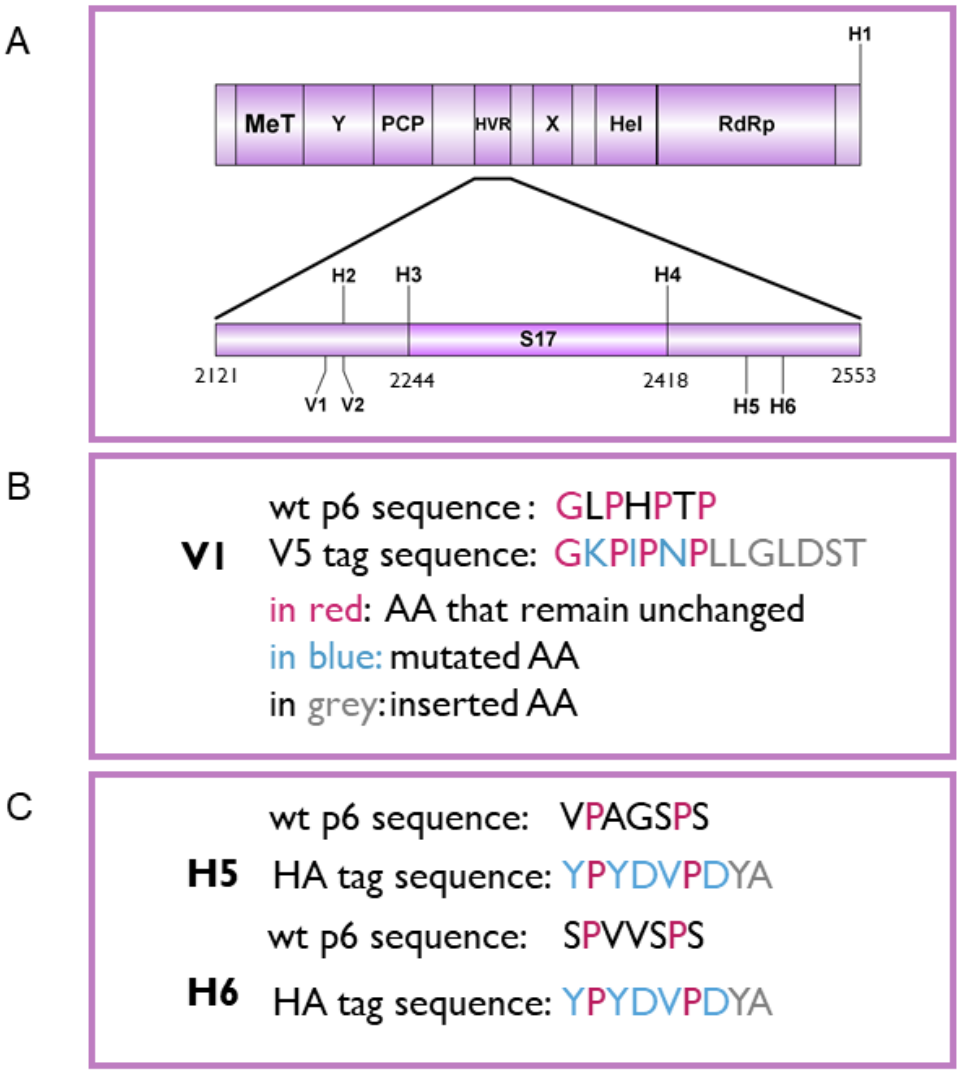

Figure 28: Insertions of HA and V5 epitopes into the ORF1 sequence. **(A)**The ORF1 and its functional domains are designated as methyltransferase (MeT), Y domain (Y), papain–like cysteine protease (PCP), hypervariable region (HVR), macro domain (X), helicase (Hel), RNA–dependent RNA polymerase (RdRp). Insertion position of an HA epitope at the C–terminus of ORF1 is localized (H1). A focus on the HVR enables to locate the human S17 ribosomal protein insertion (S17) of the HEV Kernow C–1 p6 strain [102]. Two other sites of insertion of V5 or HA epitopes are shown: V1 and V2 for V5 epitope insertions and H2 for HA epitope insertion. **(B)** Insertion strategy for the V1 epitope: Alignment of the V5 epitope and the HVR. Amino acids that remained unchanged are in red. Mutated amino acid residues are in blue and inserted amino acid residues are in grey. **(C)** Insertion strategy for the H5 and H6 epitope. The goal was to keep the proline–residues in the proline rich region unchanged. The color scheme is the same as in (B).

5.3. Replication Kinetics

5.3.1. Replication Efficacy of the p6–GLuc replicons

The luciferase activity of the p6–wt–GLuc and tagged p6–GLuc constructs was monitored to determine their replication efficacy and the impact of the inserted epitope on the replication efficacy of the replicon.
PLC3 and Huh7.5 cells were electroporated with p6–GLuc replicon RNA and plated in 24 well plates. Two clones of each replicon constructs were analyzed to compare their replication performance.
As the *Gaussia* luciferase is secreted from the cell, the supernatant was sampled over the course of 5 days starting from 1 dpe. The replication fold was determined by normalizing the obtained relative light units of all time points to 1dpe (Chapter 3.3.1).
The p6–GAD–GLuc serves as a negative control in this experiment as it is a non–replicative mutant containing a mutation from GDD to GAD in a conserved catalytic motif of the RdRp, which abolishes replication [387].
Indeed, it can be observed that the p6–GAD–GLuc non–replicative control shows a substantially lower replication fold (replication fold <2) in PLC3 cells (Fig. 29).
The tagged constructs showed different replication efficacies.
The p6–H1–GLuc and p6–H2–GLuc show a low to moderate degree of replication compared to the p6–wt–GLuc over the course of 5 days (at day 5 (13%) and (24%) respectively), whereas the other p6–GLuc HA tagged constructs (H3–H6) show a more varied replication efficacy ranging from 10% to 48% . In preliminary experiments, we tried to detect the HA–tagged ORF1 protein in lysates from p6–GLuc–electroporated PLC3 cells and the H3–H6 tagged constructs were not detected at all, while the H1 and H2 tagged ORF1 showed a faint band (data not shown). Therefore, the H3 to H6 constructs were not considered for further applications.
The insertion of the HA tag in the H1 position shows only 13% of the replication efficacy of the p6–wt–GLuc at day 5. The lower *Gaussia* luciferase expression in this construct is probably due to the insertion of the HA tag into a regulatory element, the subgenomic promoter, located between the C–terminus of the RdRp and the transcription starting site of the subgenomic RNA (Fig. 27 (B)) [97].The V5 tagged p6–GLuc constructs replicate with an efficacy of at least 65% at 5dpe compared to the p6–wt–GLuc in both cell lines. The p6–V1–GLuc clone 2 replicates most efficiently with up to 91% compared to the p6–wt–GLuc.
It is important to note that the insertion of the H2 epitope is located at the same position as the V2 tag. Although, the p6–H2–GLuc construct replicates less efficiently than the p6–V2–gluc replicon. The loss of replication capacity might be caused by their different sequence compositions.

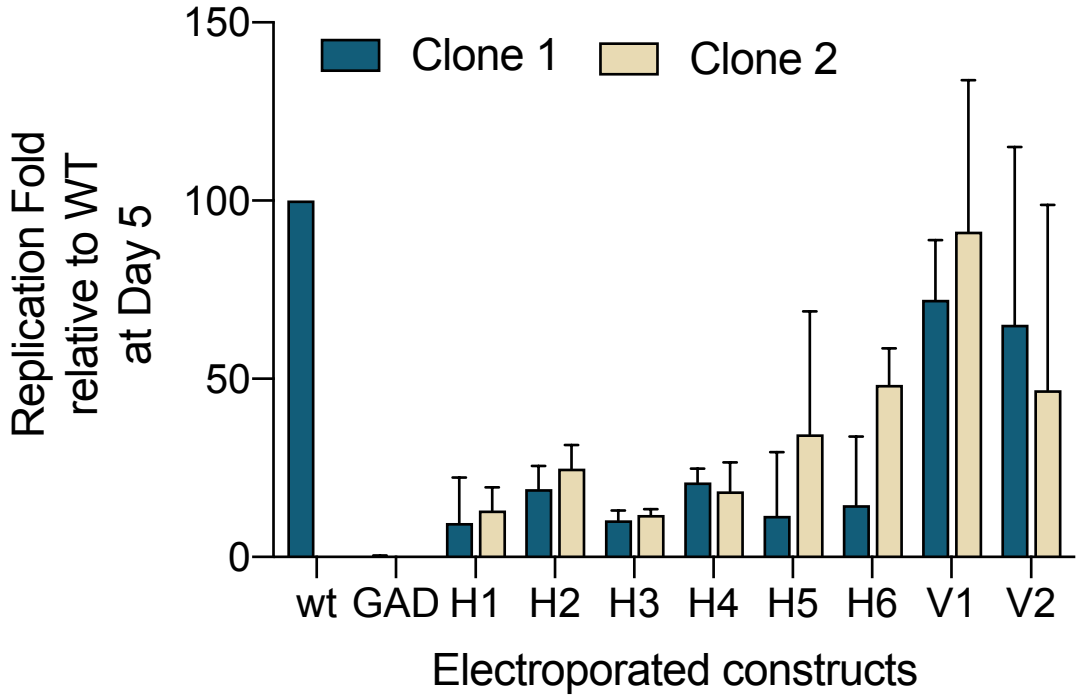

Figure 29: Replication efficacies of HEV replicons expressing tagged ORF1 in PLC3 cells as measured by luciferase activity. The relative light units (RLU) were measured everyday for 5 dpe by quantification of the *Gaussia* luciferase in the cell supernatant using a luminometer. Replication fold increases of the tagged p6–GLuc replicons and non–tagged p6-GLuc replicons (wt, GAD) were normalized to 1 dpe. The p6–GAD–GLuc is a non–replicative construct that possesses a mutation from GDD to GAD which inactivates the ORF1 polymerase. Experiments were conducted three times with 3 technical replicates. (n=3).

The replication fold over the course of 5 days of all replicons that were selected for further studies (p6–V1–GLuc, p6–V2–GLuc, p6–H1–GLuc and p6–H2–GLuc) as well as the non–tagged p6–wt–GLuc and the p6–GAD–GLuc is shown in Fig. 30. The replication fold of all constructs increases over time until 5dpe. It appears even more clearly that the V5 tagged replicons show a very similar kinetics to the non–tagged p6–wt–GLuc, whereas the HA tagged replicons show an impaired activity. The replication profile in PLC3 and Huh7.5 cells is fairly similar, however, the overall replication folds in Huh7.5 were approximatively 10 times reduced compared to those in PLC3 cells (Fig. 30).

Additionally, all constructs were analyzed in the presence of a replication inhibitor: after electroporation of PLC3 and Huh7.5 cells with the tagged and p6–wt–GLuc constructs, the replication was inhibited with sofosbuvir and monitored during 5 days (Fig. 30 (C&D)). Sofosbuvir is a nucleoside analog that was discovered as a treatment of HCV [388] and it specifically

inhibits the replication of HEV as well [328].
As a result, the replication efficacies of all constructs were significantly diminished by a factor of approximately 10 compared to their non–treated counterparts. For example, the sofosbuvir decreased replication efficacy of p6–wt–GLuc by 82% compared to the non–treated p6–wt–GLuc. These results were confirmed in Huh7.5 cells as well (Fig. 30 D). Therefore, it can be concluded that the shown kinetics were truly based on the replicative capacity of the replicon. Furthermore, the impact of sofosbuvir was proven by staining the ORF2 protein in electroporated PLC cells on coverslips untreated or treated with sofosbuvir (Appendices Fig.46). It was found that upon sofosbuvir treatment, the ORF2 staining in the cytoplasm disappeared and also the nuclear staining, while still present, appeared fainter. Thereby proving that the sofosbuvir inhibition was successful.
In conclusion, the p6–V1–GLuc and p6–V2–GLuc as well as the p6–H2–GLuc show a moderate to efficient replication with the p6–V1–GLuc construct replicating most efficiently. Also, the replication of all constructs was successfully inhibited by sofosbuvir. Therefore, the epitopes V1, V2 and H2 were inserted into the HEV p6 infectious strain. However, since the H1 insertion diminishes the transcription of subgenomic RNA, this epitope was not inserted into the p6 infectious strain but only into the ORF1 heterologously expressed from the pTM plasmid.

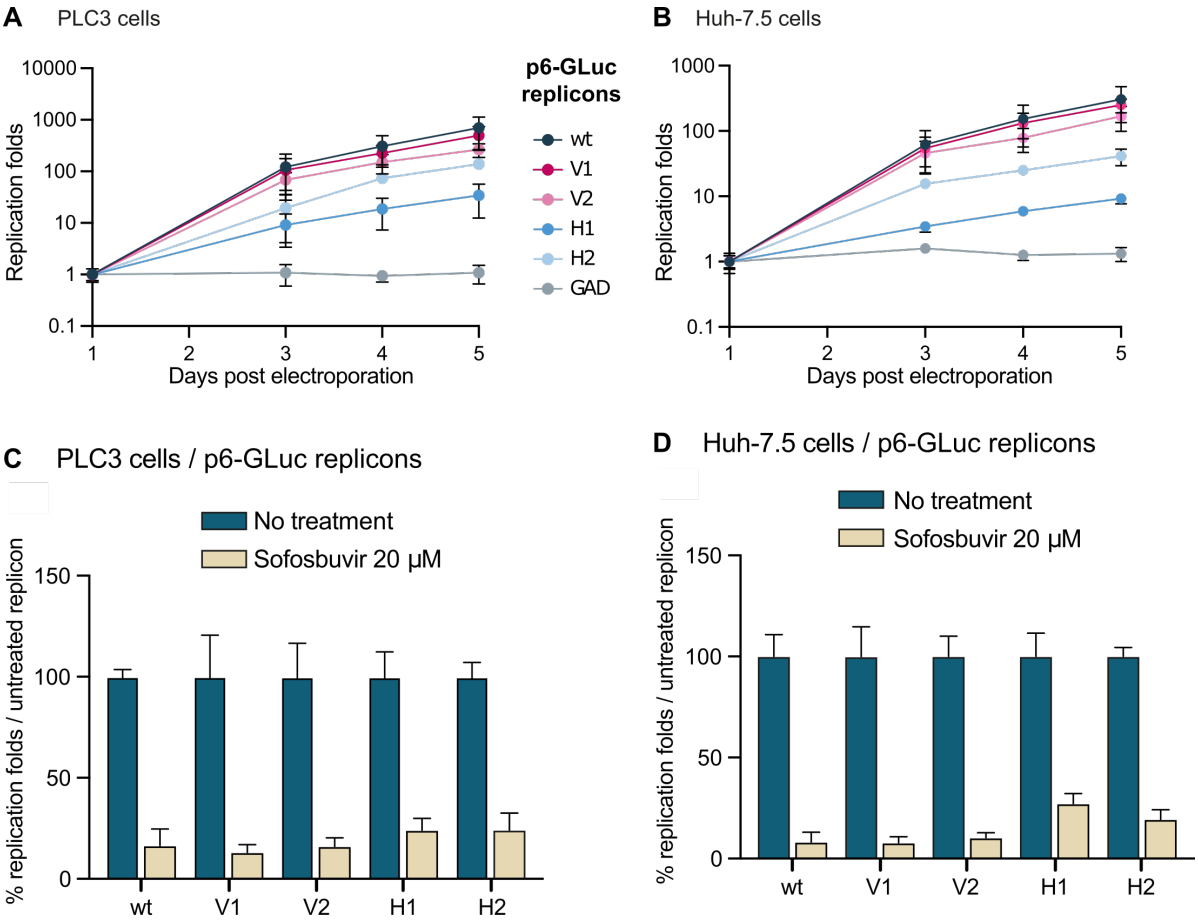

Figure 30: (A)&(B) Replication efficacies of HEV replicons expressing tagged ORF1 in PLC3 and Huh7.5 cells as measured by luciferase activity. The relative light units (RLU) were measured everyday for 5 dpe by quantification of the *Gaussia* luciferase in the cell supernatant using a luminometer. Replication fold increases of the tagged p6–GLuc replicons (V1, V2, H1, H2) and non–tagged p6–GLuc replicons (wt, GAD) were normalized to 1 dpe. The p6–GAD–GLuc is a non–replicative construct that possesses a mutation from GDD to GAD which inactivates the ORF1 polymerase. n=3. **(C)&(D)** Replication inhibition of p6–GLuc replicons in PLC3 and Huh7.5 cells in presence of sofosbuvir. Cells were electroporated with the tagged p6–GLuc replicons (V1, V2, H1, H2) or non–tagged p6–GLuc replicons (wt). Four hours post–electroporation, sofosbuvir, an effective polymerase inhibitor, was added to the cell medium at a final concentration of 20µM. The relative light units (RLU) were measured at day 5 post–electroporation by quantification of the *Gaussia* luciferase in the cell supernatants using a luminometer. Replication fold increases were normalized to 1 dpe. Percentages of replication were calculated to the non–treated corresponding construct. n=3.

5.3.2. Quantification of RNA in p6–GLuc replicon cells

The quantification of HEV RNA of the p6–GLuc replicons was performed to monitor the impact of the insertions on intracellular RNA levels.
PLC3 cells were electroporated with p6–GLuc replicon RNA and at each time point, RNA was extracted and reverse transcribed into cDNA (Chapter 3.3.2). Two qPCRs were set up in the lab targeting the orf1 gene or the *Gaussia* luciferase gene (probe design after [335] and [97]) (Fig. 31 (A)). The probe targeting the ORF1 gene enables us to quantify the genomic copy number whereas the probe targeting the GLuc gene quantifies both genomic and subgenomic RNA.
In these experiments, the p6–wt–GLuc serves as a positive control for efficient replication, the p6–GAD–GLuc is a non replicative mutant and the PBS control does not contain any viral RNA. Indeed, the PBS control did not show any amplification above background noise when targeted by the ORF1 probe or by the GLuc probe, hence its omission in Fig. 31. The p6–GAD–GLuc RNA amplification decreases from a copy number of $1.86x10^6$ for GLuc and $1.2x10^6$ for ORF1 to $2.65x10^5$ and $3.32x10^4$ copy numbers over time.
The gene copy numbers detected by the GLuc probe are approximately 10 fold higher compared to the ORF1 probe. Since the GLuc probe detects both the genomic and subgenomic genomes, the difference of a factor 10 is likely attributed to this fact.
The p6–wt–GLuc and p6–V5–GLuc RNA levels increase steadily over the course of 3 days in the case of the GLuc targeted gene (Fig. 31 (C)), while they stay relatively constant for the ORF1 targeted gene (Fig. 31 (B)). The genome copy number targeted by the ORF1 probe increases between 1.06–2.69 fold, while the increase amounts to 12–20.5 fold for GLuc targeted copy numbers. On the other hand, ORF1–probed RNA levels increase slightly over 3 days for the p6—H1-–GLuc. On the contrary, GLuc–probed RNA quantity of p6–H1–GLuc does not increase as much as the p6-–wt-–GLuc RNA copy numbers. In the case of p6—H1—GLuc, the number of ORF1–probed genome copies increases 3.1 fold over time, thereby lying in the range of the other functional constructs (Fig. 31 (B)). On the contrary, GLuc–probed RNA levels increase only by 2 fold (Fig. 31 (C)). This results led us to believe that the insertion of the H1 epitope at the C–terminus of the orf1 gene impacts the transcription of subgenomic RNA negatively.
The H2 tag was not tested in this context, since it was decided to include it in specific experiments at a later time point.
As a consequence the H1 tag was not inserted into the p6 HEV and only the V1, V2 and H2 tagged constructs were further characterized.

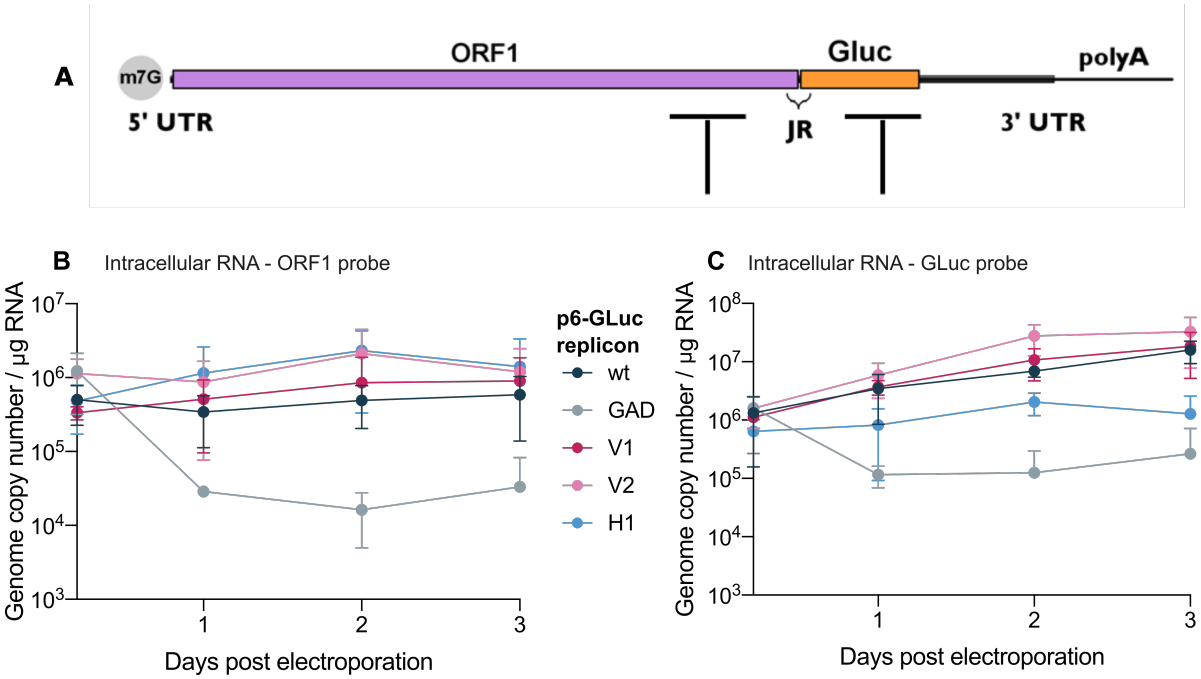

Figure 31: HEV RNA quantification in p6–GLuc electroporated–PLC3 cells expressing wild type or epitope–tagged ORF1. The probe design placement is shown in (A). Intracellular viral RNAs were quantified at 4 h, 1, 2 and 3 dpe by RT–qPCR targeting either ORF1 (B) or GLuc (C). Experiments were conducted three times with 2 technical replicates.

5.3.3. Quantification of RNA in p6 electroporated cells

To validate the insertion of the previously selected tags in the HEV p6 infectious system as well, PLC3 were electroporated with tagged or p6–wt RNA. At each time point, RNA was extracted from the cells and cellular supernatant and reverse transcribed into cDNA. For the qPCR of the orf1 gene, the probe from chapter 5.3.2 was used, while the probe targeting the ORF2/ORF3 overlap was published previously [381]. The probe targeting the ORF1 gene enables us to quantify the full genome copy number whereas the probe targeting the ORF2 gene targets both genomic and subgenomic RNA.

In addition to the analysis of intracellular RNA, the RNA of the supernatants were extracted and quantified as well, since the HEV p6 RNA can form viral particles that leave the cell.

In these experiments, the p6–wt serves as a positive control for efficient replication and the PBS negative control does not contain any viral RNA (Mock). Indeed, the amplification of the PBS control was below the limit of detection at all time points for both orf1 and orf3/2 probes (Fig. 32).

The gene copy numbers detected by the orf3/2 probe remain higher in cell lysates compared to the ORF1 probe, by approximately 2–5 fold. Since the orf3/2 probe detects both the genomic and subgenomic RNA and the orf1 probe only detects genomic RNA, it is logical that

the detected ORF2 gene copy number is higher.
Overall, the orf1 and orf2 copy numbers between the p6–wt and the tagged p6 constructs are similar. In cellular extracts, the p6–wt and V5 tagged p6 RNA increase between 4h and 3dpe and remain stable until 7dpe regarding the RNA detected by the orf1 (Fig. 32 (B)) and orf3/2 (Fig. 32 (C)) probes.
In contrast, in cell supernatants, the RNA targeted by the orf1 and the orf3/2 probes of the p6–wt and the V5 tagged constructs decreases slightly at 1 dpe and remains constant from 3dpe onwards (Fig. 32 (D,E)). Also, the RNA levels in the supernatant of orf1 and orf2/3 are similar. This is likely because of the absence of the subgenomic RNA in the cell supernatant. In general, the RNA levels of the p6–wt and the V5–tagged constructs are comparable. Thus, the RNA levels are not affected by the insertion of an V5 epitope into the orf1 gene. This is in line with the luminometry results that showed an efficient replication of the V5 tagged replicons compared to the wt replicon.
As a conclusion, the p6–V1, p6–V2 and p6–H2 constructs were subjected for further evaluation with a focus on the V1 and V2 construct.

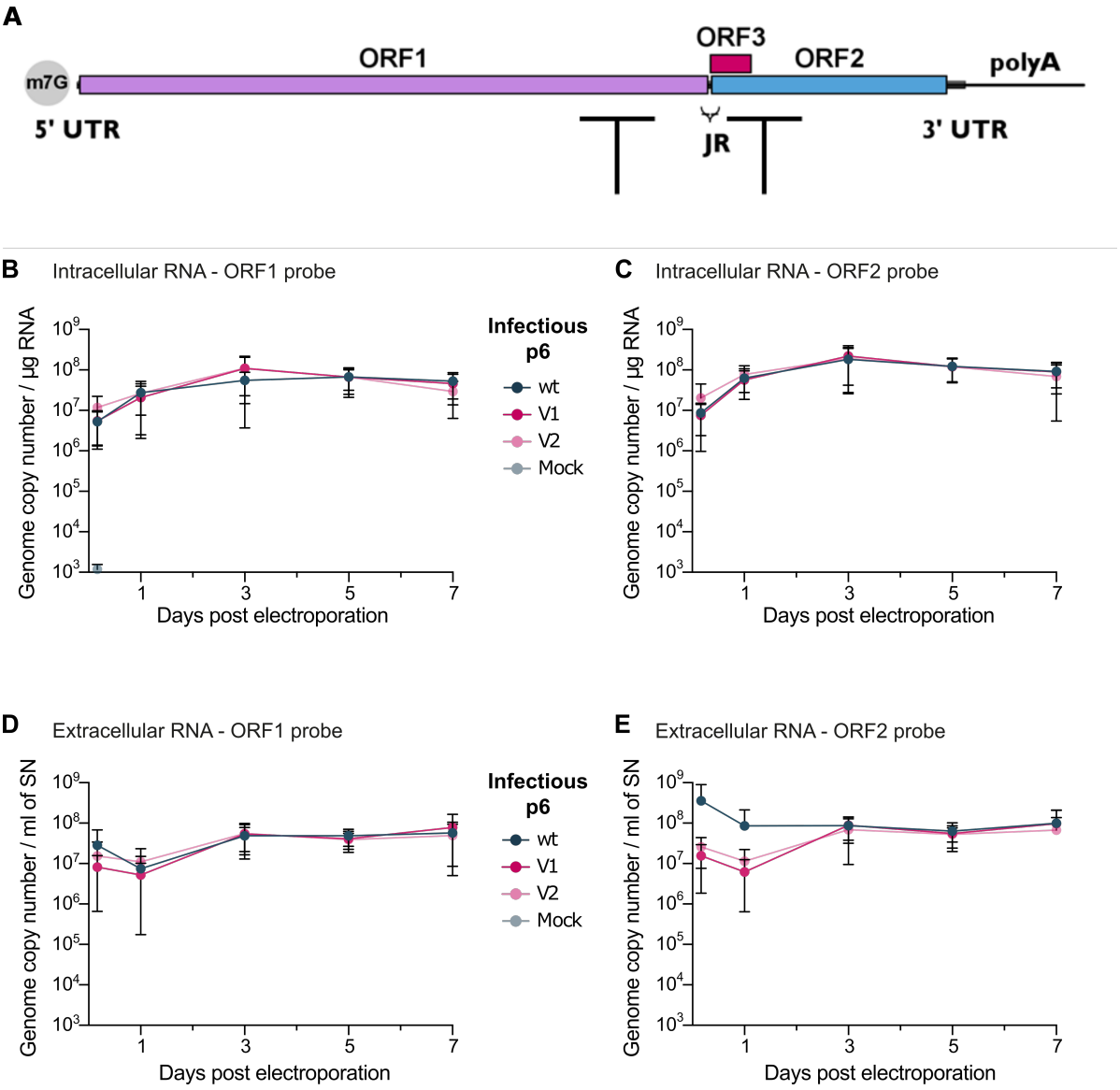

Figure 32: HEV RNA quantification in p6 electroporated–PLC3 cells expressing wild type or epitope–tagged orf1. Probe design placement is shown in (A). Intracellular (B,C) and extracellular (D,E) viral RNAs were quantified at 4 h, 1, 3, 5 and 7 dpe by RT-qPCR targeting either orf1 (B,D) or orf3/2 (C,F). Experiments were conducted three times with 2 technical replicates.

5.4. Determination of Infectious Titers

To further validate the insertion of the different tags in the HEV p6 genome, infectious titers of all constructs were determined.
Similarly to the procedures mentioned above, PLC3 cells were electroporated with HEV p6 tagged and non–tagged constructs and incubated with HEV medium 1 day after electroporation. After 10 days, the infectious supernatant was diluted in a 1/10 manner and Huh7.5 cells were infected with the pure and diluted supernatant. Three days later, the ORF2 protein was labeled by immunofluorescence and the infectious titer was measured (Chapter 3.2.3).
Furthermore, the supernatant of electroporated PLC3 and infected Huh7.5 as well as the Huh7.5 cell lysates were analyzed by western blot.

5.4.1. Validation by staining of the ORF2 protein

To measure the infectious titer of all constructs, the Huh7.5 cells were stained with anti–ORF2 antibody 1E6 (see Tab. 12) and infected cells were counted.
Measuring foci forming units revealed that the infectious titers lie between $4x10^4$/mL and $6x10^4$/mL for the p6–wt and the V5 tagged constructs. In contrast, the infectious titer of the p6–H2 lies at $2x10^4$/mL. The ratio of all titers is shown in figure 33 (A) and it can be observed that the p6–V1 and p6–V2 constructs' infectious titers are similar to the non–tagged p6 (94%). The p6–H2 construct, however, shows only 40% of the infectivity compared to the p6–wt.
The staining of the infected Huh7.5 cells was further verified by confocal microscopy. The immunofluorescence images (Fig. 33 (B)) show a cytoplasmic and nuclear localization of ORF2. The intensity and the pattern of the signal was similar between the p6–wt and the V5 tagged constructs, which is in line with the infectious titers mentioned above.
The ORF2 protein pattern of the Huh7.5 cells infected with the supernatant of H2 electroporated PLC3 cells also shows a nuclear and cytoplasmic localization, but the staining remains mainly nuclear. This seems logical since the infectivity of the p6–H2 construct is impacted due to the HA epitope.
To conclude, the V5 epitope has no significant impact on the infectivity of the tagged constructs. In contrast, the HA tag lowers the infectivity by more than 50%.

5.4.2. Analysis of Cell Supernatants and Lysates

To finish the characterization and validation of our tagged constructs, the expression of ORF1 and ORF2 after infection of Huh7.5 cells was analyzed. The supernatants of electroporated PLC3 and infected Huh7.5 as well as the Huh7.5 cell lysates were subjected to western blot

analysis.
Therefore, the ORF2 protein was detected in all three fractions and additionally, the infected Huh7.5 cell lysate was stained for the V5 tagged ORF1 as well.
In Fig. 33 (C) it can be observed that the ORF2 expression in the supernatant of PLC3 cells electroporated with the p6 wt and the tagged constructs is nearly identical. Very similar expression levels of the capsid protein concerning all constructs can be found in the supernatant of infected Huh7.5 cells as well. Although, the ORF2 expression in the supernatant of Huh7.5 cells is lower compared to those in PLC3 cell supernatants. In contrast, the ORF2 expression in lysates of Huh7.5 cells infected by the different p6 viral particles produced by PLC3 cells differs substantially. While p6–wt and V5–tagged p6 viral particles induce similar ORF2 levels in Huh7.5 cells, it is not the case for the p6–H2 particles produced by PLC3 cells. Quantification of the ORF2 band intensity show a decrease of 82% compared to the band detected in Huh7.5 infected by the p6–wt. This is in line with the previous results acquired from measuring the infectious titers and the less intense phenotype seen by confocal microscopy.
In addition, the ORF1 protein could be detected in cells infected with the p6–V1 and p6–V2 at a size of approximately 190 kDa (Fig. 33 (C)). The signal is fainter compared to the ORF2 protein signal, implying that the ORF1 protein is less expressed than the ORF2 protein.
On the other hand, the Huh7.5 cells infected by p6–H2 did not show any detectable expression of the ORF1 protein. This is likely due to the fact that this construct achieves a lower infectious titer and is less replication competent according to the luminometry experiments.
All in all, the insertion of the V5 epitope in the p6–wt appears to have little to no impact on the ORF2 expression in the supernatant or lysates of infected cells. On the contrary, the HA tag of the p6–H2 diminishes the ORF2 expression in Huh7.5 cell lysates.
In conclusion, the main focus of this study lies on the V5 tagged p6 and p6–GLuc constructs. Furthermore, the V1, V2 and the H2 epitopes were also inserted into the heterologously expressed plasmid.

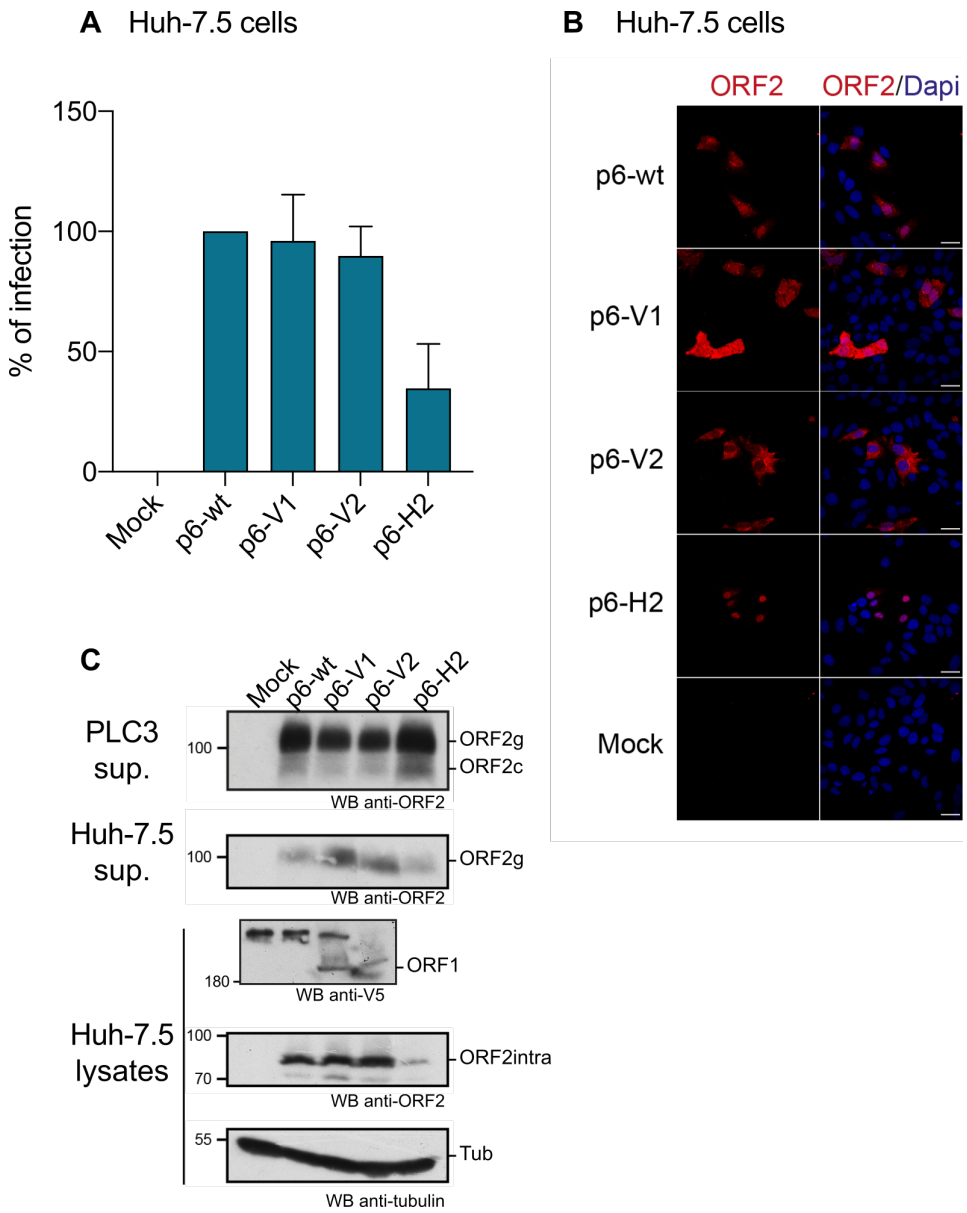

Figure 33: (A) Infectious titers of HEV p6 expressing epitope-tagged ORF1 polyprotein. Ten dpe, supernatant of PLC3 cells electroporated with p6–wt, p6–V1, p6–V2 or p6–H2 were collected to infect Huh7.5 cells. Three dpi, cells were fixed and stained with anti-ORF2 antibody (1E6). The number of positive cells from 3 experiments were counted in triplicate. Statistical analysis was performed using the Mann–Whitney test. **(B)** Huh7.5 cells were infected with the supernatant of PLC3 cells that were electroporated with HEV p6 expressing non–tagged ORF1 (p6–wt), V5–tagged (p6–V1, p6–V2) or HA–tagged (p6–H2) replicase. Huh7.5 infected with mock-electroporated PLC3 cell supernatant served as negative control (Mock). Three dpi, cells were fixed, permeabilized and stained with the anti-ORF2 antibody (1E6, red). Nuclei were stained with Dapi (blue). Scale bar = 30µm. **(C)** PLC3 cells were electroporated with p6–wt, p6–V1, p6–V2 and p6–H2. Ten dpe, proteins of cell supernatants were separated by SDS-PAGE electrophoresis, transferred onto a nitrocellulose membrane and probed with an anti-ORF2 antibody (1E6, first panel, PLC3 sup.). Huh7.5 cells were infected with PLC3 supernatants. Three dpi, Huh7.5 supernatants were also analyzed for ORF2 expression (1E6, second panel, Huh7.5 sup.). In parallel, Huh7.5 cells were lysed and total protein extracts were probed with anti–V5, ORF2 (1E6) and tubulin antibodies (last 3 panels, Huh7.5 lysates

5.5. ORF1 expression over time

The expression of the ORF1 protein was analyzed over time to study its kinetics and to examine whether or not potential cleavage products can be observed. After electroporation of the p6–GLuc replicon and the p6 infectious strain, the cells were cultured between 4h and 25d and then lysed (Chapter 3.7.1). Also, kinetic variations of ORF1 heterologously expressed was studied alongside. The ORF1 sequence is identical in all three expression systems.
Then, the proteins were separated by SDS PAGE and the V5 or HA tagged ORF1 was detected by western blot (Chapter 3.7.6).
The full length ORF1 protein has a size of approximately 194 kDa, thus a signal at a higher molecular weight than the top marker (180 kDa) is expected concerning all three systems that are being studied.

5.5.1. Expression of the ORF1 protein in p6 replicon cells

In Fig. 34 (A) the immunoblot of the V5 tagged ORF1 protein expressed through the p6–GLuc replicon is shown. Cells electroporated with the non–tagged p6–wt–GLuc replicon and the PBS control served as negative controls. Indeed, no signal for both negative controls can be observed. At higher than 180 kDa a signal was detected at all time points. This band corresponds to the full length form of ORF1, since the predicted molecular weight is calculated to be 194kDa. Interestingly, bands of smaller molecular weight were present that might correspond to potential cleavage products. In total, 6 bands can be identified and the band pattern is summed up in Tab. 26.
It is remarkable that the ORF1 protein can be observed very early on (4hpe), however, it is not clear whether this early onset expression is truly due to the replication of the replicon or a result of transcription and translation of the electroporated RNA.
The signal intensity of all bands is similar between 4hpe–12hpe, but on day 1 the intensity decreases, but is still detectable at day 3, and at later time points the ORF1 is not detectable altogether (data not shown). This is likely due to the inability of the replicon to be passed on after cell division. Also, the replicon does not produce viral particles, thus neighboring cells can not get infected.
At this point, the band pattern can not be interpreted since the V5 tag is situated in the HVR, for that reason, the N–terminus and C–terminus of each potential cleavage product is unknown.

5.5.2. Expression of the ORF1 protein in p6 electroporated cells

Next, the ORF1 expression of the p6 infectious constructs was analyzed in a similar manner. Similarly to the band pattern obtained from the p6–GLuc replicon system, the major band is detected at higher than 180 kDa and smaller bands can be seen between approximately 90 kDa and 180 kDa for the V5 tagged ORF1 (Fig. 34 (B) & Tab. 26). Contrarily to the p6–GLuc replicon kinetics, the V5 tagged ORF1 expression under the p6 infectious system can be detected until 25 dpe. In this case, the viral particles can infect neighboring cells and therefore are propagated even after several passages. The signal gradually decreases over time, but at 25 dpe the full length ORF1 and also its potential cleavage products are detected albeit less intense. The highest band intensity can be found between 4h and 3 dpe. However it is possible that the ORF1 expression at the early time points is not a result of viral replication yet, but due to translation of electroporated RNA.
Overall, the band patterns of the two different systems are similar, but several differences can be found (Tab. 26). For example, the infectious p6–V1 produces 6 bands and not 5, which lie between 90 kDa and 180 kDa. Likewise, the potential cleavage products can not be interpreted so far, since it is unknown whether the cleavage occurs at the N– or at the C–terminus of the polyprotein. The results obtained with the p6–V1 and p6–V2 were also in part confirmed by the expression of the p6–H2 construct in PLC3 cells (Fig. 47). The full length ORF1 protein was detectable at early and later time points (1dpe–25dpe), however smaller bands were not visible, even at longer exposure times.

5.5.3. Expression of the heterologously expressed ORF1 protein

The expression kinetics was also studied in H7–T7–IZ cells that heterologously express the ORF1 protein (Fig. 34 (C)). The experiments concerning this part were conducted by Cyrine Bentaleb and more details can be found in her PhD thesis manuscript. The identified minor bands are summed up in Tab. 26, the most intense bands are labeled by stars.

Table 26: Band Pattern of the ORF1 protein. Stars correspond to the in Fig. 34 marked bands.

p6–GLuc replicon	infectious p6	heterologous expression
180	180 (***)	180
150 (***)	150 (**)	160 (***)
130	120	130 (**)
120 (**)	110	110 (*)
100	100 (*)	100
95 (*)	90	95

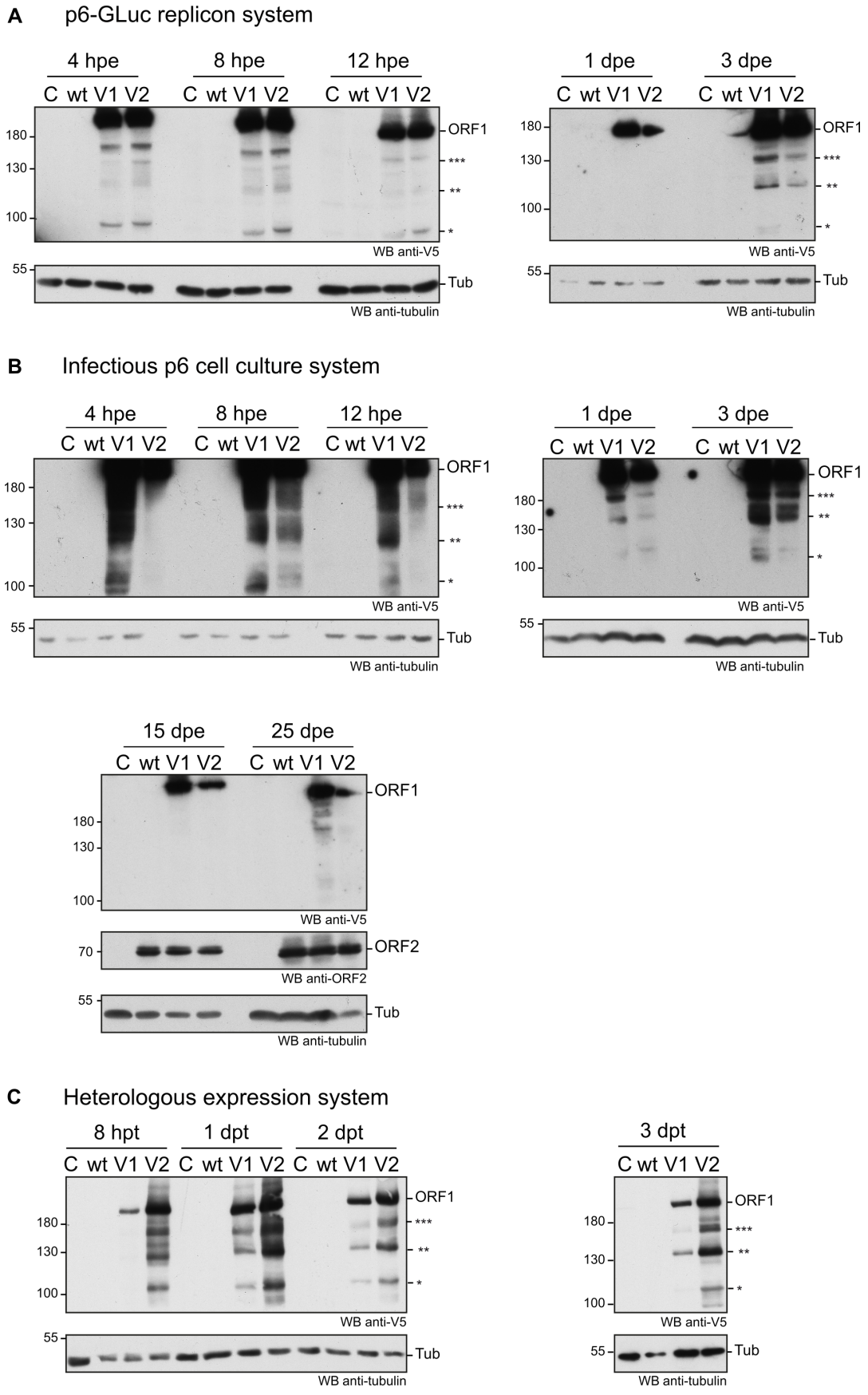

Figure 34: Expression of the V5–tagged ORF1 protein over time in different cellular systems.

Figure 34 ***(previous page)*****:** Expression of the V5–tagged ORF1 protein over time in different cellular systems. The stars indicate the most intense putative cleavage ORF1 products for each system. **(A)** Expression of the ORF1 protein in the p6–GLuc replicon system. PLC3 cells were electroporated with a replicon expressing the wild type untagged ORF1 protein (wt) or the V5–tagged ORF1 (V1 or V2). Total cell lysates were collected in presence of protease inhibitors at 4, 8, 12 hpe and 1 and 3 days post–electroporation (dpe). Mock–electroporated cells served as negative control (C). The band migrating higher than 180 kDa corresponds to the full–length ORF1 protein (ORF1). The immunoblot was probed either with an anti–V5 antibody or an anti–tubulin antibody to control for even loading. Molecular weight markers are indicated in kilodalton. **(B)** Expression of the ORF1 protein in the infectious p6 cell culture system. PLC3 cells were electroporated with the p6 infectious strain expressing the wildtype untagged ORF1 protein (wt) or the V5–tagged ORF1 (V1 or V2). Total cell lysates were collected in presence of protease inhibitors at 4, 8, 12 hpe and 1, 3, 15, 25 dpe. Mock–electroporated cells served as negative control (C). The band migrating higher than 180 kDa corresponds to the full–length ORF1 protein (ORF1). The immunoblot was probed either with an anti–V5 antibody or an anti–ORF2 (1E6) antibody or an anti–tubulin antibody to control for even loading. Molecular weight markers are indicated in kilodalton. **(C)** Heterologous expression of the HEV p6 ORF1 protein. H7–T7–IZ cells were transfected with a pTM plasmid expressing the wild type untagged ORF1 protein (wt) or the V5–tagged ORF1 (V1 or V2). Total cell lysates were collected in presence of protease inhibitors at 8 hours post–transfection (hpt), 1dpt, 2dpt and 3dpt. Mock–transfected cells served as negative control (C). The band migrating higher than 180 kDa corresponds to the full–length ORF1 protein (ORF1). The immunoblot was probed either with an anti–V5 antibody or an anti–tubulin antibody to control for even loading. Molecular weight markers are indicated in kilodalton.

5.5.4. Comparison of the ORF1 expression systems

In the previous subchapter it became apparent that the band pattern of the ORF1 protein is similar in the three expression systems used, however the potential cleavage bands have slightly different sizes dependent on the system used. It was therefore of interest to compare the band pattern while migrating all samples on the same SDS–PAGE gel.

The limiting factor in these experiments is the low intensity of the ORF1 full length expression and even more so of the smaller bands. Thus, it was decided to perform an immunoprecipitation to enrich the tagged ORF1 proteins (Chapter 3.7.7).

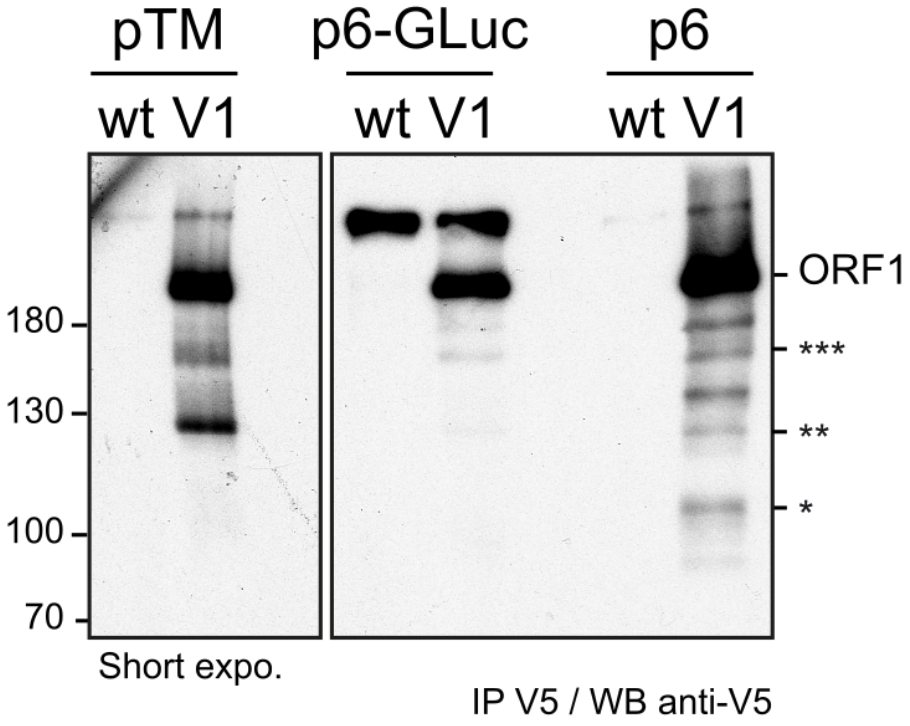

Figure 35: Immunoprecipitation of the ORF1 protein in all three expression systems. H7–T7–IZ cells were transfected with the ORF1–V1 and lysed 1dpe. PLC3 cells were electroporated with either p6–V1–GLuc or p6–V1 RNA and lysates were collected 3dpe. The IP was performed using the polyclonal goat anti–V5 antibody and the immunoblot was probed with a monoclonal mouse anti–V5 antibody (Tab.12). Cells transfected or electroporated with the non–tagged ORF1 served as a negative control. Molecular weight markers are indicated in kilodalton.

In Fig. 35 it can be observed that the intensities of the full length ORF1 protein are similar among all three systems, however, the smaller bands are detected in different intensities. Next to the full length ORF1, the heterologously expressed ORF1–V1 produces the main bands at 160 and 130kDa, the p6–V1–GLuc shows two faint bands at 180kDa and 160kDa and for the p6–V1 construct bands at 180kDa, 160kDa, 140kDa, 130kDa, 110kDa and 95kDa are detected . Following the IP of the PLC3/p6–V1, a better separated band pattern was detected compared to the crude lysate labeling (Fig. 34).
This time, the band at 160kDa (***) is in common between all tested systems. As it was stated in the previous part, the pattern is difficult to interpret, since it is unclear whether the potential cleavage occurs at the N– or at the C–terminus.

The difficulty of these experiments lies in the reproducibility of the detection of the potential cleavage product bands, since the band detectability can vary slightly among experiments. This might be due to a tight temporal regulation of their expression or their potential processing.

5.6. Cleavage of ORF1

It still remains uncertain if or how the ORF1 polyprotein might be cleaved. While a PCP domain was bioinformatically assigned in the ORF1 protein based on sequence homology [104], no enzymatic potential of this domain has been shown to date. Furthermore, a recent article challenged the borders and functionality of this domain, claiming that instead a fatty acid binding domain was identified downstream of the putative PCP domain [130]. Therefore, several protease inhibitors were tested on PLC3 cells that express the p6–GLuc replicon. The luciferase activity, the band pattern and the phenotype in regards of subcellular distribution were evaluated.
Furthermore, to exclude the possibility of the minor bands being the product of degradation, the proteasome was inhibited and the band pattern of the ORF1 protein was analyzed.
To gather more information concerning the potential cleavage products observed over time (Chapter 5.3), it was attempted to sequence all products by using mass spectrometry (MS).

5.6.1. Inhibition of the Proteasome

Proteasomes are large, multicatalytic protein complexes that cleave proteins into peptides intracellularly [389]. Usually, polymerized ubiquitin molecules serve as a signal for proteins to be shuttled towards the proteasome and subsequently being broken down proteolytically [390, 391].
In Fig. 34 it can be seen that next to the full length ORF1 protein, several bands of smaller sizes appear on western blot starting from 4hpe until 25dpe. While these bands could correspond to potential cleavage products, the possibility remains that these bands are a product of degradation. Thus, if the minor bands in question are indeed the result of protein degradation by the proteasome, they would be expected to disappear when treated with the proteasome inhibitor lactacystin.
The successful inibition of the proteasome was controlled using the HSP70 as a marker. This protein accumulates upon inhibition of the proteasome [392].
Therefore, cells electroporated with PBS, the p6–wt–GLuc and the p6–V1–GLuc replicon were treated with lactacystin and evaluated on western blot (Fig. 36, (B)). Since the lactacystin

molecule was dissolved in methanol, each sample was incubated also with methanol alone. It can be observed that while the tubulin control shows the same amount of protein in all samples, the HSP70 protein quantity increases slightly when treated with lactacystin in all three samples. As a consequence, it can be concluded that the inhibition of the proteasome was successful.

When treated with lactacystin, the tagged ORF1 protein shows a nearly identical band pattern compared to the non–treated or methanol treated samples. The full length ORF1 protein shows the strongest signal, but the typical minor bands are present as well. When comparing the intensities of the non–treated cells expressing the ORF1 protein and the lactacystin treated cells, no difference can be stated. This implies that the inhibition of the proteasome does not abolish the appearance of smaller bands. Thus, based on this experiment the observed minor bands are likely not the result of degradation by the proteasome.

In parallel, the inhibition of the proteasome was tested in H7–T7–IZ cells that were transfected with the wt–ORF1 and the tagged ORF1. The experiment was run at the same time by Cyrine Bentaleb. As can be seen in Fig. 36 (A), the same results were obtained that were previously described, corroborating the indication that the potential cleavage products are not a product of degradation.

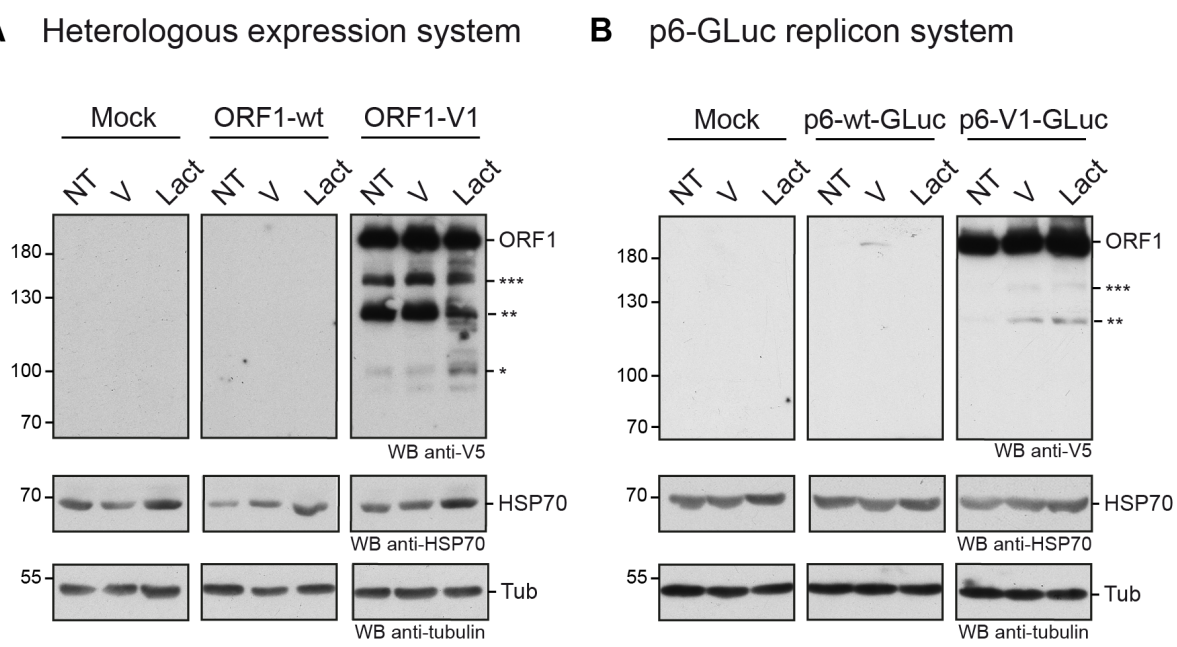

Figure 36: Treatment of cells expressing the V1–tagged ORF1 with the proteasome inhibitor lactacystin. NT: Non–treated samples, V: samples treated with methanol, since lactacystin was dissolved in methanol, lact: samples treated with 30µM lactacystin for 8h at 3dpe. HSP70 served as a positive control, since it accumulates when the proteasome is inhibited. The stars indicate the most intense putative cleavage ORF1 products. **(A)** H7–T7–IZ cells expressing the V1–tagged ORF1 treated with lactacystin show the full length ORF1 protein and smaller bands. **(B)** P6–V1–GLuc electroporated PLC3 cell lysates still show smaller bands in addition to the full length ORF1 upon treatment with lactacystin.

5.6.2. Protease Inhibition of ORF1

According to the bioinformatical analysis, that shows sequence homology to the RUBV protease domain, HEV possesses a papain like cysteine protease. Additionally, a zinc binding motif was identified within the PCP. In order to characterize these potential features, inhibitors of cysteine proteases and zinc chelators were chosen. The selection of the molecules to be tested was also based on a report by Saraswat *et al.* who analyzed the effect of a range of inhibitors and chelators on an *in vitro* model of HEV [129]. All molecules and concentrations can be found in Tab. 23.

Similarly to the luciferase kinetic experiments (Chapter 5.3.1) the replication efficacy of the p6–wt–GLuc replicon was followed over 5 days. The cells were treated with the different inhibitors right after electroporation until the endpoint of the experiment. The replication fold was calculated by comparing the RLU values of each time point to 1dpe.

Figure 37 shows the percentage of the replication fold of the p6–wt–GLuc replication treated with each molecule compared to the untreated p6–wt–GLuc. The p6–GAD–gluc and the p6–wt–GLuc treated with sofosbuvir serve as negative or non–replicative controls in this experiment.

The effect of the cysteine protease inhibitors E64d and Antipain with the concentrations used (1, 10 and 50 or 10, 100 and 200µM) on the p6–wt–GLuc replication was not significant (Chapter 7 Fig. 37 (A)). The replication fold remained at 77% or higher compared to the non–treated p6–wt–GLuc. E64d does not exhibit any cytotoxicity at the concentrations used and Antipain shows a decreased cell viability at the highest dose used (Fig. 48).

Leupeptin, a cysteine and serine protease inhibitor, showed slightly elevated inhibition at 500µM of the p6–wt–GLuc replication compared to the previously described cysteine protease inhibitors. The replication fold on day 5 is inhibited by 43%, while maintaining almost complete cell viability (Appendices Fig. 48).

The chelator EDTA did not decrease the p6–wt–GLuc replication fold at any concentration, nor was it toxic on PLC3 cells. On the other hand, the chelator TPEN showed cytotoxicity at 10µM. At the lower concentrations tested, no inhibitory effect on the replication efficacy could be stated.

Finally, the molecule Velpatasvir, that acts on the zinc binding pocket of the HCV NS5A through a yet unidentified mechanism of action, only showed a moderate effect on the replication fold of the p6–wt–GLuc replicon. Its IC_{50} on Huh7 cells expressing HCV is 50pM. At this concentration, no effect was observed but at higher concentrations it showed a moderate degree of inhibition of HEV replication (37% decrease compared to the p6–wt–GLuc).

To conclude, according to the luciferase kinetic experiments, there is little to no effect of the selected molecules on the HEV replicon replication fold. Nevertheless, it was tested whether or not any of the molecules had an impact on the band pattern of the ORF1 protein by performing a western blot (Fig. 37 (B)) against the V5 epitope. PLC3 cells electroporated with the p6–V1–gluc were incubated with all molecules listed above at the highest working concentration (concentration 3, except for TPEN where concentration 1 was used) for 3d and then lysed. Mock–electroporated PLC3 cells served as a negative control.

At 3dpe it can be observed that the band pattern does not change upon incubation with any of the compound molecules. The full length ORF1 as well as potential cleavage products are visible in a similar intensity.

Lastly, the subcellular ORF1 distribution while treated with the molecules Leupeptin, Velpatasvir and Sofosbuvir in PLC3 cells was observed at 3dpe (Fig. 37 (C)). Leupeptin and velpatasvir were chosen since they decreased the replication of the HEV replicon most compared to the other molecules tested. Sofosbuvir served as a positive control for successful HEV replication inhibition. Therefore, PLC3 cells were electroporated with the p6–V1 and with

PBS as a negative control.
It can be observed that the distribution of the ORF1 protein in the cells when treated with either Leupeptin or Velpatasvir did not change when compared to the untreated condition. Treatment with sofosbuvir, however, abolished the V5 staining in p6–V1 electroporated PLC3 cells.
In conclusion, it appears that none of the selected compounds had an effect on the replication of the p6–GLuc replicon or the expression of the ORF1 protein. Therefore, the results of Sarawat *et al.* are not applicable to our cellular system.

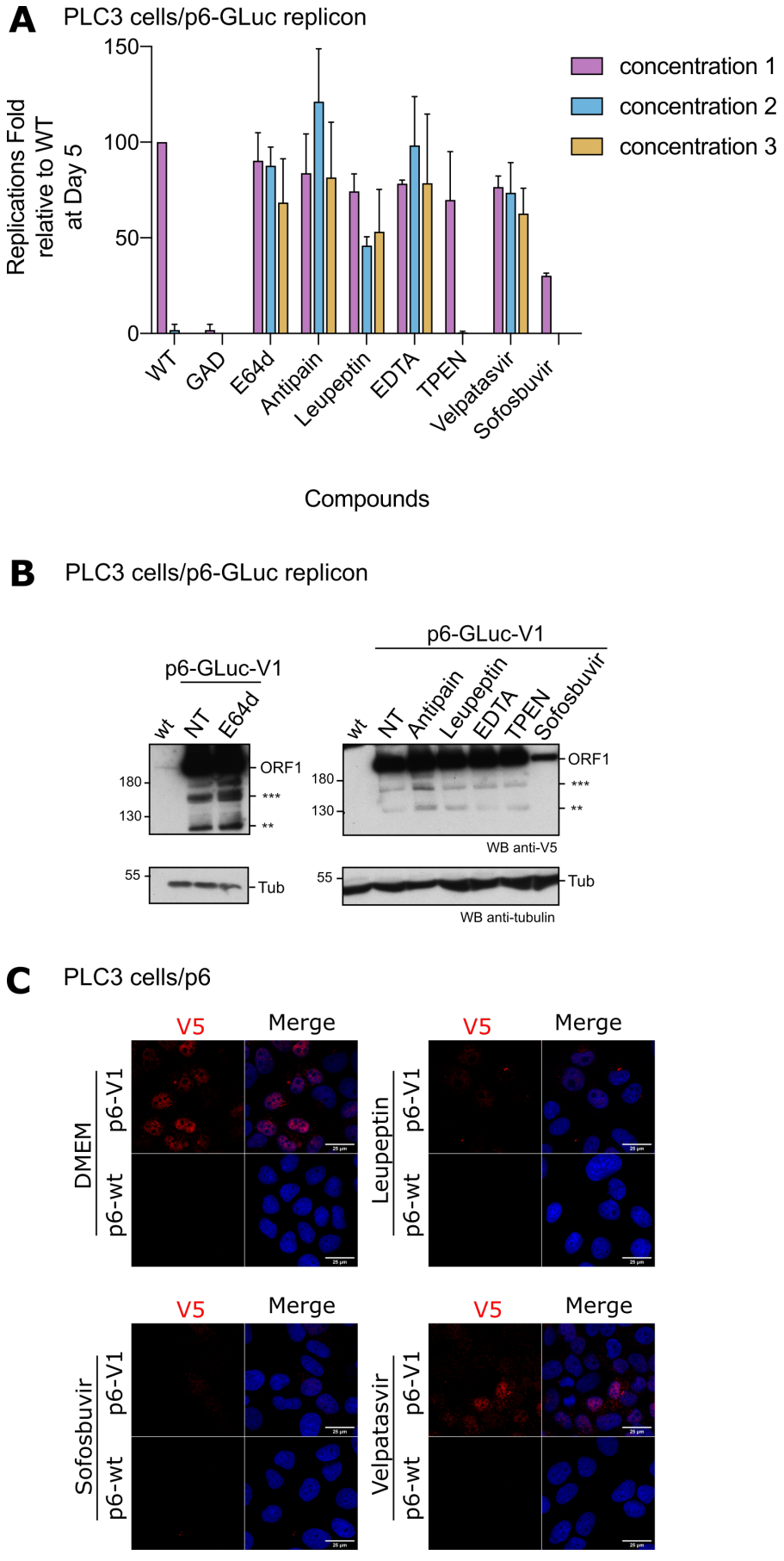

Figure 37: Treatment of electroporated PLC3 cells with protease inhibitors or ion chelators

Figure 37 *(previous page)*: (A) PLC3 cells were electroporated with the p6–wt–GLuc or the p6–GAD–GLuc replicon and treated with the following compounds: E64d, Antipain, Leupeptin, EDTA, TPEN, Velpatasvir and Sofosbuvir with three different concentrations mentioned in Tab. 23 . Replication Folds were normalized to 1dpe and then compared to the wt (=100%) at 5dpe. n=3. **(B)** PLC3 cells were electroporated with the p6–V1–GLuc and treated with the same compounds as in (A) (concentration 3). Lysates were collected at 3dpe and the western blot was revealed with the anti–V5–antibody and tubulin as a loading control. The stars indicate the most intense putative cleavage ORF1 products. **(C)** PLC3 cells were electroporated with the p6–wt and the p6–V1, seeded onto coverslips and treated with Sofosbuvir, Leupeptin and Velpatasvir at concentration 3 for 3 days. It was stained against the V5 epitope, images were taken using a confocal microscope.

5.6.3. Mass spectrometry of ORF1

Mass spectrometry (MS) is a technique that identifies protein sequences after digesting them into smaller peptides of 7 – 35 residues. The sequence of the full length ORF1 protein is already known, however the sequence of the smaller putative cleavage product bands remains mysterious. One of the difficulties of this experiment is the low abundance of the smaller bands, therefore several attempts were necessary to amplify and purify the V5–tagged bands to a maximum by performing an IP before submitting them to MS.

Therefore, PLC3 cells expressing the p6–V1 were immunoprecipitated by using a V5 antibody and the eluate was loaded onto a SDS–PAGE gel that was subsequently stained by a colloidal blue solution. On the same gel, a sample where H7–T7–IZ cells expressing the V1 tagged ORF1 protein was run side by side. At the same time, both samples were transferred onto a membrane and a western blot was performed (Chapter 3.7.8).

On the colloidal blue stained gel (Fig. 38 (A)) a band at higher than 180kDa is visible which corresponds to the full length ORF1. Unfortunately, the minor bands that can be seen on the western blot right next to it (Fig. 38 (B)), are not found on the gel, since their protein amount is not high enough. Therefore, the bands that were invisible on the colloidal blue stained gel were cut according to the western blot that was run at the same time (Fig. 38 (C&D) white and black boxes).

The bands 1–7 belong to the p6–V1 sample, bands 11–16 represent the ORF1–V1 sample and bands 8–10 correspond to bands that were specifically visible on the colloidal blue gel but not on western blot.

Band 1 was clearly identified as the full length tagged ORF1 protein. Its sequence coverage amounted to 38% and 129 spectra were observed. The N–terminus was identified but the scores of the first peptide actually were relatively low at 14 and 6. A score higher than 15 was considered reliable. Bands 2–7 show a sequence coverage of 18–32% and the spectra count was between 41 and 87. With exception of bands 3 and 5, all the other bands start with the

peptide 1–8 which corresponds to the N–terminus of the polyprotein. The C–terminus were the peptides ending at 1706 or 1734 for bands 2–7.
Similarly to the p6–V1, the sequence coverage of the heterologously expressed ORF1 ranges from 17–40%. The spectra count was slightly higher compared to the p6–V1 construct (63–195). The full length ORF1 protein was identified (band 11), but only between the peptides 1–1494. The N–terminus for the minor bands (12–16) was identified as the peptide 1–8 with a score of higher than 15 for at least one spectrum for each band. The C–terminus for all minor bands lays between the peptides 1398 and 1706.
The bands 8, 9 and 10 were visible on the colloidal blue stained gel, but they were not detected by western blot. The MS analysis shows that these bands too correspond to the full length ORF1 protein with a sequence coverage of 39, 55 and 71%. Of note, the spectra count was comparatively high too ranging from 125–672. At this point, it is unclear why the ORF1 protein, while detectable by colloidal blue staining, is not recognized by the V5 antibody on western blot. It can be speculated that these bands represent the aggregation of the ORF1 protein or parts of the ORF1 protein since they migrate at higher molecular weight.

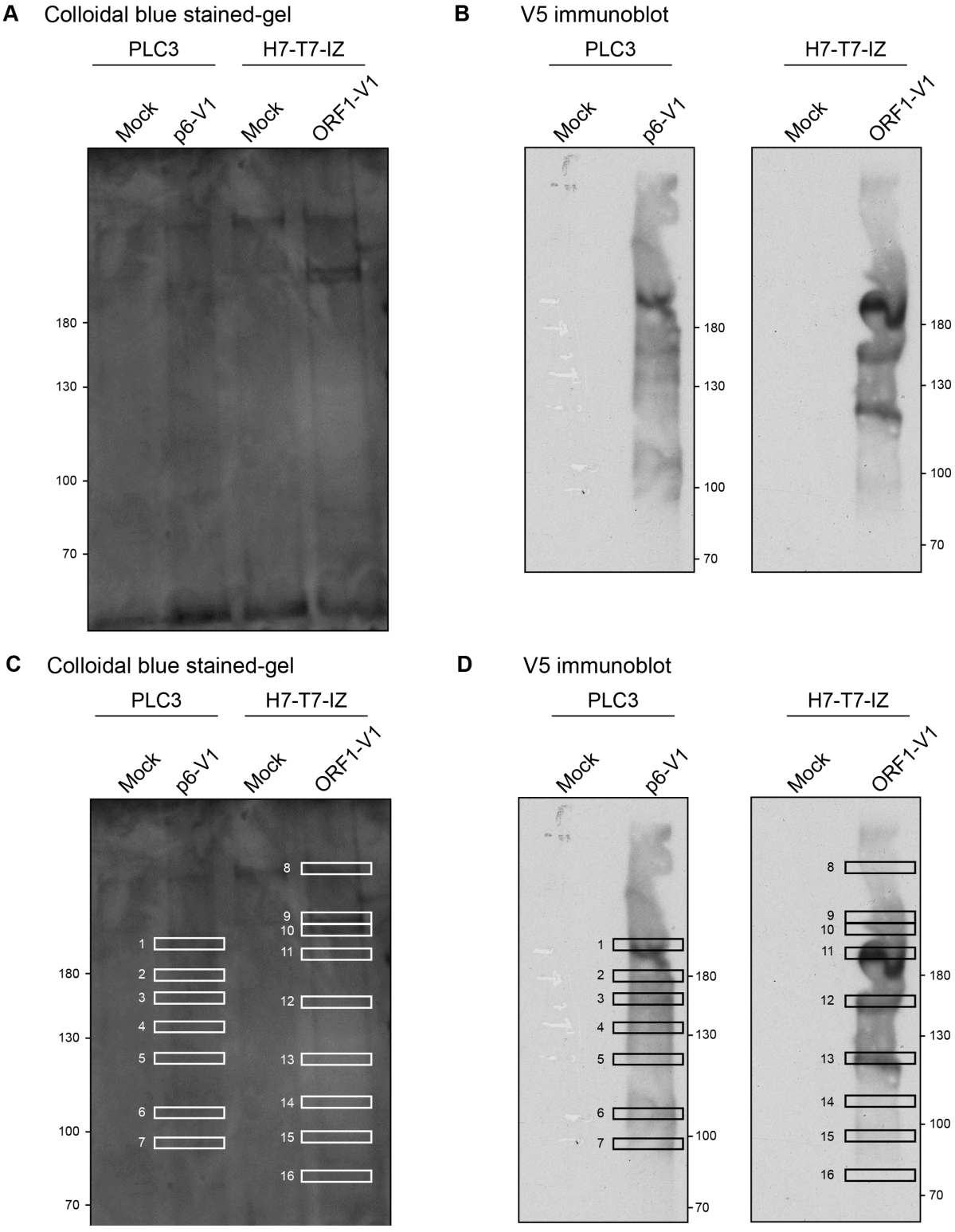

Figure 38: Immunoprecipitation of H7–T7–IZ cells expressing the ORF1–V5 protein and PLC3 cells expressing the p6–V1.

Figure 38 ***(previous page)*****:** H7–T7–IZ cells were transfected with a pTM plasmid expressing a V5–tagged ORF1 protein (ORF1-V1). PLC3 cells were electroporated with the p6–V1 construct expressing a V5–tagged ORF1 (p6–V1). Mock–transfected or –electroporated cells were used as negative controls (Mock). Lysates of each cell line were immunoprecipitated with the V5 antibody (Tab. 3). Next, the eluate was partitioned in 2 fractions and resolved by SDS–PAGE electrophoresis. Five per cent of the eluate was probed with the anti–V5 antibody (B,D) and most of the eluate was stained with colloidal blue (A,C). Following precise alignment of the revealed film and the colloidal blue stained gel, the desired bands were cut from the gel and analyzed by nano–scale liquid chromatography coupled to tandem mass spectrometry after in–gel trypsin digestion. White rectangles highlight the numbered bands of interest that were analyzed (Supplementary Fig. C,D).

Table 27: Results of the mass spectrometry analysis

Band number/construct	Sequence coverage[%]	Number of spectra	N–terminal peptides (score)	C–terminal peptides (score)
1/p6–V1	38	129	1–8 (14)	1758–1777(25)
2/p6–V1	32	87	41–53 (78)	1720–1734 (65)
3/p6–V1	31	68	54–69 (15)	1720–1734 (95)
4/p6–V1	32	83	1–8 (1)	1695–1706 (41)
5/p6–V1	30	68	41–53 (77)	1720–1734 (79)
6/p6–V1	20	48	1–8 (7)	1695–1706 (16)
7/p6–V1	18	41	1–8 (6)	1695–1706 (19)
8/ORF1–V1	39	125	1–8 (5)	1720–1734 (69)
9/ORF1–V1	55	321	1–8 (18)	1758–1777 (87)
10/ORF1–V1	71	672	1–8 (71)	1758–1777 (87)
11/ORF1–V1	35	195	1–8 (17)	1485–1494 (10)
12/ORF1–V1	40	185	1–8 (24)	1651–1662 (58)
13/ORF1–V1	31	102	1–8 (24)	1695–1706 (30)
14/ORF1–V1	19	75	1–8 (25)	1651–1662 (32)
15/ORF1–V1	17	63	1–8 (18)	1651–1662 (18)
16/ORF1–V1	17	66	1–8 (24)	1390–1398 (40)

5.7. Subcellular Fractionation of ORF1

To identify the subcellular compartment in which the ORF1 protein and potentially the viral replication site are located, cellular fractions were separated by using the subcellular fractionation kit (Tab. 10). This kit allows the extraction of the cytoplasmic soluble fraction, the cytoplasmic membranous fraction, the nuclear soluble fraction, the nuclear chromatin bound fraction and the cytoskeleton (Chapter 3.7.3).
To start with, the heterologously expressed ORF1 was analyzed by western blot (Fig. 39 (A)). The full length ORF1 protein is detected in all the fractions except the nuclear chromatin–bound fraction. Potential cleavage products are predominantly visible in the cytoplasmic fraction and in the cytoskeleton fraction.
Next, the V5 tagged replicons were analyzed. Fig. 39 (B) shows the presence of the uncleaved ORF1 protein in all subcellular fractions at 3dpe. With the exception of the nuclear chromatin bound fraction, the band pattern appears very similar throughout all fractions. The bands at 150 kDa, 130 kDa and 100 kDa show up most prominent in all extracts except for the nuclear chromatin bound fraction. This indicates that the ORF1 protein is not only present in the cytoplasm and the nucleus, but also, that it might interact with cytoplasmic membranes and also the cytoskeleton.
In Fig. 39 (C) the distribution across cellular fractions of the p6–V5 tagged ORF1 protein at 3dpe is demonstrated. The uncleaved polyprotein is present in all subcellular fractions. Potential cleavage proteins are visible as well in all fractions except for the nuclear chromatin bound extract.
The band pattern between the different fractions is similar, however, it varies especially between the cytoplasmic and the nuclear fractions. A band at 160 kDa is detected in the nuclear soluble and cytoskeleton fractions, but not in the cytoplasmic fractions.
When comparing the results obtained with the p6–GLuc replicon and the p6 infectious system, it is noticeable that the band pattern is similar. The most intense band remains the uncleaved ORF1. Potential cleavage bands appear in all fractions except for the nuclear chromatin bound fraction. However, in the replicon expressing cells and H7–T7–IZ cells expressing the ORF1 protein, there is no difference between the band patterns among the different subcellular fractions, as it is detectable in the p6 expressing cells.

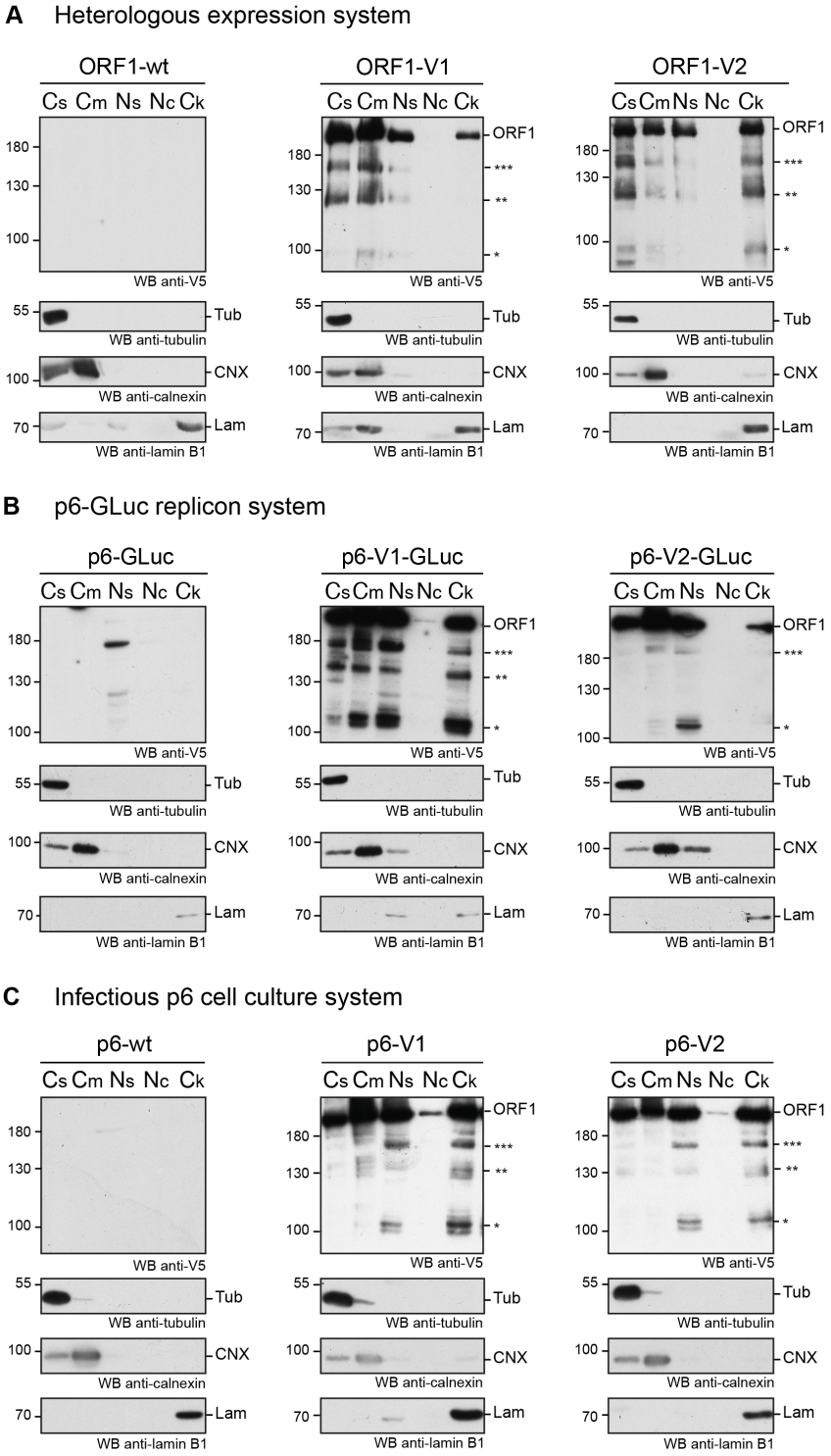

Figure 39: The ORF1 protein is expressed in different subcellular fractions.

Figure 39 *(previous page)*: (A) H7–TZ–IZ cells were transfected with the vector expressing the non–tagged ORF1 wildtype protein (ORF1–wt) and the V5–tagged ORF1 proteins (ORF1–V1, ORF1–V2). Eight hours post–transfection, cells were collected and cellular fractions were separated as follows: Cs = cytoplasmic soluble fraction, Cm = cytoplasmic membranous fraction, Ns = nuclear soluble fraction, Nc = nuclear chromatin–bound fraction, Ck = cytoskeleton. Immunoblots were probed with antibodies directed against the V5 epitope. Other antibodies were used to monitor for fraction enrichment: anti–tubulin as a marker of the cytoplasmic soluble fraction, anti–calnexin as a marker of cytoplasmic membranous fraction and anti–lamin B1 as a marker of nuclear envelope. Molecular weight markers are indicated in kilodalton. **(B)** PLC3 cells were electroporated with the p6–GLuc replicons expressing the non–tagged wildtype ORF1 (p6–wt–GLuc), and the V5–tagged ORF1 (p6–V1–GLuc, p6–V2–GLuc). Three days post–electroporation, cells were collected and cellular fractions were separated and named as above. The above-mentioned antibodies were used to reveal the immunobots. Molecular weight markers are indicated in kilodalton. **(C)** PLC3 cells were electroporated with the p6 expressing the non-tagged wildtype ORF1 (p6), and the V5–tagged ORF1 (p6–V1, p6–V2). Four hours post–electroporation, cells were collected and cellular fractions were separated and named as above. The above–mentioned antibodies were used to reveal the immunoblots. Molecular weight markers are indicated in kilodalton.

5.8. Membrane Rearrangement induced by ORF1

Whether or not the non–structural protein induces membrane rearrangement in host cells was investigated by electron microscopy (Chapter 3.5.3).

These experiments were conducted in collaboration with Pr. P. Roingeard (plateforme IBiSA, Université F. Rabelais, Tours).

Prelimiary data generated by transmission electron microscopy suggested that vesicles are formed upon HEV p6 electroporation in PLC3 cells (Fig. 40). The vesicles appear in clusters and are surrounded by an electron–dense membrane (Fig. 40 (A) white arrows). These findings suggested that HEV can indeed induce membrane rearrangement in host cells.

To test this hypothesis, we wanted to identify which role the ORF1 protein could play in this process. First, PLC3 cells electroporated with p6–V1 were subjected to a immuno–gold staining at various time points post electroporation (4hpe, 3dpe, 10dpe). All procedures were carried out by Cyrine Bentaleb at the facility of our collaboration partner.

Unfortunately, several anti–V5 antibodies were unable to detect a specific signal in PLC3 cells. As a next step, PLC3 cells electroporated with the p6–H2 was used in order to test a different primary antibody. However, even different anti–HA antibodies failed to specifically stain the ORF1 in PLC3 cells (Appendices Fig. 49).

Finally, this goal was no longer pursued during this thesis.

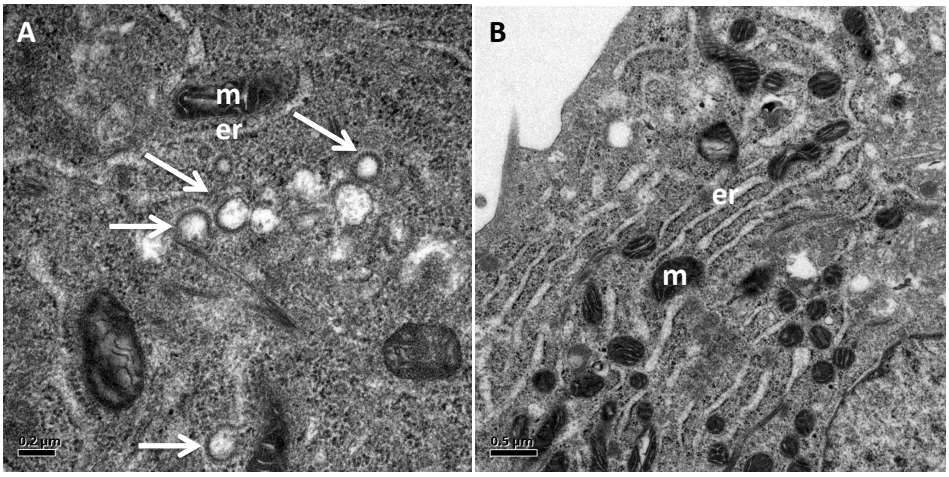

Figure 40: Ultrastructure of PLC3 cells electroporated with the HEV p6. PLC3 cells were electroporated with the p6 **(A)** or PBS **(B)** and were cultured for several days. After fixation, the cells were analyzed by transmission electron microscopy.

5.9. Subcellular Localization of ORF1

The subcellular localization of the tagged ORF1 protein was studied through immuno–labeling and *in situ* hybridization.

To begin with, the labeling of p6–V1, p6–V2 and p6–H2 in PLC3 cells will be discussed. Furthermore, the detection of HEV positive and negative RNA will be addressed.

All immuno–stainings were performed by using the p6–GLuc replicon, the p6 infectious system and the heterologous system.

First, PLC3 cells were electroporated with all tagged p6–GLuc constructs, the p6–wt–GLuc and a PBS control. At 3dpe, the cells were fixed and the V5 and HA tagged ORF1 was targeted by an anti–V5 antibody and an anti–HA antibody (Chapter 3.5.1). Unfortunately, no specific signal was detected. This might be due to a low expression of the ORF1 protein in PLC3 cells.

Next, the same experiment was repeated by using the p6 infectious system in PLC3 cells. As shown in Fig. 41 (A) the ORF1 protein is localized in the cytoplasm and the nucleus. The nuclear labeling appears stronger, however the nucleus is more condensed than the cytoplasm and might be the reason for this observation.

Furthermore, the ORF1 protein forms perinuclear aggregates that often go hand in hand with

a nuclear deformation (white arrow, Fig. 41 (A)). It is unclear what these aggregates might represent, but they were further studied in the following chapters (see 5.9.1 and 5.9.2).
However, the heterologously expressed ORF1 localizes predominantly to the cytoplasm and only shows a weak nuclear staining (Appendices, Fig. 50 (A)). Similarly to the p6–V1 staining, the ORF1 accumulates in the perinuclear region that coincides with a deformation of the nucleus. However, less accumulations were found overall when compared to the staining of the p6 infectious system.

5.9.1. Co–labeling with viral proteins

The ORF1 protein was co–labeled with several viral or cellular proteins to more accurately determine the site of viral replication.
At first, the viral capsid protein, ORF2, and the ORF1 protein were co–stained by using immuno–labeling in PLC3 cells at 3dpe. The ORF2 protein was stained with the commercial antibody 1E6 that recognizes all forms of the ORF2 protein (Fig. 41 (C&D)).
In Fig. 41 (C) it can be observed that ORF2 is distributed in the cytoplasm and the nucleus of the cell. Furthermore, it forms perinuclear aggregates that often localize next to a nuclear deformation. When co–labeled with ORF1 it can be seen that the aggregations are partially overlapping. Apart from the perinuclear foci however, the ORF1 and ORF2 do not seem to overlap. As a result, the pearson coefficient of the co–staining in the region of interest (ROI) defined as the perinuclear nugget is 0.57 (Fig.41 (B)).
Furthermore, a stack of more than 40 layers of the co–labeling between ORF1 and ORF2 was analyzed (Fig. 41 (D)). It becomes clear that the ORF1 and the ORF2 protein are both present in the periculear nugget showing similar intensities over space (Fig. 41 (D) graph).
When the tagged ORF1 and the ORF2/3 are co–expressed in H7–T7–IZ cells, an overlap in the perinuclear foci is observed as well (Fig. 50 (B)).
Next, the ORF3 protein was further examined. In PLC3 cells, the ORF3 protein appears in a spot–like pattern in the cytoplasm (Fig. 41 (E&F)). Interestingly, it also forms aggregations close to the nucleus that often lie next to a nuclear deformation. Colocalization experiments show that these foci also partially overlap with the ORF1 protein. In the ROI, a pearson coefficient of 0.54 was found between the ORF1 and the ORF3 protein in the infectious system. The pearson coefficient of this overlap is similar to the ORF2 colocalization. When the stack of the co–labeling is analyzed, it can be seen, that the intensities over space are shaped in a similar pattern (Fig. 41 (F) graph). In this case however, the ORF3 protein produces a higher intensity compared to ORF1. Additionally, it can be observed in the surfacing mode of the 3D image that the ORF3 protein seems to surround the ORF1 protein.
In the heterologous expression model the overlap between ORF1 and ORF3 in the perinuclear region is furthermore confirmed (Fig. 50 (C)).

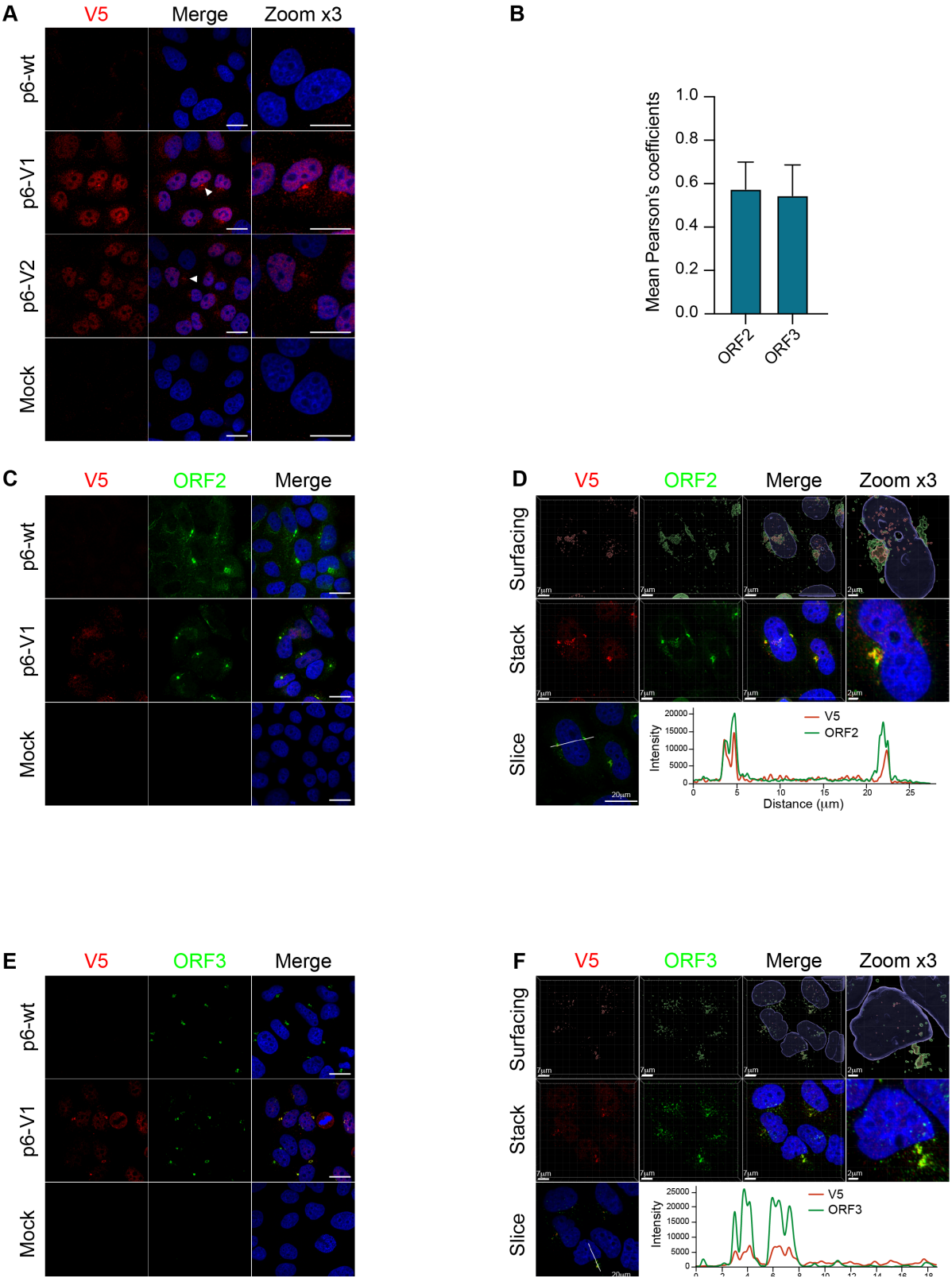

Figure 41: Co–localization of the HEV proteins in the host cell.

Figure 41 ***(previous page)*****: (A)** PLC3 cells were fixed and permeabilized 3 days after electroporation with the p6 wildtype non–tagged strain (p6) or the p6 expressing the V5–tagged ORF1 protein (p6–V1, p6–V2). Cells were stained with an anti–V5 antibody (red) and nuclei were stained with DAPI (blue) prior to analysis by confocal microscopy. Mock–electroporated cells served as negative control. Scale bar = 20µm. **(B)** Pearson coefficients were calculated using JACoP plugin from ImageJ software using the perinuclear nugget as ROI. Mean (+/– standard deviation) of 30 analyzed cells are indicated. **(C)** Co–labeling of the V5–tagged HEV replicase with ORF2 in PLC3 cells. Cells were treated as above (A). Then, the viral proteins were co–labeled with antibodies directed against the V5 epitope (ORF1, red) and ORF2 (1E6, green) prior to analysis by confocal microscopy. Scale bar = 20µm. **(D)** A stack of the co–staining performed as in (C) of at least 40 layers with an interval of 0.15µm was analyzed. A 3D surfacing (top), the stack (middle) and a graph covering the slice (bottom) are shown. **(E)** Co–labeling of the V5–tagged HEV replicase with ORF3 in PLC3 cells. Cells were treated as above (A). Then, the viral proteins were co-labeled with antibodies directed against the V5 epitope (ORF1, red) and ORF3 (green) prior to analysis by confocal microscopy. Scale bar = 20µm. **(F)** A stack of the co–staining performed as in (E) of at least 40 layers with an interval of 0.15µm was analyzed. A 3D surfacing (top), the stack (middle) and a graph covering the slice (bottom) are shown.

5.9.2. Co–labeling with cellular markers

The ORF1 protein was co–stained with several cellular markers to identify the subcellular compartment of viral replication.

Based on the results of another student in the lab, Kevin Hervouet, different markers of the recycling endosomal pathway were chosen. It was shown by him that the proteins CD71 and Rab11 colocalize with the ORF2 protein in the perinuclear aggregates [393]. CD71 is the transferrin receptor I that is localized on the plasma membrane and gets internalized via endosomes, due to which it is transferred again to the plasma membrane [394]. In Fig. 42 (A&B) the overlap between CD71 and the ORF1 protein is shown. Here, a partial colocalization (pearson coefficient of 0.42) can be observed concerning the above mentioned foci. The overlap was also further characterized as can be found in Fig. 42 (B). Similarly to the analyses performed with ORF1 and ORF2 or ORF3, a stack of images was acquired to reconstruct a 3D image. It can be observed from the surfacing representation that while also overlapping, CD71 seems to surround ORF1. The intensity graph shows an intensity over distance pattern that is very similar for both analyzed proteins, however, the intensity of CD71 around 3 fold higher than the intensity of ORF1.

Another marker of the endosomal pathway, that has been shown to be exploited by pathogens, Rab 11, was studied. Rab 11 is a small GTPase that is localized in the recycling endosome [395] and it also forms perinuclear aggregates that overlap with the aggregates formed by

the ORF1 protein (Fig. 42 (C&D)). The pearson coefficient amounts to 0.69, which marks the highest level of colocalization among all proteins tested. Indeed, the surfacing depiction shows an obvious colocalization between Rab11 and ORF1 (Fig. 42 (D)). This is further corroborated by the intensity plot of the two proteins. In this case, the ORF1 shows a higher intensity over distance than Rab11.

Protein kinase C and casein kinase substrate in neurons 2 (PACSIN2) is a lipid–binding protein that promotes the tubulation of the phosphatidic acid–containing membranes, that has been implicated in the assembly of HCV [396].

In Fig. 42 (E) it can be seen that PACSIN2 is present where the perinuclear nuggets are formed, however it does not accumulate in that region. The pearson coefficient of the overlap with ORF1 lies therefore at 0.23.

On the other hand, the Eps15 homology domain protein 1 (EHD1) is recruited by PACSIN2 alongside long tubular membranes (in the tubular recycling endosome or TRE), however it is unclear how EHD1 is recruited to these tubular endosomes [397]. The association between EHD1 and ORF1 is found regarding the perinuclear accumulations as can be seen by a pearson coefficient of 0.49 and in Fig. 43 (C).

Another cellular factor that was tested is the CD63, that belongs to the tetraspanin family. It has shown to be involved in the exit and entry of viruses [398]. In this case however, it does not seem to colocalize with the ORF1 protein (pearson coefficient of 0.1). On the other hand, it is noteworthy that the distribution pattern of CD63 differed between PBS electroporated cells and cells electroporated with HEV (Fig. 43 (A)). The CD63 protein in PBS electroporated cells is evenly distributed throughout the cytoplasm, whereas in cells electroporated with the p6–wt or tagged constructs the labeling seems stronger and more small aggregates seem to form in the vicinity of perinuclear aggregates.

In fact, several members of the tetraspanin family have been shown to be involved in the life cycle of different viruses [399]. CD81 is also a member of this family; it has been shown to interact with HCV [400, 401]. However it does not seem to directly associate with ORF1 of HEV (Fig. 43 (B)). It even seems to adopt a pattern that evades the ORF1 protein, as the pearson coefficient reaches -0.1.

All in all, it appears that HEV uses the recycling endosomal pathway during its life cycle. The colocalization within the perinuclear aggregates between the cellular markers and the ORF2 protein led to the hypothesis that viral assembly takes place in this location [393]. Based on this hypothesis, a second one can be formed: the site of viral replication might be close to the site of viral assembly.

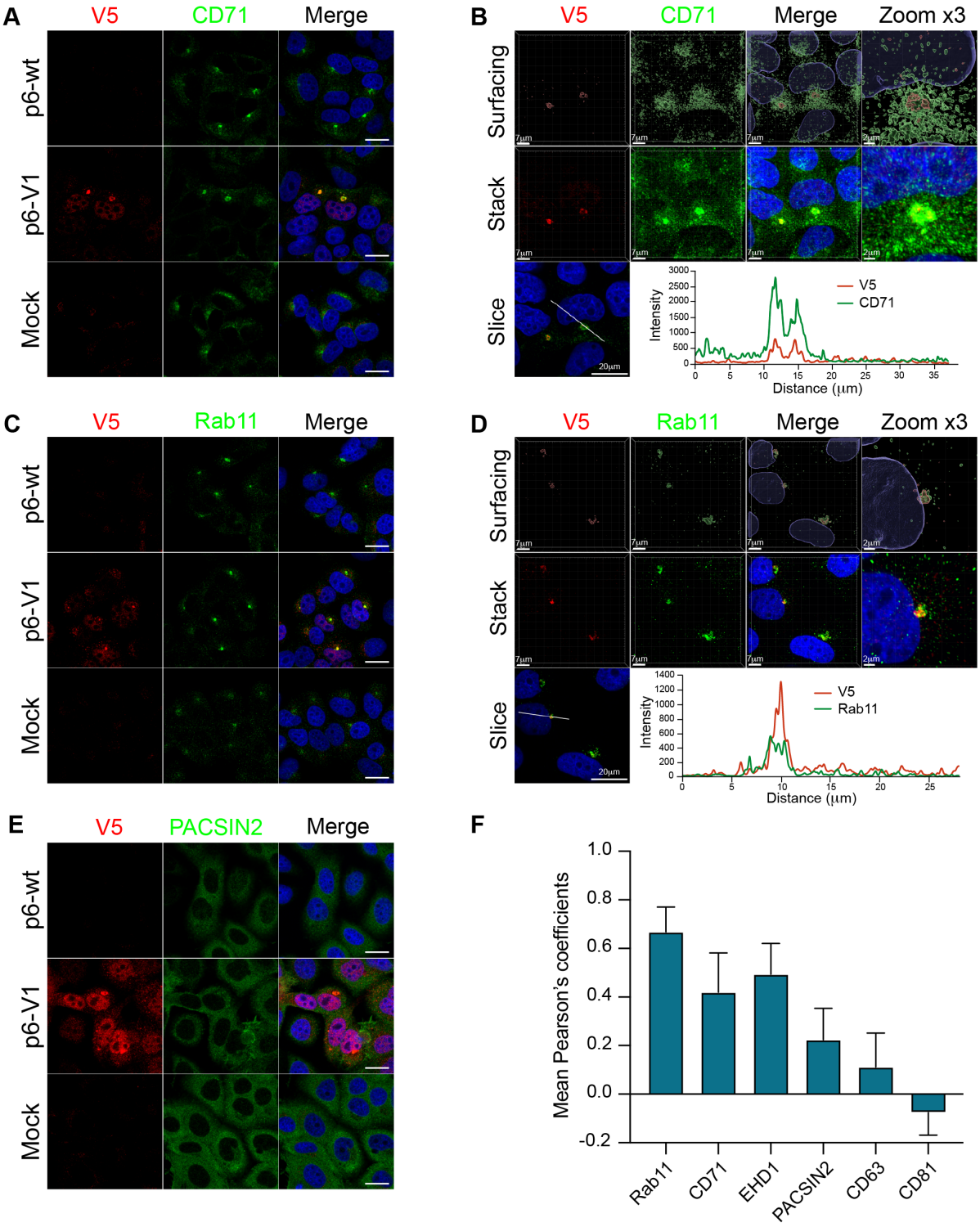

Figure 42: Co–labeling of the HEV V5–tagged ORF1 protein with several cellular markers in the p6 cell culture system.

Figure 42 ***(previous page)*****:** The wt (p6–wt) and V5–tagged ORF1 proteins (p6–V1) were expressed in PLC3 cells electroporated with the p6 HEV strain. Three dpe, cells were co–labeled with anti–V5 antibody (red) and cellular markers antibodies (green) directed against CD71 **(A&B)**, Rab11 **(C&D)** and PACSIN2(**E**). Cell nuclei were stained with DAPI (blue). Mock–electroporated cells served as negative controls (Mock). Images were taken with a confocal microscope. Scale bar = 20µm. **(B&D)** A stack of the co–staining performed as in (A) of at least 40 layers with an interval of 0.15µm was analyzed. A 3D surfacing (top), the stack (middle) and a graph covering the slice (bottom) are shown.**(F)** Pearson coefficients were calculated using JACoP plugin from ImageJ software using the perinuclear nugget as ROI. Mean (+/– standard deviation) of 30 analyzed cells are indicated.

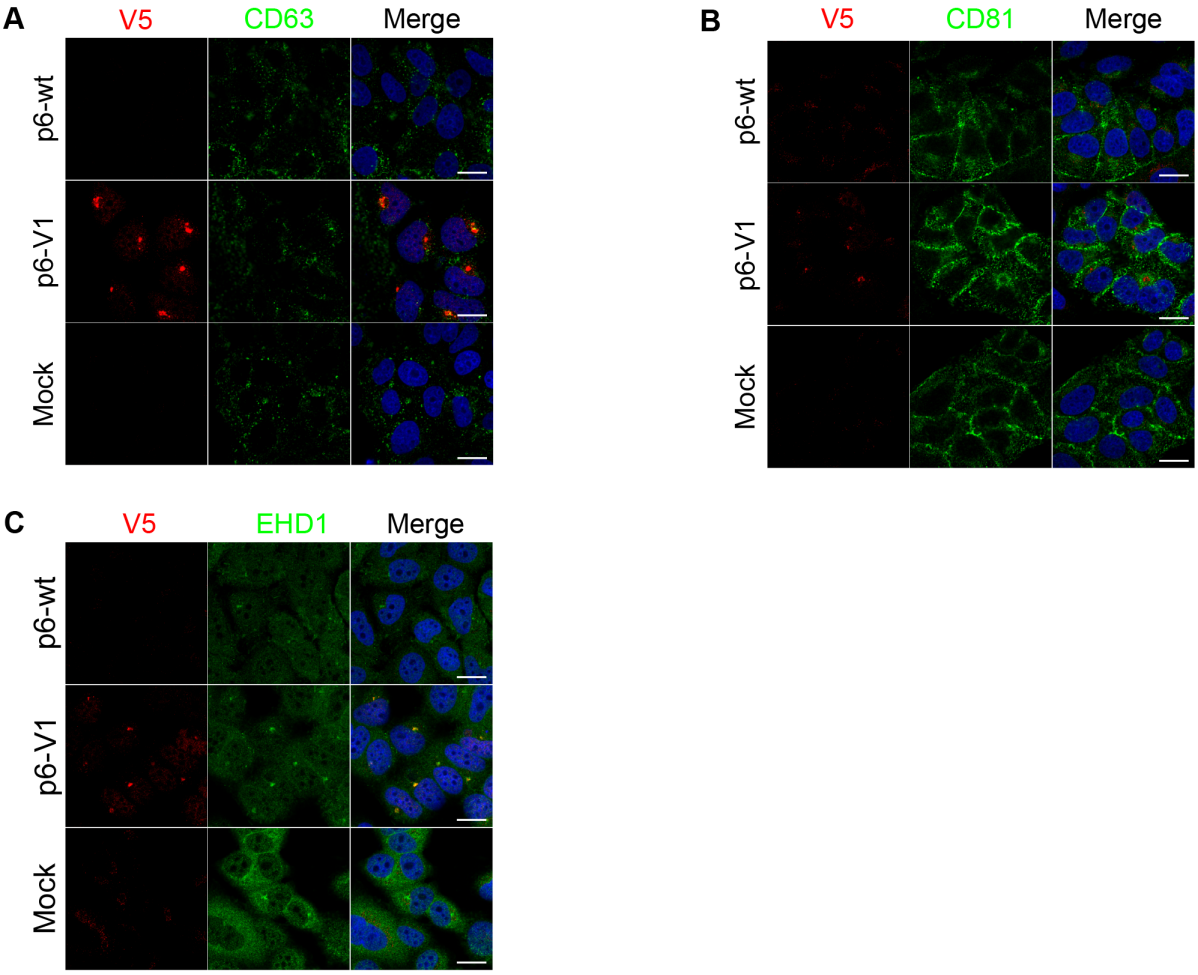

Figure 43: Co–labeling of the HEV V5–tagged ORF1 protein with the cellular markers CD63, CD81 and EHD1 in the p6 cell culture system.

Figure 43 *(previous page)*: The wt (p6–wt) and V5–tagged ORF1 protein (p6–V1) were expressed in PLC3 cells electroporated with the p6 HEV strain. Three dpe, cells were co–labeled with anti–V5 antibody (red) and cellular markers antibodies (green) directed against CD63 **(A)**, CD81 (**B**) and EHD1(**C**). Cell nuclei were stained with DAPI (blue). Mock–electroporated cells served as negative controls (Mock). Images were taken with a confocal microscope. Scale bar = 20µm.

5.9.3. Detection of HEV RNA inside the host cell

The RNA staining was performed by employing the RNAscope® method by Advanced Cell Diagnostic, Inc. (ACDbio).
The principle of this technique is the *in situ* hybridization of target specific probes to RNA and the augmentation of the fluorescent specific signal through multiple amplification steps.
Probes were designed against genomic RNA, subgenomic RNA and negative–stranded HEV RNA (Fig. 44 (A)). PLC3 cells electroporated with p6–wt RNA were first stained for genomic, subgenomic and negative–stranded RNA.
To follow the kinetics of the viral RNA localization inside the HEV–infected cells, a time course experiment was set up. P6–wt and PBS electroporated cells were fixed at 4hpe, 3dpe and 6dpe and further labeled for positive–stranded genomic and subgenomic RNA and negative–stranded RNA (Fig.44 (B)). At 4hpe, the labeling of the negative–stranded RNA is located close to the cell nucleus. Subgenomic and genomic RNA are partially colocalizing with negative–stranded RNA at 4hpe, while subgenomic RNA even seems to surround negative–stranded RNA. The pearson coefficient of the overlap between negative–stranded RNA and subgenomic RNA reaches 0.68, which corresponds to a moderate to high amount of colocalization.
At 3dpe, accumulations of especially genomic and subgenomic RNA are visible close to the cell nucleus, while they are also dispatched throughout the cell. The pearson coefficient of positive–sense RNA and negative–stranded RNA decreased slightly when compared to 4hpe from 0.51 to 0.37 for probe targets A and B and from 0.68 to 0.54 for probe targets C and B. The decrease might be caused by the loss of intensity of negative–stranded RNA. The pearson coefficient between probe targets A and C stays similar between 4hpe and 3dpe (0.39 and 0.41 respectively) as does their signal intensity.
The last time point, 6dpe, shows a more diffuse pattern for all three types of HEV RNA in PLC3 cells. The staining of the negative–stranded RNA at this time point adopts a dot–like pattern, some of them displaying a rather intense fluorescence while other foci being more diffuse. Of note, some similar intense dots (although slightly smaller) are also shown in the mock–electroporated cells. And while the subgenomic RNA is more and more dispersed throughout the cell maintaining its high intensity, the genomic RNA loses part of its signal in-

tensity. The pearson coefficient for negative–stranded RNA and genomic RNA at 6dpe stays similar to the one at 3dpe (0.38 for both of them). While the colocalization between subgenomic and negative–sense RNA decreases (0.53 to 0.43), the overlap between subgenomic and genomic RNA increases slightly (0.41 to 0.52).
Next, HEV genomic RNA was co–labeled with the ORF1 protein (Fig. 44 (D)). Therefore, PLC3 cells were electroporated with the p6–V1 construct and PBS as its negative control. The PLC3 cells were fixed at 4hpe, 3dpe and 6dpe to analyze the genomic positive–stranded RNA and ORF1 protein expression over time. At 4hpe, the ORF1 staining is of low intensity and overlaps partially with genomic RNA, the pearson coefficient is relatively low (0.39, Fig. 44 (E)). At 3dpe the ORF1 protein shows its typical nuclear distribution together with a faint staining in the cytoplasm and the more intense perinuclear accumulations. The positive–stranded genomic RNA colocalizes with the accumulations and partly with the cytoplasmic staining as well. A pearson coefficient of 0.44 was measured. At 6dpe the ORF1 protein is located in the nucleus and the cytoplasm, but the perinuclear accumulations do not occur any longer. The positive–stranded RNA staining becomes fainter and does not any more overlap with the ORF1 staining, which is also expressed by a pearson coefficient of 0.05.

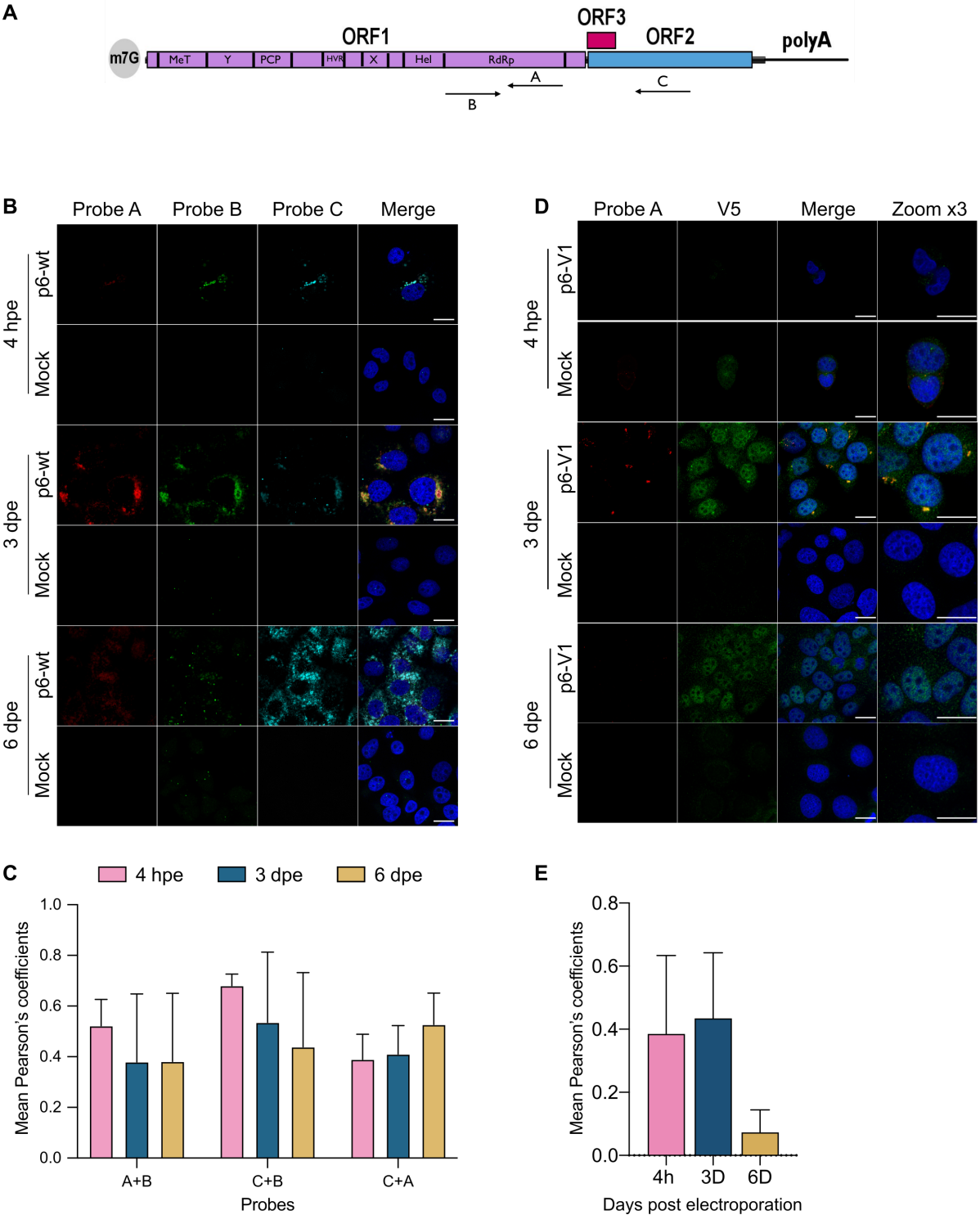

Figure 44: *in situ* labeling of positive– and negative–sense HEV RNA.

Figure 44 ***(previous page)*****:** PLC3 cells were electroporated with non–tagged p6 or V5–tagged p6 strains (p6–wt and p6–V1, respectively). Cells were grown on coverslips, fixed and stained at 4 hpe, 3 dpe and 6 dpe. Mock–electroporated cells served as negative control. Cell nuclei were stained with Dapi (blue). Images were taken on a confocal microscope. Scale bar = 20 µm. **(A)** Schematic overview of the RNAscope® probe location. Probe A targets the positive–sense genomic RNA and is located in the RdRp domain of ORF1 (purple). Probe B targets the negative–sense RNA and is also located in the RdRp but does not overlap with probe A. Probe C targets the positive–sense subgenomic RNA, by hybridizing at the ORF3 (red) / ORF2 (blue) overlap. **(B)** PLC3 cells electroporated with the p6–wt strain were sequentially stained with probes A (white), B (red) and C (green). **(C)** Pearson's correlation coefficients were calculated using JACoP plugin from ImageJ software using the whole cell as ROI. Mean (+/– standard deviation) of 25 analyzed cells are indicated. **(D)** PLC3 cells electroporated with the p6–V1 strain was stained with probes A (red) while the V5–tagged–ORF1 was stained in green. **(E)** Pearson's correlation coefficients were calculated using JACoP plugin from ImageJ software using the whole cell as ROI. Mean (+/– standard deviation) of 25 analyzed cells are indicated.

Secondly, the genomic RNA was co–labeled with the other viral proteins and two of the above mentioned cellular factors (Fig. 45). The ORF2 protein staining is characterized by a nuclear and cytoplasmic labeling together with perinuclear accumulations that often coincide with a deformation of the nucleus (Fig. 45 (A)). These accumulations were also observed for genomic positive–stranded at 3dpe as well. Indeed, the accumulations of positive–sense genomic RNA and the ORF2 protein colocalize as shown by pearson coefficients of 0.6 (Fig. 45 (E)).

Thirdly, the genomic HEV RNA was co–stained with the ORF3 protein (Fig. 45 (C)). Since the ORF3 and the ORF2 colocalize as well in this exact region, an overlap can be observed between the ORF3 protein and positive–stranded genomic RNA at 3dpe (Pearson coefficient of 0.73).

Furthermore, 2 cellular markers were examined regarding their interaction with viral RNA (Fig. 45 (B&D)). As described before, Rab11 is a protein of the endosomal recycling pathway that is found as well in the perinuclear accumulations overlapping with all three viral proteins. At 3dpe of the p6–wt in PLC3 cells, it can be observed that a partial overlap between positive–sense RNA and Rab11 is formed in the perinuclear region, reflected by a Pearson coefficient of 0.48.

Also, a partial overlap between viral genomic RNA and the tetraspanin CD63 is show in Fig. 45 (D) . The Pearson coefficient amounts to 0.53, which might indicate a partial association between CD63 and genomic positive–sense RNA. It is interesting to note, that the ORF1 protein did not seem to associate with CD63 (Fig. 43 (A) & Fig. 42 (F), however, the positive–sense genomic RNA appears to colocalize partially.

In conclusion, HEV positive– and negative–sense RNA as well as subgenomic RNA are located in the perinuclear region at 3dpe. At this time point, colocalization between positive–sense genomic RNA and all viral proteins in the nugget–shaped foci was observed, thereby further corrobating the hypothesis that viral replication and assembly take place in close proximity to each other in the perinuclear region.

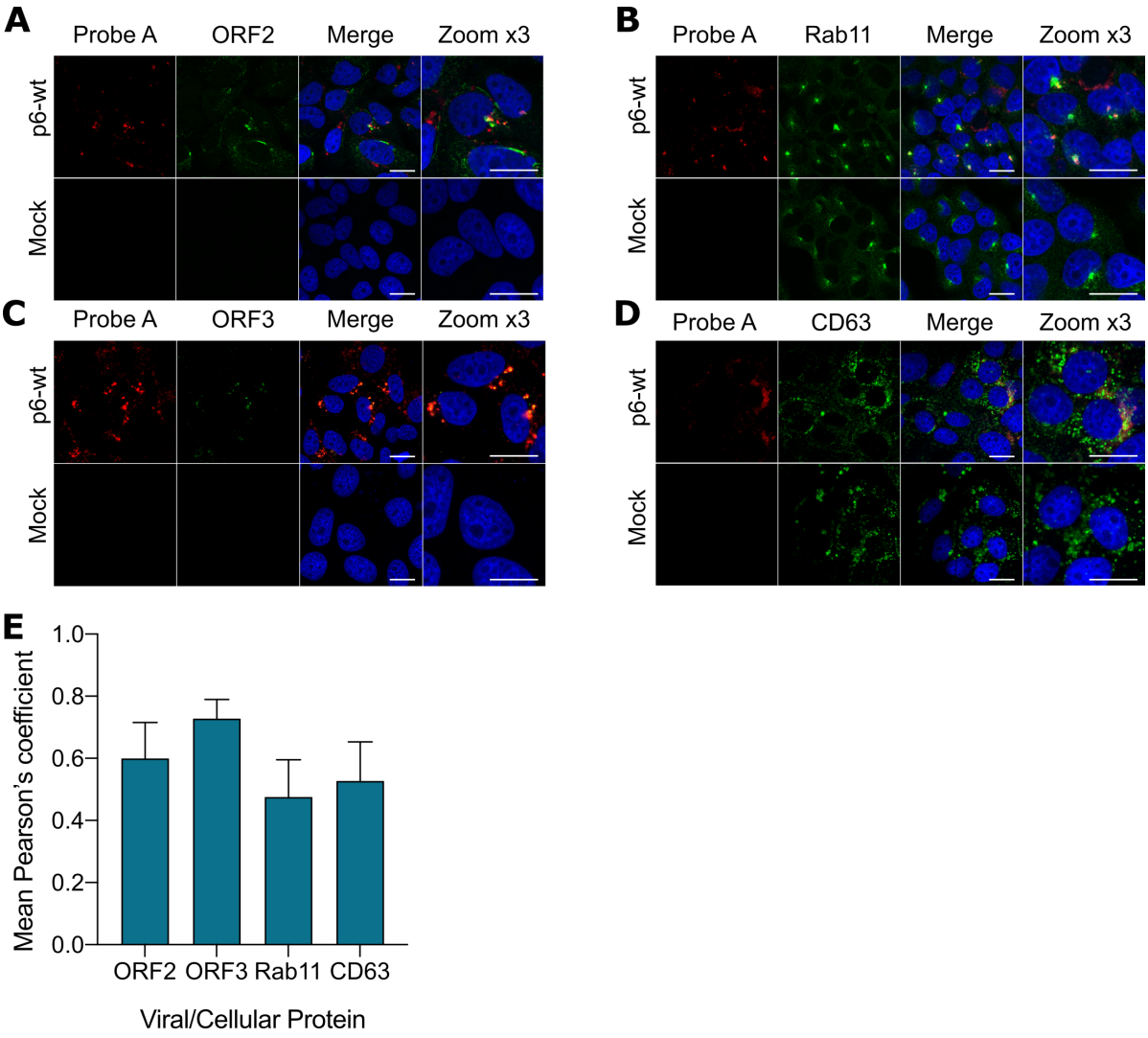

Figure 45: *In situ* labeling of positive–sense HEV RNA and viral or cellular proteins. PLC3 cells were electroporated with non–tagged p6 (p6–wt and p6–V1) or with PBS (Mock) as a negative control. Cells were grown on coverslips, fixed and stained at 3 dpe. Cell nuclei were stained with Dapi (blue). Images were taken on a confocal microscope. Scale bar = 20 µm. **(A)** PLC3 cells electroporated with the p6–wt strain was sequentially stained with probes A (red) while ORF2 protein was stained in green using the 1E6 monoclonal antibody. **(B)** PLC3 cells electroporated with the p6–wt strain was sequentially stained with probes A (red) while Rab11 was stained in green. **(C)** PLC3 cells electroporated with the p6–wt strain was sequentially stained with probes A (red) while ORF3 protein was stained in green using the polyclonal anti–ORF3 antibody. **(D)** PLC3 cells electroporated with the p6–wt strain was sequentially stained with probes A (red) while CD63 was stained in green. **(E)** Pearson's correlation coefficients were calculated using JACoP plugin from ImageJ software using the perinuclear nugget–shaped accumulations as ROI. Mean (+/– standard deviation) of 25 analyzed cells are indicated.

6. Discussion

There are still many unanswered questions regarding the life cycle of hepatitis E virus. In this study, we focused on the replication step of the virus, which involves foremost the non–structural protein ORF1. Our goal was to characterize ORF1 maturation and subcellular localization during viral replication.
Out of all three viral proteins, ORF1 is the least studied one, which is due to low expression levels and the lack of a commercial and functional antibody. Thus, we inserted different tags into ORF1 to detect the ORF1 protein.
This approach has been used in a study by Szkolnicka *et al.* which employed a transposon based screen to insert HA tags into the ORF1 protein [222]. They successfully inserted the epitope and were able to localize the ORF1 through indirect immunofluorescence in HepG2/C3A cells.
In the following, the validation of our epitope tagged systems as well as our goals to characterize the maturation and the subcellular localization of ORF1 will be discussed.

6.1. System Validation

Similarly to the approach by Szkolnicka *et al.*, we aimed to insert epitopes without disrupting viral replication [222]. Therefore, we controlled the replicative capacity by first inserting the epitope tags in a replicon containing the *Gaussia* luciferase as a read–out.
In first attempts, HA tags were inserted at the borders of the different predicted domains of the ORF1 protein. To test their replication ability, the tags were inserted into the p6–GLuc replicon and the luciferase activity was monitored over the course of 5 days. It became apparent that the insertion in these positions completely abolished replication (data not shown). One reason for this result might be that the bioinformatically assigned domains do not correspond exactly to the actual domain borders, so that the tag insertion might have interrupted the domain. Another hypothetical reason might have been the disruption of the 3D structure of the polyprotein.
To avoid a modification of the ORF1 conformation, an HA tag was thus inserted at the C–terminus of the ORF1 protein, right before the stop codon (Chapter 5.2, Fig. 28). Another advantage of this insertion site is the traceability of the tagged protein, since in the event of a possible cleavage, we can determine more precisely in which region of the protein the cleavage may occur.
As a next step, the HVR was chosen as an epitope tag insertion site, since it is the most variable part of the ORF1 genome and it is known to tolerate small insertions and deletions [102, 145]. After aligning 44 HEV ORF1 sequences, we indeed confirmed the variability of

this region. The previously mentioned study by Szkolnicka *et al.*, also found that the HVR was the most tolerant region for insertions.

At first, the HA epitopes were inserted in several strategic places (Fig. 28): The H2 position was derived from the strain LBPR–0379 that contains a S19 insertion that confers a growth advantage in cell culture [102, 145] (Fig. 28 (A)). Since this site was known to tolerate a relatively large insert (117nt), first the H2 and later the V2 were placed in this exact position.

Next, the H3 and H4 insertion sites were located at the borders of the S17, a region that is specific and unique to the Kernow C1 strain (Fig. 28 (A)). The H5 and H6 were inserted in a way that conserves the proline residues in the proline–rich region of the HVR (Fig. 28 C).

Next to the HA tags, V5 epitopes were tested as well. The V2 tag is situated in the exact same position as the H2 tag. The V1 tag on the other hand was based on a different insertion strategy: after aligning the V5 epitope sequence with the complete HVR region of the ORF1 protein, a region was identified, where 4 amino acids were identical, 3 amino acids had to be mutated and 7 amino acids needed to be inserted to reconstitute the V5 epitope with a lesser impact on the HEV genome (Fig. 28 (B)).

On day 5, the replication efficacies were compared to those of the p6–wt–GLuc (Chapter 5.3, Fig. 30 (A&B)). Out of all constructs, the p6–V1–GLuc replicon showed the most promising replication efficacy as it was comparable to the p6–wt–GLuc. By inducing the least amount of change into the HEV genome, the V1 insertion did not affect the replication efficacy significantly. Moreover, one of the tags used in the study by Szkolnicka *et al.* also identified this insertion site (shifted by one amino acid) as the most tolerable, thereby confirming the validity of our insertion choice.

The p6–V2–GLuc construct also showed a replication efficacy relatively close to the p6–wt–GLuc. However, the p6–H2–GLuc replicon replicates less efficiently even though both epitopes are situated in the exact same position. This implies that not only the insertion site matters concerning its tolerability, but also the amino acid sequence composition. On the other hand, Szkolnicka *et al.* inserted an HA tag 5 amino acids upstream of this site in a different strain while maintaining the replication ability of their replicon. Therefore, it is difficult to explain the success of one tag insertion and the defeat of the other.

Collectively, the HA tagged p6–GLuc replicons showed a lower replication efficacy compared to the wt replicon (9–34%). The H1 position is located within the subgenomic promoter that was likely disrupted by the HA insertion, which therefore reduced subgenomic expression [97]. The specific reasons for the low replicative capacity of the other HA tagged replicons are unclear. As a consequence, neither the H1 nor the H3–H6 were inserted into the p6 infectious genome. Initially, the H2 was not inserted into the p6 infectious genome either due to its lower replication efficacy compared to p6–V2–GLuc. However, when we encountered difficulty concerning the V5 antibody during the immuno–gold labeling, we tried to circumvent

the problem by using an HA antibody to continue these experiments. Since the H2 insertion is in the same position as the V2, we have included this construct in our analysis but at a later time point.
The HA tags in the H2 position on the other hand, were used in the heterologous system, since it relies on T7–driven expression and not on replication.
Next, the intracellular RNA levels of the tagged replicons were determined to further address the impact of the selected tags on the replication of the replicons (Chapter 5.3.2).
By using one probe against genomic RNA and another against subgenomic RNA, it was found that the expression levels of the p6–V1–GLuc and the p6–V2–GLuc were overall comparable to the p6–wt–GLuc. This indicates that the tag insertion does not have an impact on the expression of intracellular genomic and subgenomic RNA. Furthermore, the V1 and V2 tags were inserted into the p6 infectious genome, where the intracellular and extracellular RNA levels were verified by using probes against genomic and subgenomic RNA (Chapter 5.3.3).
In line with the previous results, the p6–V1 and the p6–V2 RNA levels behave similarly to the non–tagged p6–wt, implying that the tag insertion in these two positions do not affect HEV intra– or extracellular RNA levels (Fig. 32). In all three cases, intracellular genomic RNA reached up to $3.9x10^7$ copy numbers/µg and extracellular RNA reached up to $7.2x10^7$ copy numbers/mL.
Finally, the impact of the tags on the infectivity of HEV was studied by measuring the construct specific infectious titers (Chapter 5.4). The p6–wt showed an infectious titer of 10^4 FFU/mL, which was also reached by the p6–V1 and p6–V2 constructs. Also, the expression of ORF2 between the p6–wt and the V5 tagged p6 constructs was compared in electroporated PLC3 cells as well as Huh7.5 cells infected with viral particles produced by PLC3 cells. It was observed that the ORF2 expression in both cases remained at the same level. Thus, the insertion of a V5 tag in both positions does not abrogate viral infectiousness or the expression of the ORF2 protein.
Taken together it can be concluded that the V1 and V2 insertion positions have no impact on viral replication or viral infectivity. On the other hand, the HA tagged constructs lead to a major decrease of HEV replication, therefore they could not be used in a replicative system. The H1 and H2 insertions could be used in a heterologous expression system and the V1 and V2 epitope tags were used in all three available systems.

6.2. Maturation of the non–structural protein

After validating the insertion of the four epitope tags in at least one of the described systems, our next goal was the characterization of the maturation of ORF1. In positive–stranded RNA

viruses it is common for the non–structural or the structural proteins to undergo processing. HCV for example gets cleaved by the protease encoded by the NS3 [402] and SARS–CoV 2 possesses even 2 proteases that cleave the non–structural proteins [403, 404].
As it was previously mentioned (Chapter 1.6.2), the potential processing of the non–structural protein of HEV remains controversial in the literature [138]. While there is evidence for and against processing, most reports were using heterologously expressed ORF1 or cell free systems to acquire their data. The last reports that were using replicon systems [101, 222] were only able to detect the full length ORF1 protein by immunoblotting.
Hence, we sought to analyze the expression of the tagged non–structural protein in our three different systems: the heterologous expression, the p6–GLuc replicon and the p6 infectious systems (Chapter 5.5). In all 3 expression systems, the ORF1 protein is already expressed at early time points (4h–8hpt). A major band at higher than 180kDa can be observed that corresponds to the full length protein. At the same time, smaller bands between 90 and 180kDa are visible as well. These smaller bands that exist in lower abundance than the full length ORF1 might be the product of ORF1 cleavages. Their early expression might be due to an early requirement of these potential cleavage for the replication of HEV, but it is not clear whether replication takes place so early on, since the electroporation process delivers a substantial amount of RNA into the cell. As time progresses, the abundance of these products decreases further (Fig. 34 (C)), which can be observed in the infectious system until 25dpe, which might imply that viral replication slows down over time. In a study on poliovirus it was shown that viral replication slows down over time too, as resources are depleted in the cell [405]. The band pattern of the smaller bands between the 3 systems is similar but it is not exactly the same. Also, the potential cleavage products seem more numerous in the p6 infectious system following a V5 IP (Fig. 35). Since the sequence of these smaller bands are still unknown, it is difficult to interpret these results.
Furthermore, we aimed to address the nature of the potential cleavage bands: are they indeed specific cleavage bands or are they the product of protein degradation?
To answer this question, we decided to perform a proteasome inhibition with the specific inhibitor lactacystin [406] (Chapter 5.6.1). If the smaller bands were indeed a product of protein degradation, we would expect them to disappear after treatment with lactacystin, since protein degradation should be inhibited. To control for the successful inhibition of the proteasome, we also probed for the HSP70 protein which is known to accumulate in this case. Indeed, we observed a slight increase of this protein when the cells were treated with the inhibitor.
Upon treatment with lactacystin at 3dpe of PLC3 cells electroporated with the HEV replicon or H7–T7–IZ cells transfected with the V1–tagged ORF1, we could observe that the smaller bands between 90–180kDa were still visible on the immunoblot in both cases. The intensity of the bands of the non–treated cells and the lactacystin treated cells was comparable as well.

This implies that the observed smaller bands are likely not degradation products.
The next question surrounding the potential processing mechanism of the non–structural protein concerns the PCP domain of ORF1. The bioinformatical analysis by Koonin *et al.*, in 1992 found a sequence homology to members of the *Rubivirus* family that stated the occurrence of a PCP domain [104]. However, an enzymatic activity of this domain has yet to be proven. In a report by Saraswat *et al.*, in order to characterize the nature of the HEV protease, they used an FTC–based casein assay to determine the effects of several inhibitors on the protease activity [129]. The protease domain had been expressed in baculovirus and was purified to be used in a cell–free assay. In their inhibition assay, 12 compounds belonging to different groups of protease inhibitors (serine proteases, aspartic proteases, amino–peptidases, metallo–endoproteases, cystein proteases) were tested. Based on their choice of compounds, we selected four molecules to test their effect in a replicative system. Additionally, we chose a specific zinc–chelator since the same report revealed this ion to be required as an optimal reaction component. Lastly, the direct acting antiviral velpatasvir was chosen, a molecule that efficiently inhibits HCV replication by binding to domain I of the NS5A, which binds one zinc ion and is involved in viral replication [407, 408]. Sofosbuvir was chosen as a control as it is a nucleoside analogon that inhibits HEV replication [328]. After selecting these molecules, preliminary experiments to ensure their functionality and the permeability of the molecules were conducted using two different *Renilla* luciferase replicons: a 229E coronavirus replicon that is susceptible to all cysteine protease inhibitors and zinc chelators and an HCV replicon that can be inhibited by velpatasvir. In both cases, the expected inhibition was found at the specific working concentrations.
Next, we performed a replication kinetics experiment by using the p6–GLuc replicon with a luciferase activity read–out (Chapter 5.6.2). By comparing the non–treated p6–GLuc replicon with the compound treated replicon, we show that the HEV replication is only moderately or not at all inhibited by the selected molecules (Fig. 37 (A)). The ion chelator EDTA had no impact on HEV replication, since it is likely not very specific for zinc. TPEN, the zinc ion chelator, showed cytotoxicity at the highest dose tested and no effect at a smaller dose. Although, it could be interesting to test several intermediary doses to determine its exact cytotoxic dose and its activity on HEV replication at a non cytotoxic dose. Also, velpatasvir did not significantly impact HEV replication, even at higher doses tested, nor did it modify its subcellular localization. Therefore, the zinc binding to HEV protease may not be as essential for HEV replication as it is for HCV.
The cysteine protease inhibitors E64d, antipain and leupeptin showed a moderate degree of inhibition at the highest dose tested. However, the reduction of replication efficacy is not significantly different compared to the non–inhibited replication. These results stand in contrast to the finding published by Saraswat *et al.* [129]. Their team used a cell–free system to test

the protease inhibitors with a FTC–casein based protease assay. This is different from our GLuc replicon in PLC3 cells, since the used compounds might behave differently within cells compared to a cell–free system. In cells, drugs could get degraded or are even cytotoxic at certain concentrations, therefore the discrepancy between the results might be explained. In the context of a replicative system, the protease activity of the PCP (or a cellular protease) towards ORF1 has not yet been proven, therefore it cannot be excluded that this domain is not functional.

Next, the effect of these compounds on HEV expression was tested by western blot. All in all, it can be stated that no difference between the bands derived from the non–inhibited p6–V1–gluc versus the inhibited p6–V1–gluc could be observed. Both the band pattern and intensity remained unchanged upon treatment with all compounds. Additionally, no difference was observed between the subcellular ORF1 localization obtained by IF. Taken together, the replication kinetics, the immunoblot and IF results confirm that no impact of protease inhibitors or ion chelators on HEV replication could be observed.

On the other hand, a relatively recent report by Proudfoot *et al.* challenged the PCP domain and identified a fatty acid binding domain instead of a protease domain [130]. Additionally, the newly identified domain seems to be placed further downstream compared to the initially assigned PCP domain (Fig. 8). While these results need to be further characterized, they might offer evidence why the tested cysteine protease inhibitors had no specific impact on HEV replication. Also, it is possible that a protease of the host cell might be responsible for the processing of the ORF1 protein. Inversely, the HEV protease might target host cell proteins, however, we did not investigate these leads any further.

At last, we were interested in finding out the sequence of the observed potential cleavage products of the ORF1 protein. We used mass spectrometry to analyze the observed bands (Chapter 5.6.3). Therefore, a large IP was performed using H7–T7–IZ cells transfected with the ORF1–V1 or PLC3 cells electroporated with the p6–V1. After SDS–PAGE electrophoresis the bands of interest were cut from the colloidal blue stained gel and submitted to mass spectrometry. A western blot with the same samples was run in parallel. Since immunoblotting is a more sensitive technique, bands that were unable to be stained by the colloidal blue could still be cut according to the western blot results. In fact, only the full length ORF1 band was successfully stained by colloidal blue, since it is produced in higher amounts. The other bands were only present in low amounts, which was the limiting factor that prevented us from going further along that line. As a result, the full length ORF1 protein was identified with certainty by mass spectrometry (sequence coverage of 38% for the p6–V1 and 35% for the ORF1–V5). The analyses of the smaller bands resulted in the identification of parts of the ORF1 protein, however, they covered less sequence information, smaller number of spectra and overall lower scores per identified peptide. Indeed, the low expression levels of these products in

both analyzed systems prevented the reliable identification of their cleavage sites. However, it appeared that the N–terminus of the identified smaller bands was stable and corresponded to the N–terminus of the polyprotein. This could hint towards a cleavage from the C–terminus rather than from the N–terminus.
In addition, an immunoprecipitation with an anti–HA–antibody using H7–T7–IZ lysates that expressed the ORF1–H1 was used to identify the sequence of potential cleavage products. By using the anti–HA–antibody we hoped to increase the amount of protein that can be coupled to the beads, however, the MS/MS analysis did not yield any detectable ORF1 sequence (data not shown).
All in all, the results from the MS confirmed that the detected protein bands of lower abundance contained parts of the ORF1 protein, but no conclusive sequence identification could be attributed to the potential cleavage products.

6.3. Membrane Rearrangement

The next objective of this study was to investigate whether the viral replicase induces membrane rearrangement in host cells. It is common for positive–standed RNA viruses to induce membrane rearrangement in cells and preliminary data from our lab suggested that HEV could induce the formation of clusters of vesicles inside the host cell cytoplasm (Chapter 5.8). However, a closer analysis of PLC3 cells showed that these vesicles are likely the result of an over–active Golgi apparatus which is specific for this cell line, as these vesicles were also present in mock–electroporated cells.
Furthermore, we were not successful in detecting the ORF1 protein in PLC3 cells electroporated with the p6–V1 or the p6–H2 using immuno–gold labeling. The tight temporal regulation and the low expression levels of ORF1 are likely responsible for the absence of ORF1 detection in cryo–sections.
As a result, whether or not ORF1 induces membrane rearrangement remains inconclusive.

6.4. Subcellular Localization of HEV Replication

In which subcellular compartment does HEV replication take place? Generally, positive–sense single stranded RNA viruses replicate in the cytoplasm of the cell.
In previous studies on HEV, the non–structural protein was found in the cytoplasm colocalizing with the other viral proteins and markers of the ERGIC, Golgi and exosomes [166, 222]. To answer this question in our system, we were interested in the localization of the ORF1 protein in the cell, but also the localization of viral genomic and subgenomic RNA.
To begin with, subcellular fractionation of cells expressing the ORF1 protein was undertaken,

that isolates two cytoplasmic fractions, two nuclear fractions and the cytoskeleton (Chapter 5.7). Interestingly, the ORF1 protein was dispersed throughout all the subcellular fractions in all three systems used. Of note, the full length protein was present in all fractions, and the potential cleavage products were observed in all fractions except the nuclear chromatin bound fraction. In this fraction, the abundance of the full length ORF1 was the lowest as well. It is further interesting to note, that the band pattern varied slightly among the different fractions. In the p6 infectious system, one band at 150kDa appeared only in the nuclear soluble and cytoskeleton fractions and was not visible in the two cytoplasmic fractions. The heterologously expressed ORF1–V1 and –V2 showed a less intense band pattern in the nuclear soluble fraction compared to the other systems. However, without the sequence information it is difficult to interpret the band pattern. It is possible however, that certain potential cleavage products are required only in certain fractions if they serve a specific purpose.

In line with these results are the findings of the ORF1 protein localization obtained by immunofluorescence (Chapter 5.9.1). Both the heterologously expressed ORF1 and the infectious p6–ORF1 are localized throughout the cell in the cytoplasm and the nucleus. Again, the staining of the heterologously expressed ORF1–V1 is less intense in the nucleus than in the cytoplasm, thereby confirming the finding observed by subcellular fractionation. Unfortunately, the p6–V1–GLuc replicon was unable to be detected in PLC3 cells by IF. This is likely due to a lower expression of the ORF1 protein in the cell. The nuclear labeling of the ORF1 protein stands in contrast to the findings reported by Szkolnicka *et al.* who showed a cytoplasmic only localization of the ORF1. The difference in localization might be due to different strains of the genotype 3 HEV being used. The Kernow p6 strain contains a S17 insertion in the HVR of the ORF1 that potentially could act as a nuclear localization signal (NLS) [409]. Furthermore it is not uncommon even for RNA virus non–structural proteins to exert functions non–related to viral replication, which could be an explanation for their localization in the nucleus (Dengue virus [410], SFV [411], Equine arteritis virus [412] non–structural proteins are found in the nucleus at early stages of infection, but it is not yet known for which exact reason they are transported to the nucleus). However, it is still unclear if the full length ORF1 or potential cleavage products migrate into the nucleus and which purpose it serves.

The ORF1 labeling also shows peri–nuclear nugget–shaped accumulations that often coincide with a nuclear deformation. This pattern has been previously observed for the ORF2 and ORF3 protein of the Kernow C1 strain as well [393]. Indeed, a partial overlap between the ORF1 and the other viral proteins was observed in the present study, which is in line with the findings reported by Szkolnicka *et al.*. In the perinuclear nugget–shaped accumulations, the pearson coefficient for the overlap between ORF1 and ORF2 amounts to 0.57 and between ORF1 and ORF3 it is 0.54. These coefficients are moderate, but show a certain degree of overlap between the ORF1 and the other viral proteins. Also, when the ORF1–V1 was (het-

erologously) expressed on its own, only few cells were observed that showed the perinuclear accumulations. However, when co–expressed with ORF2 or ORF3, the nugget–shaped accumulations were visible more abundantly. This might indicate, that the ORF1 protein does not induce these structures by itself.

As it was reported by Bentaleb *et al.*, the ORF2 protein colocalizes with several cellular factors located in the endosomal recycling compartment (ERC), indicating the site of HEV assembly. Interestingly, an overlap between ORF1 and the same factors has been found in this study as well (Chapter 5.9.2) [393]. The ERC is responsible for mediating cargo to the plasma membrane and it is involved in several cellular processes. Pathogens such as viruses have been hijacking the ERC during infection [413, 414]. ORF1 partially overlaps with the factors Rab11, CD71 and EHD1 (Fig. 42&43).

The transferrin receptor I, CD71, is a membrane glycoprotein responsible for cellular iron uptake [415]. It is localized at the plasma membrane, gets internalized via endosomes and is transported back to the plasma membrane [394]. Additionally, it serves as a receptor for arenaviruses [416]. Upon HEV infection, it forms perinuclear nugget–shaped foci that overlap with all viral proteins. The pearson coefficient for the overlap with ORF1 is relatively low which is probably due to an only partial overlap in the previously mentioned foci.

Rab11 (a small GTPase) is a key player in the ERC and is involved in processes such as promoting epithelial and endothelial barrier integrity, sensing and immobilizing pathogens, and repairing pathogen–induced cellular damage. Many bacterial or viral pathogens exploit Rab11 trafficking to invade or escape from the host cells [395]. The pearson coefficient between ORF1 and Rab11 is higher compared to the coefficient between ORF1 and CD71, which is likely attributed to the fact that the Rab11 staining is primarily located to the perinuclear accumulations.

Protein kinase C and casein kinase substrate in neurons (PACSIN) family members are involved in several cellular processes such as clathrin–dependent and –independent endocytosis, caveolae formation, vesicle trafficking, actin dynamics, and cell migration [417–421]. Furthermore, PACSIN2 (also known as syndapin 2) is implicated in the propagation of HIV [422, 423] and it interacts with the NS5A of HCV to promote viral assembly [396]. The ERC is functionally interconnected with the tubular recycling endosome (TRE) whose morphogenesis is controlled by PACSIN2 [424–428]. Also, PACSIN2 recruits EHD1 to the TRE [397, 429]. The overlap between ORF1 and EHD1 is also mainly focused in the perinuclear nugget–shaped foci. Therefore it can be stated that the ORF1 localization extends to the TRE. The viral proteins ORF2 and ORF3 co–distribute with markers of the late endosome CD63 and CD81, which are tetraspanins found in multivesicular bodies (MVBs). Also, Szkolnicka *et al.* observed colocalization between ORF1 and CD63 as well as CD151 [222]. However, no colocalization was observed for ORF1 and these two cellular proteins. This might indicate that

ORF1 of the p6 strain specifically localizes to the ERC and the TRE and not late endosomes. Taken together, these results suggest that the place of viral replication is in close proximity to the site of HEV assembly.

To confirm this first evidence, we were looking to localize HEV RNA within the cell (Chapter 5.9.3). An indicator for the replication of RNA viruses (that are not retroviruses) is the occurrence of double stranded RNA. Initially, it was planned to stain double stranded RNA with the antibody J2 in PLC3 cells electroporated with the HEV p6. Unfortunately, the antibody staining at 3dpe did not reveal any specific labeling. This may be caused by low expression levels of double stranded RNA due to a slow replication of the virus.

Therefore, we were opting for a technique that can specifically and sensitively detect HEV RNA in fixed cells and we decided to set up the RNAscope® technique for *in situ* hybridization. This technique was also used to successfully visualize HCV and Zika RNA in fixed cells [245, 430].

The negative–sense RNA is primarily an indicator for viral replication since its only purpose serves as a template for positive–stranded RNA. It can be seen that HEV negative–sense RNA was most prevalent at early time points and its intensity faded over time (Fig. 44). This points towards an early onset of HEV replication that slows down over time as it was seen on the expression of ORF1 and potential cleavage products on Western blot (Fig. 34).

Positive–stranded genomic RNA was further co–stained with all viral proteins at 3dpe. Indeed, positive–stranded genomic RNA did co–localize with ORF1, ORF2 and ORF3 in the perinuclear foci indicated by Pearson coefficients of 0.44, 0.49 and 0.57, respectively.

Positive–stranded RNA was also co–labeled with the cellular factors Rab11 localized in the ERC and CD63 in the late endosomes. Similarly to the co–staining of ORF1, Rab11 was found to overlap partially with postive–sense RNA. However, while ORF1 did not appear to colocalize with CD63, positive–sense RNA showed a higher degree of colocalization. Taken together, the visualization of RNA corroborates the hypothesis that the site of HEV replication and assembly are in close proximity to each other.

6.5. Conclusion

To conclude, we successfully inserted two V5 epitopes (V1 and V2) into the HVR of ORF1 of HEV that allowed the detection of the ORF1–tagged protein by anti–V5 antibodies, while the replication of the virus or the replicon is not negatively impacted. Furthermore, genomic and subgenomic RNA levels as well as the infectivity of the newly generated constructs remained comparable to those of the non–tagged p6–wt.

By using the V5 tagged HEV, it was found that the ORF1 protein is detected very early on after electroporation and is still detectable after 5 passages (4hpe–25dpe). Moreover, next to the full–length ORF1 protein that has an expected size of 194kDa, smaller bands that could correspond to potential cleavage products were visible too. These bands are likely not the result of degradation, as the inhibition of the proteasome did not abrogate the occurrence of these proteins. Unfortunately, we did not fully identify the sequence of these bands, however, it seems that they are rather cleaved from the C–terminus than the N–terminus, as the identified peptides of all minor bands matched the N–terminus of the full–length ORF1 protein.

The nature of the protease that might be responsible for the potential processing is unclear, as cysteine protease inhibitors did not result in a lowered replication capacity.

It also remained inconclusive whether or not the viral replicase induces host cell membrane rearrangement as positive–sense RNA viruses usually do. Unfortunately, the tagged ORF1 protein could not be detected by immuno–electron microscopy.

On the other hand, the ORF1 localization was identified by immuno–labeling. It was observed that the ORF1 protein localizes to the cell nucleus and is diffused in the cytoplasm to lower extent. It also forms perinuclear nugget–shaped foci in which it co–localizes with the other viral proteins ORF2 and ORF3. This site has recently been characterized as a hypothetical site of HEV assembly, that recruits cellular proteins of the ERC (Rab11, CD71, EHD1) [393]. Indeed, the ORF1 protein also co–localizes to these proteins implying that the site for viral replication and viral assembly are in close proximity to each other. Finally, *in situ* hybridization of HEV positive– and negative–stranded RNA corroborates these findings as co–localization with the previously mentioned viral and cellular proteins can be stated.

All in all, this study helped to gain a better understanding of the possible maturation of the HEV viral replicase and the localization of its replication site in host cells.

7. Perspectives

This report on the characterization of the hepatitis E virus replicase opens up new possibilities for further studies. By using the described cell culture system and/or the different V5 tagged constructs, new leads could be pursued in the future.

In order to characterize especially the PCP domain of HEV, it may be a worthwhile to explore further the idea of the potential fatty acid binding domain. A collaboration with the team of Proudfoot *et al.* who published their results in 2020 could be of interest. In this context, it could be an idea to test FABD binding competitors on the HEV replicon to characterize this potential domain further.

The p6–Gluc replicon could also be used to evaluate a more important number of FABD binding competitos or inhibitors of the HEV replication in general, since the *Gaussia* luciferase read–out is compatible with a high–throughput screening assay. This would allow to characterize the replication through the mechanism of action of different compounds and at the same time it could potentially lead to an opportunity to develop a treatment against the virus. It would also be possible to use a replicon with GFP in place of the *Gaussia* luciferase to set up a high–throughput assay so that the read–out could be analyzed by a high–content imaging platform.

Furthermore, the sequencing of the potential cleavage products of the ORF1 protein still needs to be improved. The low abundance of the proteins of interest likely calls for more sensitive technologies. Unfortunately, there is not yet a universally used improved technique for this goal, however, the latest developments in the domain of protein sequencing need to be followed. For example, it is possible to couple mass spectrometers with a nanopore ion source in order to sequence single molecules. The techniques improves sensitivity and allows for the detection of post–translational modifications [431]. Other new technologies consist of DNA technologies for protein sequencing and biological and solid state nanopores, that are however, only in the early steps of development [431].

Finally, the localization of ORF1 could be further characterized. In preliminary experiments we mutated a potential nuclear localization signal (NLS) that was described by Kenney&Meng in 2015 [409] to analyze the effect of this signal on the subcellular localization of ORF1. Unfortunately, the NLS mutants were no longer replication competent and could not be further studied. However, it would be possible to only mutate part of the NLS or the S17 region (that contains the NLS) could be inserted into a different strain of the same genotype to study its effect on the ORF1 localization. Also, it would be interesting to confirm the subcellular localization of HEV that we observed in our cell culture systems also in *in vivo* tissue samples. It would be feasible to perform not only indirect immuno–labeling of the non–structural protein but also *in situ* RNA hybridization to detect positive– and negative–stranded RNA in those samples.

To conclude, it would be very interesting to establish collaborations as well as use the newest state–of–the-art techniques to pursue the goal to characterize the replication step of the HEV life cycle.

References

[1] T. L. Meister, J. Bruening, D. Todt, and E. Steinmann, “Cell culture systems for the study of hepatitis e virus,” *Antivir Res*, vol. 163, pp. 34–49, 2019.

[2] R. Fu, C. Decker, and V. Thi, “Cell culture models for hepatitis e virus,” *Viruses*, vol. 11, no. 7, p. 608, 2019.

[3] M. Balayan, A. Andjaparidze, S. Savinskaya, E. Ketiladze, D. Braginsky, A. Savinov, and V. Poleschuk, “Evidence for a virus in non-A, non-B hepatitis transmitted via the fecal-oral route.,” *Intervirology*, vol. 20, no. 1, pp. 23–31, 1983.

[4] M. Khuroo, “Study of an epidemic of non-A, non-B hepatitis possibility of another human hepatitis virus distinct from post-transfusion non-A, non-B type,” *Am J Medicine*, vol. 68, no. 6, pp. 818–824, 1980.

[5] R. Purcell, “The discovery of the hepatitis viruses.,” *Gastroenterology*, vol. 104, no. 4, pp. 955–63, 1993.

[6] G. Reyes, M. Purdy, J. Kim, K. Luk, L. Young, K. Fry, and D. Bradley, “Isolation of a cDNA from the virus responsible for enterically transmitted non-A, non-B hepatitis,” *Science*, vol. 247, no. 4948, pp. 1335–1339, 1990.

[7] A. W. Tam, M. M. Smith, M. E. Guerra, C. Huang, D. W. Bradley, K. E. Fry, and G. R. Reyes, “Hepatitis e virus (HEV): molecular cloning and sequencing of the full-length viral genome,” *Virology*, vol. 185, no. 1, pp. 120–131, 1991.

[8] D. B. Smith, P. Simmonds, I. members of the on the of Group, S. Jameel, S. U. Emerson, T. J. Harrison, X. Meng, H. Okamoto, W. H. der Poel, and M. A. Purdy, “Consensus proposals for classification of the family hepeviridae,” *J Gen Virol*, vol. 95, no. Pt_10, pp. 2223–2232, 2014.

[9] A. Kelly, N. Netzler, and P. White, “Ancient recombination events and the origins of hepatitis e virus,” *Bmc Evol Biol*, vol. 16, no. 1, p. 210, 2016.

[10] S. U. Emerson, H. Nguyen, J. Graff, D. A. Stephany, A. Brockington, and R. H. Purcell, “In vitro replication of hepatitis e virus (HEV) genomes and of an HEV replicon expressing green fluorescent protein,” *J Virol*, vol. 78, no. 9, pp. 4838–4846, 2004.

[11] P. P. Primadharsini, S. Nagashima, and H. Okamoto, “Genetic variability and evolution of hepatitis e virus.,” *Viruses*, vol. 11, no. 5, 2019.

[12] A. Andonov, M. Robbins, J. Borlang, J. Cao, T. Hatchette, A. Stueck, Y. Deschambault, K. Murnaghan, J. Varga, and L. Johnston, "Rat hepatitis e virus linked to severe acute hepatitis in an immunocompetent patient," *J Infect Dis*, vol. 220, no. 6, pp. 951–955, 2019.

[13] S. Sridhar, C. Yip, S. Wu, J. Cai, A. Zhang, K. Leung, T. Chung, J. Chan, W. Chan, J. Teng, A. Rex, V. Cheng, H. Chen, S. Lau, P. Woo, N. Xia, C. Lo, and K. Yuen, "Rat hepatitis e virus as cause of persistent hepatitis after liver transplant," *Emerg Infect Dis*, vol. 24, no. 12, pp. 2241–2250, 2018.

[14] S. Lhomme, M. Migueres, F. Abravanel, O. Marion, N. Kamar, and J. Izopet, "Hepatitis e virus: How it escapes host innate immunity," *Nato Adv Sci Inst Se*, vol. 8, no. 3, p. 422, 2020.

[15] "WHO $\{|\}$ hepatitis e," 2017.

[16] C. Adlhoch, A. Avellon, S. A. Baylis, A. R. Ciccaglione, E. Couturier, R. de Sousa, J. Epštein, S. Ethelberg, M. Faber, Á. Fehér, S. Ijaz, H. Lange, Z. Manďáková, K. Mellou, A. Mozalevskis, R. Ruska, V. Rizzi, B. Said, L. Sundqvist, L. Thornton, M. E. Tosti, W. van Pelt, E. Aspinall, D. Domanovic, E. Severi, J. Takkinen, and H. R. Dalton, "Hepatitis e virus: Assessment of the epidemiological situation in humans in europe, 2014/15," *J Clin Virol*, vol. 82, pp. 9–16, 2016.

[17] G. Zehender, E. Ebranati, A. Lai, C. Luzzago, S. Paladini, C. Tagliacarne, C. Galli, M. Galli, M. Ciccozzi, A. R. Zanetti, and L. Romanò, "Phylogeography and phylodynamics of european genotype 3 hepatitis e virus," *Infect Genetics Evol*, vol. 25, pp. 138–143, 2014.

[18] ECDC, "Facts about hepatitis e," 2017.

[19] H. R. Dalton, N. Kamar, J. J. van Eijk, B. N. Mclean, P. Cintas, R. P. Bendall, and B. C. Jacobs, "Hepatitis e virus and neurological injury," *Nat Rev Neurol*, vol. 12, no. 2, pp. 77–85, 2016.

[20] N. Kamar, R. Bendall, L. Florence, N. Xia, S. Ijaz, J. Izopet, and H. R. Dalton, "Hepatitis e," *Lancet*, vol. 379, no. 9835, pp. 2477–2488, 2012.

[21] J. H. Hoofnagle, K. E. Nelson, and R. H. Purcell, "Hepatitis e," *New Engl J Medicine*, vol. 367, no. 13, pp. 1237–1244, 2012.

[22] Y. Debing, D. Moradpour, J. Neyts, and J. Gouttenoire, "Update on hepatitis e virology: Implications for clinical practice," *J Hepatol*, vol. 65, no. 1, pp. 200–212, 2016.

[23] E. Tsega, K. Krawczynski, B. Hansson, E. Nordenfelt, Y. Negusse, W. Alemu, and Y. Bahru, "Outbreak of acute hepatitis e virus infection among military personnel in northern ethiopia," *J Med Virol*, vol. 34, no. 4, pp. 232–236, 1991.

[24] M. M. C, J. He, K. C. Hyams, E. Ahmed, I. O. Khalid, and M. Carl, "Acute hepatitis e infection during the 1988 floods in khartoum, sudan," *T Roy Soc Trop Med H*, vol. 88, no. 2, p. 177, 1994.

[25] J. Guthmann, H. Klovstad, D. Boccia, N. Hamid, L. Pinoges, J. Nizou, M. Tatay, F. Diaz, A. Moren, R. Grais, I. Ciglenecki, E. Nicand, and P. Guerin, "A large outbreak of hepatitis e among a displaced population in darfur, sudan, 2004: The role of water treatment methods," *Clin Infect Dis*, vol. 42, no. 12, pp. 1685–1691, 2006.

[26] P. Woo, S. Lau, J. Teng, A. K. Tsang, M. Joseph, E. Wong, Y. Tang, S. Sivakumar, J. Xie, R. Bai, R. Wernery, U. Wernery, and K. Yuen, "New hepatitis e virus genotype in camels, the middle east," *Emerg Infect Dis*, vol. 20, no. 6, pp. 1044–1048, 2014.

[27] A. Rasche, M. Saqib, A. M. Liljander, S. Bornstein, A. Zohaib, S. Renneker, K. Steinhagen, R. Wernery, M. Younan, I. Gluecks, M. Hilali, B. E. Musa, J. Jores, U. Wernery, J. Drexer, C. Drosten, and V. Corman, "Hepatitis e virus infection in dromedaries, north and east africa, united arab emirates, and pakistan, 1983–2015," *Emerg Infect Dis*, vol. 22, no. 7, pp. 1249–1252, 2016.

[28] S. Kumar, S. Subhadra, B. Singh, and B. Panda, "Hepatitis e virus: the current scenario," *Int J Infect Dis*, vol. 17, no. 4, pp. e228–e233, 2013.

[29] T. Ahmad, J. Hui, T. Musa, M. Behzadifar, and M. Baig, "Seroprevalence of hepatitis e virus infection in pregnant women: a systematic review and meta-analysis," *Ann Saudi Med*, vol. 40, no. 2, pp. 136–146, 2020.

[30] F. Farshadpour, S. Taherkhani, and R. Taherkhani, "Hepatitis e virus infection during pregnancy: The overlooked cause of maternal and fetal mortality," *Infect Disord - Drug Targets*, vol. 19, no. 3, pp. 334–336, 2019.

[31] X. Meng, P. G. Halbur, M. S. Shapiro, S. Govindarajan, J. D. Bruna, I. K. Mushahwar, R. H. Purcell, and S. U. Emerson, "Genetic and experimental evidence for Cross-Species infection by swine hepatitis e virus," *J Virol*, vol. 72, no. 12, pp. 9714–9721, 1998.

[32] X. Cheng, S. Wang, X. Dai, C. Shi, Y. Wen, M. Zhu, S. Zhan, and J. Meng, "Rabbit as a novel animal model for hepatitis e virus infection and vaccine evaluation," *Plos One*, vol. 7, no. 12, p. e51616, 2012.

[33] D. M. Yugo, C. M. Cossaboom, and X. Meng, "Naturally occurring animal models of human hepatitis e virus infection," *Ilar J*, vol. 55, no. 1, pp. 187–199, 2014.

[34] R. Mar, B. Mínguez, R. Gironés, R. Francisco, J. Quer, and M. Buti, "Phylogenetic demonstration of hepatitis e infection transmitted by pork meat ingestion," *J Clin Gastroenterol*, vol. 49, no. 2, pp. 165–168, 2015.

[35] P. Colson, P. Borentain, B. Queyriaux, M. Kaba, V. Moal, P. Gallian, L. Heyries, D. Raoult, and R. Gerolami, "Pig liver sausage as a source of hepatitis e virus transmission to humans," *J Infect Dis*, vol. 202, no. 6, pp. 825–834, 2010.

[36] C. Niederhauser, N. Widmer, M. Hotz, C. Tinguely, S. Fontana, G. Allemann, M. Borri, L. Infanti, A. Sarraj, J. Sigle, M. Stalder, J. Thierbach, S. Waldvogel, T. Wiengand, M. Züger, and P. Gowland, "Current hepatitis e virus seroprevalence in swiss blood donors and apparent decline from 1997 to 2016," vol. 23, no. 35, p. 1700616, 2018.

[37] P. Kokkinos, I. Kozyra, S. Lazic, M. Bouwknegt, S. Rutjes, K. Willems, R. Moloney, R. A. de Husman, A. Kaupke, E. Legaki, D. M, N. Cook, A. Rzeżutka, T. Petrovic, and A. Vantarakis, "Harmonised investigation of the occurrence of human enteric viruses in the leafy green vegetable supply chain in three european countries," *Food Environ Virol*, vol. 4, no. 4, pp. 179–191, 2012.

[38] P. E. Hewitt, S. Ijaz, S. R. Brailsford, R. Brett, S. Dicks, B. Haywood, I. T. Kennedy, A. Kitchen, P. Patel, J. Poh, K. Russell, K. I. Tettmar, J. Tossell, U. Ines, and R. S. Tedder, "Hepatitis e virus in blood components: a prevalence and transmission study in southeast england," *Lancet*, vol. 384, no. 9956, pp. 1766–1773, 2014.

[39] D. Domanović, R. Tedder, J. Blümel, H. Zaaijer, P. Gallian, C. Niederhauser, S. Oliveras, O. Joan, F. Boland, L. Harritshøj, M. Nascimento, A. Ciccaglione, C. Politis, C. Adlhoch, B. Flan, O. Wahiba, G. Rautmann, P. Strengers, and P. Hewitt, "Hepatitis e and blood donation safety in selected european countries: a shift to screening?," *Eurosurveillance*, vol. 22, no. 16, p. 30514, 2017.

[40] C. Pilar, R. Carlota, R. Eugenio, and A. Mas, "Hepatitis e virus in industrialized countries: The silent threat," *Biomed Res Int*, vol. 2016, pp. 1–17, 2016.

[41] I. Ditah, F. Ditah, P. Devaki, C. Ditah, P. S. Kamath, and M. Charlton, "Current epidemiology of hepatitis e virus infection in the united states: Low seroprevalence in the national health and nutrition evaluation survey," *Hepatology*, vol. 60, no. 3, pp. 815–822, 2014.

[42] J. Izopet, P. Tremeaux, O. Marion, M. Migueres, N. Capelli, C. Sabine, J. Mansuy, F. Abravanel, N. Kamar, and S. Lhomme, "Hepatitis e virus infections in europe," *J Clin Virol*, vol. 120, pp. 20–26, 2019.

[43] S. Emerson, H. Nguyen, U. Torian, K. Mather, and A. Firth, "An essential RNA element resides in a central region of hepatitis e virus ORF2," *J Gen Virol*, vol. 94, no. Pt_7, pp. 1468–1476, 2013.

[44] N. Kamar, J. Izopet, N. Pavio, R. Aggarwal, A. Labrique, H. Wedemeyer, and H. R. Dalton, "Hepatitis e virus infection," *Nat Rev Dis Primers*, vol. 3, no. 1, p. nrdp201786, 2017.

[45] H. Wedemeyer, S. Pischke, and M. P. Manns, "Pathogenesis and treatment of hepatitis e virus infection," *Gastroenterology*, vol. 142, no. 6, pp. 1388–1397.e1, 2012.

[46] D. B. Rein, G. A. Stevens, J. Theaker, J. S. Wittenborn, and S. T. Wiersma, "The global burden of hepatitis e virus genotypes 1 and 2 in 2005," *Hepatology*, vol. 55, no. 4, pp. 988–997, 2012.

[47] U. Navaneethan, M. Mohajer, and M. T. Shata, "Hepatitis e and pregnancy: understanding the pathogenesis," *Liver Int*, vol. 28, no. 9, pp. 1190–1199, 2008.

[48] Y. Guillois, F. Abravanel, T. Miura, N. Pavio, V. Vaillant, S. Lhomme, F. S. Guyader, N. Rose, J. Saux, L. A. King, J. Izopet, and E. Couturier, "High proportion of asymptomatic infections in an outbreak of hepatitis e associated with a Spit-Roasted piglet, france, 2013," *Clin Infect Dis*, vol. 62, no. 3, pp. 351–357, 2016.

[49] B. Said, S. Ijaz, G. Kafatos, L. Booth, L. H. Thomas, A. Walsh, M. Ramsay, D. Morgan, and H. E. Team, "Hepatitis e outbreak on cruise ship," *Emerg Infect Dis*, vol. 15, no. 11, pp. 1738–1744, 2009.

[50] M. Faber, N. Willrich, M. Schemmerer, C. Rauh, R. Kuhnert, K. Stark, and J. Wenzel, "Hepatitis e virus seroprevalence, seroincidence and seroreversion in the german adult population," *J Viral Hepatitis*, vol. 25, no. 6, pp. 752–758, 2018.

[51] E. B. Haagsma, A. P. van den Berg, R. J. Porte, C. A. Benne, H. Vennema, J. H. Reimerink, and M. P. Koopmans, "Chronic hepatitis e virus infection in liver transplant recipients," *Liver Transplant*, vol. 14, no. 4, pp. 547–553, 2008.

[52] N. Kamar, J. Mansuy, O. Cointault, J. Selves, F. Abravanel, M. Danjoux, P. Otal, L. Esposito, D. Durand, J. Izopet, and L. Rostaing, "Hepatitis e Virus-Related cirrhosis in

kidney-and Kidney–Pancreas-Transplant recipients," *Am J Transplant*, vol. 8, no. 8, pp. 1744–1748, 2008.

[53] R. Gérolami, V. Moal, and P. Colson, "Chronic hepatitis e with cirrhosis in a Kidney-Transplant recipient," *New Engl J Medicine*, vol. 358, no. 8, pp. 859–860, 2008.

[54] P. Colson, M. Kaba, J. Moreau, and P. Brouqui, "Hepatitis e in an HIV-infected patient," *J Clin Virol*, vol. 45, no. 4, pp. 269–271, 2009.

[55] H. R. Dalton, R. P. Bendall, F. E. Keane, R. S. Tedder, and S. Ijaz, "Persistent carriage of hepatitis e virus in patients with HIV infection," *New Engl J Medicine*, vol. 361, no. 10, pp. 1025–1027, 2009.

[56] K. Alain, S. Franziska, P. Bürgisser, A. Witteck, K. E. Darling, H. Kovari, L. Kaiser, J. Evison, L. Elzi, V. Fuente, J. Jost, D. Moradpour, F. Abravanel, J. Izpopet, M. Cavassini, and S. of the Study, "Hepatitis e virus seroprevalence and chronic infections in patients with HIV, switzerland," *Emerg Infect Dis*, vol. 17, no. 6, pp. 1074–1078, 2011.

[57] A. Tamura, Y. K. Shimizu, T. Tanaka, K. Kuroda, Y. Arakawa, K. Takahashi, S. Mishiro, K. Shimizu, and M. Moriyama, "Persistent infection of hepatitis e virus transmitted by blood transfusion in a patient with t-cell lymphoma," *Hepatol Res*, vol. 37, no. 2, pp. 113–120, 2007.

[58] J. Versluis, S. D. Pas, H. J. Agteresch, R. A. de Man, J. Maaskant, M. E. Schipper, A. D. Osterhaus, J. J. Cornelissen, and A. A. van der Eijk, "Hepatitis e virus: an underestimated opportunistic pathogen in recipients of allogeneic hematopoietic stem cell transplantation," *Blood*, vol. 122, no. 6, pp. 1079–1086, 2013.

[59] S. Pischke, J. Hartl, S. D. Pas, A. W. Lohse, B. C. Jacobs, and A. A. der Eijk, "Hepatitis e virus: Infection beyond the liver?," *J Hepatol*, vol. 66, no. 5, pp. 1082–1095, 2017.

[60] M. Takahashi, T. Tanaka, H. Takahashi, Y. Hoshino, S. Nagashima, Jirintai, H. Mizuo, Y. Yazaki, T. Takagi, M. Azuma, E. Kusano, N. Isoda, K. Sugano, and H. Okamoto, "Hepatitis e virus (HEV) strains in serum samples can replicate efficiently in cultured cells despite the coexistence of HEV antibodies: Characterization of HEV virions in blood circulation," *J Clin Microbiol*, vol. 48, no. 4, pp. 1112–1125, 2010.

[61] S. Nagashima, S. Jirintai, M. Takahashi, T. Kobayashi, Tanggis, T. Nishizawa, T. Kouki, T. Yashiro, and H. Okamoto, "Hepatitis e virus egress depends on the exosomal pathway, with secretory exosomes derived from multivesicular bodies," *J Gen Virol*, vol. 95, no. Pt_10, pp. 2166–2175, 2014.

[62] P. Rawla, J. Raj, A. Kannemkuzhiyil, J. Aluru, K. Thandra, and M. Gajendran, "A systematic review of the Extra-Hepatic manifestations of hepatitis e virus infection," *Medical Sci*, vol. 8, no. 1, p. 9, 2020.

[63] F. Abravanel, J. Pique, E. Couturier, F. Nicot, C. Dimeglio, S. Lhomme, J. Chiabrando, K. Saune, J. Péron, N. Kamar, S. Evrard, H. de Valk, P. Cintas, J. Izopet, and H. study group, "Acute hepatitis e in french patients and neurological manifestations," *J Infection*, vol. 77, no. 3, pp. 220–226, 2018.

[64] T. Horvatits and S. Pischke, "Extrahepatic manifestations and HEV, the genotype matters," *Ebiomedicine*, vol. 36, pp. 3–4, 2018.

[65] J. van Eijk, H. R. Dalton, P. Ripellino, R. G. Madden, C. Jones, M. Fritz, C. Gobbi, G. Melli, E. Pasi, J. Herrod, R. F. Lissmann, H. H. Ashraf, M. Abdelrahim, O. Masri, M. Fraga, D. Benninger, T. Kuntzer, V. Aubert, R. Sahli, D. Moradpour, B. Hélène, S. Attarian, R. Gérolami, P. Colson, M. T. Giordani, J. Hartl, S. Pischke, N. X. Lin, B. N. Mclean, R. P. Bendall, M. Panning, J. Peron, N. Kamar, J. Izopet, B. C. Jacobs, N. van Alfen, and B. van Engelen, "Clinical phenotype and outcome of hepatitis e virus–associated neuralgic amyotrophy," *Neurology*, vol. 89, no. 9, pp. 909–917, 2017.

[66] O. Stevens, K. G. Claeys, K. Poesen, V. Saegeman, and P. Damme, "Diagnostic challenges and clinical characteristics of hepatitis e Virus–Associated Guillain-Barré syndrome," *Jama Neurol*, vol. 74, no. 1, p. 26, 2016.

[67] A. Belbézier, A. Deroux, S. Françoise, B. Colombe, A. Bosseray, C. Wintenberger, P. Dumanoir, M. Lugosi, B. Isabelle, V. Leroy, M. Maignan, C. Roselyne, D. Viglino, M. Vaillant, L. Minotti, E. Lagrange, O. Epaulard, D. Chantal, S. Lhomme, J. Lupo, S. Larrat, P. Morand, C. Schwebel, A. Vilotitch, J. Bosson, and L. Bouillet, "Screening of hepatitis e in patients presenting for acute neurological disorders," *J Infect Public Heal*, vol. 13, no. 7, pp. 1047–1050, 2020.

[68] N. Kamar, J. Izopet, P. Cintas, C. Garrouste, U. E, O. Cointault, and L. Rostaing, "Hepatitis e Virus-Induced neurological symptoms in a Kidney-Transplant patient with chronic hepatitis," *Am J Transplant*, vol. 10, no. 5, pp. 1321–1324, 2010.

[69] F. Fousekis, I. Mitselos, and D. Christodoulou, "Extrahepatic manifestations of hepatitis e virus: An overview," *Clin Mol Hepatology*, vol. 26, no. 1, pp. 16–23, 2020.

[70] R. Shi, M. Soomro, R. She, Y. Yang, T. Wang, Q. Wu, H. Li, and W. Hao, "Evidence of hepatitis e virus breaking through the blood–brain barrier and replicating in the central nervous system," *J Viral Hepatitis*, vol. 23, no. 11, pp. 930–939, 2016.

[71] J. Tian, R. Shi, T. Liu, R. She, Q. Wu, J. An, W. Hao, and M. Soomro, “Brain infection by hepatitis e virus probably via damage of the Blood-Brain barrier due to alterations of tight junction proteins,” *Front Cell Infect Mi*, vol. 9, p. 52, 2019.

[72] D. A. Bello, G. C, A. Josse, L. Rostaing, J. Izopet, and N. Kamar, “Successful treatment of hepatitis e virus-associated cryoglobulinemic membranoproliferative glomerulonephritis with ribavirin,” *Transpl Infect Dis*, vol. 17, no. 2, pp. 279–283, 2015.

[73] M. Premkumar, D. Rangegowda, C. Vashishtha, V. Bhatia, J. Khumuckham, and B. Kumar, “Acute viral hepatitis e is associated with the development of myocarditis,” *Case Reports Hepatology*, vol. 2015, pp. 1–6, 2015.

[74] T. Dougherty, S. Bashir, M. Adam, and M. Borum, “Acute myopericarditis due to hepatitis e virus infection: The first reported case in the western hemisphere,” *J Gastrointest Dig Syst*, vol. 2016, no. 01, 2016.

[75] K. Woolson, A. Forbes, L. Vine, L. Beynon, M. L, V. Panayi, J. Hunter, R. Madden, T. Glasgow, A. Kotecha, H. Dalton, L. Mihailescu, U. Warshow, H. Hussaini, J. Palmer, B. Mclean, B. Haywood, R. Bendall, and H. Dalton, “Extra-hepatic manifestations of autochthonous hepatitis e infection,” *Aliment Pharm Therap*, vol. 40, no. 11-12, pp. 1282–1291, 2014.

[76] Z. Aiqin, X. Dongming, T. Kejun, Z. Yun, and Z. Aiqin, “LONG QT SYNDROME AND TORSADES DE POINTS IN a PATIENT WITH ACUTE HEPATITIS e VIRUS INFECTION: AN UNUSUAL CASE,” *Heart*, vol. 98, no. Suppl 2, p. E222, 2012.

[77] S. Haffar, F. Bazerbachi, L. Prokop, K. D. Watt, H. M. Murad, and S. T. Chari, “Frequency and prognosis of acute pancreatitis associated with fulminant or non-fulminant acute hepatitis a: A systematic review,” *Pancreatology*, vol. 17, no. 2, pp. 166–175, 2017.

[78] D. M. Parenti, W. Steinberg, and P. Kang, “Infectious causes of acute pancreatitis,” *Pancreas*, vol. 13, no. 4, pp. 356–371, 1996.

[79] L. Xing, K. Kato, T. Li, N. Takeda, T. Miyamura, L. Hammar, and R. Cheng, “Recombinant hepatitis e capsid protein Self-Assembles into a Dual-Domain t = 1 particle presenting native virus epitopes,” *Virology*, vol. 265, no. 1, pp. 35–45, 1999.

[80] L. Xing, T. Li, N. Mayazaki, M. N. Simon, J. S. Wall, M. Moore, C. Wang, N. Takeda, T. Wakita, T. Miyamura, and H. R. Cheng, “Structure of hepatitis e virion-sized particle reveals an RNA-dependent viral assembly pathway,” *J Biol Chem*, vol. 285, no. 43, pp. 33175–33183, 2010.

[81] T. Yamashita, Y. Mori, N. Miyazaki, H. R. Cheng, M. Yoshimura, H. Unno, R. Shima, K. Moriishi, T. Tsukihara, T. Li, N. Takeda, T. Miyamura, and Y. Matsuura, "Biological and immunological characteristics of hepatitis e virus-like particles based on the crystal structure," *Proc National Acad Sci*, vol. 106, no. 31, pp. 12986–12991, 2009.

[82] M. Rossmann and J. Johnson, "Icosahedral RNA virus structure," *Annu Rev Biochem*, vol. 58, no. 1, pp. 533–569, 1989.

[83] T. Shiota, T. Li, S. Yoshizaki, T. Kato, T. Wakita, and K. Ishii, "The hepatitis e virus capsid C-Terminal region is essential for the viral life cycle: Implication for viral genome encapsidation and particle stabilization," *J Virol*, vol. 87, no. 10, pp. 6031–6036, 2013.

[84] S. He, J. Miao, Z. Zheng, T. Wu, M. Xie, M. Tang, J. Zhang, M. Ng, and N. Xia, "Putative receptor-binding sites of hepatitis e virus," *J Gen Virol*, vol. 89, no. 1, pp. 245–249, 2008.

[85] M. Takahashi, K. Yamada, Y. Hoshino, H. Takahashi, K. Ichiyama, T. Tanaka, and H. Okamoto, "Monoclonal antibodies raised against the ORF3 protein of hepatitis e virus (HEV) can capture HEV particles in culture supernatant and serum but not those in feces," *Arch Virol*, vol. 153, no. 9, p. 1703, 2008.

[86] N. Capelli, O. Marion, M. Dubois, S. Allart, B. Justine, S. Lhomme, F. Abravanel, J. Izopet, and C. Sabine, "Vectorial release of hepatitis e virus in polarized human hepatocytes," *J Virol*, vol. 93, no. 4, 2018.

[87] O. Marion, S. Lhomme, M. Nayrac, M. Dubois, M. Pucelle, M. Requena, M. Migueres, F. Abravanel, J. Peron, N. Carrere, B. Suc, P. Delobel, N. Kamar, and J. Izopet, "Hepatitis e virus replication in human intestinal cells," *Gut*, vol. 69, no. 5, p. 901, 2020.

[88] K. Yamina, X. Meng, R. H. Purcell, and S. U. Emerson, "Evidence that the genomic RNA of hepatitis e virus is capped," *J Virol*, vol. 73, no. 10, pp. 8848–8850, 1999.

[89] V. P. Nair, S. Anang, C. Subramani, A. Madhvi, K. Bakshi, A. Srivastava, Shalimar, B. Nayak, K. C. Ranjith, and M. Surjit, "Endoplasmic reticulum stress induced synthesis of a novel viral factor mediates efficient replication of genotype-1 hepatitis e virus," *Plos Pathog*, vol. 12, no. 4, p. e1005521, 2016.

[90] J. Graff, U. Torian, H. Nguyen, and S. U. Emerson, "A bicistronic subgenomic mRNA encodes both the ORF2 and ORF3 proteins of hepatitis e virus," *J Virol*, vol. 80, no. 12, pp. 5919–5926, 2006.

[91] K. Ichiyama, K. Yamada, T. Tanaka, S. Nagashima, Jirintai, M. Takahashi, and H. Okamoto, "Determination of the 5-terminal sequence of subgenomic RNA of hepatitis e virus strains in cultured cells," *Arch Virol*, vol. 154, no. 12, pp. 1945–1951, 2009.

[92] Y. Huang, T. Opriessnig, P. Halbur, and X. Meng, "Initiation at the third In-Frame AUG codon of open reading frame 3 of the hepatitis e virus is essential for viral infectivity in vivo," *J Virol*, vol. 81, no. 6, pp. 3018–3026, 2007.

[93] J. Zhang, M. H. Ng, N. Xia, S. Lau, X. Che, T. Chau, S. Lai, and S. W. Im, "Conformational antigenic determinants generated by interactions between a bacterially expressed recombinant peptide of the hepatitis e virus structural protein," *J Med Virol*, vol. 64, no. 2, pp. 125–132, 2001.

[94] M. Surjit, S. Jameel, and S. K. Lal, "The ORF2 protein of hepatitis e virus binds the 5 region of viral RNA," vol. 78, no. 1, pp. 320–328, 2004.

[95] C. Huang, D. Nguyen, J. Fernandez, K. Y. Yun, K. E. Fry, D. W. Bradley, A. W. Tam, and G. R. Reyes, "Molecular cloning and sequencing of the mexico isolate of hepatitis e virus (HEV)," *Virology*, vol. 191, no. 2, pp. 550–558, 1992.

[96] M. Parvez, "The hepatitis e virus ORF1 X-domain residues form a putative macrodomain protein/Appr-1-pase catalytic-site, critical for viral RNA replication," *Gene*, vol. 566, no. 1, pp. 47–53, 2015.

[97] Q. Ding, I. Nimgaonkar, N. F. Archer, Y. Bram, B. Heller, R. E. Schwartz, and A. Ploss, "Identification of the intragenomic promoter controlling hepatitis e virus subgenomic RNA transcription," *Mbio*, vol. 9, no. 3, pp. e00769–18, 2018.

[98] J. Graff, H. Nguyen, C. Yu, W. R. Elkins, M. Claire, R. H. Purcell, and S. U. Emerson, "The open reading frame 3 gene of hepatitis e virus contains a cis-Reactive element and encodes a protein required for infection of macaques," vol. 79, no. 11, pp. 6680–6689, 2005.

[99] D. Cao, Y. Huang, and X. Meng, "The nucleotides on the Stem-Loop RNA structure in the junction region of the hepatitis e virus genome are critical for virus replication," vol. 84, no. 24, pp. 13040–13044, 2010.

[100] S. Agrawal, D. Gupta, and S. Panda, "The 3 end of hepatitis e virus (HEV) genome binds specifically to the viral RNA-Dependent RNA polymerase (RdRp)," vol. 282, no. 1, pp. 87–101, 2001.

[101] X. Ju, G. Xiang, M. Gong, R. Yang, J. Qin, Y. Li, Y. Nan, Y. Yang, Q. Zhang, and Q. Ding, "Identification of functional cis-acting RNA elements in the hepatitis e virus genome required for viral replication," *Plos Pathog*, vol. 16, no. 5, p. e1008488, 2020.

[102] P. Shukla, H. Nguyen, K. Faulk, K. Mather, U. Torian, R. Engle, and S. Emerson, "Adaptation of a genotype 3 hepatitis e virus to efficient growth in cell culture depends on an inserted human gene segment acquired by recombination," vol. 86, no. 10, pp. 5697–5707, 2012.

[103] P. Artimo, M. Jonnalagedda, K. Arnold, D. Baratin, G. Csardi, E. de Castro, S. Duvaud, V. Flegel, A. Fortier, E. Gasteiger, A. Grosdidier, C. Hernandez, V. Ioannidis, D. Kuznetsov, R. Liechti, S. Moretti, K. Mostaguir, N. Redaschi, G. Rossier, I. Xenarios, and H. Stockinger, "ExPASy: SIB bioinformatics resource portal," *Nucleic Acids Res*, vol. 40, no. W1, pp. W597–W603, 2012.

[104] E. Koonin, A. Gorbalenya, M. Purdy, M. Rozanov, G. Reyes, and D. Bradley, "Computer-assisted assignment of functional domains in the nonstructural polyprotein of hepatitis e virus: delineation of an additional group of positive-strand RNA plant and animal viruses," *Proc National Acad Sci*, vol. 89, no. 17, pp. 8259–8263, 1992.

[105] S. Kenney and X. Meng, "Hepatitis e virus genome structure and replication strategy," *Csh Perspect Med*, vol. 9, no. 1, p. a031724, 2018.

[106] E. Decroly, F. Ferron, J. Lescar, and B. Canard, "Conventional and unconventional mechanisms for capping viral mRNA.," *Nat Rev Microbiol*, vol. 10, no. 1, pp. 51–65, 2011.

[107] M. N. Rozanov, E. V. Koonin, and A. E. Gorbalenya, "Conservation of the putative methyltransferase domain: a hallmark of the 'Sindbis-like' supergroup of positive-strand RNA viruses," *J Gen Virol*, vol. 73, no. 8, pp. 2129–2134, 1992.

[108] T. Ahola and L. Kääriäinen, "Reaction in alphavirus mRNA capping: formation of a covalent complex of nonstructural protein nsP1 with 7-methyl-GMP.," *Proc National Acad Sci*, vol. 92, no. 2, pp. 507–511, 1995.

[109] Y. Huang, Y. Hsu, Y. Han, and M. Meng, "mRNA guanylation catalyzed by the S-Adenosylmethionine-dependent guanylyltransferase of bamboo mosaic virus," *J Biol Chem*, vol. 280, no. 13, pp. 13153–13162, 2005.

[110] J. Magden, N. Takeda, T. Li, P. Auvinen, T. Ahola, T. Miyamura, A. Merits, and L. Kääriäinen, "Virus-Specific mRNA capping enzyme encoded by hepatitis e virus," *J Virol*, vol. 75, no. 14, pp. 6249–6255, 2001.

[111] G. Balistreri, J. Caldentey, L. Kääriäinen, and T. Ahola, “Enzymatic defects of the nsP2 proteins of semliki forest virus Temperature-Sensitive mutants,” *J Virol*, vol. 81, no. 6, pp. 2849–2860, 2007.

[112] L. Vasiljeva, A. Merits, P. Auvinen, and L. Kääriäinen, “Identification of a novel function of the AlphavirusCapping apparatus RNA 5-TRIPHOSPHATASE ACTIVITY OF nsp2,” *J Biol Chem*, vol. 275, no. 23, pp. 17281–17287, 2000.

[113] Y. Li, T. Shih, Y. Hsu, Y. Han, Y. Huang, and M. Meng, “The Helicase-Like domain of plant potexvirus replicase participates in formation of RNA 5 cap structure by exhibiting RNA 5-Triphosphatase activity,” *J Virol*, vol. 75, no. 24, pp. 12114–12120, 2001.

[114] P. Das, A. Merits, and A. Lulla, “Functional cross-talk between distant domains of chikungunya virus non-structural protein 2 is decisive for its RNA-modulating activity,” *J Biol Chem*, vol. 289, no. 9, pp. 5635–5653, 2014.

[115] Y. A. Karpe and K. S. Lole, “NTPase and 5 to 3 RNA Duplex-Unwinding activities of the hepatitis e virus helicase domain,” *J Virol*, vol. 84, no. 7, pp. 3595–3602, 2010.

[116] S. Emerson, M. Zhang, X. Meng, H. Nguyen, S. M. Claire, S. Govindarajan, Y. Huang, and R. Purcell, “Recombinant hepatitis e virus genomes infectious for primates: Importance of capping and discovery of a cis-reactive element,” *Proc National Acad Sci*, vol. 98, no. 26, pp. 15270–15275, 2001.

[117] A. Pichlmair, O. Schulz, C. Tan, T. I. Näslund, P. Liljeström, F. Weber, and C. e Sousa, “RIG-I-Mediated antiviral responses to Single-Stranded RNA bearing 59-Phosphates,” *Science*, vol. 314, no. 5801, pp. 997–1001, 2006.

[118] M. Parvez, “Mutational analysis of hepatitis e virus ORF1 ”Y-domain”: effects on RNA replication and virion infectivity,” *World J Gastroentero*, vol. 23, no. 4, pp. 590–602, 2017.

[119] J. Borkakoti, G. Ahmed, A. Rai, and P. Kar, “Report of novel H105R, D29N, V27A mutations in the methyltransferase region of the HEV genome in patients with acute liver failure,” *J Clin Virol*, vol. 91, pp. 1–4, 2017.

[120] N. Mishra, A. M. Walimbe, and V. A. Arankalle, “Hepatitis e virus from india exhibits significant amino acid mutations in fulminant hepatic failure patients,” *Virus Genes*, vol. 46, no. 1, pp. 47–53, 2013.

[121] T. Ahola, P. Laakkonen, H. Vihinen, and L. Kääriäinen, “Critical residues of semliki forest virus RNA capping enzyme involved in methyltransferase and guanylyltransferase-like activities.,” *J Virol*, vol. 71, no. 1, pp. 392–397, 1997.

[122] W. HUEY-LAN, O. JULES, and S. VICTOR, "Mutagenesis of the sindbis virus nsP1 protein: Effects on methyltransferase activity and viral infectivity," *Virology*, vol. 217, no. 2, pp. 527–531, 1996.

[123] P. Laakkonen, T. Ahola, and L. Kääriäinen, "The effects of palmitoylation on membrane association of semliki forest virus RNA capping enzyme," *J Biol Chem*, vol. 271, no. 45, pp. 28567–28571, 1996.

[124] G. Milligan, M. Parenti, and A. I. Magee, "The dynamic role of palmitoylation in signal transduction," *Trends Biochem Sci*, vol. 20, no. 5, pp. 181–186, 1995.

[125] B. D. protocols in protein science, "Papain-like cysteine proteases," *Current protocols in protein science*, 2000.

[126] C. Voshavar, "Protease inhibitors for the treatment of HIV/AIDS: recent advances and future challenges," *Curr Top Med Chem*, vol. 19, no. 18, pp. 1571–1598, 2019.

[127] M. Parvez, "Molecular characterization of hepatitis e virus ORF1 gene supports a papain-like cysteine protease (PCP)-domain activity," *Virus Res*, vol. 178, no. 2, pp. 553–556, 2013.

[128] D. Paliwal, S. Panda, N. Kapur, S. Varma, and H. Durgapal, "Hepatitis e virus (HEV) protease: a chymotrypsin-like enzyme that processes both non-structural (pORF1) and capsid (pORF2) protein," *J Gen Virol*, vol. 95, no. Pt_8, pp. 1689–1700, 2014.

[129] S. Saraswat, M. Chaudhary, and D. Sehgal, "Hepatitis e virus cysteine protease has papain like properties validated by in silico modeling and Cell-Free inhibition assays," *Front Cell Infect Mi*, vol. 9, p. 478, 2020.

[130] A. Proudfoot, A. Hyrina, M. Holdorf, A. O. Frank, and D. Bussiere, "First crystal structure of a nonstructural hepatitis e viral protein identifies a putative novel Zinc-Binding protein," *J Virol*, vol. 93, no. 13, 2019.

[131] I. Ansari, S. Nanda, H. Durgapal, S. Agrawal, S. Mohanty, D. Gupta, S. Jameel, and S. Panda, "Cloning, sequencing, and expression of the hepatitis e virus (HEV) nonstructural open reading frame 1 (ORF1).," *J Med Virol*, vol. 60, no. 3, pp. 275–83, 2000.

[132] S. Ropp, A. Tam, B. Beames, M. Purdy, and T. Frey, "Expression of the hepatitis e virus ORF1," *Arch Virol*, vol. 145, no. 7, pp. 1321–1337, 2000.

[133] D. Sehgal, S. Thomas, M. Chakraborty, and S. Jameel, "Expression and processing of the hepatitis e virus ORF1 nonstructural polyprotein," *Virol J*, vol. 3, no. 1, p. 38, 2006.

[134] S. Suppiah, Y. Zhou, and T. K. Frey, "Lack of processing of the expressed ORF1 gene product of hepatitis e virus," *Virol J*, vol. 8, no. 1, p. 245, 2011.

[135] Y. A. Karpe and K. S. Lole, "Deubiquitination activity associated with hepatitis e virus putative papain-like cysteine protease," *J Gen Virol*, vol. 92, no. 9, pp. 2088–2092, 2011.

[136] M. A. Purdy, J. Lara, and Y. E. Khudyakov, "The hepatitis e virus polyproline region is involved in viral adaptation," *Plos One*, vol. 7, no. 4, p. e35974, 2012.

[137] R. Pudupakam, S. P. Kenney, L. Córdoba, Y. Huang, B. A. Dryman, L. Tanya, W. F. Pierson, and X. Meng, "Mutational analysis of the hypervariable region of hepatitis e virus reveals its involvement in the efficiency of viral RNA replication," vol. 85, no. 19, pp. 10031–10040, 2011.

[138] L. Robert, I. Nimgaonkar, and A. Ploss, "Hepatitis e virus replication," *Viruses*, vol. 11, no. 8, p. 719, 2019.

[139] R. Pudupakam, Y. Huang, T. Opriessnig, P. Halbur, F. Pierson, and X. Meng, "Deletions of the hypervariable region (HVR) in open reading frame 1 of hepatitis e virus do not abolish virus infectivity: Evidence for attenuation of HVR deletion mutants in vivo," *J Virol*, vol. 83, no. 1, pp. 384–395, 2009.

[140] D. B. Smith, M. A. Purdy, and P. Simmonds, "Genetic variability and the classification of hepatitis e virus," *J Virol*, vol. 87, no. 8, pp. 4161–4169, 2013.

[141] C. Tsai, B. Ma, Y. Sham, S. Kumar, and R. Nussinov, "Structured disorder and conformational selection," *Proteins Struct Funct Bioinform*, vol. 44, no. 4, pp. 418–427, 2001.

[142] K. A. Dunker, C. J. Oldfield, J. Meng, P. Romero, J. Y. Yang, J. Chen, V. Vacic, Z. Obradovic, and V. N. Uversky, "The unfoldomics decade: an update on intrinsically disordered proteins," *Bmc Genomics*, vol. 9, no. Suppl 2, p. S1, 2008.

[143] S. P. Kenney and X. Meng, "The lysine residues within the human ribosomal protein s17 sequence naturally inserted into the viral nonstructural protein of a unique strain of hepatitis e virus are important for enhanced virus replication," *J Virol*, vol. 89, no. 7, pp. 3793–3803, 2015.

[144] P. Shukla, H. Nguyen, U. Torian, R. Engle, K. Faulk, H. Dalton, R. Bendall, F. Keane, R. Purcell, and S. Emerson, "Cross-species infections of cultured cells by hepatitis e virus and discovery of an infectious virus–host recombinant," *Proc National Acad Sci*, vol. 108, no. 6, pp. 2438–2443, 2011.

[145] H. Nguyen, U. Torian, K. Faulk, K. Mather, R. Engle, E. Thompson, H. Bonkovsky, and S. Emerson, "A naturally occurring human/hepatitis e recombinant virus predominates in serum but not in faeces of a chronic hepatitis e patient and has a growth advantage in cell culture," *J Gen Virol*, vol. 93, no. 3, pp. 526–530, 2012.

[146] Y. Debing, C. Ramière, K. Dallmeier, G. Piorkowski, M. Trabaud, F. Lebossé, C. Scholtès, M. Roche, L. Catherine, X. de Lamballerie, P. André, and J. Neyts, "Hepatitis e virus mutations associated with ribavirin treatment failure result in altered viral fitness and ribavirin sensitivity," *J Hepatol*, vol. 65, no. 3, pp. 499–508, 2016.

[147] C. Li, Y. Debing, G. Jankevicius, J. Neyts, I. Ahel, B. Coutard, and B. Canard, "Viral macro domains reverse protein ADP-Ribosylation," *J Virol*, vol. 90, no. 19, pp. 8478–8486, 2016.

[148] Y. M. Alhammad and A. R. Fehr, "The viral macrodomain counters host antiviral ADP-Ribosylation," *Viruses*, vol. 12, no. 4, p. 384, 2020.

[149] M. R. Martzen, M. S. M, S. L. Spinelli, F. M. Torres, S. Fields, E. J. Grayhack, and E. M. Phizicky, "A biochemical genomics approach for identifying genes by the activity of their products," *Science*, vol. 286, no. 5442, pp. 1153–1155, 1999.

[150] G. I. Karras, G. Kustatscher, H. R. Buhecha, M. D. Allen, C. Pugieux, F. Sait, M. Bycroft, and A. G. Ladurner, "The macro domain is an ADP-ribose binding module," *Embo J*, vol. 24, no. 11, pp. 1911–1920, 2005.

[151] M. Egloff, H. Malet, Á. Putics, M. Heinonen, H. Dutartre, A. Frangeul, A. Gruez, V. Campanacci, C. Cambillau, J. Ziebuhr, T. Ahola, and B. Canard, "Structural and functional basis for ADP-Ribose and Poly(ADP-Ribose) binding by viral macro domains," *J Virol*, vol. 80, no. 17, pp. 8493–8502, 2006.

[152] J. Amé, C. Spenlehauer, and G. de Murcia, "The PARP superfamily," *Bioessays*, vol. 26, no. 8, pp. 882–893, 2004.

[153] D. Corda and M. Girolamo, "Functional aspects of protein mono-ADP-ribosylation," *Embo J*, vol. 22, no. 9, pp. 1953–1958, 2003.

[154] A. E. Gorbalenya, E. V. Koonin, and M. Lai, "Putative papain-related thiol proteases of positive strand RNA viruses identification of rubi and aphthovirus proteases and delineation of a novel conserved domain associated with proteases of rubi, alpha and coronaviruses," *Febs Lett*, vol. 288, no. 1-2, pp. 201–205, 1991.

[155] M. D. Allen, A. M. Buckle, S. C. Cordell, J. Löwe, and M. Bycroft, "The crystal structure of AF1521 a protein from archaeoglobus fulgidus with homology to the non-histone domain of MacroH2A," *J Mol Biol*, vol. 330, no. 3, pp. 503–511, 2003.

[156] Y. Nan, Z. Ma, R. Wang, Y. Yu, H. Kannan, B. Fredericksen, and Y. Zhang, "Enhancement of interferon induction by ORF3 product of hepatitis e virus," *J Virol*, vol. 88, no. 15, pp. 8696–8705, 2014.

[157] S. Anang, C. Subramani, V. P. Nair, S. Kaul, N. Kaushik, C. Sharma, A. Tiwari, R. CT, and M. Surjit, "Identification of critical residues in hepatitis e virus macro domain involved in its interaction with viral methyltransferase and ORF3 proteins," *Sci Rep-uk*, vol. 6, no. 1, p. 25133, 2016.

[158] N. Ojha and K. S. Lole, "Hepatitis e virus ORF1 encoded macro domain protein interacts with light chain subunit of human ferritin and inhibits its secretion," *Mol Cell Biochem*, vol. 417, no. 1-2, pp. 75–85, 2016.

[159] L. Chen, L. Hu, T. Chan, G. Tsao, D. Xie, K. Huo, L. Fu, S. Ma, B. Zheng, and X. Guan, "Chromodomain helicase/adenosine triphosphatase DNA binding protein 1–like (CHD1l) gene suppresses the nucleus-to-mitochondria translocation of nur77 to sustain hepatocellular carcinoma cell survival," *Hepatology*, vol. 50, no. 1, pp. 122–129, 2009.

[160] M. Singleton and W. D. of bacteriology, "Modularity and specialization in superfamily 1 and 2 helicases," *Journal of bacteriology*, 2002.

[161] Y. A. Karpe and K. S. Lole, "RNA 5-Triphosphatase activity of the hepatitis e virus helicase domain," *J Virol*, vol. 84, no. 18, pp. 9637–9641, 2010.

[162] G. Kadaré and A. Haenni, "Virus-encoded RNA helicases.," *J Virol*, vol. 71, no. 4, pp. 2583–2590, 1997.

[163] P. Devhare, K. Sharma, V. Mhaindarkar, V. Arankalle, and K. Lole, "Analysis of helicase domain mutations in the hepatitis e virus derived from patients with fulminant hepatic failure: Effects on enzymatic activities and virus replication," *Virus Res*, vol. 184, pp. 103–110, 2014.

[164] V. Mhaindarkar, K. Sharma, and K. S. Lole, "Mutagenesis of hepatitis e virus helicase motifs: Effects on enzyme activity," *Virus Res*, vol. 179, pp. 26–33, 2014.

[165] S. Mahilkar, M. S. Paingankar, and K. S. Lole, "Hepatitis e virus RNA-dependent RNA polymerase: RNA template specificities, recruitment and synthesis," *J Gen Virol*, vol. 97, no. 9, pp. 2231–2242, 2016.

[166] S. Rehman, N. Kapur, H. Durgapal, and S. Panda, “Subcellular localization of hepatitis e virus (HEV) replicase,” *Virology*, vol. 370, no. 1, pp. 77–92, 2008.

[167] A. Osterman, T. Stellberger, A. Gebhardt, M. Kurz, C. C. Friedel, P. Uetz, H. Nitschko, A. Baiker, and V. M. G, “The hepatitis e virus intraviral interactome,” *Sci Rep-uk*, vol. 5, no. 1, p. 13872, 2015.

[168] K. D. Pingale, G. D. Kanade, and Y. A. Karpe, “Hepatitis e virus polymerase binds to IFIT1 to protect the viral RNA from IFIT1-mediated translation inhibition,” *J Gen Virol*, vol. 100, no. 3, pp. 471–483, 2019.

[169] B. Haldipur, P. Bhukya, V. Arankalle, and K. Lole, “Positive regulation of hepatitis e virus replication by MicroRNA-122,” *J Virol*, vol. 92, no. 11, pp. e01999–17, 2018.

[170] C. L. Jopling, M. Yi, A. M. Lancaster, S. M. Lemon, and P. Sarnow, “Modulation of hepatitis c virus RNA abundance by a Liver-Specific MicroRNA,” *Science*, vol. 309, no. 5740, pp. 1577–1581, 2005.

[171] R. D. Kunden, S. Ghezelbash, J. Q. Khan, and J. A. Wilson, “Location specific annealing of miR-122 and other small RNAs defines an hepatitis c virus 5 UTR regulatory element with distinct impacts on virus translation and genome stability,” *Nucleic Acids Res*, vol. 48, no. 16, pp. gkaa664–, 2020.

[172] J. Henke, D. Goergen, J. Zheng, Y. Song, C. G. Schüttler, C. Fehr, C. Jünemann, and M. Niepmann, “microRNA-122 stimulates translation of hepatitis c virus RNA,” *Embo J*, vol. 27, no. 24, pp. 3300–3310, 2008.

[173] A. P. Roberts, A. P. Lewis, and C. L. Jopling, “miR-122 activates hepatitis c virus translation by a specialized mechanism requiring particular RNA components,” *Nucleic Acids Res*, vol. 39, no. 17, pp. 7716–7729, 2011.

[174] E. S. Machlin, P. Sarnow, and S. M. Sagan, “Masking the 5 terminal nucleotides of the hepatitis c virus genome by an unconventional microRNA-target RNA complex,” *Proc National Acad Sci*, vol. 108, no. 8, pp. 3193–3198, 2011.

[175] T. Masaki, K. C. Arend, Y. Li, D. Yamane, M. D. R, T. Kato, T. Wakita, N. J. Moorman, and S. M. Lemon, “miR-122 stimulates hepatitis c virus RNA synthesis by altering the balance of viral RNAs engaged in replication versus translation,” *Cell Host Microbe*, vol. 17, no. 2, pp. 217–228, 2015.

[176] D. K. Conrad, F. Giering, C. Erfurth, A. Neumann, C. Fehr, G. Meister, and M. Niepmann, “microRNA-122 dependent binding of ago2 protein to hepatitis c virus RNA is

associated with enhanced RNA stability and translation stimulation," *Plos One*, vol. 8, no. 2, p. e56272, 2013.

[177] S. Lhomme, N. Kamar, F. Nicot, J. Ducos, M. Bismuth, V. Garrigue, P. Joelle, I. Ollivier, A. Elodie, O. Goria, H. Barth, P. Perrin, K. Saune, M. Dubois, R. Carcenac, C. Lefebvre, N. Jeanne, F. Abravanel, and J. Izopet, "Mutation in the hepatitis e virus polymerase and outcome of ribavirin therapy," *Antimicrob Agents Ch*, vol. 60, no. 3, pp. 1608–1614, 2016.

[178] Y. Debing, A. Gisa, K. Dallmeier, S. Pischke, B. Bremer, M. Manns, H. Wedemeyer, P. Suneetha, and J. Neyts, "A mutation in the hepatitis e virus RNA polymerase promotes its replication and associates with ribavirin treatment failure in organ transplant recipients," *Gastroenterology*, vol. 147, no. 5, pp. 1008–1011.e7, 2014.

[179] D. Todt, T. Meister, and E. Steinmann, "Hepatitis e virus treatment and ribavirin therapy: viral mechanisms of nonresponse," *Curr Opin Virol*, vol. 32, pp. 80–87, 2018.

[180] M. A. Purdy, M. K. A, K. Krawczynski, J. Spelbring, G. R. Reyes, and D. W. Bradley, "Preliminary evidence that a trpE-HEV fusion protein protects cynomolgus macaques against challenge with wild-type hepatitis e virus (HEV)," *J Med Virol*, vol. 41, no. 1, pp. 90–94, 1993.

[181] S. Jameel, M. Zafrullah, M. Ozdener, and S. Panda, "Expression in animal cells and characterization of the hepatitis e virus structural proteins.," *J Virol*, vol. 70, no. 1, pp. 207–16, 1996.

[182] J. Graff, Y. Zhou, U. Torian, H. Nguyen, M. Claire, C. Yu, R. H. Purcell, and S. U. Emerson, "Mutations within potential glycosylation sites in the capsid protein of hepatitis e virus prevent the formation of infectious virus particles," *J Virol*, vol. 82, no. 3, pp. 1185–1194, 2008.

[183] M. Zafrullah, M. Ozdener, R. Kumar, S. Panda, and S. Jameel, "Mutational analysis of glycosylation, membrane translocation, and cell surface expression of the hepatitis e virus ORF2 protein.," *J Virol*, vol. 73, no. 5, pp. 4074–82, 1999.

[184] M. Xu, N. Behloul, J. Wen, J. Zhang, and J. Meng, "Role of asparagine at position 562 in dimerization and immunogenicity of the hepatitis e virus capsid protein," *Infect Genetics Evol*, vol. 37, pp. 99–107, 2016.

[185] M. Ankavay, J. Dubuisson, and L. Cocquerel, "Le virus de l'hépatite e - un virus méconnu qui se dévoile," *Médecine Sci*, vol. 34, no. 12, pp. 1071–1078, 2018.

[186] C. Montpellier, C. Wychowski, I. M. Sayed, J. Meunier, J. Saliou, M. Ankavay, A. Bull, A. Pillez, F. Abravanel, F. Helle, E. Brochot, H. Drobecq, R. Farhat, A. Cécile-Marie, J. G. Haddad, J. Izopet, P. Meuleman, A. Goffard, J. Dubuisson, and L. Cocquerel, "Hepatitis e virus lifecycle and identification of 3 forms of the ORF2 capsid protein," *Gastroenterology*, vol. 154, no. 1, pp. 211–223.e8, 2018.

[187] M. Kalia and S. Jameel, "Virus entry paradigms," *Amino Acids*, vol. 41, no. 5, pp. 1147–1157, 2011.

[188] M. Kalia, V. Chandra, S. Rahman, D. Sehgal, and S. Jameel, "Heparan sulfate proteoglycans are required for cellular binding of the hepatitis e virus ORF2 capsid protein and for viral infection," *J Virol*, vol. 83, no. 24, pp. 12714–12724, 2009.

[189] H. Yu, S. Li, C. Yang, M. Wei, C. Song, Z. Zheng, Y. Gu, H. Du, J. Zhang, and N. Xia, "Homology model and potential virus-capsid binding site of a putative HEV receptor grp78," *J Mol Model*, vol. 17, no. 5, pp. 987–995, 2011.

[190] L. John, S. Thomas, O. Herchenröder, B. M. Pützer, and S. Schaefer, "Hepatitis e virus ORF2 protein activates the Pro-Apoptotic gene CHOP and Anti-Apoptotic heat shock proteins," *Plos One*, vol. 6, no. 9, p. e25378, 2011.

[191] M. Surjit, B. Varshney, and S. K. Lal, "The ORF2 glycoprotein of hepatitis e virus inhibits cellular NF- activity by blocking ubiquitination mediated proteasomal degradation of I in human hepatoma cells," *Bmc Biochem*, vol. 13, no. 1, p. 7, 2012.

[192] Y. Qi, F. Zhang, L. Zhang, T. J. Harrison, W. Huang, C. Zhao, W. Kong, C. Jiang, and Y. Wang, "Hepatitis e virus produced from cell culture has a lipid envelope," *Plos One*, vol. 10, no. 7, p. e0132503, 2015.

[193] M. Zafrullah, M. Ozdener, S. Panda, and S. Jameel, "The ORF3 protein of hepatitis e virus is a phosphoprotein that associates with the cytoskeleton.," vol. 71, no. 12, pp. 9045–53, 1997.

[194] S. Tyagi, S. Jameel, and S. K. Lal, "Self-Association and mapping of the interaction domain of hepatitis e virus ORF3 protein," *J Virol*, vol. 75, no. 5, pp. 2493–2498, 2001.

[195] Q. Ding, B. Heller, J. M. Capuccino, B. Song, I. Nimgaonkar, G. Hrebikova, J. E. Contreras, and A. Ploss, "Hepatitis e virus ORF3 is a functional ion channel required for release of infectious particles," *Proc National Acad Sci*, vol. 114, no. 5, pp. 1147–1152, 2017.

[196] H. Kannan, S. Fan, D. Patel, I. Bossis, and Y. Zhang, "The hepatitis e virus open reading frame 3 product interacts with microtubules and interferes with their dynamics," *J Virol*, vol. 83, no. 13, pp. 6375–6382, 2009.

[197] J. Gouttenoire, A. Pollán, L. Abrami, N. Oechslin, J. Mauron, M. Matter, J. Oppliger, D. Szkolnicka, V. Thi, G. F. van der Goot, and D. Moradpour, "Palmitoylation mediates membrane association of hepatitis e virus ORF3 protein and is required for infectious particle secretion," *Plos Pathog*, vol. 14, no. 12, p. e1007471, 2018.

[198] R. Ratra, K. Anindita, and S. K. Lal, "The ORF3 protein of hepatitis e virus interacts with hemopexin by means of its 26 amino acid N-Terminal hydrophobic domain II †," *Biochemistry-us*, vol. 47, no. 7, pp. 1957–1969, 2008.

[199] E. Tolosano and F. Altruda, "Hemopexin: Structure, function, and regulation," *Dna Cell Biol*, vol. 21, no. 4, pp. 297–306, 2002.

[200] H. Korkaya, S. Jameel, D. Gupta, S. Tyagi, R. Kumar, M. Zafrullah, M. Mazumdar, S. Lal, L. Xiaofang, D. Sehgal, S. Das, and D. Sahal, "The ORF3 protein of hepatitis e virus binds to src homology 3 domains and activates MAPK," *J Biol Chem*, vol. 276, no. 45, pp. 42389–42400, 2001.

[201] S. Tyagi, H. Korkaya, M. Zafrullah, S. Jameel, and S. K. Lal, "The phosphorylated form of the ORF3 protein of hepatitis e virus interacts with its non-glycosylated form of the major capsid protein, ORF2," *J Biol Chem*, vol. 277, no. 25, pp. 22759–22767, 2002.

[202] S. Tyagi, M. Surjit, A. Roy, S. Jameel, and S. K. Lal, "The ORF3 protein of hepatitis e virus interacts with liver-specific alpha1-Microglobulin and its precursor alpha1-Microglobulin/Bikunin precursor (AMBP) and expedites their export from the hepatocyte," *J Biol Chem*, vol. 279, no. 28, pp. 29308–29319, 2004.

[203] S. Emerson, H. Nguyen, U. Torian, and R. Purcell, "ORF3 protein of hepatitis e virus is not required for replication, virion assembly, or infection of hepatoma cells in vitro," *J Virol*, vol. 80, no. 21, pp. 10457–10464, 2006.

[204] A. Zarrinpar, R. P. Bhattacharyya, and W. A. Lim, "The structure and function of proline recognition domains," *Sci Stke*, vol. 2003, no. 179, pp. re8–re8, 2003.

[205] K. Yamada, M. Takahashi, Y. Hoshino, H. Takahashi, K. Ichiyama, S. Nagashima, T. Tanaka, and H. Okamoto, "ORF3 protein of hepatitis e virus is essential for virion release from infected cells," *J Gen Virol*, vol. 90, no. 8, pp. 1880–1891, 2009.

[206] S. Nagashima, M. Takahashi, Jirintai, T. Tanaka, K. Yamada, T. Nishizawa, and H. Okamoto, "A PSAP motif in the ORF3 protein of hepatitis e virus is necessary for virion release from infected cells," *J Gen Virol*, vol. 92, no. 2, pp. 269–278, 2011.

[207] D. Cao and X. Meng, "Molecular biology and replication of hepatitis e virus," *Emerg Microbes Infec*, vol. 1, no. 8, p. e17, 2012.

[208] T. Shiota, T. Li, Y. Nishimura, S. Yoshizaki, R. Sugiyama, M. Shimojima, M. Saijo, H. Shimizu, R. Suzuki, T. Wakita, M. Muramatsu, and K. Ishii, "Integrin is involved in non-enveloped hepatitis e virus infection," *Virology*, vol. 536, pp. 119–124, 2019.

[209] T. S. Guu, Z. Liu, Q. Ye, D. A. Mata, K. Li, C. Yin, J. Zhang, and Y. Tao, "Structure of the hepatitis e virus-like particle suggests mechanisms for virus assembly and receptor binding," *Proc National Acad Sci*, vol. 106, no. 31, pp. 12992–12997, 2009.

[210] P. Holla, I. Ahmad, Z. Ahmed, and S. Jameel, "Hepatitis e virus enters liver cells through a dynamin-2, clathrin and membrane Cholesterol-Dependent pathway," *Traffic*, vol. 16, no. 4, pp. 398–416, 2015.

[211] N. Kapur, D. Thakral, H. Durgapal, and S. Panda, "Hepatitis e virus enters liver cells through receptor-dependent clathrin-mediated endocytosis," *J Viral Hepatitis*, vol. 19, no. 6, pp. 436–448, 2012.

[212] Z. Zheng, J. Miao, M. Zhao, M. Tang, A. E. Yeo, H. Yu, J. Zhang, and N. Xia, "Role of heat-shock protein 90 in hepatitis e virus capsid trafficking," *J Gen Virol*, vol. 91, no. 7, pp. 1728–1736, 2010.

[213] X. Yin, C. Ambardekar, Y. Lu, and Z. Feng, "Distinct entry mechanisms for nonenveloped and Quasi-Enveloped hepatitis e viruses," vol. 90, no. 8, pp. 4232–4242, 2016.

[214] K. Himmelsbach, D. Bender, and E. Hildt, "Life cycle and morphogenesis of the hepatitis e virus," *Emerg Microbes Infec*, vol. 7, no. 1, pp. 1–12, 2018.

[215] X. Zhou, L. Xu, Y. Wang, W. Wang, D. Sprengers, H. J. Metselaar, M. P. Peppelenbosch, and Q. Pan, "Requirement of the eukaryotic translation initiation factor 4F complex in hepatitis e virus replication," *Antivir Res*, vol. 124, pp. 11–19, 2015.

[216] J. Perttila, P. Spuul, and T. Ahola, "Early secretory pathway localization and lack of processing for hepatitis e virus replication protein pORF1," *J Gen Virol*, vol. 94, no. Pt_4, pp. 807–816, 2012.

[217] S. Nagashima, M. Takahashi, S. Jirintai, T. Tanaka, T. Nishizawa, J. Yasuda, and H. Okamoto, "Tumour susceptibility gene 101 and the vacuolar protein sorting pathway are required for the release of hepatitis e virions," *J Gen Virol*, vol. 92, no. 12, pp. 2838–2848, 2011.

[218] S. Nagashima, M. Takahashi, T. Kobayashi, Tanggis, T. Nishizawa, T. Nishiyama, P. Primadharsini, and H. Okamoto, "Characterization of the Quasi-Enveloped hepatitis e virus particles released by the cellular exosomal pathway," *J Virol*, vol. 91, no. 22, pp. e00822–17, 2017.

[219] S. U. Emerson, H. T. Nguyen, U. Torian, D. Burke, R. Engle, and R. H. Purcell, "Release of genotype 1 hepatitis e virus from cultured hepatoma and polarized intestinal cells depends on open reading frame 3 protein and requires an intact PXXP motif," *J Virol*, vol. 84, no. 18, pp. 9059–9069, 2010.

[220] F. Lecaille, J. Kaleta, and D. Brömme, "Human and parasitic papain-like cysteine proteases: their role in physiology and pathology and recent developments in inhibitor design.," *Chem Rev*, vol. 102, no. 12, pp. 4459–88, 2002.

[221] G. D. Kanade, K. D. Pingale, and Y. A. Karpe, "Activities of thrombin and factor xa are essential for replication of hepatitis e virus and are possibly implicated in ORF1 polyprotein processing," *J Virol*, vol. 92, no. 6, pp. e01853–17, 2018.

[222] D. Szkolnicka, A. Pollán, N. Silva, N. Oechslin, J. Gouttenoire, and D. Moradpour, "Recombinant hepatitis e viruses harboring tags in the ORF1 protein," *J Virol*, vol. 93, no. 19, 2019.

[223] M. Ulasli, M. Verheije, C. Haan, and F. Reggiori, "Qualitative and quantitative ultrastructural analysis of the membrane rearrangements induced by coronavirus," *Cell Microbiol*, vol. 12, no. 6, pp. 844–861, 2010.

[224] R. R. Novoa, G. Calderita, R. Arranz, J. Fontana, H. Granzow, and C. Risco, "Virus factories: associations of cell organelles for viral replication and morphogenesis," *Biol Cell*, vol. 97, no. 2, pp. 147–172, 2005.

[225] C. Netherton, K. Moffat, E. Brooks, and T. Wileman, "A guide to viral inclusions, membrane rearrangements, factories, and viroplasm produced during virus replication.," *Adv Virus Res*, vol. 70, pp. 101–82, 2007.

[226] R. FC, E. JF, and W. TH, "The effect of poliomyelitis virus upon cells in tissue cultures.," *J Clin Investigation*, vol. 29, no. 6, p. 841, 1950.

[227] M. Reissig, D. W. Howes, and J. L. Melnick, “SEQUENCE OF MORPHOLOGICAL CHANGES IN EPITHELIAL CELL CULTURES INFECTED WITH POLIOVIRUS,” *J Exp Medicine*, vol. 104, no. 3, pp. 289–304, 1956.

[228] J. A. den Boon, A. Diaz, and P. Ahlquist, “Cytoplasmic viral replication complexes,” *Cell Host Microbe*, vol. 8, no. 1, pp. 77–85, 2010.

[229] E. Westaway, J. Mackenzie, M. Kenney, M. Jones, and A. Khromykh, “Ultrastructure of kunjin virus-infected cells: colocalization of NS1 and NS3 with double-stranded RNA, and of NS2B with NS3, in virus-induced membrane structures.,” *J Virol*, vol. 71, no. 9, pp. 6650–6661, 1997.

[230] K. W. Pedersen, Y. van der Meer, N. Roos, and E. J. Snijder, “Open reading frame 1a-Encoded subunits of the arterivirus replicase induce endoplasmic Reticulum-Derived Double-Membrane vesicles which carry the viral replication complex,” *J Virol*, vol. 73, no. 3, pp. 2016–2026, 1999.

[231] D. A. Suhy, T. H. Giddings, and K. Kirkegaard, “Remodeling the endoplasmic reticulum by poliovirus infection and by individual viral proteins: an Autophagy-Like origin for Virus-Induced vesicles,” *J Virol*, vol. 74, no. 19, pp. 8953–8965, 2000.

[232] S. Froshauer, J. Kartenbeck, and A. Helenius, “Alphavirus RNA replicase is located on the cytoplasmic surface of endosomes and lysosomes.,” *J Cell Biology*, vol. 107, no. 6, pp. 2075–2086, 1988.

[233] T. Hatta, S. Bullivant, and R. Matthews, “Fine structure of vesicles induced in chloroplasts of chinese cabbage leaves by infection with turnip yellow mosaic virus,” *J Gen Virol*, vol. 20, no. 1, pp. 37–50, 1973.

[234] M. Schwartz, J. Chen, M. Janda, M. Sullivan, J. den Boon, and P. Ahlquist, “A Positive-Strand RNA virus replication complex parallels form and function of retrovirus capsids,” *Mol Cell*, vol. 9, no. 3, pp. 505–514, 2002.

[235] P. Ahlquist, A. O. Noueiry, W. Lee, D. B. Kushner, and B. T. Dye, “Host factors in Positive-Strand RNA virus genome replication,” *J Virol*, vol. 77, no. 15, pp. 8181–8186, 2003.

[236] R. Inés, A. Merz, A. Chiramel, J. Lee, P. Chlanda, U. Haselman, S. Rachel, A. Habermann, S. Hoppe, S. Kallis, P. Walther, C. Antony, K. Jacomine, and R. Bartenschlager, “Three-Dimensional architecture and biogenesis of membrane structures associated with hepatitis c virus replication,” *Plos Pathog*, vol. 8, no. 12, p. e1003056, 2012.

[237] K. Knoops, M. Kikkert, S. H. van den Worm, Z. J. C, Y. van der Meer, A. J. Koster, M. A. Mommaas, and E. J. Snijder, "SARS-Coronavirus replication is supported by a reticulovesicular network of modified endoplasmic reticulum," *Plos Biol*, vol. 6, no. 9, p. e226, 2008.

[238] B. van der Hoeven, D. Oudshoorn, A. J. Koster, E. J. Snijder, M. Kikkert, and M. Bárcena, "Biogenesis and architecture of arterivirus replication organelles," *Virus Res*, vol. 220, pp. 70–90, 2016.

[239] M. K. Pietilä, M. J. van Hemert, and T. Ahola, "Purification of highly active alphavirus replication complexes demonstrates altered fractionation of multiple cellular membranes," *J Virol*, vol. 92, no. 8, pp. e01852–17, 2018.

[240] J. Lee, J. Marshall, and D. Bowden, "Characterization of rubella virus replication complexes using antibodies to Double-Stranded RNA," *Virology*, vol. 200, no. 1, pp. 307–312, 1994.

[241] D. Magliano, J. A. Marshall, D. Bowden, N. Vardaxis, J. Meanger, and J. Lee, "Rubella virus replication complexes are Virus-Modified lysosomes," *Virology*, vol. 240, no. 1, pp. 57–63, 1998.

[242] J. A. den Boon, "ExPasy," 0.

[243] D. Lenggenhager, J. Gouttenoire, M. Malehmir, M. Bawohl, H. Hanna, S. Kreutzer, D. Semela, J. Neuweiler, S. Hürlimann, P. Aepli, M. Fraga, R. Sahli, L. Terracciano, R. Laura, B. Müllhaupt, C. Sempoux, D. Moradpour, A. Weber, D. Lenggenhager, J. Gouttenoire, M. Malehmir, M. Bawohl, H. Hanna, S. Kreutzer, D. Semela, J. Neuweiler, S. Hürlimann, P. Aepli, M. Fraga, R. Sahli, L. Terracciano, R. Laura, B. Müllhaupt, C. Sempoux, D. Moradpour, and A. Weber, "Visualization of hepatitis e virus RNA and proteins in the human liver," 2017.

[244] M. Kumar, P. Hooda, M. Khanna, U. Patel, and D. Sehgal, "Development of BacMam induced hepatitis e virus replication model in hepatoma cells to study the polyprotein processing," *Front Microbiol*, vol. 11, p. 1347, 2020.

[245] D. Liu, P. R. Tedbury, S. Lan, A. D. Huber, P. M. N, J. Ji, E. Michailidis, M. Saeed, T. P. Ndongwe, L. C. Bassit, R. F. Schinazi, R. Ralston, C. M. Rice, and S. G. Sarafianos, "Visualization of positive and negative sense viral RNA for probing the mechanism of Direct-Acting antivirals against hepatitis c virus," *Viruses*, vol. 11, no. 11, p. 1039, 2019.

[246] Y. Wang, H. Liu, S. Liu, C. Yang, Y. Jiang, S. Wang, A. Liu, M. P. Peppelenbosch, N. Kamar, Q. Pan, and J. Zhao, "Incidence, predictors and prognosis of genotype 4

hepatitis e related liver failure: A tertiary nested case-control study," *Liver Int*, vol. 39, no. 12, pp. 2291–2300, 2019.

[247] J. Wu and Z. J. Chen, "Innate immune sensing and signaling of cytosolic nucleic acids," *Immunology*, vol. 32, no. 1, pp. 461–488, 2014.

[248] T. Kawai and S. Akira, "Toll-like receptors and their crosstalk with other innate receptors in infection and immunity," *Immunity*, vol. 34, no. 5, pp. 637–650, 2011.

[249] L. A. Durfee, N. Lyon, K. Seo, and J. M. Huibregtse, "The ISG15 conjugation system broadly targets newly synthesized proteins: Implications for the antiviral function of ISG15," *Mol Cell*, vol. 38, no. 5, pp. 722–732, 2010.

[250] G. C. Sen, "Novel functions of interferon-induced proteins," *Semin Cancer Biol*, vol. 10, no. 2, pp. 93–101, 2000.

[251] X. Li, J. Blackford, and B. Hassel, "RNase l mediates the antiviral effect of interferon through a selective reduction in viral RNA during encephalomyocarditis virus infection.," *J Virol*, vol. 72, no. 4, pp. 2752–9, 1998.

[252] M. J. Clemens, "PKR—A protein kinase regulated by double-stranded RNA," *Int J Biochem Cell Biology*, vol. 29, no. 7, pp. 945–949, 1997.

[253] J. Myoung, J. Lee, and K. Min, "Methyltransferase of a cell culture-adapted hepatitis e inhibits the MDA5 receptor signaling pathway," *J Microbiol*, vol. 57, no. 12, pp. 1126–1131, 2019.

[254] Y. Nan, Y. Yu, Z. Ma, S. K. Khattar, B. Fredericksen, and Y. Zhang, "Hepatitis e virus inhibits type i interferon induction by ORF1 products," *J Virol*, vol. 88, no. 20, pp. 11924–11932, 2014.

[255] E. Bagdassarian, V. Doceul, M. Pellerin, A. Demange, L. Meyer, N. Jouvenet, and N. Pavio, "The Amino-Terminal region of hepatitis e virus ORF1 containing a methyltransferase (Met) and a Papain-Like cysteine protease (PCP) domain counteracts type i interferon response," *Viruses*, vol. 10, no. 12, p. 726, 2018.

[256] T. Uchida, T. Aye, X. Ma, F. Iida, T. Shikata, M. Ichikawa, T. Rikihisa, and K. Win, "An epidemic outbreak of hepatitis e in yangon of myanmar: Antibody assay and animal transmission of the virus," *Pathol Int*, vol. 43, no. 3, pp. 94–98, 1993.

[257] S. Tsarev, T. Tsareva, S. Emerson, S. Govindarajan, M. Shapiro, J. Gerin, and R. Purcell, "Successful passive and active immunization of cynomolgus monkeys against hepatitis e," *Proc National Acad Sci*, vol. 91, no. 21, pp. 10198–10202, 1994.

[258] V. Arankalle, M. Favorov, M. Chadha, D. Phule, and K. Banerjee, “Rhesus monkeys infected with hepatitis e virus (HEV) from the former USSR are immune to subsequent challenge with an indian strain of HEV.,” *Acta Virol*, vol. 37, no. 6, pp. 515–8, 1993.

[259] M. S. Hakim, W. Wang, W. M. Bramer, J. Geng, F. Huang, R. A. de Man, M. P. Peppelenbosch, and Q. Pan, “The global burden of hepatitis e outbreaks: a systematic review,” *Liver Int*, vol. 37, no. 1, pp. 19–31, 2017.

[260] J. Zhang, S. Li, T. Wu, Q. Zhao, M. Ng, and N. Xia, “Hepatitis e virus: neutralizing sites, diagnosis, and protective immunity,” *Rev Med Virol*, vol. 22, no. 5, pp. 339–349, 2012.

[261] Z. Tang, M. Tang, M. Zhao, G. Wen, F. Yang, W. Cai, S. Wang, Z. Zheng, and N. Xia, “A novel linear neutralizing epitope of hepatitis e virus,” *Vaccine*, vol. 33, no. 30, pp. 3504–3511, 2015.

[262] C. Sabine, M. Dubois, P. Célia, T. Bonnefois, S. Lhomme, B. Justine, B. You, S. Simoneau, P. Gleizes, B. Flan, F. Abravanel, and J. Izopet, “Characterization of the lipid envelope of exosome encapsulated HEV particles protected from the immune response,” *Biochimie*, vol. 141, pp. 70–79, 2017.

[263] A. Brown, J. S. Halliday, L. Swadling, R. G. Madden, R. Bendall, J. G. Hunter, J. Maggs, P. Simmonds, D. B. Smith, L. Vine, M. Cara, J. Collier, D. Bonsall, K. Jeffery, S. Dunachie, P. Klenerman, J. Izopet, N. Kamar, H. R. Dalton, and E. Barnes, “Characterization of the specificity, functionality, and durability of host T-Cell responses against the Full-Length hepatitis e virus,” *Hepatology*, vol. 64, no. 6, pp. 1934–1950, 2016.

[264] T. Wu, J. Zhang, Z. Su, J. Liu, X. Wu, X. Wu, C. Lin, S. Ou, Q. Yan, W. J. Shih, and N. Xia, “Specific cellular immune response in hepatitis e patients,” *Intervirology*, vol. 51, no. 5, pp. 322–327, 2009.

[265] M. Shata, A. Barrett, N. Shire, S. Abdelwahab, M. Sobhy, E. Daef, E. S.S., M. Hashem, R. Engle, R. Purcell, S. Emerson, G. Strickland, and K. Sherman, “Characterization of hepatitis e-specific cell-mediated immune response using IFN-gamma ELISPOT assay,” *J Immunol Methods*, vol. 328, no. 1-2, pp. 152–161, 2007.

[266] A. Gisa, P. Suneetha, P. Behrendt, S. Pischke, B. Bremer, C. Falk, M. Manns, M. Cornberg, H. Wedemeyer, and A. Kraft, “Cross-genotype-specific t-cell responses in acute hepatitis e virus (HEV) infection,” *J Viral Hepatitis*, vol. 23, no. 4, pp. 305–315, 2016.

[267] P. Suneetha, S. Pischke, V. Schlaphoff, J. Grabowski, P. Fytili, A. Gronert, B. Bremer, A. Markova, J. Jaroszewicz, C. Bara, M. P. Manns, M. Cornberg, and H. Wedemeyer,

"Hepatitis e virus (HEV)-specific t-cell responses are associated with control of HEV infection," *Hepatology*, vol. 55, no. 3, pp. 695–708, 2012.

[268] S. Prabhu, P. Gupta, H. Durgapal, S. Rath, S. Gupta, S. Acharya, and S. Panda, "Study of cellular immune response against hepatitis e virus (HEV)," *J Viral Hepatitis*, vol. 18, no. 8, pp. 587–594, 2011.

[269] A. Naik, A. Goel, V. Agrawal, A. N. Sarangi, N. Chhavi, V. Singh, S. Jameel, and R. Aggarwal, "Changes in gene expression in liver tissue from patients with fulminant hepatitis e," *World J Gastroentero*, vol. 21, no. 26, pp. 8032–8042, 2015.

[270] R. Srivastava, R. Aggarwal, S. Sachdeva, M. Alam, S. Jameel, and S. Naik, "Adaptive immune responses during acute uncomplicated and fulminant hepatitis e," *J Gastroen Hepatol*, vol. 26, no. 2, pp. 306–311, 2011.

[271] A. Jana, P. Behrendt, B. Bremer, P. Suneetha, A. Gisa, F. Rinker, M. P. Manns, M. Cornberg, H. Wedemeyer, and A. R. Kraft, "Hepatitis e virus ORF 1 induces proliferative and functional t-cell responses in patients with ongoing and resolved hepatitis e," *Liver Int*, vol. 38, no. 2, pp. 266–277, 2018.

[272] E. Shin, P. Sung, and S. Park, "Immune responses and immunopathology in acute and chronic viral hepatitis," *Nat Rev Immunol*, vol. 16, no. 8, pp. 509–523, 2016.

[273] M. Favorov, H. Fields, M. Purdy, T. Yashina, A. Aleksandrov, M. Alter, D. Yarasheva, D. Bradley, and H. Margolis, "Serologic identification of hepatitis e virus infections in epidemic and endemic settings," *J Med Virol*, vol. 36, no. 4, pp. 246–250, 1992.

[274] E. Clayson, K. Myint, R. Snitbhan, D. Vaughn, B. Innis, L. Chan, P. Cheung, and M. Shrestha, "Viremia, fecal shedding, and IgM and IgG responses in patients with hepatitis e," *J Infect Dis*, vol. 172, no. 4, pp. 927–933, 1995.

[275] J. Hartl, B. Otto, R. Madden, G. Webb, K. Woolson, L. Kriston, E. Vettorazzi, A. W. Lohse, H. Dalton, and S. Pischke, "Hepatitis e seroprevalence in europe: A Meta-Analysis," *Viruses*, vol. 8, no. 8, p. 211, 2016.

[276] R. Bendall, V. Ellis, S. Ijaz, R. Ali, and H. Dalton, "A comparison of two commercially available anti-HEV IgG kits and a re-evaluation of anti-HEV IgG seroprevalence data in developed countries," *J Med Virol*, vol. 82, no. 5, pp. 799–805, 2010.

[277] T. Vollmer, J. Diekmann, M. Eberhardt, C. Knabbe, and J. Dreier, "Monitoring of Anti-Hepatitis e virus antibody seroconversion in asymptomatically infected blood donors:

Systematic comparison of nine commercial Anti-HEV IgM and IgG assays," *Viruses*, vol. 8, no. 8, p. 232, 2016.

[278] C. Yu, R. Engle, J. Bryan, S. Emerson, and R. Purcell, "Detection of immunoglobulin m antibodies to hepatitis e virus by class capture enzyme immunoassay," *Clin Diagn Lab Immun*, vol. 10, no. 4, pp. 579–586, 2003.

[279] A. D. W, A. F. Majdalawieh, A. G. Mesleh, O. M. Abdalla, and G. K. Nasrallah, "Laboratory challenges in the diagnosis of hepatitis e virus," vol. 67, no. 4, pp. 466–480, 2018.

[280] S. A. Baylis, J. Blümel, S. Mizusawa, K. Matsubayashi, H. Sakata, Y. Okada, M. C. Nübling, K. O. Hanschmann, and H. Group, "World health organization international standard to harmonize assays for detection of hepatitis e virus RNA," *Emerg Infect Dis*, vol. 19, no. 5, pp. 729–735, 2013.

[281] S. A. Baylis, K. Hanschmann, J. Blümel, M. C. Nübling, and H. Group, "Standardization of hepatitis e virus (HEV) nucleic acid amplification Technique-Based assays: an initial study to evaluate a panel of HEV strains and investigate laboratory performance," *J Clin Microbiol*, vol. 49, no. 4, pp. 1234–1239, 2011.

[282] N. Kamar, H. R. Dalton, F. Abravanel, and J. Izopet, "Hepatitis e virus infection," *Clin Microbiol Rev*, vol. 27, no. 1, pp. 116–138, 2014.

[283] E. B. Haagsma, R. Annelies, A. P. van den Berg, R. J. Porte, and H. G. Niesters, "Treatment of chronic hepatitis e in liver transplant recipients with pegylated interferon alpha-2b," *Liver Transplant*, vol. 16, no. 4, pp. 474–477, 2010.

[284] N. Kamar, F. Abravanel, J. Selves, C. Garrouste, L. Esposito, L. Lavayssière, O. Cointault, D. Ribes, I. Cardeau, M. Nogier, J. Mansuy, F. Muscari, J. Peron, J. Izopet, and L. Rostaing, "Influence of immunosuppressive therapy on the natural history of genotype 3 Hepatitis-E virus infection after organ transplantation," *Transplantation*, vol. 89, no. 3, p. 353, 2010.

[285] N. Kamar, L. Rostaing, F. Abravanel, C. Garrouste, L. Esposito, C. Isabelle, J. Mansuy, J. Selves, J. Peron, P. Otal, F. Muscari, and J. Izopet, "Pegylated interferon-alpha for treating chronic hepatitis e virus infection after liver transplantation," *Clin Infect Dis*, vol. 50, no. 5, pp. e30–e33, 2010.

[286] N. Kamar, F. Abravanel, C. Garrouste, C. Isabelle, J. Mansuy, H. Weclawiak, J. Izopet, and L. Rostaing, "Three-month pegylated interferon-alpha-2a therapy for chronic hep-

atitis e virus infection in a haemodialysis patient," *Nephrol Dial Transpl*, vol. 25, no. 8, pp. 2792–2795, 2010.

[287] V. Mallet, E. Nicand, P. Sultanik, C. Chakvetadze, S. Tessé, E. Thervet, L. Mouthon, P. Sogni, and S. Pol, "Brief communication: Case reports of ribavirin treatment for chronic hepatitis e," *Ann Intern Med*, vol. 153, no. 2, p. 85, 2010.

[288] S. Pischke, S. Hardtke, U. Bode, S. Birkner, C. Chatzikyrkou, W. Kauffmann, C. L. Bara, J. Gottlieb, J. Wenzel, M. P. Manns, and H. Wedemeyer, "Ribavirin treatment of acute and chronic hepatitis e: a single-centre experience," *Liver Int*, vol. 33, no. 5, pp. 722–726, 2013.

[289] Y. Debing, S. U. Emerson, Y. Wang, Q. Pan, J. Balzarini, K. Dallmeier, and J. Neyts, "Ribavirin inhibits in vitro hepatitis e virus replication through depletion of cellular GTP pools and is moderately synergistic with alpha interferon," *Antimicrob Agents Ch*, vol. 58, no. 1, pp. 267–273, 2014.

[290] S. Crotty, C. E. Cameron, and R. Andino, "RNA virus error catastrophe: Direct molecular test by using ribavirin," *Proc National Acad Sci*, vol. 98, no. 12, pp. 6895–6900, 2001.

[291] H. Tejero, F. Montero, and J. Nuño, *Theories of Lethal Mutagenesis: From Error Catastrophe to Lethal Defection*, vol. 392. 2015.

[292] E. Thomas, M. G. Ghany, and J. T. Liang, "The application and mechanism of action of ribavirin in therapy of hepatitis c," *Antivir Chem Chemother*, vol. 23, no. 1, pp. 1–12, 2012.

[293] S. Lhomme, C. Garrouste, N. Kamar, K. Saune, F. Abravanel, J. Mansuy, M. Dubois, L. Rostaing, and J. Izopet, "Influence of polyproline region and macro domain genetic heterogeneity on HEV persistence in immunocompromised patients," *J Infect Dis*, vol. 209, no. 2, pp. 300–303, 2014.

[294] S. Lhomme, F. Abravanel, M. Dubois, S. Karine, L. Rostaing, N. Kamar, and J. Izopet, "Hepatitis e virus quasispecies and the outcome of acute hepatitis e in Solid-Organ transplant patients," *J Virol*, vol. 86, no. 18, pp. 10006–10014, 2012.

[295] D. Todt, A. Gisa, A. Radonic, A. Nitsche, P. Behrendt, P. Suneetha, S. Pischke, B. Bremer, R. J. Brown, M. P. Manns, M. Cornberg, T. C. Bock, E. Steinmann, and H. Wedemeyer, "In vivo evidence for ribavirin-induced mutagenesis of the hepatitis e virus genome," *Gut*, vol. 65, no. 10, pp. 1733–1743, 2016.

[296] Y. Debing and J. Neyts, “Antiviral strategies for hepatitis e virus,” *Antivir Res*, vol. 102, pp. 106–118, 2014.

[297] E. van Wezel, J. de Bruijne, K. Damman, M. Bijmolen, A. van den Berg, E. Verschuuren, G. Ruigrok, R. A, and M. Knoester, “Sofosbuvir add-on to ribavirin treatment for chronic hepatitis e virus infection in solid organ transplant recipients does not result in sustained virological response,” *Open Forum Infect Dis*, vol. 6, no. 8, 2019.

[298] M. Drinane, X. Wang, and K. Watt, “Sofosbuvir and ribavirin eradication of refractory hepatitis e in an immunosuppressed kidney transplant recipient,” *Hepatology*, vol. 69, no. 5, pp. 2297–2299, 2019.

[299] M. C. Donnelly, S. N. Imlach, F. Abravanel, S. Ramalingam, I. Johannessen, J. Petrik, A. R. Fraser, J. Campbell, P. Bramley, H. R. Dalton, P. C. Hayes, N. Kamar, and K. J. Simpson, “Sofosbuvir and daclatasvir Anti–Viral therapy fails to Clear HEV viremia and restore reactive t cells in a HEV/HCV Co-Infected liver transplant recipient,” *Gastroenterology*, vol. 152, no. 1, pp. 300–301, 2017.

[300] N. Kamar and Q. Pan, “No clear evidence for an effect of sofosbuvir against hepatitis e virus in organ transplant patients,” *Hepatology*, vol. 69, no. 4, pp. 1846–1847, 2019.

[301] D. Todt, N. Moeller, D. Praditya, V. Kinast, M. Friesland, M. Engelmann, L. Verhoye, I. Sayed, P. Behrendt, V. Thi, P. Meuleman, and E. Steinmann, “The natural compound silvestrol inhibits hepatitis e virus (HEV) replication in vitro and in vivo,” *Antivir Res*, vol. 157, pp. 151–158, 2018.

[302] N. E. Netzler, D. Tuipulotu, S. G. Vasudevan, J. M. Mackenzie, and P. A. White, “Antiviral candidates for treating hepatitis e virus infection,” *Antimicrob Agents Ch*, vol. 63, no. 6, 2019.

[303] S. Haffar, F. Bazerbachi, and J. R. Lake, “Making the case for the development of a vaccination against hepatitis e virus,” *Liver Int*, vol. 35, no. 2, pp. 311–316, 2015.

[304] C. Yang, H. Pan, M. Wei, X. Zhang, N. Wang, Y. Gu, H. Du, J. Zhang, S. Li, and N. Xia, “Hepatitis e virus capsid protein assembles in 4M urea in the presence of salts,” *Protein Sci*, vol. 22, no. 3, pp. 314–326, 2013.

[305] S. Li, J. Zhang, Z. He, Y. Gu, R. Liu, J. Lin, Y. Chen, M. Ng, and N. Xia, “Mutational analysis of essential interactions involved in the assembly of hepatitis e virus capsid,” *J Biol Chem*, vol. 280, no. 5, pp. 3400–3406, 2005.

[306] S. Li, X. Tang, J. Seetharaman, C. Yang, Y. Gu, J. Zhang, H. Du, W. J. Shih, C. Hew, J. Sivaraman, and N. Xia, "Dimerization of hepatitis e virus capsid protein e2s domain is essential for Virus–Host interaction," *Plos Pathog*, vol. 5, no. 8, p. e1000537, 2009.

[307] J. Zhang, X. Zhang, S. Huang, T. Wu, Y. Hu, Z. Wang, H. Wang, H. Jiang, Y. Wang, Q. Yan, M. Guo, X. Liu, J. Li, C. Yang, Q. Tang, R. Jiang, H. Pan, Y. Li, W. J. Shih, M. Ng, F. Zhu, and N. Xia, "Long-Term efficacy of a hepatitis e vaccine," *New Engl J Medicine*, vol. 372, no. 10, pp. 914–922, 2015.

[308] F. Zhu, J. Zhang, X. Zhang, C. Zhou, Z. Wang, S. Huang, H. Wang, C. Yang, H. Jiang, J. Cai, Y. Wang, X. Ai, Y. Hu, Q. Tang, X. Yao, Q. Yan, Y. Xian, T. Wu, Y. Li, J. Miao, M. Ng, J. Shih, and N. Xia, "Efficacy and safety of a recombinant hepatitis e vaccine in healthy adults: a large-scale, randomised, double-blind placebo-controlled, phase 3 trial," *Lancet*, vol. 376, no. 9744, pp. 895–902, 2010.

[309] J. Zhang, C.-b. Liu, R.-c. Li, Y.-m. Li, Y.-j. Zheng, Y.-p. Li, D. Luo, B.-b. Pan, Y. Nong, S. Ge, J.-h. Xiong, J. Shih, M. Ng, and N.-s. Xia, "Randomized-controlled phase II clinical trial of a bacterially expressed recombinant hepatitis e vaccine," *Vaccine*, vol. 27, no. 12, pp. 1869–1874, 2009.

[310] J. Zhang, X. Zhang, C. Zhou, Z. Wang, S. Huang, X. Yao, Z. Liang, T. Wu, J. Li, Q. Yan, C. Yang, H. Jiang, H. Huang, Y. Xian, W. J. Shih, M. Ng, Y. Li, J. Wang, F. Zhu, and N. Xia, "Protection against hepatitis e virus infection by naturally acquired and vaccine-induced immunity," *Clin Microbiol Infec*, vol. 20, no. 6, pp. O397–O405, 2014.

[311] T. Kumai, A. Fan, Y. Harabuchi, and E. Celis, "Cancer immunotherapy: moving forward with peptide t cell vaccines," *Curr Opin Immunol*, vol. 47, pp. 57–63, 2017.

[312] M. Melssen and C. L. Slingluff, "Vaccines targeting helper t cells for cancer immunotherapy," *Curr Opin Immunol*, vol. 47, pp. 85–92, 2017.

[313] N. Behloul, S. Baha, Z. Liu, W. Wei, Y. Zhu, Y. Rao, R. Shi, and J. Meng, "Design and development of a chimeric vaccine candidate against zoonotic hepatitis e and foot-and-mouth disease," *Microb Cell Fact*, vol. 19, no. 1, p. 137, 2020.

[314] S. Kamili, "Toward the development of a hepatitis e vaccine," *Virus Res*, vol. 161, no. 1, pp. 93–100, 2011.

[315] M. Zhang, S. U. Emerson, H. Nguyen, R. Engle, S. Govindarajan, W. C. Blackwelder, J. Gerin, and R. H. Purcell, "Recombinant vaccine against hepatitis e: duration of protective immunity in rhesus macaques," *Vaccine*, vol. 20, no. 27-28, pp. 3285–3291, 2002.

[316] M. Shrestha, R. Scott, D. Joshi, M. P. Mammen, G. Thapa, N. Thapa, K. Myint, M. Fourneau, R. A. Kuschner, S. Shrestha, M. David, J. Seriwatana, D. W. Vaughn, A. Safary, T. P. Endy, and B. L. Innis, "Safety and efficacy of a recombinant hepatitis e vaccine," *New Engl J Medicine*, vol. 356, no. 9, pp. 895–903, 2007.

[317] P. O. Yarbough, "Hepatitis e virus," *Intervirology*, vol. 42, no. 2-3, pp. 179–184, 1999.

[318] Y. Tong, M. Zhan, J. Lu, Y. Bai, and S. Bi, "[Immunogenicity of recombinant HEV ORF2 protein expressed in pichia pastoris].," *Zhonghua Shi Yan He Lin Chuang Bing Du Xue Za Zhi Zhonghua Shiyan He Linchuang Bingduxue Zazhi Chin J Exp Clin Virology*, vol. 16, no. 1, pp. 23–6, 2002.

[319] Y. Ma, S. Lin, Y. Gao, M. Li, W. Luo, J. Zhang, and N. Xia, "Expression of ORF2 partial gene of hepatitis e virus in tomatoes and immunoactivity of expression products," *World J Gastroentero*, vol. 9, no. 10, pp. 2211–2215, 2003.

[320] V. A. Arankalle, K. S. Lole, T. M. Deshmukh, S. Srivastava, and U. S. Shaligram, "Challenge studies in rhesus monkeys immunized with candidate hepatitis e vaccines: DNA, DNA-prime-protein-boost and DNA-protein encapsulated in liposomes," *Vaccine*, vol. 27, no. 7, pp. 1032–1039, 2009.

[321] S. Kamili, J. Spelbring, D. Carson, and K. Krawczynski, "Protective efficacy of hepatitis e virus DNA vaccine administered by gene gun in the cynomolgus macaque model of infection," *J Infect Dis*, vol. 189, no. 2, pp. 258–264, 2004.

[322] J. Pillot, Sharma, Y. Lazizi, A. Budkowska, C. Dauguet, M. Galimand, and J. Sarthou, "Immunological characterization of a viral agent involved in epidemic and sporadic non-A,non-B hepatitis," *Ann De L'institut Pasteur Virologie*, vol. 138, no. 1, pp. 145–158, 1987.

[323] H. Okamoto, "Genetic variability and evolution of hepatitis e virus," *Virus Res*, vol. 127, no. 2, pp. 216–228, 2007.

[324] T. Tanaka, M. Takahashi, E. Kusano, and H. Okamoto, "Development and evaluation of an efficient cell-culture system for hepatitis e virus," *J Gen Virol*, vol. 88, no. 3, pp. 903–911, 2007.

[325] Q. Wu, J. An, R. She, R. Shi, W. Hao, M. Soomro, X. Yuan, J. Yang, and J. Wang, "Detection of genotype 4 swine hepatitis e virus in systemic tissues in Cross-Species infected rabbits," *Plos One*, vol. 12, no. 1, p. e0171277, 2017.

[326] S. Panda, I. Ansari, H. Durgapal, S. Agrawal, and S. Jameel, “The in Vitro-Synthesized RNA from a cDNA clone of hepatitis e virus is infectious,” *J Virol*, vol. 74, no. 5, pp. 2430–2437, 2000.

[327] R. Johne, P. Dremsek, J. Reetz, G. Heckel, M. Hess, and R. G. Ulrich, “Hepeviridae: An expanding family of vertebrate viruses,” *Infect Genetics Evol*, vol. 27, pp. 212–229, 2014.

[328] V. Thi, Y. Debing, X. Wu, C. M. Rice, J. Neyts, D. Moradpour, and J. Gouttenoire, “Sofosbuvir inhibits hepatitis e virus replication in vitro and results in an additive effect when combined with ribavirin,” *Gastroenterology*, vol. 150, no. 1, pp. 82–85.e4, 2016.

[329] V. Thi, X. Wu, R. L. Belote, U. Andreo, C. N. Takacs, J. P. Fernandez, V. Luis, S. Prallet, C. C. Decker, R. M. Fu, B. Qu, K. Uryu, H. Molina, M. Saeed, E. Steinmann, S. Urban, R. R. Singaraja, W. M. Schneider, S. M. Simon, and C. M. Rice, “Stem cell-derived polarized hepatocytes,” *Nat Commun*, vol. 11, no. 1, p. 1677, 2020.

[330] L. Xu, W. Wang, Y. Li, X. Zhou, Y. Yin, Y. Wang, R. A. de Man, L. van der Laan, F. Huang, N. Kamar, M. P. Peppelenbosch, and Q. Pan, “RIG-I is a key antiviral interferon-stimulated gene against hepatitis e virus regardless of interferon production,” *Hepatology*, vol. 65, no. 6, pp. 1823–1839, 2017.

[331] H. Nguyen, P. Shukla, U. Torian, K. Faulk, and S. Emerson, “Hepatitis e virus genotype 1 infection of swine kidney cells in vitro is inhibited at multiple levels,” *J Virol*, vol. 88, no. 2, pp. 868–877, 2014.

[332] S. Drave, Y. Debing, S. Walter, D. Todt, M. Engelmann, M. Friesland, H. Wedemeyer, J. Neyts, P. Behrendt, and E. Steinmann, “Extra-hepatic replication and infection of hepatitis e virus in neuronal-derived cells,” *J Viral Hepatitis*, vol. 23, no. 7, pp. 512–521, 2016.

[333] X. Zhou, F. Huang, L. Xu, Z. Lin, F. M. de Vrij, A. A. C, M. van der Kroeg, M. Zhao, Y. Yin, W. Wang, W. Cao, Y. Wang, S. A. Kushner, J. Peron, L. Alric, R. A. de Man, B. C. Jacobs, J. J. van Eijk, E. M. Aronica, D. Sprengers, H. J. Metselaar, C. I. de Zeeuw, H. R. Dalton, N. Kamar, M. P. Peppelenbosch, and Q. Pan, “Hepatitis e virus infects neurons and brains,” *J Infect Dis*, vol. 215, no. 8, pp. 1197–1206, 2017.

[334] L. Knegendorf, S. A. Drave, V. Thi, Y. Debing, R. J. Brown, F. W. Vondran, K. Resner, M. Friesland, T. Khera, M. Engelmann, B. Bremer, H. Wedemeyer, P. Behrendt, J. Neyts, T. Pietschmann, D. Todt, and E. Steinmann, “Hepatitis e virus replication and interferon

responses in human placental cells," *Hepatology Commun*, vol. 2, no. 2, pp. 173–187, 2018.

[335] X. Yin, X. Li, C. Ambardekar, Z. Hu, S. Lhomme, and Z. Feng, "Hepatitis e virus persists in the presence of a type III interferon response," *Plos Pathog*, vol. 13, no. 5, p. e1006417, 2017.

[336] X. Wu, V. Thi, P. Liu, C. N. Takacs, K. Xiang, L. Andrus, J. Gouttenoire, D. Moradpour, and C. M. Rice, "Pan-Genotype hepatitis e virus replication in stem Cell–Derived hepatocellular systems," *Gastroenterology*, vol. 154, no. 3, pp. 663–674.e7, 2018.

[337] R. H. Purcell and S. U. Emerson, "Animal models of hepatitis a and e," *Ilar J*, vol. 42, no. 2, pp. 161–177, 2001.

[338] Y. Choi, X. Zhang, C. Tran, and B. Skinner, "Expression profiles of host immune response-related genes against HEV genotype 3 and genotype 1 infections in rhesus macaques," *J Viral Hepatitis*, vol. 25, no. 8, pp. 986–995, 2018.

[339] R. H. Purcell, R. E. Engle, S. Govindarajan, R. Herbert, M. Claire, W. R. Elkins, A. Cook, C. Shaver, M. Beauregard, J. Swerczek, and S. U. Emerson, "Pathobiology of hepatitis e: lessons learned from primate models," *Emerg Microbes Infec*, vol. 2, no. 1, pp. 1–6, 2019.

[340] S. Tsarev, T. Tsareva, S. Emerson, M. Rippy, P. Zack, M. Shapiro, and R. Purcell, "Experimental hepatitis e in pregnant rhesus monkeys: Failure to transmit hepatitis e virus (HEV) to offspring and evidence of naturally acquired antibodies to HEV," *J Infect Dis*, vol. 172, no. 1, pp. 31–37, 1995.

[341] N. Gardinali, J. Guimarães, J. Melgaço, Y. Kevorkian, F. de Bottino, Y. Vieira, A. de da Silva, D. Pinto, L. da Fonseca, L. Vilhena, E. Uiechi, M. da Silva, J. Moran, R. Marchevsky, O. Cruz, R. Otonel, A. Alfieri, J. de Oliveira, A. Gaspar, and M. Pinto, "Cynomolgus monkeys are successfully and persistently infected with hepatitis e virus genotype 3 (HEV-3) after long-term immunosuppressive therapy," *Plos One*, vol. 12, no. 3, p. e0174070, 2017.

[342] F. Huang, C. Yang, X. Zhou, W. Yu, and Q. Pan, "Rhesus macaques persistently infected with hepatitis e shed virus into urine," *J Hepatol*, vol. 64, no. 6, pp. 1446–1447, 2016.

[343] J. Gouilly, Q. Chen, J. Siewiera, G. Cartron, C. Levy, M. Dubois, A. Reem, J. Izopet, J. Nabila, and H. Costa, "Genotype specific pathogenicity of hepatitis e virus at the human maternal-fetal interface," *Nat Commun*, vol. 9, no. 1, p. 4748, 2018.

[344] R. H. Purcell, H. Nguyen, M. Shapiro, R. E. Engle, S. Govindarajan, W. C. Blackwelder, D. C. Wong, J. Prieels, and S. U. Emerson, "Pre-clinical immunogenicity and efficacy trial of a recombinant hepatitis e vaccine," *Vaccine*, vol. 21, no. 19-20, pp. 2607–2615, 2003.

[345] S. P. Kenney and X. J. Meng, "Hepatitis e virus: Animal models and zoonosis.," *Annu Rev Anim Biosci*, vol. 7, pp. 427–448, 2019.

[346] A. Feagins, T. Opriessnig, D. Guenette, P. Halbur, and X. Meng, "Detection and characterization of infectious hepatitis e virus from commercial pig livers sold in local grocery stores in the USA," *J Gen Virol*, vol. 88, no. 3, pp. 912–917, 2007.

[347] C. M. Cossaboom, L. Córdoba, B. J. Sanford, P. Piñeyro, S. P. Kenney, B. A. Dryman, Y. Wang, and X. Meng, "Cross-species infection of pigs with a novel rabbit, but not rat, strain of hepatitis e virus isolated in the united states," *J Gen Virol*, vol. 93, no. Pt_8, pp. 1687–1695, 2012.

[348] F. Huang, Y. Li, W. Yu, S. Jing, J. Wang, F. Long, Z. He, C. Yang, Y. Bi, W. Cao, C. Liu, X. Hua, and Q. Pan, "Excretion of infectious hepatitis e virus into milk in cows imposes high risks of zoonosis," *Hepatology*, vol. 64, no. 2, pp. 350–359, 2016.

[349] X. Meng, *Swine Hepatitis E Virus: Cross-Species Infection and Risk in Xenotransplantation*. 2003.

[350] M. Bouwknegt, S. A. Rutjes, C. Reusken, S. Norbert, K. Frankena, M. C. de Jong, A. de Husman, and W. H. van der Poel, "The course of hepatitis e virus infection in pigs after contact-infection and intravenous inoculation," *Bmc Vet Res*, vol. 5, no. 1, p. 7, 2009.

[351] T. Williams, C. Kasorndorkbua, P. Halbur, G. Haqshenas, D. Guenette, T. Toth, and X. Meng, "Evidence of extrahepatic sites of replication of the hepatitis e virus in a swine model," *J Clin Microbiol*, vol. 39, no. 9, pp. 3040–3046, 2001.

[352] J. Schlosser, M. Eiden, V. Ariel, C. Fast, P. Dremsek, E. Lange, R. G. Ulrich, and M. H. Groschup, "Natural and experimental hepatitis e virus genotype 3 - infection in european wild boar is transmissible to domestic pigs," *Vet Res*, vol. 45, no. 1, p. 121, 2014.

[353] B. J. Sanford, T. Opriessnig, S. P. Kenney, B. A. Dryman, L. Córdoba, and X. Meng, "Assessment of the cross-protective capability of recombinant capsid proteins derived from pig, rat, and avian hepatitis e viruses (HEV) against challenge with a genotype 3 HEV in pigs," *Vaccine*, vol. 30, no. 44, pp. 6249–6255, 2012.

[354] B. J. Sanford, B. A. Dryman, Y. Huang, A. R. Feagins, L. Tanya, and X. Meng, "Prior infection of pigs with a genotype 3 swine hepatitis e virus (HEV) protects against subsequent challenges with homologous and heterologous genotypes 3 and 4 human HEV," *Virus Res*, vol. 159, no. 1, pp. 17–22, 2011.

[355] I. Sayed, A. Elkhawaga, and E. Mohamed, "In vivo models for studying hepatitis e virus infection; updates and applications," *Virus Res*, vol. 274, p. 197765, 2019.

[356] H. Ma, L. Zheng, Y. Liu, C. Zhao, T. J. Harrison, Y. Ma, S. Sun, J. Zhang, and Y. Wang, "Experimental infection of rabbits with rabbit and genotypes 1 and 4 hepatitis e viruses," *Plos One*, vol. 5, no. 2, p. e9160, 2010.

[357] J. Han, Y. Lei, L. Liu, P. Liu, J. Xia, Y. Zhang, H. Zeng, L. Wang, L. Wang, and H. Zhuang, "SPF rabbits infected with rabbit hepatitis e virus isolate experimentally showing the chronicity of hepatitis," *Plos One*, vol. 9, no. 6, p. e99861, 2014.

[358] L. Wang, J. Xia, L. Wang, and Y. Wang, "Experimental infection of rabbits with genotype 3 hepatitis e virus produced both chronicity and kidney injury," *Gut*, vol. 66, no. 3, pp. gutjnl–2016–312023, 2016.

[359] B. Liu, Y. Chen, Y. Sun, Y. Nan, H. Li, T. Du, J. A. Hiscox, Q. Zhao, and E. Zhou, "Experimental infection of rabbit with swine-derived hepatitis e virus genotype 4," *Vet Microbiol*, vol. 229, pp. 168–175, 2019.

[360] J. Xia, L. Liu, L. Wang, Y. Zhang, H. Zeng, P. Liu, Q. Zou, L. Wang, and H. Zhuang, "Experimental infection of pregnant rabbits with hepatitis e virus demonstrating high mortality and vertical transmission," *J Viral Hepatitis*, vol. 22, no. 10, pp. 850–857, 2015.

[361] T. LI, S. Yuriko, A. Yasushi, T. Hiroshi, M. Tatsuo, and T. Naokazu, "Mice are not susceptible to hepatitis e virus infection," *J Vet Med Sci*, vol. 70, no. 12, pp. 1359–1362, 2008.

[362] F. Huang, W. Zhang, G. Gong, C. Yuan, Y. Yan, S. Yang, L. Cui, J. Zhu, Z. Yang, and X. Hua, "Experimental infection of balb/c nude mice with hepatitis e virus," *Bmc Infect Dis*, vol. 9, no. 1, p. 93, 2009.

[363] P. Meuleman, L. Libbrecht, R. Vos, B. de Hemptinne, K. Gevaert, J. Vandekerckhove, T. Roskams, and L. Geert, "Morphological and biochemical characterization of a human liver in a uPA-SCID mouse chimera," *Hepatology*, vol. 41, no. 4, pp. 847–856, 2005.

[364] L. Foquet, E. M. Wilson, L. Verhoye, M. Grompe, L. Geert, J. Bial, and P. Meuleman, *Successful Engraftment of Human Hepatocytes in uPA-SCID and FRG® KO Mice*. 2016.

[365] L. Allweiss, S. Gass, K. Giersch, A. Groth, J. Kah, T. Volz, G. Rapp, A. Schöbel, A. W. Lohse, S. Polywka, S. Pischke, E. Herker, M. Dandri, and M. Lütgehetmann, "Human liver chimeric mice as a new model of chronic hepatitis e virus infection and preclinical drug evaluation," *J Hepatol*, vol. 64, no. 5, pp. 1033–1040, 2016.

[366] I. M. Sayed and P. Meuleman, "Murine tissues of human liver chimeric mice are not susceptible to hepatitis e virus genotypes 1 and 3," *J Infect Dis*, vol. 216, no. 7, pp. 919–920, 2017.

[367] M. D. van de Garde, S. D. Pas, G. W. van Oord, L. Gama, Y. Choi, R. A. de Man, A. Boonstra, and T. Vanwolleghem, "Interferon-alpha treatment rapidly clears hepatitis e virus infection in humanized mice," *Sci Rep-uk*, vol. 7, no. 1, p. 8267, 2017.

[368] I. M. Sayed, L. Verhoye, L. Cocquerel, F. Abravanel, L. Foquet, C. Montpellier, Y. Debing, A. Farhoudi, C. Wychowski, J. Dubuisson, L. Geert, J. Neyts, J. Izopet, T. Michiels, and P. Meuleman, "Study of hepatitis e virus infection of genotype 1 and 3 in mice with humanised liver," *Gut*, vol. 66, no. 5, p. 920, 2017.

[369] T. Li, S. Yoshizaki, Y. Ami, Y. Suzaki, S. P. Yasuda, K. Yoshimatsu, J. Arikawa, N. Takeda, and T. Wakita, "Susceptibility of laboratory rats against genotypes 1, 3, 4, and rat hepatitis e viruses," *Vet Microbiol*, vol. 163, no. 1-2, pp. 54–61, 2013.

[370] T. Li, T. Yang, S. Yoshizaki, Y. Ami, Y. Suzaki, K. Ishii, N. Kishida, M. Shirakura, H. Asanuma, N. Takeda, and T. Wakita, "Ferret hepatitis e virus infection induces acute hepatitis and persistent infection in ferrets," *Vet Microbiol*, vol. 183, pp. 30–36, 2016.

[371] T. Li, S. Yoshizaki, T. Yang, M. Kataoka, T. Nakamura, Y. Ami, S. Yuriko, N. Takeda, and T. Wakita, "Production of infectious ferret hepatitis e virus in a human hepatocarcinoma cell line PLC/PRF/5," *Virus Res*, vol. 213, pp. 283–288, 2016.

[372] W. Li, Q. Sun, R. She, D. Wang, X. Duan, J. Yin, and Y. Ding, "Experimental infection of mongolian gerbils by a genotype 4 strain of swine hepatitis e virus," *J Med Virol*, vol. 81, no. 9, pp. 1591–1596, 2009.

[373] Y. Yang, R. Shi, R. She, M. Soomro, J. Mao, F. Du, Y. Zhao, and C. Liu, "Effect of swine hepatitis e virus on the livers of experimentally infected mongolian gerbils by swine hepatitis e virus," *Virus Res*, vol. 208, pp. 171–179, 2015.

[374] Y. Hong, Z. He, W. Tao, T. Fu, Y. Wang, and Y. Chen, "Experimental infection of Z:ZCLA mongolian gerbils with human hepatitis e virus," *World J Gastroentero*, vol. 21, no. 3, pp. 862–867, 2015.

[375] W. Yu, C. Yang, Y. Bi, F. Long, Y. Li, J. Wang, and F. Huang, “Characterization of hepatitis e virus infection in tree shrew (Tupaia belangeri chinensis),” *Bmc Infect Dis*, vol. 16, no. 1, p. 80, 2016.

[376] G. Haqshenas, H. Shivaprasad, P. Woolcock, D. Read, and X. Meng, “Genetic identification and characterization of a novel virus related to human hepatitis e virus from chickens with hepatitis–splenomegaly syndrome in the united states,” *J Gen Virol*, vol. 82, no. 10, pp. 2449–2462, 2001.

[377] P. Billam, F. Pierson, W. Li, L. T, R. Duncan, and X. Meng, “Development and validation of a Negative-Strand-Specific reverse Transcription-PCR assay for detection of a chicken strain of hepatitis e virus: Identification of nonliver replication sites,” *J Clin Microbiol*, vol. 46, no. 8, pp. 2630–2634, 2008.

[378] H. Guo, E. Zhou, Z. Sun, and X. Meng, “Protection of chickens against avian hepatitis e virus (avian HEV) infection by immunization with recombinant avian HEV capsid protein,” *Vaccine*, vol. 25, no. 15, pp. 2892–2899, 2007.

[379] M. von Nordheim, M. Boinay, R. Leisi, C. Kempf, and C. Ros, “Cutthroat trout Virus—Towards a virus model to support hepatitis e research,” *Viruses*, vol. 8, no. 10, p. 289, 2016.

[380] K. J. Blight, M. J. A, and C. M. Rice, “Highly permissive cell lines for subgenomic and genomic hepatitis c virus RNA replication,” *J Virol*, vol. 76, no. 24, pp. 13001–13014, 2002.

[381] N. Jothikumar, T. L. Cromeans, B. H. Robertson, X. Meng, and V. R. Hill, “A broadly reactive one-step real-time RT-PCR assay for rapid and sensitive detection of hepatitis e virus,” *J Virol Methods*, vol. 131, no. 1, pp. 65–71, 2006.

[382] K. Murata and M. Wolf, “Cryo-electron microscopy for structural analysis of dynamic biological macromolecules,” *Biochimica Et Biophysica Acta Bba - Gen Subj*, vol. 1862, no. 2, pp. 324–334, 2018.

[383] B. Ford, “Transmission electron microscope,” 0.

[384] F. Sigworth, “A Maximum-Likelihood approach to Single-Particle image refinement,” *J Struct Biol*, vol. 122, no. 3, pp. 328–339, 1998.

[385] S. Scheres, “A bayesian view on Cryo-EM structure determination,” *J Mol Biol*, vol. 415, no. 2-4, pp. 406–418, 2012.

[386] S. H. Scheres, H. Gao, M. Valle, G. T. Herman, P. P. Eggermont, J. Frank, and J. Carazo, "Disentangling conformational states of macromolecules in 3D-EM through likelihood optimization," *Nat Methods*, vol. 4, no. 1, pp. 27–29, 2007.

[387] M. van der Heijden and J. Bol, "Composition of alphavirus-like replication complexes: involvement of virus and host encoded proteins," *Arch Virol*, vol. 147, no. 5, pp. 875–898, 2002.

[388] I. Gentile, F. Borgia, A. Buonomo, G. Castaldo, and G. Borgia, "A novel promising therapeutic option against hepatitis c virus: An oral nucleotide NS5B polymerase inhibitor sofosbuvir," *Curr Med Chem*, vol. 20, no. 30, pp. 3733–3742, 2013.

[389] L. D. Fricker, "Proteasome inhibitor drugs," *Annu Rev Pharmacol*, vol. 60, no. 1, pp. 1–20, 2019.

[390] A. Hershko and A. Ciechanover, "THE UBIQUITIN SYSTEM," *Annu Rev Biochem*, vol. 67, no. 1, pp. 425–479, 1998.

[391] T. Ravid and M. Hochstrasser, "Diversity of degradation signals in the ubiquitin proteasome system," *Nat Rev Mol Cell Bio*, vol. 9, no. 9, pp. 679–689, 2008.

[392] D. Kim, S. Kim, and G. C. Li, "Proteasome inhibitors MG132 and lactacystin hyperphosphorylate HSF1 and induce hsp70 and hsp27 expression," *Biochem Bioph Res Co*, vol. 254, no. 1, pp. 264–268, 1999.

[393] C. Bentaleb, K. Hervouet, C. Montpellier, C. Camuzet, J. Burlaud-Gaillard, M. Ferrié, E. Werkmeister, K. Metzger, N. L. Janampa, J. Marlet, J. Roux, C. Deffaud, A. Goffard, Y. Rouillé, J. Dubuisson, P. Roingeard, C.-M. Aliouat-Denis, and L. Cocquerel, "The Endocytic Recycling Compartment Serves as a Viral Factory for Hepatitis E Virus." Posté sur bioRxiv le 14 octobre 2021., Oct. 2021.

[394] H. Kawabata, "Transferrin and transferrin receptors update," *Free Radical Bio Med*, vol. 133, pp. 46–54, 2019.

[395] A. Guichard, V. Nizet, and E. Bier, "RAB11-mediated trafficking in host–pathogen interactions," *Nat Rev Microbiol*, vol. 12, no. 9, pp. 624–634, 2014.

[396] L. P. Nguyen, S. C. Tran, S. Suetsugu, Y. Lim, and S. B. Hwang, "PACSIN2 interacts with nonstructural protein 5A and regulates hepatitis c virus assembly," *J Virol*, vol. 94, no. 5, 2020.

[397] M. Sharma, S. Giridharan, J. Rahajeng, N. Naslavsky, and S. Caplan, "MICAL-L1 links EHD1 to tubular recycling endosomes and regulates receptor recycling," *Mol Biol Cell*, vol. 20, no. 24, pp. 5181–5194, 2009.

[398] M. S. Pols and J. Klumperman, "Trafficking and function of the tetraspanin CD63," *Exp Cell Res*, vol. 315, no. 9, pp. 1584–1592, 2009.

[399] L. Florin and T. Lang, "Tetraspanin assemblies in virus infection," *Front Immunol*, vol. 9, p. 1140, 2018.

[400] P. Pileri, Y. Uematsu, S. Campagnoli, G. Galli, F. Falugi, R. Petracca, A. J. Weiner, M. Houghton, D. Rosa, G. Grandi, and S. Abrignani, "Binding of hepatitis c virus to CD81," *Science*, vol. 282, no. 5390, pp. 938–941, 1998.

[401] B. Grigorov, J. Molle, E. Rubinstein, F. Zoulim, and B. Bartosch, "CD81 large extracellular loop-containing fusion proteins with a dominant negative effect on HCV cell spread and replication," *J Gen Virol*, vol. 98, no. 7, pp. 1646–1657, 2017.

[402] R. Bartenschlager, A. L, J. Mous, and H. Jacobsen, "Nonstructural protein 3 of the hepatitis c virus encodes a serine-type proteinase required for cleavage at the NS3/4 and NS4/5 junctions," *J Virol*, vol. 67, no. 7, pp. 3835–3844, 1993.

[403] N. Barretto, D. Jukneliene, K. Ratia, Z. Chen, A. D. Mesecar, and S. C. Baker, "The Papain-Like protease of severe acute respiratory syndrome coronavirus has deubiquitinating activity," *J Virol*, vol. 79, no. 24, pp. 15189–15198, 2005.

[404] B. Y. M, S. E. John, and A. D. Mesecar, "The SARS-coronavirus papain-like protease: Structure, function and inhibition by designed antiviral compounds," *Antivir Res*, vol. 115, pp. 21–38, 2015.

[405] R. R. Regoes, S. Crotty, R. Antia, and M. M. Tanaka, "Optimal replication of poliovirus within cells," *Am Nat*, vol. 165, no. 3, pp. 364–373, 2005.

[406] G. Fenteany, R. F. Standaert, W. S. Lane, S. Choi, E. Corey, and S. L. Schreiber, "Inhibition of proteasome activities and Subunit-Specific Amino-Terminal threonine modification by lactacystin," *Science*, vol. 268, no. 5211, pp. 726–731, 1995.

[407] T. L. Tellinghuisen, J. Marcotrigiano, A. E. Gorbalenya, and C. M. Rice, "The NS5A protein of hepatitis c virus is a zinc metalloprotein*," *J Biol Chem*, vol. 279, no. 47, pp. 48576–48587, 2004.

[408] D. B. Ascher, J. Wielens, T. L. Nero, L. Doughty, C. J. Morton, and M. W. Parker, "Potent hepatitis c inhibitors bind directly to NS5A and reduce its affinity for RNA," *Sci Rep-uk*, vol. 4, no. 1, p. 4765, 2014.

[409] S. P. Kenney and X. Meng, "Identification and fine mapping of nuclear and nucleolar localization signals within the human ribosomal protein s17," *Plos One*, vol. 10, no. 4, p. e0124396, 2015.

[410] P. Selvin, J. Luis, R. José, O. Juan, F. Carlos, G. Ana, and R. del Angel, "Nuclear localization of non-structural protein 3 (NS3) during dengue virus infection," *Arch Virol*, vol. 166, no. 5, pp. 1439–1446, 2021.

[411] J. Peranen, M. Rikkonen, P. Liljestrom, and L. Kaariainen, "Nuclear localization of semliki forest virus-specific nonstructural protein nsP2," *J Virol*, vol. 64, no. 5, pp. 1888–1896, 1990.

[412] M. A. Tijms, Y. van der Meer, and E. J. Snijder, "Nuclear localization of non-structural protein 1 and nucleocapsid protein of equine arteritis virus," *J Gen Virol*, vol. 83, no. 4, pp. 795–800, 2002.

[413] F. R. Maxfield and M. T. E, "Endocytic recycling," *Nat Rev Mol Cell Bio*, vol. 5, no. 2, pp. 121–132, 2004.

[414] V. Sílvia and M. Amorim, "Recycling endosomes and viral infection," *Viruses*, vol. 8, no. 3, p. 64, 2016.

[415] S. Rothenberger, E. W. Mullner, and L. C. Kuhn, "The mRNA-binding protein which controls ferritin and transferrin receptor expression is conserved during evolution," *Nucleic Acids Res*, vol. 18, no. 5, pp. 1175–1179, 1990.

[416] S. R. Radoshitzky, J. Abraham, C. F. Spiropoulou, J. H. Kuhn, D. Nguyen, W. Li, J. Nagel, P. J. Schmidt, J. H. Nunberg, N. C. Andrews, M. Farzan, and H. Choe, "Transferrin receptor 1 is a cellular receptor for new world haemorrhagic fever arenaviruses," *Nature*, vol. 446, no. 7131, pp. 92–96, 2007.

[417] B. Qualmann, M. M. Kessels, and R. B. Kelly, "Molecular links between endocytosis and the actin cytoskeleton," *J Cell Biology*, vol. 150, no. 5, pp. F111–F116, 2000.

[418] B. Qualmann and R. B. Kelly, "Syndapin isoforms participate in Receptor-Mediated endocytosis and actin organization," *J Cell Biology*, vol. 148, no. 5, pp. 1047–1062, 2000.

[419] C. Hansen, G. Howard, and B. J. Nichols, "Pacsin 2 is recruited to caveolae and functions in caveolar biogenesis," *J Cell Sci*, vol. 124, no. 16, pp. 2777–2785, 2011.

[420] Y. Senju, Y. Itoh, K. Takano, S. Hamada, and S. Suetsugu, “Essential role of PACSIN2/syndapin-II in caveolae membrane sculpting,” *J Cell Sci*, vol. 124, no. 12, pp. 2032–2040, 2011.

[421] B. de Kreuk, M. Nethe, F. Mar, E. C. Anthony, P. J. Hensbergen, A. M. Deelder, M. Plomann, and P. L. Hordijk, “The F-BAR domain protein PACSIN2 associates with rac1 and regulates cell spreading and migration,” *J Cell Sci*, vol. 124, no. 14, pp. 2375–2388, 2011.

[422] S. Popov, E. Popova, M. Inoue, Y. Wu, and H. Göttlinger, “HIV-1 gag recruits PACSIN2 to promote virus spreading,” *Proc National Acad Sci*, vol. 115, no. 27, p. 201801849, 2018.

[423] R. Duyne and E. O. Freed, “HIV-1 packs in PACSIN2 for cell-to-cell spread,” *Proc National Acad Sci*, vol. 115, no. 27, p. 201808821, 2018.

[424] K. Dhawan, N. Naslavsky, and S. Caplan, “Sorting nexin 17 (SNX17) links endosomal sorting to eps15 homology domain protein 1 (EHD1)–mediated fission machinery,” *J Biol Chem*, vol. 295, no. 12, pp. 3837–3850, 2020.

[425] N. Naslavsky, J. Rahajeng, M. Sharma, M. Jovi, and S. Caplan, “Interactions between EHD proteins and Rab11-FIP2: a role for EHD3 in early endosomal transport,” *Mol Biol Cell*, vol. 17, no. 1, pp. 163–177, 2006.

[426] P. J. Cullen and F. Steinberg, “To degrade or not to degrade: mechanisms and significance of endocytic recycling,” *Nat Rev Mol Cell Bio*, vol. 19, no. 11, pp. 679–696, 2018.

[427] N. Naslavsky and S. Caplan, “EHD proteins: key conductors of endocytic transport,” *Trends Cell Biol*, vol. 21, no. 2, pp. 122–131, 2011.

[428] S. Caplan, N. Naslavsky, L. M. Hartnell, R. Lodge, R. S. Polishchuk, J. G. Donaldson, and J. S. Bonifacino, “A tubular EHD1-containing compartment involved in the recycling of major histocompatibility complex class i molecules to the plasma membrane,” *Embo J*, vol. 21, no. 11, pp. 2557–2567, 2002.

[429] A. Braun, R. Pinyol, R. Dahlhaus, D. Koch, P. Fonarev, B. D. Grant, M. M. Kessels, and B. Qualmann, “EHD proteins associate with syndapin i and II and such interactions play a crucial role in endosomal recycling,” *Mol Biol Cell*, vol. 16, no. 8, pp. 3642–3658, 2005.

[430] F. Wang, J. Flanagan, N. Su, L. Wang, S. Bui, A. Nielson, X. Wu, H. Vo, X. Ma, and Y. Luo, "RNAscope a novel in situ RNA analysis platform for Formalin-Fixed, Paraffin-Embedded tissues," *J Mol Diagnostics*, vol. 14, no. 1, pp. 22–29, 2012.

[431] J. Alfaro, P. Bohländer, M. Dai, M. Filius, C. J. Howard, X. F. van Kooten, S. Ohayon, A. Pomorski, S. Schmid, A. Aksimentiev, E. V. Anslyn, G. Bedran, C. Cao, M. Chinappi, E. Coyaud, C. Dekker, G. Dittmar, N. Drachman, R. Eelkema, D. Goodlett, S. Hentz, U. Kalathiya, N. L. Kelleher, R. T. Kelly, Z. Kelman, S. Kim, B. Kuster, R. David, S. Lindsay, G. Maglia, E. M. Marcotte, J. P. Marino, C. Masselon, M. Mayer, P. Samaras, K. Sarthak, L. Sepiashvili, D. Stein, M. Wanunu, M. Wilhelm, P. Yin, A. Meller, and C. Joo, "The emerging landscape of single-molecule protein sequencing technologies," *Nat Methods*, vol. 18, no. 6, pp. 604–617, 2021.

Appendices

A. Inhibition with Sofosbuvir

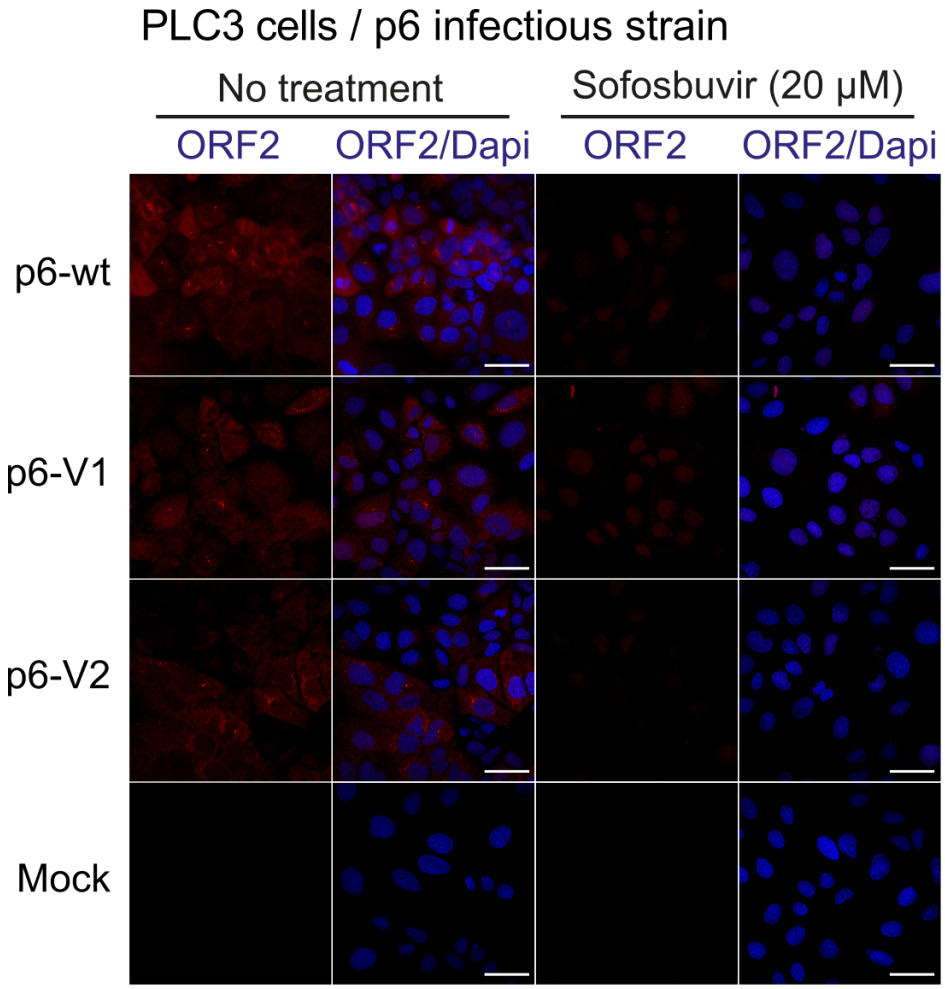

Figure 46: Immunofluorescence of p6-electroporated PLC3 cells in presence of sofosbuvir (20µM). Three days post–electroporation with the infectious p6–wt, p6–V1 or p6–V2 strain, PLC3 cells were fixed and stained in red with an anti-ORF2 antibody (1E6, Millipore). Nuclei were stained with Dapi (blue). Mock–electroporated PLC3 cells served as negative control. Scale bar = 20 µM

B. Kinetics of the HA–tagged ORF1

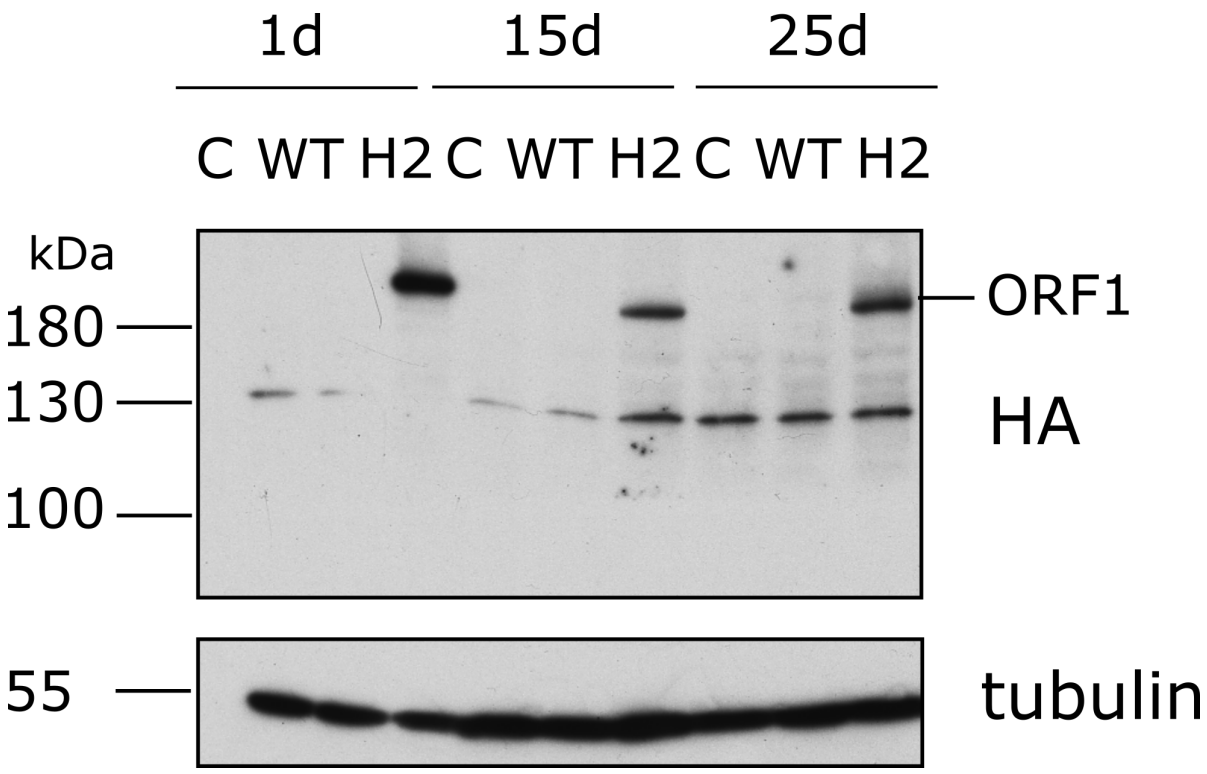

Figure 47: PLC3 cells were electroporated with the p6 infectious strain expressing the wildtype untagged ORF1 protein (wt) or the HA–tagged ORF1 (H2). Total cell lysates were collected in presence of protease inhibitors at 1, 15 and 25 dpe. Mock–electroporated cells served as negative control (C). The band migrating higher than 180 kDa corresponds to the full–length ORF1 protein (ORF1). The immunoblot was probed either with an anti–HA antibody or an anti–tubulin antibody to control for even loading. Molecular weight markers are indicated in kilodalton.

C. MTS assay of PLC3 cells

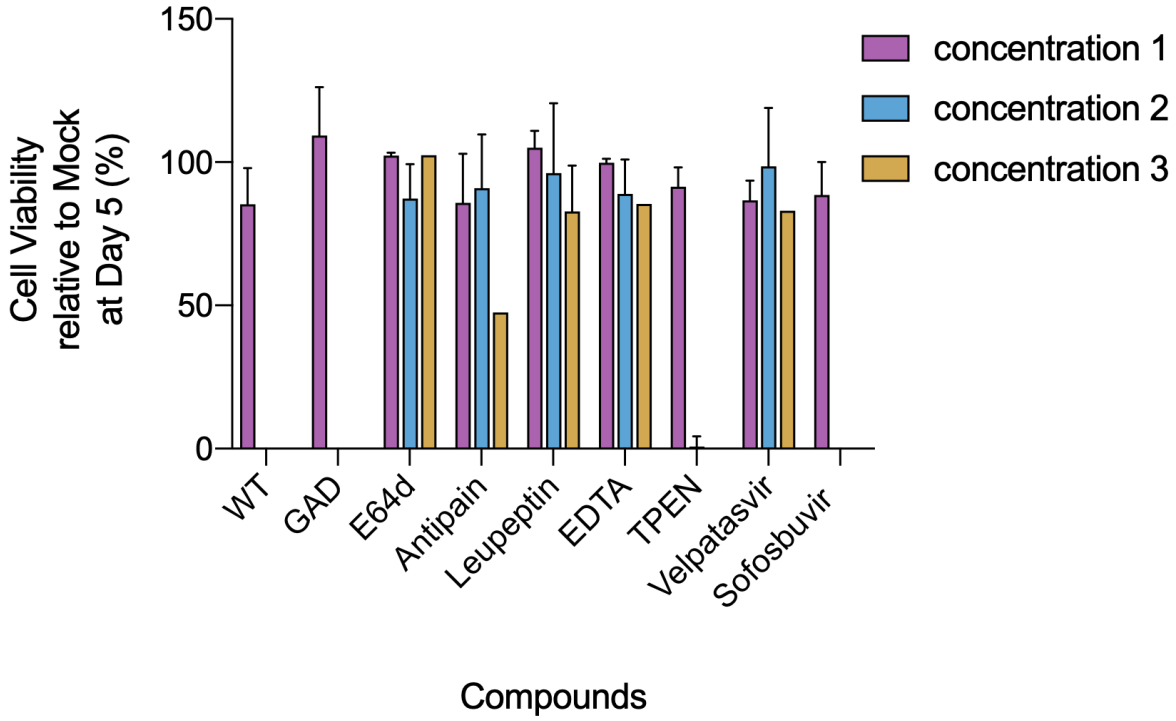

Figure 48: Cell viability assay of electroporated PLC3 cells with protease inhibitors and ion chelators. PLC3 cell were electroporate with the p6–V1–GLuc replicon and treated with the following compounds: E64d, Antipain, Leupeptin, EDTA, TPEN, Velpatasvir and Sofosbuvir with three different concentrations mentioned in Tab. 23. Cell viability was normalized to mock electroporated PLC3 cells (=100%) at 5dpe.

D. Immuno–gold staining of the HA–tagged ORF1

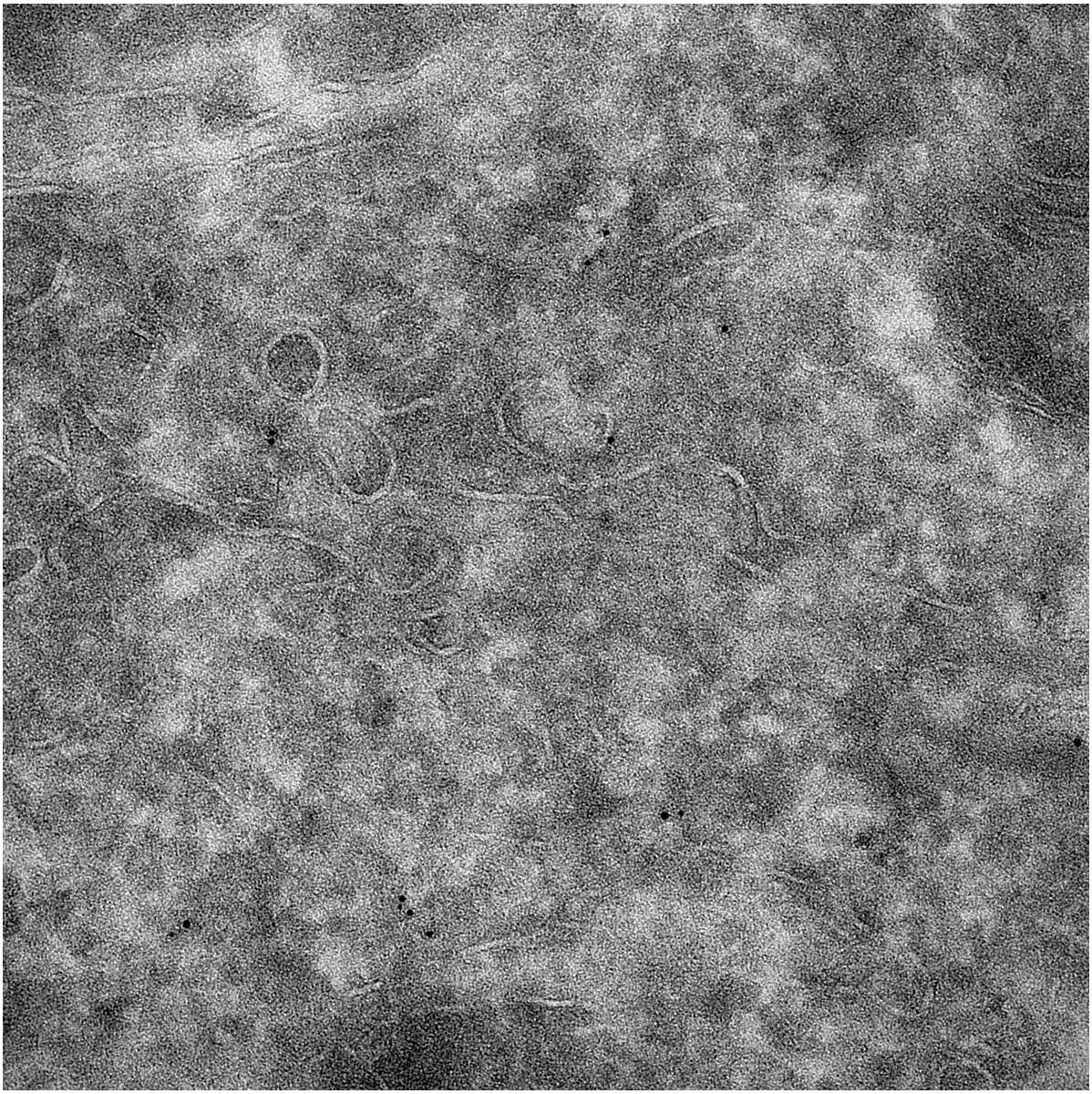

Figure 49: Immuno–gold staining of p6–H2 electroporated PLC3 cells. PLC3 cells were electroporated with the p6–H2 and fixed at 3dpe. An anti–HA antibody was used to stain the ORF1 protein, the secondary antibody was coupled to gold beads with a size of 6nm. No specific signal was detected and overall only few beads were visible.

E. Subcellular Localization of the heterologously expressed ORF1

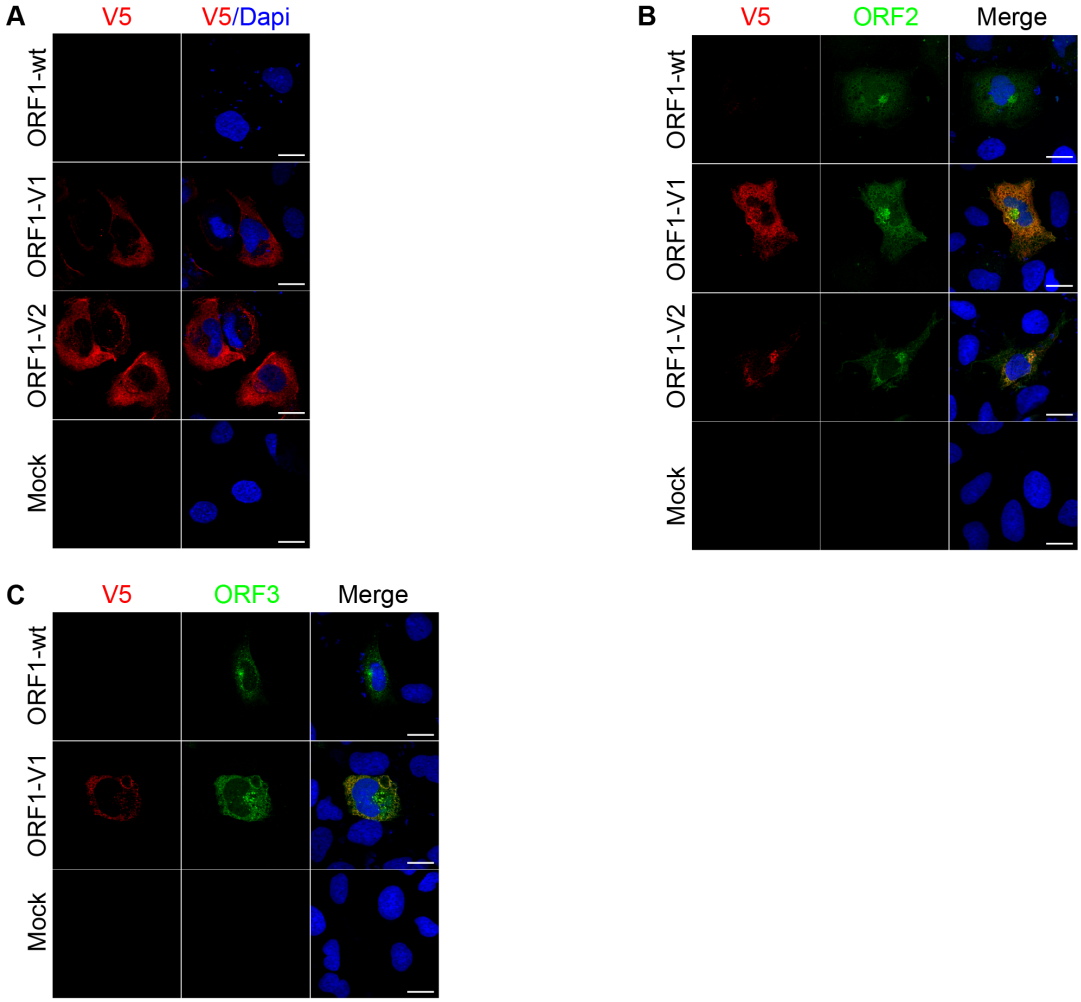

Figure 50: (A) H7–T7–IZ cells expressing either the wildtype ORF1 (ORF1–wt) or the V5–tagged ORF1 proteins (ORF1–V1, ORF1–V2) were fixed and permeabilized 8 h after transfection. Cells were stained with an anti–V5 antibody (red) and nuclei were stained with DAPI (blue) prior to analysis by confocal microscopy. Mock–transfected cells served as negative control. Scale bar = 20µm. **(B)** Co–labeling of the V5–tagged HEV replicase with ORF2 in H7–T7–IZ cells. Cells were treated as above. Then, the viral proteins were co–labeled with antibodies directed against the V5 epitope (ORF1, red) and ORF2 (1E6, green) prior to analysis by confocal microscopy. Scale bar = 20µm. **(C)** Co–labeling of the V5–tagged HEV replicase with ORF3 in H7–T7–IZ cells. Cells were treated as above. Then, the viral proteins were co–labeled with antibodies directed against the V5 epitope (ORF1, red) and ORF3 (green) prior to analysis by confocal microscopy. Scale bar = 20µm.

F. Article: Characterization of the Hepatitis E Virus Replicase

frontiers in Microbiology

ORIGINAL RESEARCH
published: 24 February 2022
doi: 10.3389/fmicb.2022.828636

Processing and Subcellular Localization of the Hepatitis E Virus Replicase: Identification of Candidate Viral Factories

*Karoline Metzger[1†], Cyrine Bentaleb[1†], Kévin Hervouet[1], Virginie Alexandre[1], Claire Montpellier[1], Jean-Michel Saliou[2], Martin Ferrié[1], Charline Camuzet[1], Yves Rouillé[1], Cécile Lecoeur[1], Jean Dubuisson[1], Laurence Cocquerel[1] and Cécile-Marie Aliouat-Denis[1]**

[1] CNRS, INSERM, CHU Lille, Institut Pasteur de Lille, U1019 – UMR 9017 – Center for Infection and Immunity of Lille (CIIL), Université de Lille, Lille, France, [2] CNRS, Inserm, CHU Lille, Institut Pasteur de Lille, UMR2014 – US41 – Plateformes Lilloises de Biologie and Santé (PLBS), Université de Lille, Lille, France

OPEN ACCESS

Edited by:
Vaithilingaraja Arumugaswami, University of California, Los Angeles, United States

Reviewed by:
Kavita Satish Lole, National Institute of Virology (ICMR), India
Deepak Sehgal, Shiv Nadar University, India

***Correspondence:**
Cécile-Marie Aliouat-Denis
cecile.aliouat@univ-lille.fr

[†] These authors have contributed equally to this work and share first authorship

Specialty section:
This article was submitted to Virology, a section of the journal Frontiers in Microbiology

Received: *03 December 2021*
Accepted: *01 February 2022*
Published: *24 February 2022*

Citation:
Metzger K, Bentaleb C, Hervouet K, Alexandre V, Montpellier C, Saliou J-M, Ferrié M, Camuzet C, Rouillé Y, Lecoeur C, Dubuisson J, Cocquerel L and Aliouat-Denis C-M (2022) Processing and Subcellular Localization of the Hepatitis E Virus Replicase: Identification of Candidate Viral Factories. Front. Microbiol. 13:828636. doi: 10.3389/fmicb.2022.828636

Hepatitis E virus (HEV) is the major cause of acute hepatitis worldwide. HEV is a positive-sense RNA virus expressing three open reading frames (ORFs). ORF1 encodes the ORF1 non–structural polyprotein, the viral replicase which transcribes the full-length genome and a subgenomic RNA that encodes the structural ORF2 and ORF3 proteins. The present study is focused on the replication step with the aim to determine whether the ORF1 polyprotein is processed during the HEV lifecycle and to identify where the replication takes place inside the host cell. As no commercial antibody recognizes ORF1 in HEV-replicating cells, we aimed at inserting epitope tags within the ORF1 protein without impacting the virus replication efficacy. Two insertion sites located in the hypervariable region were thus selected to tolerate the V5 epitope while preserving HEV replication efficacy. Once integrated into the infectious full-length Kernow C-1 p6 strain, the V5 epitopes did neither impact the replication of genomic nor the production of subgenomic RNA. Also, the V5-tagged viral particles remained as infectious as the wildtype particles to Huh-7.5 cells. Next, the expression pattern of the V5-tagged ORF1 was compared in heterologous expression and replicative HEV systems. A high molecular weight protein (180 kDa) that was expressed in all three systems and that likely corresponds to the unprocessed form of ORF1 was detected up to 25 days after electroporation in the p6 cell culture system. Additionally, less abundant products of lower molecular weights were detected in both in cytoplasmic and nuclear compartments. Concurrently, the V5-tagged ORF1 was localized by confocal microscopy inside the cell nucleus but also as compact perinuclear substructures in which ORF2 and ORF3 proteins were detected. Importantly, using *in situ* hybridization (RNAScope®), positive and negative-strand HEV RNAs were localized in the perinuclear substructures of HEV-producing cells. Finally, by simultaneous detection of HEV genomic RNAs and viral proteins in these substructures, we identified candidate HEV factories.

Keywords: HEV p6, positive-strand RNA virus, ORF1 processing, *Gaussia* luciferase replicon, epitope tag, RNA hybridization, endocytic recycling compartment, replication complexes

INTRODUCTION

Hepatitis E virus (HEV) is one of the leading causes of acute hepatitis worldwide (WHO, 2021). Amongst the 20 million infections estimated by WHO every year, 3.3 million cases are symptomatic. Although HEV infection is usually self-resolving in the general population with a mortality rate of 0.5 to 4% due to fulminant hepatitis, the immunocompromised patients, mainly organ transplant recipients, may suffer from chronic hepatitis and cirrhosis (Lhomme et al., 2020). Elevated mortality rates (up to 25%) have also been recorded among pregnant women in developing countries as well as in patients with pre-existing liver diseases (Pérez-Gracia et al., 2017; Lhomme et al., 2020; Webb and Dalton, 2020). In addition, both chronic and acute HEV infections can lead to neurological disorders or kidney injuries and impaired renal function (Lhomme et al., 2020; Webb and Dalton, 2020).

Hepatitis E virus is classified in the *Hepeviridae* family and the four genotypes (gt 1-gt 4) that account for most of the human infections, are included within the *Orthohepevirus A* genus (Smith and Simmonds, 2018). HEV gt 1 and 2 are transmitted through fecal-oral route and can cause large, primarily waterborne outbreaks in resource-limited settings. Ingestion of undercooked swine or game meat is the primary mode of zoonotic transmission of HEV gt 3 and 4 in middle- and high-income areas (Kamar et al., 2017).

The HEV genome is a positive-sense, 5′-capped, single-stranded RNA of ∼7.2 kb in length. It is organized into three open reading frames (ORFs): ORF1, ORF2, and ORF3 (Wang and Meng, 2021). ORF1 encodes the ORF1 non-structural polyprotein, which contains several functional domains essential for viral replication. ORF2 encodes the ORF2 viral capsid protein, which is involved in particle assembly, binding to host cells and eliciting neutralizing antibodies (Schofield et al., 2000; Shiota et al., 2013). ORF3 encodes a small multifunctional phosphoprotein involved in virion morphogenesis and egress [reviewed in Glitscher and Hildt (2021)]. ORF2 and ORF3 are partially overlapping and the corresponding proteins are translated from a subgenomic RNA of 2.2 kb in length (Graff et al., 2006). Another small viral protein, named ORF4, only expressed in genotype 1 HEV, was shown to interact with several host and viral proteins and enhance viral replication (Nair et al., 2016; Yadav et al., 2021).

ORF1 is the largest ORF in the viral genome and encodes a non-structural polyprotein where several domains have been bioinformatically assigned based on homology with Rubi-like viruses, i.e., *Rubivirus*, *Betateravirus,* and *Benyvirus* (Koonin et al., 1992). Although several domains such as methyltransferase (Met), helicase (Hel) and RNA-dependent RNA polymerase (RdRp) have been reported to be enzymatically active, the function of the Y and X-domains as well as the highly disordered hypervariable region (HVR) remain elusive (Wang and Meng, 2021; **Figure 1C**). In addition, the precise location of the protease region (known as papain-like cysteine protease, PCP) and its enzymatic activity are still a matter of debate (LeDesma et al., 2019; Proudfoot et al., 2019). Whether or not the HEV polyprotein gets processed by the PCP or cellular proteases remains a difficult question to address considering the low expression level of the polyprotein in HEV cell culture systems as well as the scarcity of functional specific antibodies (Debing et al., 2016; Lenggenhager et al., 2017; Nimgaonkar et al., 2018; Kenney and Meng, 2019).

In this study, we sought to characterize the ORF1 replicase. The insertion of epitope tags into the HEV replicase came to us as the best strategy to track the polyprotein inside the host cell and identify its potential cleavage products. The HVR was chosen based on amino acid (aa) ORF1 sequence alignments as well as its capacity to tolerate inserted fragments arising either from duplication of viral genome or from human genes (Shukla et al., 2011, 2012; Nguyen et al., 2012; Johne et al., 2014; Lhomme et al., 2014). Additionally, the HVR region of the HEV83-2-27 strain of gt 3 has been recently reported to tolerate the insertion of an HA epitope and a small luciferase reporter gene (Szkolnicka et al., 2019). In our study, we attempted to insert V5 or HA epitopes into the HVR of gt 3 Kernow C-1 p6 strain, taking advantage of the homology existing between the HEV and V5 epitope aa sequences and also of a naturally occurring insertion in the HEV genome (Nguyen et al., 2012; **Figure 1C**). At first, a p6-GLuc replicon expressing the *Gaussia Luciferase* (*GLuc*) reporter gene under the control of the epitope tagged-ORF1 was used to select insertion sites that did not impact replication efficacy (Shukla et al., 2012; Emerson et al., 2013; **Figure 1B**). Two positions located into the HVR were selected as the V5 insertions did neither impact the *Gaussia* luciferase secretion nor the transcription of genomic and subgenomic viral RNAs. Also, the V5-tagged viral particles remained as infectious as the wildtype particles to Huh-7.5 cells. Next, the expression of the selected epitope-tagged ORF1 was analyzed in the p6-GLuc replicon, heterologous and p6 cell culture systems. The full-length ORF1 protein as well as less abundant products of lower molecular weight were detected in all systems, both in cytoplasmic and nuclear compartments. Simultaneous detection of HEV genomic / subgenomic RNAs by fluorescence *in situ* hybridization (RNAscope®) and ORF1 protein by immunofluorescence identified candidate HEV replication complexes as compact perinuclear nuggets in which ORF2 and ORF3 proteins were also detected. Finally, partial co-localization of viral proteins with cellular markers of the endocytic recycling compartment (ERC) unveiled the composition of the HEV replication factories.

MATERIALS AND METHODS

Plasmids

The plasmid pBlueScript SK (+) carrying the DNA of the full-length genome of HEV gt 3 Kernow C-1 p6 strain (GenBank accession number JQ679013) was kindly provided by Dr. S.U. Emerson (**Figure 1A**). The HEV p6-wt-GLuc replicon, constructed from the HEV gt 3 Kernow C-1 p6 strain was also obtained from Dr. Emerson (**Figure 1B**). This replicon possesses a *Gaussia Luciferase* (*GLuc*) reporter gene that substitutes the 5′ part of the ORF2 gene and most part of the ORF3 gene (Shukla et al., 2012; Emerson et al., 2013). A p6-GAD-GLuc mutant

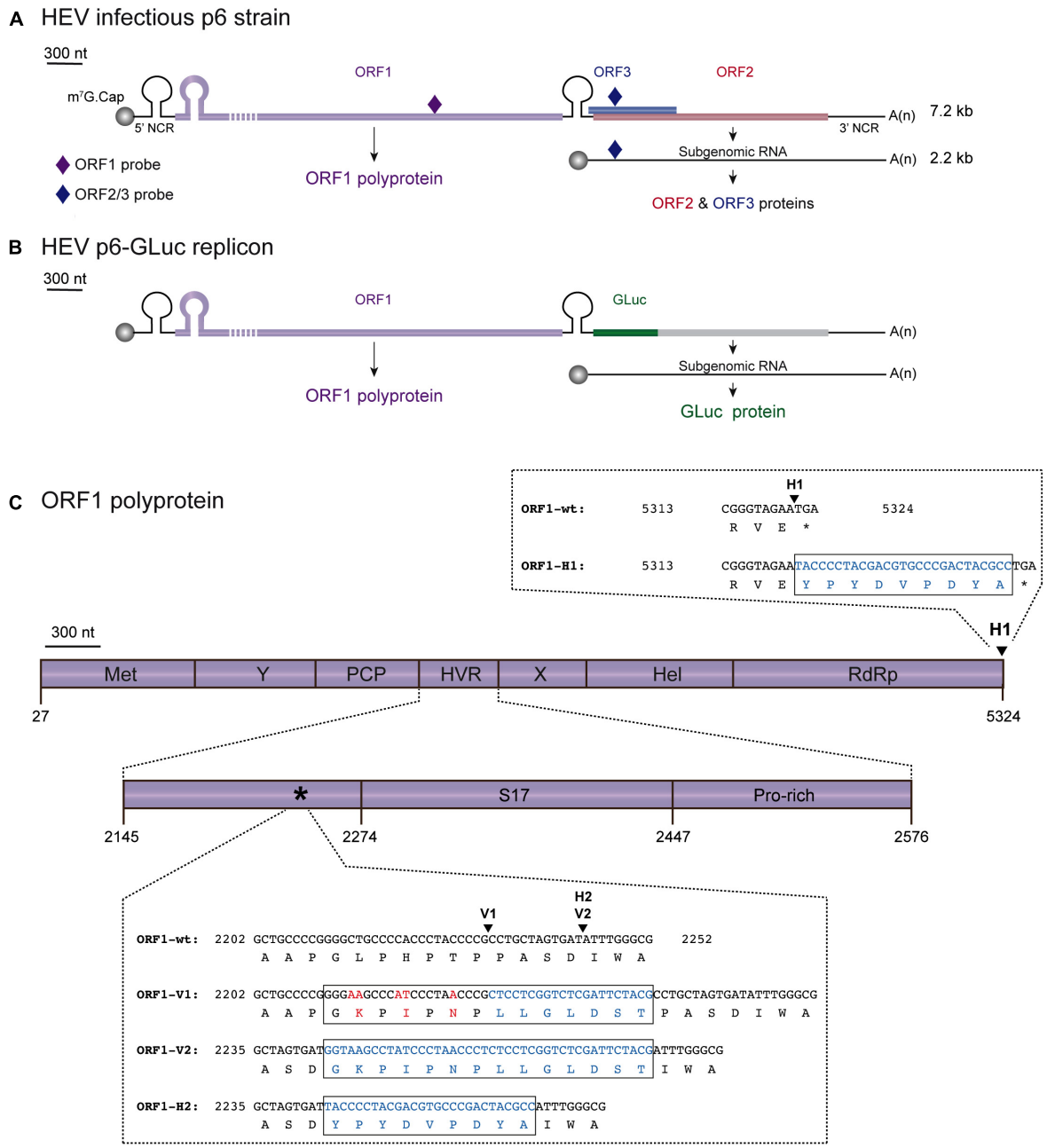

FIGURE 1 | Localization scheme of epitope tag insertions within the ORF1 polyprotein of HEV. **(A)** Scheme of the HEV Kernow C-1 p6 (GenBank accession number JQ679013) genome and encoded proteins. The full-length HEV genome (7.2 kb) is composed of 5′ and 3′ non coding regions (NCR) as well as three open reading frames: ORF1 (purple) encoding the HEV replicase, ORF2 (red) and ORF3 (blue) encoding the capsid and a small phosphoprotein, respectively. The HEV subgenomic RNA of 2.2 kb is depicted as a thin black line. The probes used in RT-qPCR experiments are located as small colored rhombus: ORF1-specific probe (dark purple) and ORF2/ORF3-specific probe (dark blue). The full-length of the ORF1 protein cannot be represented at the scheme scale (purple dashed lines). **(B)** Scheme of the HEV p6-GLuc replicon genome and encoded proteins. The *Gaussia* luciferase (GLuc, green) replaces the ORF3 and the N-terminus of ORF2 in the HEV p6-GLuc replicon. **(C)** The ORF1 is enlarged and its functional domains are designated as methyltransferase (MeT), Y domain (Y), papain-like cysteine protease (PCP), hypervariable region (HVR), macro- or X-domain (X), helicase (Hel), RNA-dependent RNA polymerase (RdRp). Insertion position of an HA epitope at the C-terminus of ORF1 is localized (H1, arrowhead). C-terminal nucleotide and aa sequences of RdRp are detailed for the ORF1 untagged wildtype (ORF1-wt) and HA-tagged (ORF1-H1) proteins with inserted epitope sequence highlighted in blue (box). A focus on the HVR enables to locate the human S17 ribosomal protein insertion (S17) of the HEV Kernow C-1 p6 strain and the prolin-rich region (Pro-rich). An asterisk points at the 2,202–2,252 region whose nucleotide and aa sequences are detailed (box). Two other sites of insertion of V5 or HA epitopes are shown (arrowheads): V1 and V2 for V5 epitope insertions and H2 for HA epitope insertion. Part of the HVR sequences of the wild-type (ORF1-wt) as well as the epitope-tagged ORF1 are presented (ORF1-V1, ORF1-V2, ORF1-H2). Mutated nucleotides and aa residues are in red. Inserted nucleotides and aa residues are in blue.

replicon in which the ORF1 polymerase active site GDD was mutated to GAD to prevent any replication was used as a negative control (Emerson et al., 2013).

The plasmids pTM-ORF1, pTM-ORF3/2 and pTM empty vector were kindly provided by Dr. J. Gouttenoire from the University of Lausanne (Switzerland) and have been previously described (Lenggenhager et al., 2017). The pTM-ORF1 vector contains the full-length sequence of the ORF1 protein. The pTM empty vector, was used as a negative control.

Epitope Tag Insertions

The HA and V5 epitopes were inserted in three different positions of the ORF1 sequence (**Figure 1C**). According to the insertion position, the constructs harboring the HA epitope are named H1 or H2 and the constructs harboring the V5 epitope are named V1 or V2. The pBlueScript SK(+) harboring the p6-GLuc replicon was used as a template. Sequences of the primers used to make the tagged ORF1 constructs can be found in **Table 1**. Prior to the fusion PCR step, DNA fragments located upstream and downstream to the epitope insertion sites were amplified by PCR using the Q5® High-Fidelity 2× Master Mix (NEB) with relevant primers (**Table 1**) on a ProFlex PCR system (Life Technologies). After purification, fragments were ligated by performing a fusion PCR. The fused fragments were amplified by another PCR using the relevant external primer pairs (**Table 1**). Next, pBlueScript SK(+) harboring the p6-GLuc / p6 genomes or pTM-ORF1 vectors and epitope-tagged inserts were restricted by the suitable restriction enzymes (**Table 1**) and subsequently ligated using the T4 DNA ligase (NEB). Finally, *E. coli* (strain TOP10) were transformed with the ligated plasmid, selected clones were grown overnight at 37°C under agitation and the plasmid DNA was extracted and purified using the NucleoSpin plasmid Mini or Midi kit (Macherey-Nagel).

Capped mRNA Synthesis

First, the plasmid DNA of p6-GLuc and p6 constructs were linearized using the MluI restriction enzyme (NEB). Next, the DNA was mixed with sodium acetate (3 M, pH 5.5) and chloroform /isoamyl alcohol (96v / 4v) and centrifuged at 14,000 rpm for 4 min. Following precipitation with

TABLE 1 | Sequences of primers and probes used to make the epitope tagged-ORF1 constructs and to quantify the genomic and subgenomic HEV RNAs by RT-qPCR.

Primer/probe name	Primer/probe sequence (5′- > 3′)	Restriction enzyme / epitope / reference
H1-Up-F-ext	GTCATGCATGGTATTTGAAAATGACTTTTCGG	NsiI
H1-Up-R-int	**GGCGTAGTCGGGCACGTCGTAGGGGTA**TTCTACCCGCTGTATGATGGAATTTG	HA
H1-Do-F-int	**TACCCCTACGACGTGCCCGACTACGCC**TGAATAACATGTTTGTTGCATCGCCC	HA
H1-Do-R-ext	TGGTCGCGAAGTTGCTGGCCACGGCC	NruI
H2-Up-F-ext	GCGATATCCAAGGGCATGCGCCGGTTG	EcoRV
H2-Up-R-int	**GGCGTAGTCGGGCACGTCGTAGGGGTA**ATCACTAGCAGGCGGGGTAGGG	HA
H2-Do-F-int	**TACCCCTACGACGTGCCCGACTACGCC**ATTTGGGCGTTACCACCGCCCTCCG	HA
H2-V1-V2-Do-R-ext	TGCATATGTAGCAGCAACAGGTG	NdeI
V1-F-ext	GAGGCGGCCGCCCCTGCTTCGGCTGCTGCCCCG**GGGAAGCCCATCCCTAACCCGCTCCT CGGTCTCGATTCTACG**CCTGCTAGTGATATTTGGGCG	NotI / V5
V2-Up-F-ext	AGGCGGCCGCCCCTGC	NotI
V2-Up-R-int	**CGTAGAATCGAGACCGAGGAGAGGGTTAGGGATAGGCTTACC**ATCACTAGCAGGCGGG GTAGGG	V5
V2-Do-F-int	**GGTAAGCCTATCCCTAACCCTCTCCTCGGTCTCGATTCTACG**ATTTGGGCGTTACCACC GCCCTCCG	V5
RT-qPCR—Fwd ORF1 primer	AAGACATTCTGCGCTTTGTT	Yin et al., 2017
RT-qPCR—Rev ORF1 primer	TGACTCCTCATAAGCATCGC	Yin et al., 2017
RT-qPCR—ORF1 probe	CCGTGGTTCCGTGCCATTGA	Yin et al., 2017
RT-qPCR—Fwd ORF2 primer	GGTGGTTTCTGGGGTGAC	Jothikumar et al., 2006
RT-qPCR—Rev ORF2 primer	AGGGGTTGGTTGGATGAA	Jothikumar et al., 2006
RT-qPCR—ORF2 probe	TGATTCTCAGCCCTTCGC	Jothikumar et al., 2006
RT-qPCR—Fwd GLuc primer	TCTGTGTGTGGACTGCACAA	Ding et al., 2018, this study
RT-qPCR—Rev GLuc primer	TGGATCTTGCTGGCAAAGGT	Ding et al., 2018, this study
RT-qPCR—GLuc probe	GGCTTGCCAACGTGCAGTGT	Ding et al., 2018, this study

Each primer is named according to (i) the epitope insertion site (H1, H2, V1 or V2), (ii) upstream (Up) or downstream (Do) fragment, (iii) forward (F) or reverse (R) sense and (iv) external (ext) or internal (int) position.
First, upstream and downstream fragments are amplified separately for each construct (i.e., for p6-H1-GLuc: upstream fragment amplified using H1-Up-F-ext / H1-Up-R-int and downstream fragment amplified using H1-Do-F-int / H1-Do-R-ext).
Second, upstream and downstream fragments are fused thanks to the overlapping region.
Third, the whole fragment containing the epitope is amplified using external primers (i.e., for p6-H1-GLuc: H1-Up-F-ext / H1-Do-R-ext).
Note that the same primer H2-V1-V2-Do-R-ext was used for p6-H2-GLuc, p6-V1-GLuc and p6-V2-GLuc constructs.
The p6-V1-GLuc construct was made using a single round of amplification and one primer pair: V1-F-ext / H2-V1-V2-Do-R-ext.
Restriction sites are underlined in external primers.
HA or V5 epitope sequence is highlighted in bold.
Primers and probes used in RT-qPCR are listed.
Fwd, forward; Rev, reverse.

absolute ethanol, the DNA was washed twice with 70% ethanol, dried and suspended in RNase free water. The capped mRNAs were synthetized by *in-vitro* transcription of the MluI-linearized DNA according to the mMESSAGE mMACHINE kit (Ambion) procedure and stored at −80°C before electroporation in PLC3 cells.

Cell Culture and Transfection

PLC3 cells are a subclone of the PLC/PRF/5 (CRL-8024) hepatoma cells and were characterized as highly replicative and productive cell line for HEV (Montpellier et al., 2018). PLC3 cells were cultured in Dulbecco's modified Eagle's medium (DMEM, ThermoFisher Scientific) containing 10% inactivated fetal calf serum and 1% non-essential aa (ThermoFisher Scientific, DMEM complete).

Capped mRNA of either luciferase p6 replicons (p6-wt-GLuc, p6-GAD-GLuc mutant replicons and HA- or V5-ORF1-tagged p6-GLuc replicons, named as p6-H1-GLuc, p6-H2-Gluc, p6-V1-GLuc and p6-V2-GLuc) or p6 infectious strains (p6-wt and V5-tagged ORF1 p6 constructs named as p6-V1 and p6-V2) were electroporated in PLC3 cells as follows. After trypsinization, cells were suspended in DMEM complete medium and washed twice in Opti-MEM medium (ThermoFisher Scientific). Three million cells were electroporated with 10 μg of RNA and suspended in DMEM complete medium.

Huh-7.5 cells (RRID:CVCL_7927) are hepatoma cells derived from Huh-7 cells (Blight et al., 2002). They were grown and electroporated with the luciferase p6 replicons as described above.

Electroporated PLC3 or Huh-7.5 cells were treated with the HEV-replication inhibitor sofosbuvir (Selleck Chemicals) at 20 μM final concentration as previously published (DaoThi et al., 2016; Farhat et al., 2018).

Huh-7-derived H7-T7-IZ cells (Romero-Brey et al., 2012) stably expressing the T7 RNA polymerase were kindly provided by Dr. R. Bartenschlager (University of Heidelberg, Germany). H7-T7-IZ cells were maintained in a DMEM completed medium supplemented with 50 μg/ml of Zeocin (InvivoGen) and used for transfection of the T7 promoter-driven pTM expression vectors. The pTM plasmids were transfected into H7-T7-IZ cells using TransIT®-LT1 Transfection Reagent (Mirus Bio LLC) following the manufacturer's recommendations with a ratio ADN to transfection reagent of 1 to 3.

PLC3 cells were authenticated by STR profiling (Multiplexion). Huh-7.5 and H7-T7-IZ cells were authenticated by Multiplex Cell Authentication (Multiplexion).

Luciferase Assay

The electroporated cells were seeded in 24-well plates (80,000 cells/well) and incubated for 5 days at 37°C and 5% CO_2. The supernatants were sampled at 1, 3, 4 and 5 days post-electroporation (dpe) and stored at −20°C until luminometer reading.

The supernatants were centrifuged at 14,000 rpm for 5 min and next, the samples were diluted 1:100 in 1× passive lysis buffer (Promega) and 5 μl were transferred into a white Nunc 96-well plate. At 1 s after injection of 20 μl of the substrate solution (Renilla Luciferase Assay System, Promega), relative light units (RLUs) were acquired on a Centro XS^3 LB 960 luminometer (Berthold Technologies) during 10 s.

Quantification of Viral RNA

After electroporation of PLC3 cells with the p6 luciferase replicons or the infectious p6 strains, total RNA was extracted from cellular supernatants (QIAamp Viral RNA Mini kit, Qiagen) or cells (NucleoSpin RNA plus kit, Macherey-Nagel) at different time post-electroporation (4 hpe–7 dpe). The RNA was next converted to cDNA by using a polydT primer and following the AffinityScript Multiple Temperature cDNA Synthesis kit instructions (Agilent Technologies). In order to quantify the HEV genome, a standard curve was prepared by diluting the *in vitro*-transcribed HEV p6 plasmid in total RNA extracted from mock electroporated PLC3 cells. For the quantification of intra- and extra-cellular HEV RNA, primers and probes were designed against genomic and subgenomic RNAs according to previously published literature (**Table 1**; Jothikumar et al., 2006; Yin et al., 2017; Ding et al., 2018). The viral RNA copy numbers were quantified by qPCR (TaqMan Gene Expression Assay, MGB-FAM-dye, ThermoFisher Scientific) using the QuantStudio3 Thermocycler (Applied Biosystems).

Cell Lysis, Subcellular Fractionation and Immunoblotting

The cells were lysed in B1 buffer (100 mM NaCl, 2 mM EDTA, 1% Triton-X100, 50 mM Tris–HCl, 0.1% SDS) including 1 mM PMSF and 1 × protease inhibitors (cOmplete™ protease inhibitor cocktail, Roche) and stored at −20°C in 1 × Laemmli buffer until usage. Subcellular fractionation was performed using the subcellular protein fractionation kit for cultured cells following the supplier instructions (ThermoFisher Scientific).

The non-infectious samples were heated at 70°C for 10 min while the infectious samples were inactivated at 80°C for 20 min. Samples were then loaded on an 8% SDS-PAGE gel and then transferred onto a nitrocellulose membrane (Hybond-ECL, Amersham). The membrane was incubated in blocking buffer (1 × PBS with 5% milk and 0.2% Tween-20) for 1 h at RT under constant shaking. The primary antibody (**Table 2**) was incubated overnight at 4°C under constant shaking in 1 × PBS containing 0.2% Tween-20 and 2% BSA. The membrane was washed three times with a solution of 1 × PBS and 0.2% Tween-20, which was followed by an incubation with a suited peroxidase-conjugated secondary antibody in blocking buffer for 45 min at RT. The membrane was washed again three times. Finally, the proteins were detected by chemiluminescence using the Pierce ECL Western Blotting Substrate (Life Technologies) and a developer.

Infectious Titers

After electroporation of PLC3 cells with p6-wt, p6-V1 or p6-V2 RNA or PBS, 1 × 10^6 cells were seeded into T-75 flasks in DMEM complete medium. Eight hours after seeding, the medium was changed to HEV medium: DMEM/M199 (1v:1v),

TABLE 2 | List of primary antibodies used in this study.

Name	Target / epitope	Host species / isotype / clonality*	Supplier / reference	Antibody registry number	Dilution used in IF	Dilution used in IB/IP
V5	GKPIPNPLLGLDST	Mouse IgG2a	Abcam	AB_471093	1:500	n/a
V5	GKPIPNPLLGLDST	Mouse IgG2a	Invitrogen	AB_2792973	n/a	1:1000
V5	GKPIPNPLLGLDST	Goat Polyclonal	Abcam	AB_307037	n/a	IP**
HA	YPYDVPDYA	Rat IgG1	Roche	AB_2687407	1:250	1:1000
HEV ORF2 (1E6)	GDSRVVIQDYDNQHEQDRPTPSPA	Mouse IgG2b	Millipore	AB_827236	1:800	1:1000
HEV ORF3	ANPPDHSAPLGVTRPSAPPLPHVVDLPQLGPRR	Rabbit Polyclonal	S. Emerson (Graff et al., 2005)	n/a	1:1000	n/a
CD63	Tetraspanin—Large extracellular loop	Mouse IgG1	BD Pharmingen	AB_396297	1:100	n/a
CD71	Transferrin receptor	Mouse IgG1	Santa Cruz	AB_1120670	1:100	n/a
CD81	Tetraspanin—Large extracellular loop	Mouse IgG1	S. Levy (Oren et al., 1990)	AB_627192	1:100	n/a
Rab11	Rab11	Rabbit (D4F5)	Cell Signaling	AB_10693925	1:100	n/a
MICAL-L1	Molecule Interacting with CasL-like1	Rabbit Polyclonal	Abcam	n/a	1:100	n/a
EHD1	Eps15 homology domain protein 1	Rabbit Polyclonal	Abcam	AB_10864800	1:1000	n/a
PACSIN2	Protein Kinase C and Casein Kinase Substrate in Neurons 2	Rabbit Polyclonal	MyBiosource	n/a	1:1000	n/a
γ-Tubulin	γ-Tubulin N-terminal region	Mouse IgG1	Sigma-Aldrich	AB_532292	n/a	1:4000
Lamin B1	Nuclear envelope marker	Rabbit Polyclonal	Abcam	AB_443298	n/a	1:1000
SP-1	Human Specificity Protein 1 (aa 18–303)—soluble nuclear fraction marker	Rabbit Polyclonal	Thermofisher	AB_2546641	n/a	1:2000
Calnexin	Human Calnexin—ER membrane marker	Rabbit Polyclonal	Abcam	AB_2069006	n/a	1:1000

**When clonality is not mentioned, the antibody is monoclonal.*
***The antibody quantity used in immunoprecipitation is given in the Materials and Methods section.*
IF, immunofluorescence; IB, immunoblot; IP, immunoprecipitation; n/a, non-applicable.

1 mg/ml of lipid-rich albumin (AlbuMAX^{TM} I Lipid-rich BSA, ThermoFisher Scientific), 1% non-essential aa and 1% pyruvate sodium (ThermoFisher Scientific). Then, the HEV producing cells were incubated at 32°C and 5% CO_2 for 10 days.

Next, Huh-7.5 cells seeded into coated 96-well plates (8,000 cells/well) were infected with undiluted and serially diluted supernatants from HEV-producing cells. The inoculum was removed after 8 h and cells were overlaid with fresh medium. Three days post-infection at 37°C and 5% CO_2, cells were fixed and processed for indirect immunofluorescence with anti-ORF2 antibody 1E6 (Millipore). For confocal microscopy analysis, Huh-7.5 cells were seeded on glass coverslips in 24-well plates and infected with 500 μl of undiluted infectious cell supernatant.

Indirect Immunofluorescence

Cells were first fixed with 3% paraformaldehyde for 20 min, washed three times with 1 × PBS, then permeabilized for 5 min with cold methanol and subsequently with 0.5% Triton X-100 for 30 min. Cells were incubated with 10% goat serum diluted in 1 × PBS for 30 min at RT and then stained with primary antibodies (**Table 2**) for 30 min at RT followed by three washes with 1 × PBS and then incubated with a suited secondary antibodies for 20 min at RT. DAPI (4′,6-diamidino-2-phenylindole, 1:500) was used to stain the nuclei. Finally, coverslips were mounted with Mowiol®4–88 (Calbiochem) on glass slides. Cells were analyzed using an LSM880 confocal laser-scanning microscope (Zeiss) using a ×63/1.4 numerical aperture oil immersion lens. The images were next processed using the ImageJ and Fiji softwares.

Colocalization studies were performed by calculating the Pearson's Correlation Coefficient (PCC) using the JACoP plugin of ImageJ and Fiji softwares. The PCC examines the relationship between the intensities of pixels from two channels in the same image. Twenty-to-thirty whole cells or regions of interest (ROI) were analyzed to calculate the PCC mean. A PCC of 1 indicates perfect correlation, 0 no correlation, and −1 a perfect anti-correlation.

Immunoprecipitations

Immunoprecipitations (IP) were performed with cell lysates of either electroporated PLC3 cells (3 dpe) or transfected H7-T7-IZ cells (1 dpt). Protein G sepharose beads (GE Healthcare, 40 μl per IP) were equilibrated in B1 lysis buffer by washing and centrifuging them at 6,000 rpm at 4°C. The beads were then incubated with the anti-V5 goat polyclonal antibody (Abcam, 1 μg of anti-V5 per mg of total proteins) in B1 buffer overnight at 4°C on a spinning wheel. The cell lysates were pre-cleared with 40 μl of beads without specific antibodies for 30 min on a spinning wheel. Next, the pre-cleared cell lysates were added to the antibody-bound beads for 2 h at RT. After this, the beads were washed six times with 1 × PBS containing 0.5% NP-40. The samples were heated for 10 min at 70°C or inactivated at 80°C for 20 min and loaded on an 8% SDS-PAGE gel.

Mass Spectrometry Analysis

Proteins were resolved by SDS-PAGE. Colloïdal blue stained bands corresponding to ORF1 proteins in WB were cut for

in-gel digestion with trypsin. NanoLC-MS/MS analyses of the protein digests were performed on an UltiMate-3000 RSLCnano System coupled to a Q-Exactive instrument (Thermo Fisher Scientific), as previously described (Montpellier et al., 2018). Collected raw data were processed and converted into *.mgf peak list format with Proteome Discoverer 1.4 (Thermo Fisher Scientific). MS/MS data were interpreted using search engine Mascot (version 2.4.0, Matrix Science) with a tolerance on mass measurement of 0.2 Da for precursor and 0.2 Da for fragment ions, against a composite target decoy database (40,584 total entries) built with Swissprot *Homo sapiens* database (TaxID = 9,606, 20 May 2016, 20,209 entries) fused with the sequences of ORF1 (p6_AFD33683) and a list of classical contaminants (119 entries). Carbamidomethylation of cysteine residues, oxidation of methionine residues, protein N-terminal acetylation and propionamidation of cysteine residues were searched as variable modifications. Up to one trypsin missed cleavage was allowed. Semi-specific cleavage was also authorized.

In situ Labeling of Viral RNA

The RNAscope® is a branched DNA *in situ* hybridization technology that specifically and sensitively detects RNA in fixed cells or tissues. First, three pools of dual Z-shaped probes of 18–25 nucleotides were designed against the HEV genomic and subgenomic RNAs (Advanced Cell Diagnostics Bio-Techne, ACD Bio, **Figure 8A**). Two probes need to bind next to each other to produce a specific signal. Each target probe set contains a pool of 20 oligo ZZ pairs.

PLC3 cells electroporated with p6-wt or p6-V1 infectious strains were fixed in 3% PFA for 20 min. Coverslips holding the fixed cells were attached to glass slides with a drop of nail polish and hydrophobic barriers were drawn around them with the ImmEdge Hydrophobic Barrier Pen (ACD Bio). Next, fixed cells were pre-treated according to the supplier instructions (RNAscope® H_2O_2 and Protease Reagents). First, the cells were treated with H_2O_2 for 10 min at RT and then washed twice with 1 × PBS. Next, the protease III was diluted 1:15 and incubated for 15 min at RT; slides were washed twice. Then, the RNAscope assay was carried out following the user manual precisely (RNAscope Detection Kit Multiplex Fluorescent Reagent Kit v2 (Wang et al., 2012; Liu et al., 2019). The positive and negative strand of genomic viral RNAs were targeted by probe A (ref. 1030631-C2, ACD Bio) and probe B (ref. 579841-C3, ACD Bio), respectively (**Figure 8A**). Probe C (ref. 586651-C1, ACD Bio) targeted the positive strand of subgenomic RNA (**Figure 8A**). The RNAs were labeled using the Opal 520, Opal 570 and Opal 650 as fluorophores (Akoya Biosciences). Subsequently, immunofluorescent labeling using either the anti-V5, 1E6 or anti-ORF3 antibodies could be performed (**Table 2**). Finally, coverslips were mounted and cells were analyzed by confocal microscopy as mentioned above.

Statistical Analysis

Mann–Whitney statistical tests were performed with R version 3.6.1. Any test with a p value < 0.05 is declared as significant.

RESULTS

Insertion of Epitope Tags in the ORF1 Polyprotein of Hepatitis E Virus

Since there is no commercial antibody that recognizes the ORF1 protein in HEV-replicating cells, we first sought to insert epitope tags in the ORF1 sequence in a way to preserve the HEV replication and to allow the characterization of the HEV replicase. We aligned 44 aa sequences from different HEV genotypes to identify variable regions which are generally more prone to accept epitope insertions without impacting viral replication. Indeed, the HVR stood out as the region with the highest divergence of the entire HEV genome, thus confirming previous reports (Muñoz-Chimeno et al., 2020). Focusing on the HVR, we next aligned several epitope aa sequences with that of HEV in an aim to identify similar aa and to ease epitope insertion with the least disruption. Such a location highly similar to the V5 epitope aa sequence was found in the HVR (**Figure 1C**). While 4 aa residues remained unchanged (G729, P731, P733, P735), 3 were mutated (L730K, H732I, T734N) and 7 were inserted to generate the full V5 epitope (V1, **Figure 1C**). In a second approach, we took advantage of the report by Nguyen et al. (2012) to insert a V5 and a HA epitope tags at position 2,143 (V2, H2, **Figure 1C**; Nguyen et al., 2012). These authors isolated a HEV gt3 strain from a chronically infected patient in which the human S19 ribosomal coding sequence was inserted at that corresponding position and led to a HEV replication advantage in cell culture (Nguyen et al., 2012). Finally, a HA tag was also introduced at the C-terminus of the RdRp, since avoiding an insertion within the ORF1 protein was supposed to maintain viral replication (H1, **Figure 1C**).

Replication of HEV p6 Replicons Expressing Epitope-Tagged ORF1

To evaluate whether epitope insertions modify the replication efficacies, we made use of the HEV *Gaussia* luciferase replicon (GLuc) in which the *GLuc* reporter gene is transcribed by the ORF1 viral replicase (**Figure 1B**; Shukla et al., 2012; Emerson et al., 2013). The luciferase, secreted in cell supernatants, is used as a readout of ORF1 replication efficacy. To measure the impact of V5 and HA epitope insertion on HEV replication, we electroporated the *GLuc* replicons expressing wt ORF1 (p6-wt-GLuc), polymerase-inactivated GAD mutant (p6-GAD-GLuc), HA-tagged ORF1 (p6-H1-GLuc, p6-H2-GLuc) or V5-tagged ORF1 (p6-V1-GLuc, p6-V2-GLuc) in PLC3 and Huh-7.5 cells, which have been described as efficient HEV cell culture systems (Farhat et al., 2018; Montpellier et al., 2018). The replication efficacies were analyzed over a course of 5 days post-electroporation (dpe) and replication folds (normalized to 1 dpe) were compared (**Figures 2A,B**). The p6-H1-GLuc and p6-H2-GLuc replicons, respectively, showed a 95 and 80% reduction of replication efficacies at 5 dpe, as compared to the p6-wt-GLuc replicon in PLC3 cells. In Huh-7.5 cells, the replications efficacies of both constructs were also drastically reduced (97 and 76% reduction for p6-H1-GLuc and p6-H2-GLuc, respectively). Due to poor replication efficacies, these constructs were not further characterized. In contrast, the replication kinetics of the

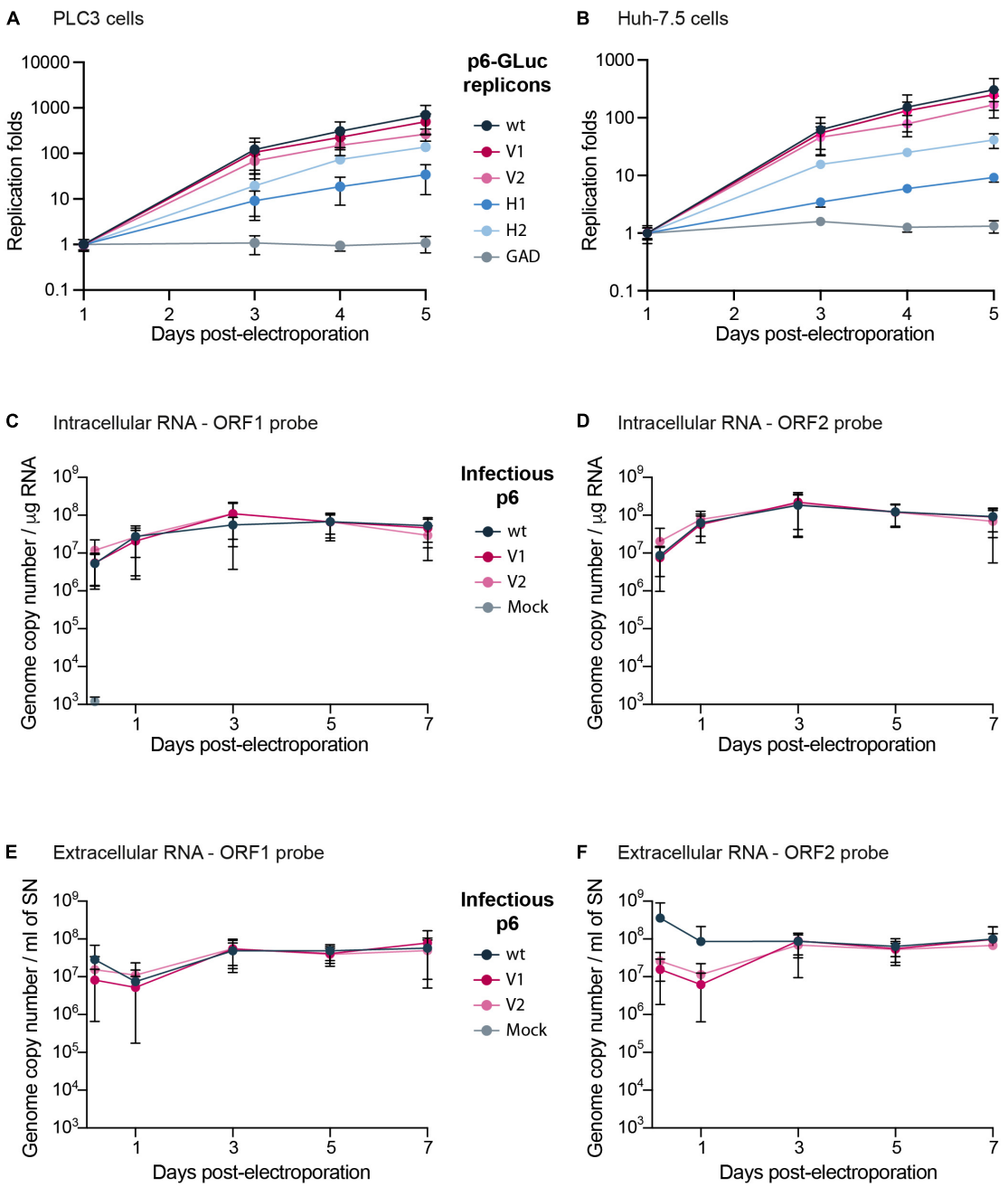

FIGURE 2 | Replication efficacies of HEV p6 replicons and infectious strain expressing epitope-tagged ORF1. **(A,B)** Replication efficacies of HEV replicons expressing tagged ORF1 in PLC3 **(A)** and Huh-7.5 cells **(B)** as measured by luciferase activity. The relative light units (RLU) were measured everyday for 5 days post-electroporation (dpe) by quantification of the *Gaussia* luciferase in the cell supernatants using a luminometer. Replication fold increases of the tagged p6-GLuc replicons (V1, V2, H1, H2) and non-tagged p6-GLuc replicons (wt, GAD) were normalized to 1 dpe. The p6-GAD-GLuc is a non-replicative construct that possesses a mutation from GDD to GAD which inactivates the ORF1 polymerase. Experiments were conducted three times with three technical replicates. **(C–F)** HEV RNA quantification in p6 electroporated-PLC3 cells expressing wild type or epitope-tagged ORF1. Intracellular **(C,D)** and extracellular **(E,F)** viral RNAs were quantified at 4 h post-electroporation (hpe), 1, 3, 5, and 7 dpe by RT-qPCR targeting either ORF1 **(C,E)** or ORF2 **(D,F)**. Mock-electroporated cells were used as negative controls and fluorescence signal was at or below the detection limit. Experiments were conducted three times with two technical replicates.

p6-V1-GLuc and p6-V2-GLuc replicons were similar to that of p6-wt-GLuc, in both PLC3 and Huh-7.5 cell lines (**Figures 2A,B**). Thus, the V5 epitope insertions at the selected positions in the ORF1 HVR do not alter HEV replication.

Of note, in the presence of sofosbuvir (20 μM), a nucleotide analog that efficiently inhibits HCV and HEV polymerases (DaoThi et al., 2016; Farhat et al., 2018), the replication efficacies of all replicons were inhibited at 5 dpe by 76 to 87% in

PLC3 cells and by 73 to 92% in Huh-7.5 cells (**Supplementary Figures 1A,B**). These results indicate that the insertion of epitope tags in the ORF1 does not affect the sofosbuvir efficacy to inhibit HEV replication.

Replication of HEV Infectious Genome Expressing Epitope-Tagged ORF1

The V5 epitope was next introduced into the p6 infectious full-length genome at two positions, leading to the p6-V1 and p6-V2 constructs (**Figure 1C**). Intra- and extracellular HEV RNA levels were measured from 4 h post-electroporation (4 hpe) to 7 dpe, by RT-qPCR using probes against the genomic RNA (ORF1 probe, **Figure 1A** and **Table 1**) or the genomic and subgenomic RNAs (ORF2 probe, **Figure 1A** and **Table 1**). The intracellular RNA levels increased rapidly for p6-V1 and p6-V2 constructs within 1 dpe to reach approximately 1×10^8 copies / μg RNA (ORF1 probe, **Figure 2C**) and 2×10^8 copies / μg RNA (ORF2 probe, **Figure 2D**) at 3 dpe. Then, the RNA levels decreased slightly but remained above 3×10^7 (ORF1 probe, **Figure 2C**) and 7×10^7 (ORF2 probe, **Figure 2D**) copies / μg RNA at 7 dpe. The intracellular RNA copy numbers of the p6-V1 and p6-V2 constructs followed similar kinetics to that of p6-wt from 4 hpe to 7 dpe. In the cell supernatants, all RNA copy numbers decreased during the first day, then increased to reach a level of 5.5×10^7 (ORF1 probe, **Figure 2E**) and 9×10^7 (ORF2 probe, **Figure 2F**) copies / ml at 3 dpe and remained constant toward the end of the experiment. The RNA levels measured for the p6-V1 and p6-V2 constructs in the cell supernatants were comparable to the p6-wt RNA level evolution. Moreover, to check whether ORF2 expression from subgenomic RNA was not altered, PLC3 cells electroporated with the p6-V1 or p6-V2 constructs were processed for ORF2 immunofluorescence (**Supplementary Figure 1C**). V5-tagged-HEV-producing cells displayed an ORF2 fluorescent labeling similar to that of p6-wt-electroporated cells. Additionally, the expression of ORF2 was inhibited by sofosbuvir as a much lower fluorescent signal could be visualized in the treated electroporated cells compared to the non-treated cells (**Supplementary Figure 1C**). Taken together, these results indicate that the insertions of V5 epitopes at the selected positions in ORF1 HVR do not affect replication efficacy of the p6 genome in PLC3 cells.

Expression and Processing of the V5-Tagged Hepatitis E Virus Replicase

We next sought to analyze the expression and processing of the ORF1 polyprotein in HEV replicative systems. Since the ORF1 protein has been largely studied in heterologous expression systems, we compared the expression and maturation of V5-tagged ORF1 in replicative and heterologous systems. For this purpose, the V5-tagged ORF1 were cloned downstream of the T7 promoter into the pTM plasmid and expressed in H7-T7-IZ cells, as previously described (Lenggenhager et al., 2017).

First, the expression of the V5-tagged ORF1 was analyzed from 8 h (8 hpt) to 3 days post-transfection (3 dpt) in the H7-T7-IZ heterologous expression system. As early as 8 hpt, the ORF1 protein was detectable by anti-V5 immunoblot as a major band migrating above 180 kDa, a size that corresponds to the expected molecular weight of the full-length ORF1 (**Figure 3A**). This major band was present at every time points and was accompanied by several lower molecular weight bands of lesser intensity, ranging from 95 to 170 kDa, which may correspond to ORF1 cleavage products (**Figure 3A**, stars). Second, the expression kinetics of the V5-tagged ORF1 protein was monitored by immunoblot, from 4 hpe to 3 dpe, in PLC3 cells electroporated with the p6-wt-GLuc, p6-V1-GLuc and p6-V2-GLuc replicons (**Figure 3B**). As early as 4 hpe, a band of high signal intensity was detected above 180 kDa, which corresponds to the full-length ORF1 protein. Additionally, several bands of lower molecular weights (95 to 170 kDa) were also detected and may correspond to potential cleavage products of the ORF1 polyprotein. At 3 dpe, the overall smaller-size band pattern ranging from 95 to 170 kDa was comparable to the band profile observed at early time points. At last, the expression profiles of the V5-tagged ORF1 in PLC3 electroporated with the p6 infectious strains (p6-wt, p6-V1, p6-V2, **Figure 3C**) were compared to the profiles of ORF1 expressed in the replicon and heterologous systems (**Figures 3A,B**, respectively). Similarly, the most intense band was migrating above 180 kDa at every time points and smaller bands were identified between 95 and 180 kDa. The V5-tagged ORF1 expression signal was more intense at early time points (4 hpe–3 dpe) when compared to later time points (15 and 25 dpe, **Figure 3C**). The V5-tagged ORF1 expression level decreased but was still detectable at 15 and 25 dpe, as it was for the ORF2 capsid protein, thus showing that the HEV expressing a V5-tagged replicase is able to fulfill its infectious cycle in the long-term. Thus, the successful expression of ORF1 polyprotein allowed the detection of an abundant full-length protein but also of less abundant smaller size products in the three systems analyzed.

To exclude that the V5-tagged ORF1 minor bands were due to protein degradation, proteasome inhibition experiments were conducted (**Supplementary Figure 2**). Upon treatment with lactacystin (30 μM for 8 h), the V5-tagged ORF1 minor bands were still detectable in both H7-T7-IZ and PLC3 cells and their pattern remained unchanged. As a control, we probed for HSP70 protein that accumulated in the lactacystin-treated conditions, indicating that the proteasome inhibition was successful (Liao et al., 2006; Young and Heikkila, 2010). Thus, these minor ORF1 bands are likely not the result of proteasome degradation.

In an aim to identify these potential ORF1 cleavage products, V5-immunoprecipitations were set up from cell lysates produced from all three systems (**Figures 4A,B**). The pattern of the smaller-size ORF1 proteins differed from one expression system to another with some proteins migrating at the same size (**Figures 4A,B**, stars). Minor ORF1 bands appeared more numerous in the p6 infectious cell culture system than in other systems. As better ORF1 expression levels were achieved in both the heterologous and p6 cell culture systems, V5-immunoprecipitations were scaled up from these two systems and trypsin-digests of some ORF1 selected products were analyzed by nano-scale liquid chromatography coupled to tandem mass spectrometry (**Table 3**). The full-length V5-tagged ORF1 proteins, expressed in the heterologous and infectious p6 cell culture systems, were identified with 35 and 38% of

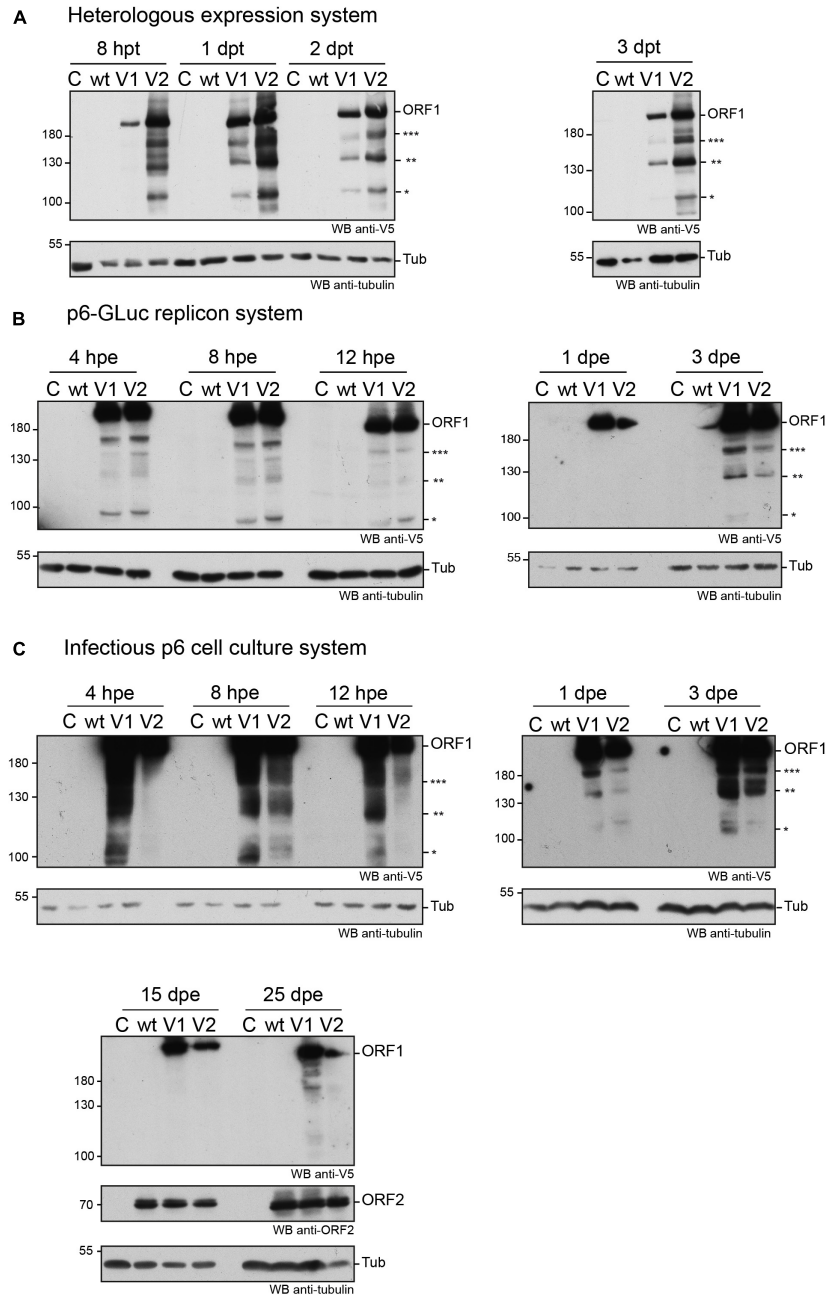

FIGURE 3 | Expression of the V5-tagged ORF1 protein over time in different cellular systems. **(A)** Heterologous expression of the HEV p6 ORF1 protein. H7-T7-IZ cells were transfected with a pTM plasmid expressing the wild type untagged ORF1 protein (wt) or the V5-tagged ORF1 (V1 or V2). The H7-T7-IZ cells constitutively express the T7 polymerase and the ORF1 gene lies under the control of a T7 promoter. Total cell lysates were collected in presence of protease inhibitors at 8 h post-transfection (hpt) and 1, 2, and 3 days post-transfection (dpt). Mock-transfected cells served as negative control (C). The band migrating higher than 180 kDa corresponds to the full-length ORF1 protein (ORF1). The immunoblot was probed either with an anti-V5 antibody or an anti-γ-tubulin antibody to control for even loading. Molecular weight markers are indicated in kilodaltons. Stars indicate lower molecular weight ORF1 products. **(B)** Expression of the ORF1 protein in the p6-GLuc replicon system. PLC3 cells were electroporated with a replicon expressing the wild type untagged ORF1 protein (wt) or the V5-tagged ORF1 (V1 or V2). Total cell lysates were collected in presence of protease inhibitors at 4, 8, and 12 hpe and 1 and 3 dpe. Mock-electroporated cells served as negative control (C). The band migrating higher than 180 kDa corresponds to the full-length ORF1 protein (ORF1). The immunoblot was probed either with an anti-V5 antibody or an anti-γ-tubulin antibody to control for even loading. Molecular weight markers are indicated in kilodaltons. Stars indicate lower molecular weight ORF1 products. **(C)** Expression of the ORF1 protein in the infectious p6 cell culture system. PLC3 cells were electroporated with *in vitro* transcribed genomic RNA of the p6 infectious strain expressing the wild type untagged ORF1 protein (wt) or the V5-tagged ORF1 (V1 or V2). Total cell lysates were collected in presence of protease inhibitors at 4, 8, 12 hpe and 1, 3, 15, 25 dpe. Mock-electroporated cells served as negative control (C). The band migrating higher than 180 kDa corresponds to the full-length ORF1 protein (ORF1). The immunoblot was probed either with an anti-V5 antibody or an anti-ORF2 (1E6) antibody or an anti-γ-tubulin antibody to control for even loading. Molecular weight markers are indicated in kilodaltons. Stars indicate lower molecular weight ORF1 products.

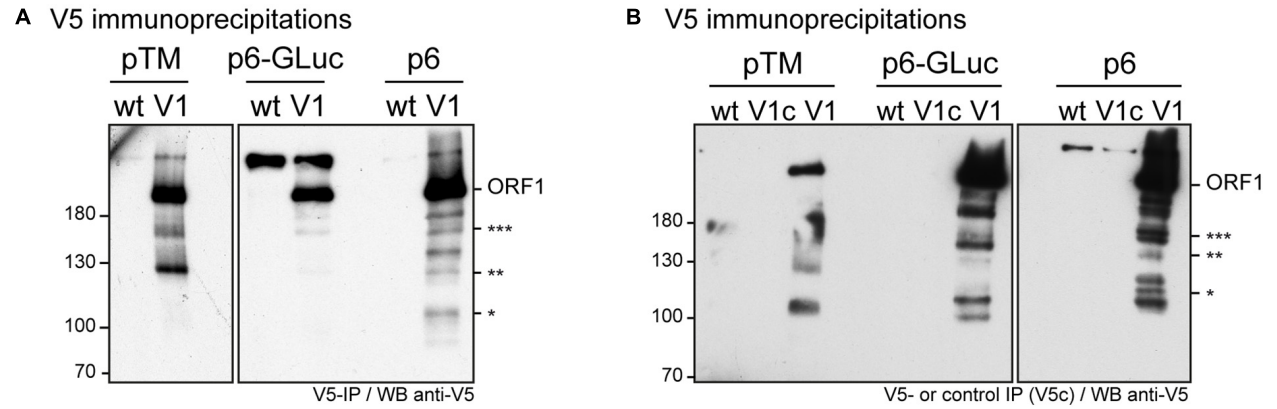

FIGURE 4 | Immunoprecipitation of the V5-tagged ORF1 protein expressed in different cellular systems. **(A)** HEV p6 ORF1 protein was heterologously expressed in H7-T7-IZ cells following transfection with the pTM plasmid carrying the untagged (wt) or V5-tagged (V1) construct (left panel). One dpt, total cell lysates were immunoprecipitated with the polyclonal goat anti-V5 antibody. HEV p6 protein was expressed in the replicon (p6-GLuc) and p6 cell culture (p6) systems (right panel). Three dpe, PLC3 cells lysates expressing either the untagged (wt) or the V5-tagged (V1) ORF1 proteins were immunoprecipitated using the polyclonal goat anti-V5 antibody. Immunoblots were revealed with a mouse anti-V5 monoclonal antibody. Molecular weight markers are indicated in kilodaltons. Stars indicate lower molecular weight ORF1 products. **(B)** In the same conditions as above, the control immunoprecipitations were conducted on the lysates expressing the V5-tagged ORF1 in all three systems using protein G sepharose beads without antibody (lanes V1c). The other lanes are labeled as in panel **(A)**. Molecular weight markers are indicated in kilodaltons. Stars indicate lower molecular weight ORF1 products.

peptide coverage, respectively. In spite of several attempts to reach sufficiently pure tagged-ORF1 protein in high-enough quantity, the peptide coverage of smaller size ORF1 proteins was not sufficient to identify any potential cleavage sites. Overall, the N-terminus of the V5-tagged ORF1 protein bands was better covered than the C-terminus, suggesting a limited processing at the polyprotein N-terminus especially in the heterologous system. Some higher molecular weight products (bands 8–10, **Table 3**), visible on the Coomassie-stained gel, but not detected by the V5 antibody, could correspond to ORF1 oligomers.

TABLE 3 | Mass spectrometry analysis.

Band number / construct	Coverage (%)	Number of identified spectra	N-term. identified peptides (NSI)	C-term. identified peptides (NSI)
1 / p6-V1	38	129	1–8 (2)	1,758–1,777 (1)
2 / p6-V1	32	87	41–53 (1)	1,720–1,734 (1)
3 / p6-V1	31	68	86–94 (1)	1,720–1,734 (1)
4 / p6-V1	32	83	41–53 (2)	1,695–1,706 (1)
5 / p6-V1	30	68	41–53 (1)	1,720–1,734 (1)
6 / p6-V1	20	48	41–53 (1)	1,651–1,662 (1)
7 / p6-V1	18	41	86–94 (2)	1,403–1,414 (1)
8 / ORF1-V1	39	125	41–53 (2)	1,720–1734 (1)
9 / ORF1-V1	55	321	1–8 (3)	1,758–1,777 (3)
10 / ORF1-V1	71	672	1–8 (4)	1,758–1,777 (7)
11 / ORF1-V1	35	195	1–8 (10)	1,405–1,419 (2)
12 / ORF1-V1	40	185	1–8 (2)	1,651–1,662 (1)
13 / ORF1-V1	31	102	1–8 (2)	1,695–1,706 (1)
14 / ORF1-V1	19	75	1–8 (2)	1,651–1,662 (1)
15 / ORF1-V1	17	63	1–8 (2)	1,390–1,398 (1)
16 / ORF1-V1	17	66	1–8 (2)	1,390–1,398 (1)

The full-length ORF1-V1 of the p6 Kernow C-1 strain is 1,779 aa in length.
Bands 8–10 were visible on the colloidal blue stained gel but were not detected by the V5 antibody.
NSI, number of spectrums identifying peptide.
Peptides identified only once with a score lower than 25 were not taken into account.

We next performed subcellular fractionation of V5-tagged ORF1 expressing cells (**Figures 5A,B**). The V5-tagged ORF1 full-length protein (>180 kDa) was detected by immunoblot in the soluble and membranous cytoplasmic fractions (Cs, Cm) as well as in the nuclear soluble fraction (Ns) and the nuclear envelope fraction (Ne) of p6-GLuc and p6 expression systems. The nuclear chromatin-bound fraction (Nc) only displayed a weak V5 signal in both expression systems. Also, smaller bands, migrating between 100 and 180 kDa (already detected in **Figure 3**), that could correspond to potential cleavage products of the ORF1 polyprotein, were detected in all fractions except in the Nc fraction. Notably, a subtle change in the band pattern was visible in the V5-tagged ORF1 expressed in PLC3 electroporated with the p6-V1: a signal was detected at 160 kDa in the Ns and Ne fractions (**Figure 5B**, three stars). This band was not detected either the Cs or the Cm fractions. Together, these results suggest that the ORF1 protein is likely partitioned in different cell compartments.

V5-Tagged Hepatitis E Virus p6 Remains Infectious in Cell Culture

We also determined the impact of V5 insertions on HEV infectivity. Huh-7.5 cells were infected with the supernatant of PLC3 cells that were electroporated with p6-wt, p6-V1 or p6-V2 RNAs (**Figure 6**). Three days post-infection, Huh-7.5 cells were processed for anti-ORF2 indirect immunofluorescence. ORF2-positive cells were counted and each positive cell focus was considered as one focus forming unit (FFU). When compared to the p6-wt, p6-V1 and p6-V2 strains produced infectious

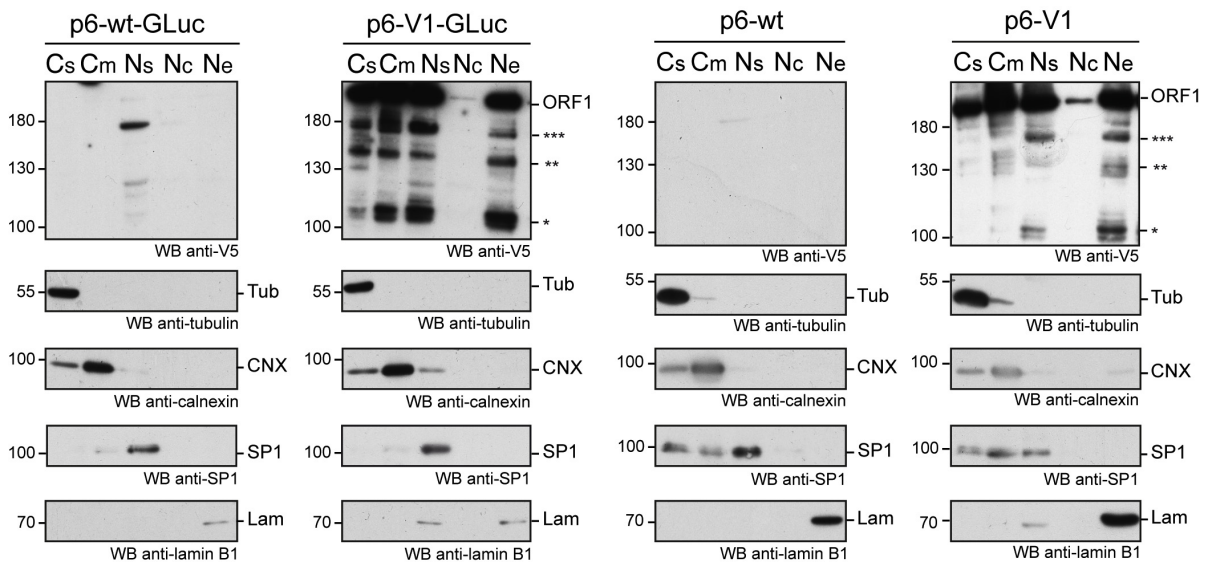

FIGURE 5 | The ORF1 protein is expressed in different cellular compartments. **(A)** PLC3 cells were electroporated with the p6-GLuc replicons expressing the non-tagged wildtype ORF1 (p6-wt-GLuc), and the V5-tagged ORF1 (p6-V1-GLuc). Three dpe, cells were collected and cellular fractions were separated as follows: Cs, cytoplasmic soluble fraction; Cm, cytoplasmic membranous fraction; Ns, nuclear soluble fraction; Nc, nuclear chromatin-bound fraction; Ne, Nuclear envelope. Immunoblots were probed with a mouse monoclonal antibody directed against the V5 epitope. Other antibodies were used to monitor for fraction enrichment: anti-γ-tubulin as a marker of the cytoplasmic soluble fraction, anti-calnexin as a marker of cytoplasmic membranous fraction, anti-SP1 as a marker of nuclear soluble fraction and anti-lamin B1 as a marker of nuclear envelope. Molecular weight markers are indicated in kilodaltons. Stars indicate lower molecular weight ORF1 products. **(B)** PLC3 cells were electroporated with the p6 expressing the non-tagged wildtype ORF1 (p6-wt), and the V5-tagged ORF1 (p6-V1). Four hpe, cells were collected and cellular fractions were separated and named as above. The above-mentioned antibodies were used to reveal the immunoblots. Molecular weight markers are indicated in kilodaltons. Stars indicate lower molecular weight ORF1 products.

titers that were not significantly different (**Figure 6A**, respective Mann–Whitney *p* values of 1 and 0.4), indicating that V5-epitope insertions did not alter HEV assembly and infectivity. Analysis by confocal microscopy also showed similar numbers of ORF2-positive cells and staining patterns when comparing Huh-7.5 cells that were infected with p6-wt versus V5-tagged p6 (**Figure 6B**).

Of note, at 10 dpe, ORF2 protein expression was also controlled by immunoblot in the PLC3 cell supernatants that were used to infect Huh-7.5 cells (**Figure 6C**, PLC3 sup.). The ORF2 protein was detected as efficiently in all PLC3 supernatants irrespective of the electroporated p6 strain. After 3 days of infection with PLC3 supernatants producing p6-wt and V5-tagged-p6 particles, the ORF2 protein was also detected in lysates and supernatants of Huh-7.5 cells (**Figure 6C**, Huh-7.5 sup., Huh-7.5 lysates). Moreover, the V5-tagged ORF1 protein could also be detected in Huh-7.5 cell lysates. These data confirm that the V5-epitope insertions do not affect production and infectivity of HEV particles.

Subcellular Localization of the Epitope-Tagged ORF1 Replicase and Co-localization With ORF2 and ORF3 Proteins

We next took advantage of replicative epitope-tagged ORF1 constructs to analyze the subcellular localization of ORF1 replicase by confocal imaging. PLC3 cells were electroporated with p6-wt, p6-V1 and p6-V2 RNAs. At 3 dpe, cells were first processed for single V5 staining. The V5 antibody mostly displayed a nuclear staining as well as cytoplasmic accumulation in the vicinity of the nucleus (**Figure 7A**, white arrowheads). Secondly, double immunostainings with antibodies directed against the V5 epitope and ORF2 or ORF3 proteins were performed. Interestingly, the ORF2 and ORF3 stainings partially overlapped with the V5 staining in peri-nuclear nugget-like substructures (**Figures 7C,E**), a finding that was corroborated by calculating the Pearson's correlation coefficients (PCC, **Figure 7B**). In line with these observations, super-resolution confocal microscopy analyses of PLC3 cells electroporated with p6-V1 and co-labeled with either V5 / ORF2 or V5 / ORF3 antibodies, showed a total overlap of fluorescence intensities between the V5 signal and both the ORF2 and ORF3 signals (**Figures 7D,F**). Altogether these results indicate that V5-tagged ORF1, ORF2 and ORF3 proteins are co-distributed in compact structures located in the vicinity of the nucleus of HEV-producing cells.

Since the ORF1 protein has been largely studied in heterologous expression systems, we next wanted to compare the subcellular localization of V5-tagged ORF1 in replicative and heterologous systems. Eight hours post-transfection with the V5-tagged constructs, a mostly cytoplasmic reticular labeling was observed in H7-T7-IZ

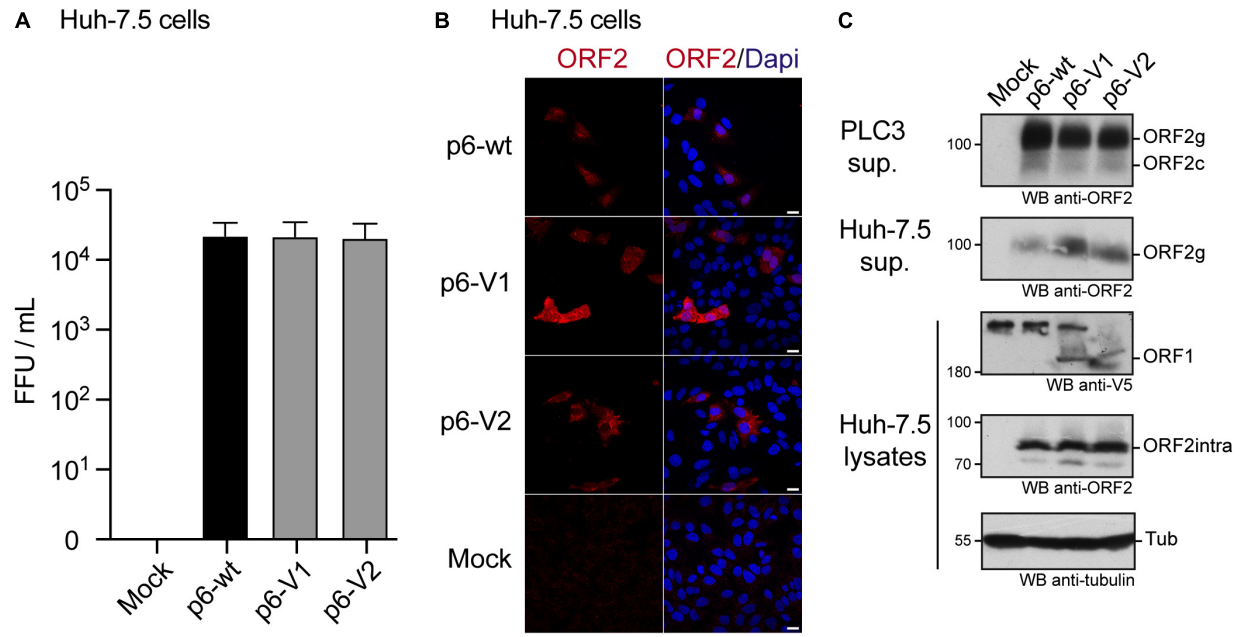

FIGURE 6 | Infection of Huh-7.5 cells by HEV p6 expressing V5-tagged ORF1 polyprotein. **(A)** Infectious titers of HEV p6 expressing epitope-tagged ORF1 polyprotein. Ten dpe, supernatants of PLC3 cells electroporated with p6-wt, p6-V1 or p6-V2 were collected to infect Huh-7.5 cells. Three days post-infection, Huh-7.5 cells were fixed and stained with an anti-ORF2 antibody (1E6). The number of ORF2-positive cells from three independent experiments were counted and used to calculate infectious titers in focus forming unit (FFU/mL). Statistical analysis was performed using the Mann–Whitney test. **(B)** Immunofluorescence of HEV p6-infected Huh-7.5 cells. Huh-7.5 cells were infected with the supernatants of PLC3 cells that were electroporated with HEV p6 expressing non-tagged ORF1 (p6-wt) or V5-tagged (p6-V1, p6-V2) replicase as mentioned above. Three days post-infection, cells were processed for anti-ORF2 immunofluorescence (1E6, red) prior to analysis by confocal microscopy. Cell nuclei were stained with Dapi (blue). Huh-7.5 cells infected with mock-electroporated PLC3 cell supernatant served as negative control (Mock). Scale bar = 20 μm. **(C)** Expression of epitope-tagged ORF1 and ORF2 proteins in the p6 cell culture system. PLC3 cells were electroporated with p6-wt, p6-V1 or p6-V2. Ten dpe, total protein extracts were submitted to Western blot and probed with an anti-ORF2 antibody (1E6, first panel, PLC3 sup.). Huh-7.5 cells were infected with PLC3 supernatants. Three days post-infection, Huh-7.5 supernatants were also analyzed for ORF2 expression (1E6, second panel, Huh-7.5 sup.). In parallel, Huh-7.5 cells were lysed and total protein extracts were probed with anti-V5, -ORF2 (1E6) and -γ-tubulin antibodies (last three panels, Huh-7.5 lysates). Molecular weight markers are indicated in kilodaltons. ORF1, full-length protein; ORF2g, glycosylated form of ORF2; ORF2c, cleaved form of ORF2; ORF2intra, intracellular ORF2 form; Tub, γ-tubulin.

cells (**Supplementary Figure 3A**). Also, in H7-T7-IZ cells co-transfected with the V5-tagged ORF1 and ORF2/ORF3 expressing plasmids, partial staining overlaps of the V5-tagged replicase with ORF2 and ORF3 proteins were visible in the cytoplasm but also in perinuclear accumulations (**Supplementary Figures 3B,C**). Thus, the heterologous system recapitulates the partial co-distribution of V5-tagged ORF1 with ORF2/ORF3 that was also observed in perinuclear substructures of HEV-producing cells.

In order to locate HEV replication sites, we implemented a highly sensitive technology (RNAscope®) to detect viral RNA. Three probes were designed to specifically hybridize to the positive- and negative- HEV RNA strands (**Figure 8A**). The probes A and C target the positive strand of the genomic and subgenomic HEV RNAs, respectively. The probe B targets the negative strand of the genomic RNA. The p6-wt-electroporated PLC3 cells were fixed at 4 hpe, 3 and 6 dpe and, then submitted to *in situ* hybridization using probes A, B and C sequentially. A fluorescent signal was detected for each of the 3 probes in discrete perinuclear foci in the host cell as early as 4 hpe (**Figure 8B**). While fluorescent staining of the negative-sense RNA (probe B) and subgenomic RNA (probe C) overlapped ($PCC_{B/C} = 0.68 \pm 0.05$, **Figure 8C**), the staining of probe A only partially overlapped with the formers ($PCC_{B/A} = 0.52 \pm 0.10$, $PCC_{A/C} = 0.39 \pm 0.10$, **Figure 8C**). Three dpe, the positive-stranded-RNA staining (probes A and C) further expanded all around the cell nuclei while the negative-stranded-RNA staining (probe B) remained more condensed as perinuclear foci. At 6 dpe, the staining of genomic and subgenomic positive-sense RNAs adopted a diffuse pattern in the cytoplasm with a $PCC_{A/C}$ reaching 0.53 ± 0.12. The negative-stranded-RNA staining was closer to a dot-like fainter pattern while the staining overlap with the 2 other probes decreased ($PCC_{A/B} = 0.38 \pm 0.27$, $PCC_{B/C} = 0.44 \pm 0.29$). At every time points, the probe C staining surrounded the probe A staining while the probe B staining was the faintest of all.

Next, positive-sense genomic RNA (probe A) were co-labeled with the viral proteins ORF1, ORF2 and ORF3 (**Figures 8D–F**). At 3 dpe, the V5-tagged ORF1 protein co-localized with the positive-sense genomic RNA within the previously identified perinuclear foci with a strong PCC of 0.76 ± 0.11 (**Figures 8D,G**). The viral RNA also co-distributed with ORF2 and ORF3 proteins at 3 dpe in p6-wt-electroporated PLC3 cells (**Figure 8G**, $PCC_{A/ORF2} = 0.60 \pm 0.12$, $PCC_{A/ORF3} = 0.73 \pm 0.06$). These

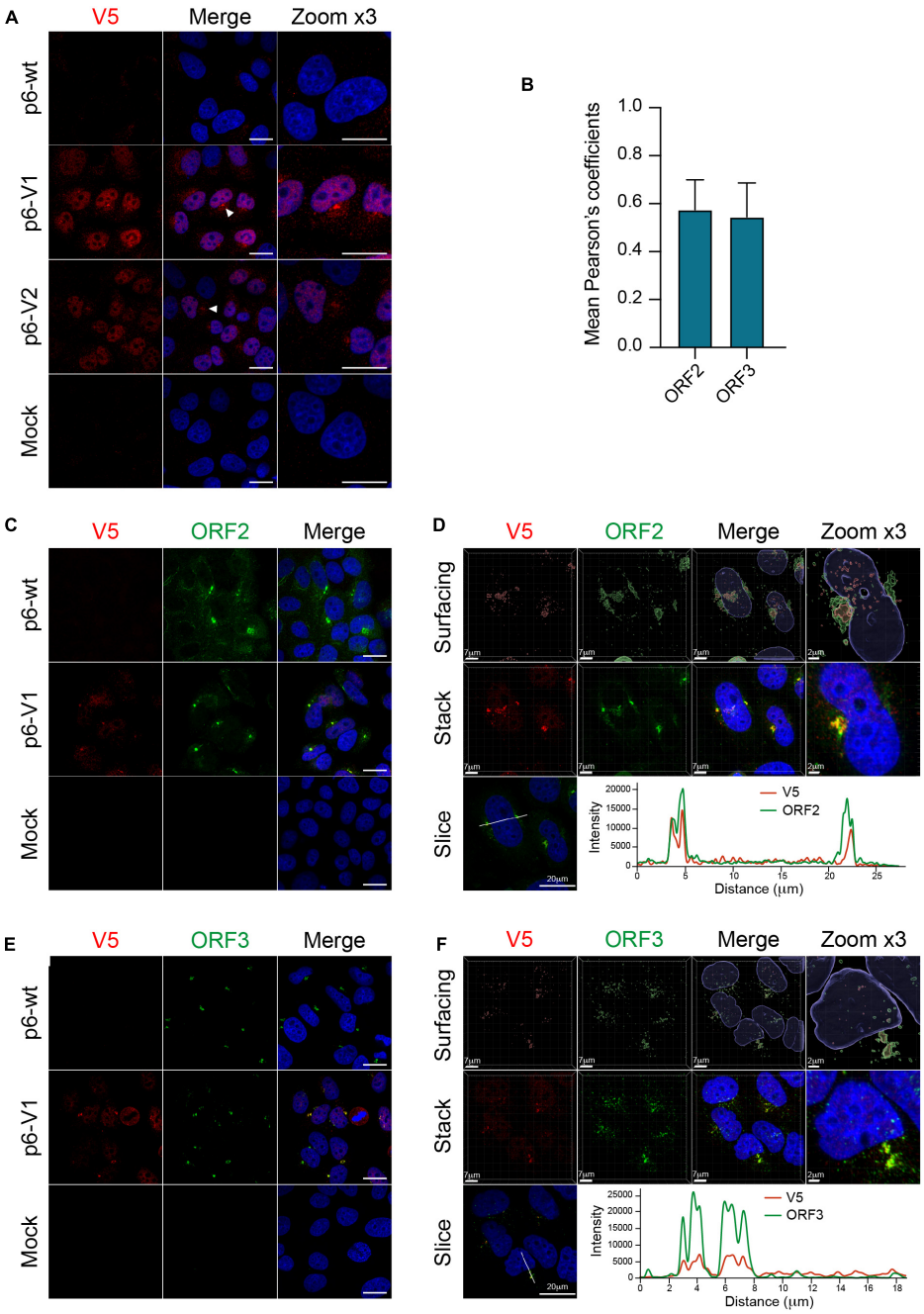

FIGURE 7 | Co-localization of the V5-tagged ORF1 and ORF2/ORF3 proteins in the host cell. **(A)** PLC3 cells were electroporated with the p6 strain expressing either the untagged (p6-wt) or the V5-tagged ORF1 (p6-V1, p6-V2) proteins. Three dpe, cells were processed for immunofluorescence using an anti-V5 antibody (red) prior to analysis by confocal microscopy. Perinuclear nugget-like structures are shown (white arrowheads). The cell nuclei were stained with DAPI (blue). Mock-electroporated cells served as negative control. Scale bar = 20 µm. **(B)** Regions of interest (ROI) were drawn around the perinuclear nugget-like structures on images taken from PLC3 cells electroporated with p6-V1 and co-labeled with antibodies directed against the V5 epitope and the ORF2 **(C)** or the ORF3 proteins **(E)**. ROI were used to determine Pearson's correlation coefficients (PCC) between V5-tagged ORF1 and ORF2 (ORF2) labeling or V5-tagged ORF1 and ORF3 (ORF3) labeling using JACoP plugin from ImageJ software. PCC means (± standard deviation) were calculated from 30 different ROI. **(C–E)** Co-labeling of the V5-tagged HEV ORF1 replicase with ORF2/ORF3 in PLC3 cells. PLC3 cells were electroporated with p6-wt or p6-V1. Three dpe, viral proteins were co-labeled with antibodies directed against the V5 epitope (red, V5) and (i) ORF2 [1E6, green, **(C)**] or (ii) ORF3 [green, **(E)**] prior to analysis by confocal microscopy. Mock-electroporated cells served as negative control. Antibodies used are listed in **Table 2**. Scale bar = 20 µm. **(D–F)** PLC3 cells electroporated with p6-V1 and co-stained with anti-V5 and (i) anti-ORF2 **(D)** or (ii) anti-ORF3 antibodies **(F)** were analyzed by confocal microscopy with a high resolution Airyscan module. On the top, volume rendering of the 3D z-stacks (Surfacing) using the Imaris software are shown to visualize the V5-tagged ORF1/ORF2 **(D)** or ORF1/ORF3 **(F)** substructures. In the middle, z-stacks are shown. On the bottom, line graphs show the fluorescence intensities of V5-tagged ORF1 and ORF2 or ORF3 staining measured every 50 nm across the region of interest highlighted by the white line in the micrograph shown on the left. Scale bars show the indicated length.

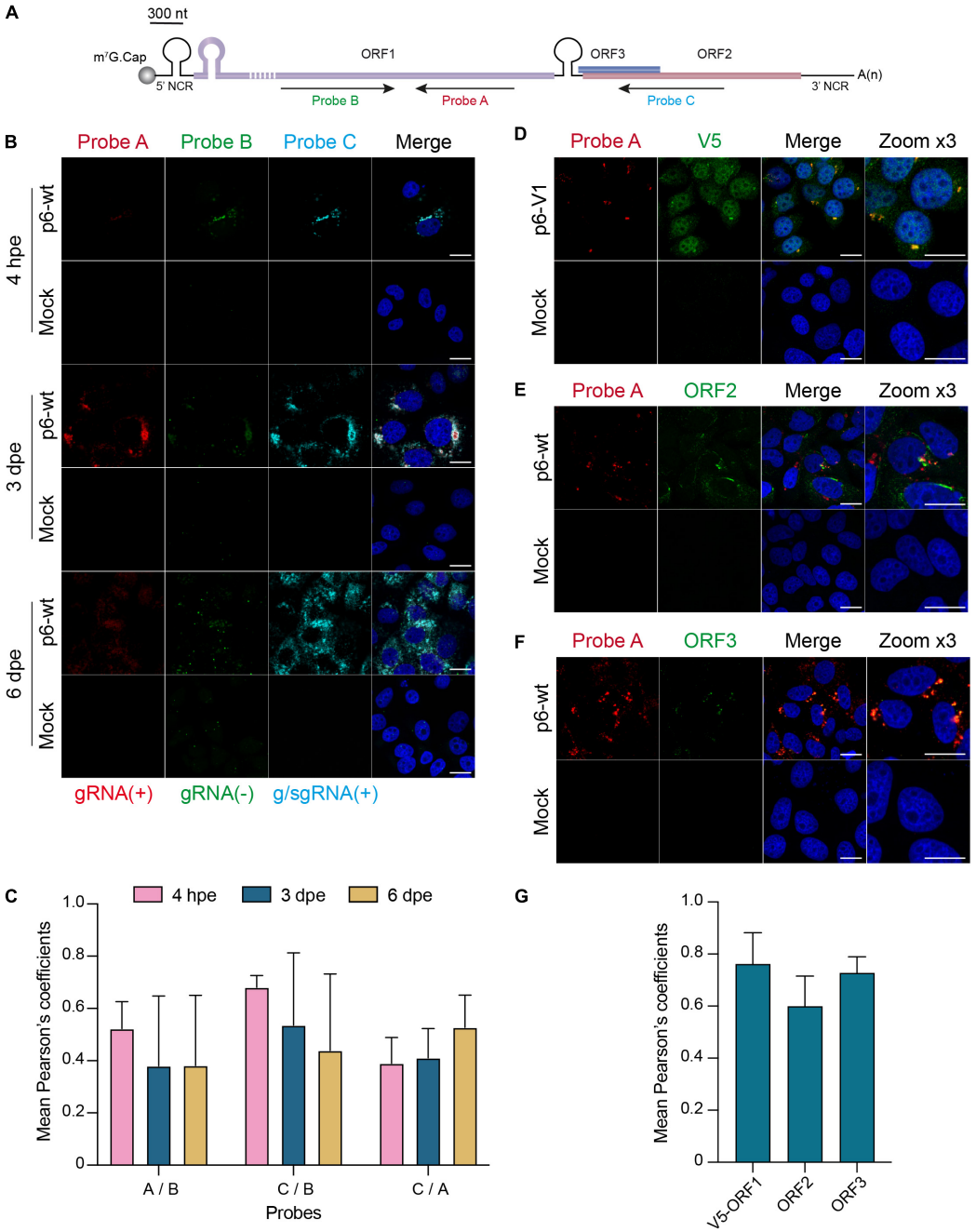

FIGURE 8 | *In situ* labeling of positive- and negative-sense HEV RNAs. PLC3 cells were electroporated with untagged (p6-wt) or V5-tagged (p6-V1) p6 strains. Cells were grown on coverslips, fixed at 4 hpe, 3 and 6 dpe and processed for *in situ* RNAscope® hybridization. Cell nuclei were stained with Dapi (blue). Images were taken on a confocal microscope. Mock-electroporated cells served as negative control. Scale bar = 20 μm. **(A)** Schematic overview of the RNAscope® probe location. Probe A targets the positive-sense genomic RNA and is located in the RdRp domain of ORF1 (purple). Probe B targets the negative-sense RNA and is also located in the RdRp but does not overlap with probe A. Probe C targets the positive-sense subgenomic RNA, by hybridizing at the ORF3 (blue) / ORF2 (red) overlap. The full-length of the ORF1 protein cannot be represented at the scheme scale (purple dashed lines). **(B)** PLC3 cells electroporated with the p6-wt strain were sequentially stained with probes A [red, gRNA(+)], B [green, gRNA(-)] and C [cyan, g/sgRNA(+)] at 4 hpe, 3 and 6 dpe. gRNA(+), positive-stranded genomic RNA; gRNA(-), negative-stranded genomic RNA; g/sgRNA(+), positive-stranded genomic and subgenomic RNAs. **(C)** Immunofluorescence images of whole PLC3 cells electroporated with p6-wt and co-labeled with probes A, B and C were used to determine PCC using JACoP plugin from ImageJ software. PCC means (± standard deviation) were calculated from 30 analyzed whole cells. **(D–F)** Three dpe, PLC3 cells electroporated with the p6-V1 construct were stained with probe A (red) and (i) the anti-V5 antibody [green, **(D)**], (ii) the anti-ORF2 [green, 1E6, **(E)**] or (iii) the anti-ORF3 [green, **(F)**]. **(G)** Regions of interest (ROI) were drawn around the perinuclear nugget-like structures on images taken from PLC3 cells electroporated with p6-V1 or p6-wt and co-labeled with probe A and anti-V5, anti-ORF2 or anti-ORF3 antibody. Twenty ROI were used to calculate mean PCC (± standard deviation) between probe A and V5-tagged ORF1 (V5-ORF1) labeling or probe A and ORF2 labeling (ORF2) or probe A and ORF3 labeling (ORF3) using JACoP plugin from ImageJ software.

accumulations were also located in the perinuclear proximity of the cell (**Figures 8E,F**).

Identification of the Hepatitis E Virus-Induced Substructures

Recently, the ORF2 and ORF3 proteins were reported to colocalize with cellular markers of the endocytic recycling compartment (ERC) in perinuclear substructures (Bentaleb et al., 2021). To further delineate whether the V5-tagged ORF1 was also present in these substructures, we conducted co-labeling experiments of the V5-tagged-ORF1 with ERC markers such as CD71, Rab11, EHD1 and PACSIN2 in PLC3 cells electroporated with p6-V1 (**Figure 9** and **Supplementary Figure 3D**). The V5-tagged ORF1 staining overlapped with CD71 and Rab11 staining in the perinuclear substructures (**Figures 9A,C**). Analyses of super-resolution confocal microscopy images further strengthened these observations showing a total overlap of fluorescence intensities between V5-tagged-ORF1 and CD71 (**Figure 9B**) as well as between V5-tagged ORF1 and Rab11 (**Figure 9D**) in the perinuclear substructures. The V5-tagged ORF1 colocalized best with Rab11 (PCC = 0.67 $\pm$ 0.08) whereas the colocalization was moderate with CD71 and EHD1 (PCC = 0.42 $\pm$ 0.13 and 0.49 $\pm$ 0.10, respectively, **Figure 9F**). No colocalization was found between V5-tagged ORF1 and PACSIN2 (PCC = 0.22 $\pm$ 0.11, **Figure 9F** and **Supplementary Figure 3D**). In addition, contrary to a previous report (Szkolnicka et al., 2019; Bentaleb et al., 2021), no colocalization was found between V5-tagged ORF1 and CD63 or CD81, two markers of multivesicular bodies, while CD81 labeling appeared surrounding the V5-tagged ORF1 signal (**Figure 9F** and **Supplementary Figures 3E,F**).

DISCUSSION

Due to its low expression level, its tight regulation in time and space as well as a lack of a commercial antibody (Lenggenhager et al., 2017), the non-structural ORF1 protein is the least studied of the three HEV proteins. Thus, the insertion of epitope tags within the HEV replicase appeared as a practical strategy to characterize the subcellular localization and processing of ORF1 polyprotein. Indeed, a transposon-based approach to insert HA epitopes in the ORF1 genome has been recently used to characterize the subcellular localization of the HEV replicase (Szkolnicka et al., 2019). Similarly, we aimed at finding positions within ORF1 where epitope tags could be inserted without disturbing viral replication. After aligning 44 HEV strains, the HVR appeared as the least conserved domain in the ORF1 sequence. In addition, while presenting the highest divergence of the entire HEV genome (Muñoz-Chimeno et al., 2020), the HVR is known to tolerate inserted fragments arising either from duplication of viral genome or from human genes which were reported to confer better replication efficacies or adaptation to cell culture (Shukla et al., 2011, 2012; Nguyen et al., 2012; Johne et al., 2014; Lhomme et al., 2014).

Recently, a cell culture model derived from the PLC/PRF/5 cell line has been established in the laboratory to efficiently produce HEV particles from the Kernow C-1 p6 strain (Shukla et al., 2012; Montpellier et al., 2018). In a first approach to identify non-disruptive insertion sites, the ORF1 HVR aa sequence of the Kernow C-1 p6 strain was aligned with those of common epitope tags. Four aa of the HVR were matching with the V5 tag sequence, while 3 aa had to be mutated and 7 had to be inserted to construct the full V5 epitope aa sequence (V1, **Figure 1**). Secondly, a V5 or HA epitope (V2 and H2, **Figure 1**) were inserted into the Kernow C-1 p6 strain in the position where the S19 insertion was found in a different strain (LBPR-0379) to confer a replication advantage in cell culture (Nguyen et al., 2012; Shukla et al., 2012). Lastly, an HA epitope was inserted at the C-terminus of the ORF1 coding sequence to avoid impacting the structure of the ORF1 protein and thereby perturb replication (H1, **Figure 1**).

At first, the epitopes were inserted into the p6-GLuc replicon in order to determine the impact of the tag insertion on its replicative ability. The luciferase activity was measured over time. Result analyses led to the conclusion that the H1 insertion diminishes the expression of the subgenomic genes, as luciferase activity was greatly decreased, which is likely due to the disruption of the subgenomic promoter region (Ding et al., 2018). Therefore, insertion at the H1 position is likely to also impact replication in the p6 context but could be of use in the heterologous expression system. Next, H2 and V2 insertions, which were placed in the same position, impacted the subgenomic expression differently. While the p6-V2-GLuc showed similar luciferase activity to the non-tagged p6-wt-GLuc, the p6-H2-GLuc construct showed a decreased replication efficacy. Thus, the aa sequence composition of the epitope, and not only the insertion position, may impact the replicase activity by modifying its conformational structure. Out of the four tagged replicons tested, replication efficacies of the p6-V1-GLuc and p6-V2-GLuc constructs appeared the least affected by epitope insertion. The luciferase activity of these constructs resembled those of the non-tagged p6-wt-GLuc. Moreover, the quantification of extracellular and intracellular viral RNA over the course of 7 days displayed similar kinetics in PLC3 cells expressing the p6-wt or the V5-tagged p6 constructs, thus strengthening the fact that the V5 insertions within the ORF1 HVR did not disturb the HEV replication. In line with these results, the infectivity of the V5-tagged p6 constructs was not altered when compared to p6-wt. Therefore, the V5-tagged constructs were selected to delineate the ORF1 features.

One of our goal was to characterize the processing of the ORF1 protein. Polyproteins encoded by positive stranded RNA viruses are commonly subjected to cleavage by viral and/or cellular proteases (Ploss and Dubuisson, 2012; Gu and Rice, 2013; Baggen et al., 2021; V'kovski et al., 2021). However, in the HEV field, the literature on ORF1 cleavage is highly controversial as there is evidence for and against cleavage of the non-structural protein (LeDesma et al., 2019).

In an aim to study potential processing of HEV replicase, expression of the V5-tagged ORF1 protein was analyzed over time by immunoblotting. In the three different systems tested in this study, the full-length ORF1 protein and smaller bands that may correspond to potential ORF1 cleavage products were detected, especially at earlier time points. This could reflect the early need for ORF1 to replicate RNA at the viral cycle

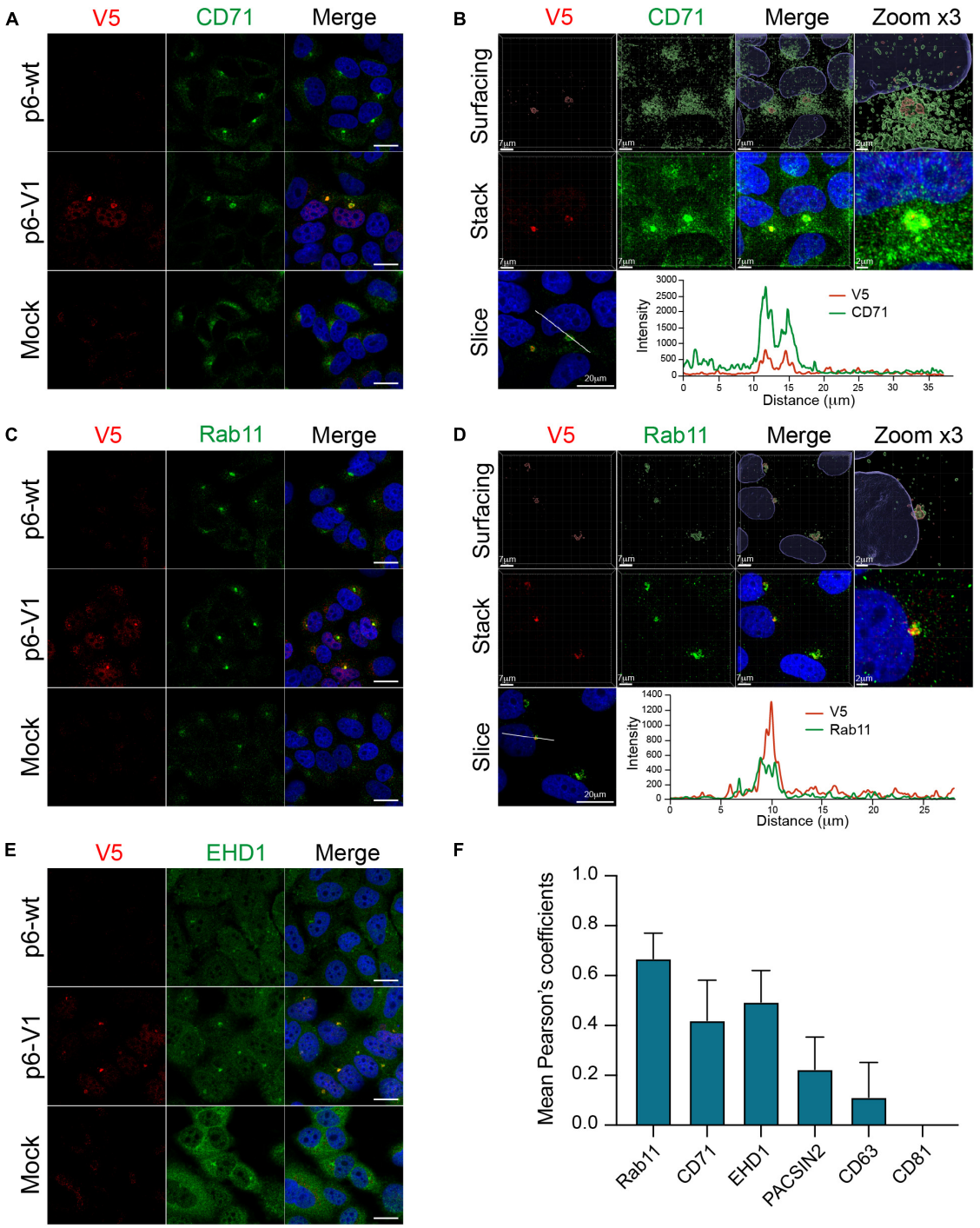

FIGURE 9 | Co-labeling of the HEV V5-tagged ORF1 protein with several cellular markers. The wt (p6-wt) and V5-tagged (p6-V1) ORF1 proteins were expressed in PLC3 cells electroporated with the p6 HEV strain. Three dpe, cells were co-labeled with anti-V5 antibody (red) and cellular markers antibodies (green) directed against CD71 **(A,B)**, Rab11 **(C,D)**, EHD1 **(E)**. Cell nuclei were stained with DAPI (blue). Mock-electroporated cells served as negative controls (Mock). Images were taken with a confocal microscope. Antibodies used are listed in **Table 2**. Scale bar = 20 µm. PLC3 cells electroporated with p6-V1 and co-stained with anti-V5 and antibodies directed against CD71 **(B)** and Rab11 **(D)** were analyzed by confocal microscopy with a high resolution Airyscan module. On the top, volume rendering of the 3D z-stacks (Surfacing) using the Imaris software are shown to visualize the V5-tagged ORF1/CD71 or Rab11 substructures. In the middle, z-stacks are shown. On the bottom, line graphs show the fluorescence intensities of V5-tagged ORF1 and CD71/Rab11 staining measured every 50 nm across the region of interest highlighted by the white line in the micrograph shown on the left. Scale bars show the indicated length. **(F)** Regions of interest (ROI) were drawn around the perinuclear nugget-like structures on the immunofluorescence images of p6-V1 electroporated PLC3 cells co-labeled with antibodies directed against the V5 epitope and CD71, Rab11, EHD1 **(A,C,E)** and PACSIN2, CD63 and CD81 (**Supplementary Figures 3D–F**). Thirty ROI were used to calculate PCC (± standard deviation) using JACoP plugin from ImageJ software.

onset. Although full-length ORF1 protein was identified by mass spectrometry with certainty, full sequence identification of the smaller products was less robust due to their lower expression levels. The ORF1 protein expressed heterologously does not seem to be processed from its N-terminus while in the p6 infectious system, more ORF1 potential cleavage products were detected and the N-terminus of the protein also seemed more stable than the C-terminus. The expression of more numerous potential cleavage products in the p6 infectious system may suggest the requirement of all viral proteins as well as cellular proteins to achieve the full ORF1 processing. As the possibility of degradation cannot be fully excluded, we inhibited the proteasome with lactacystin and noted that the observed band pattern and ORF1 quantity remained unchanged. Thus, the minor ORF1 products may be the result of natural viral and/or cellular processing rather than artefactual degradation. Furthermore, the ORF1 protein and its potential cleavage products were detected in different cellular compartments with slightly different patterns. For example, a band of 160 kDa was only present in the nuclear fraction enriched from the p6 cell culture system. This result may point to the requirement of an ORF1 processing before or upon its translocation into the nucleus. Nevertheless, without any sequence information, it remained difficult to assess to which domain of the ORF1 protein this product may correspond.

RNA viruses generally replicate in the cytoplasm. In previous studies, the ORF1 protein was found in the cytoplasm colocalizing with ORF2 and ORF3 viral proteins, and ERGIC/Golgi markers (Rehman et al., 2008; Szkolnicka et al., 2019). In our study, the V5-tagged ORF1 proteins, expressed in the replicon, heterologous and p6 cell culture expression systems, displayed both a cytoplasmic and nuclear localization as assessed by subcellular fractionation and immunofluorescence experiments. The use of the Kernow C-1 p6 strain, that contains the S17 human ribosomal protein insertion in which an element could act as a nuclear localization signal (NLS), may account for this discrepancy (Kenney and Meng, 2015). However, mutations of the conserved aa in the S17 NLS disrupted the replication efficacy of the p6-GLuc replicon and did not inhibit the nuclear localization as assessed by immunofluorescence staining or immunoblot analysis of subcellular fractions in the heterologous system (data not shown). In addition, we observed perinuclear aggregations of the ORF1 protein that often coincide with a deformation of the nucleus. Recently, ORF2 and ORF3 proteins as well as cellular markers of the ERC such as Rab11 and CD71 were reported to locate to this region in HEV-producing cells (Bentaleb et al., 2021). Interestingly, we confirmed partial overlaps of the ORF1 protein with ORF2 and ORF3 viral proteins as well as several cellular markers of the ERC, especially in the nugget-like perinuclear region. These results indicate that the place of viral replication is in close proximity to the site of virus assembly. Indeed, in other viruses such as Dengue virus, replication and assembly take place in the same subcellular compartment (Welsch et al., 2009).

Lastly, to formerly identify the HEV replication site, we aimed at locating the negative-sense HEV RNA in the host cell. To that end, the RNAscope® technique, which enabled to specifically target and visualize the positive- and negative-RNA-strands of hepatitis C virus and the positive-RNA-strand of Zika virus, was implemented (Wang et al., 2012; Liu et al., 2019). We managed to locate positive-sense genomic and subgenomic HEV RNAs as well as the negative-sense RNA in the cell. Moreover, co-distributions of the positive-sense genomic RNA with ORF1, ORF2 and ORF3 viral proteins were visible within the nugget-like perinuclear foci. In conclusion, we demonstrated that viral replication and assembly take place in close proximity in HEV-producing cells, in perinuclear nugget-like structures that may constitute the HEV viral factories.

DATA AVAILABILITY STATEMENT

The original contributions presented in the study are included in the article/**Supplementary Material**, further inquiries can be directed to the corresponding author/s.

AUTHOR CONTRIBUTIONS

KM, CB, KH, VA, CM, J-MS, MF, CC, YR, CL, JD, LC, and C-MA-D performed research and/or analyzed data. KM and C-MA-D wrote the manuscript. All authors contributed to the article and approved the submitted version.

FUNDING

This work was supported by a grant from the French agency ANRS-Maladies infectieuses émergentes. KM was supported by a fellowship from the French Ministery of Research and Higher Education. CB and KH were supported by fellowships from the French agency ANRS-Maladies infectieuses émergentes. MF was supported by a fellowship from the Lille Pasteur Institute and Région Hauts-de-France.

ACKNOWLEDGMENTS

We would like to thank Suzanne U. Emerson (NIH, United States), Jérôme Gouttenoire (University of Lausanne) and Ralph Bartenschlager (University of Heidelberg) for providing us with reagents. We would also like to thank the imaging core facility of the BioImaging Center Lille-Nord de France for access to the instruments. We would also further like to thank Grégoire Savary (UMR9020, CANTHER, Univ. Lille) and Benoit Pourcet (U1011-EGID, Univ. Lille) for sharing their expertise and equipment to perform the RNAScope® technique.

SUPPLEMENTARY MATERIAL

The Supplementary Material for this article can be found online at: https://www.frontiersin.org/articles/10.3389/fmicb.2022.828636/full#supplementary-material

REFERENCES

Baggen, J., Vanstreels, E., Jansen, S., and Daelemans, D. (2021). Cellular host factors for SARS-CoV-2 infection. *Nat. Microbiol.* 6, 1219–1232. doi: 10.1038/s41564-021-00958-0

Bentaleb, C., Hervouet, K., Montpellier, C., Camuzet, C., Burlaud-Gaillard, J., Ferrié, M., et al. (2021). The endocytic recycling compartment serves as a viral factory for hepatitis E virus. *Biorxiv*[Preprint]. doi: 10.1101/2021.10.14.464345 Biorxiv 2021.10.14.464345,

Blight, K. J., McKeating, J. A., and Rice, C. M. (2002). Highly permissive cell lines for subgenomic and genomic Hepatitis C virus RNA replication. *J. Virol.* 76, 13001–13014. doi: 10.1128/jvi.76.24.13001-13014.2002

DaoThi, V. L., Debing, Y., Wu, X., Rice, C. M., Neyts, J., Moradpour, D., et al. (2016). Sofosbuvir inhibits Hepatitis E virus replication in vitro and results in an additive effect when combined with ribavirin. *Gastroenterology* 150, 82–85.e4. doi: 10.1053/j.gastro.2015.09.011

Debing, Y., Moradpour, D., Neyts, J., and Gouttenoire, J. (2016). Update on hepatitis E virology: implications for clinical practice. *J. Hepatol.* 65, 200–212. doi: 10.1016/j.jhep.2016.02.045

Ding, Q., Nimgaonkar, I., Archer, N. F., Bram, Y., Heller, B., Schwartz, R. E., et al. (2018). Identification of the intragenomic promoter controlling Hepatitis E virus subgenomic RNA transcription. *mBio* 9:e00769-18. doi: 10.1128/mbio.00769-18

Emerson, S. U., Nguyen, H. T., Torian, U., Mather, K., and Firth, A. E. (2013). An essential RNA element resides in a central region of hepatitis E virus ORF2. *J. Gen. Virol.* 94, 1468–1476. doi: 10.1099/vir.0.051870-0

Farhat, R., Ankavay, M., Lebsir, N., Gouttenoire, J., Jackson, C. L., Wychowski, C., et al. (2018). Identification of GBF1 as a cellular factor required for hepatitis E virus RNA replication. *Cell. Microbiol.* 20:e12804. doi: 10.1111/cmi.12804

Glitscher, M., and Hildt, E. (2021). Hepatitis E virus egress and beyond – the manifold roles of the viral ORF3 protein. *Cell Microbiol.* 23:e13379. doi: 10.1111/cmi.13379

Graff, J., Nguyen, H., Yu, C., Elkins, W. R., St Claire, M., Purcell, R. H., et al. (2005). The open reading frame 3 gene of Hepatitis E virus contains a cis-reactive element and encodes a protein required for infection of macaques. *J. Virol.* 79, 6680–6689. doi: 10.1128/jvi.79.11.6680-6689.2005

Graff, J., Torian, U., Nguyen, H., and Emerson, S. U. (2006). A bicistronic subgenomic mRNA encodes both the ORF2 and ORF3 proteins of Hepatitis E virus. *J. Virol.* 80, 5919–5926. doi: 10.1128/jvi.00046-06

Gu, M., and Rice, C. M. (2013). Structures of hepatitis C virus nonstructural proteins required for replicase assembly and function. *Curr. Opin. Virol.* 3, 129–136. doi: 10.1016/j.coviro.2013.03.013

Johne, R., Reetz, J., Ulrich, R. G., Machnowska, P., Sachsenröder, J., Nickel, P., et al. (2014). An ORF1-rearranged hepatitis E virus derived from a chronically infected patient efficiently replicates in cell culture. *J. Viral Hepatitis* 21, 447–456. doi: 10.1111/jvh.12157

Jothikumar, N., Cromeans, T. L., Robertson, B. H., Meng, X. J., and Hill, V. R. (2006). A broadly reactive one-step real-time RT-PCR assay for rapid and sensitive detection of hepatitis E virus. *J. Virol. Methods* 131, 65–71. doi: 10.1016/j.jviromet.2005.07.004

Kamar, N., Izopet, J., Pavio, N., Aggarwal, R., Labrique, A., Wedemeyer, H., et al. (2017). Hepatitis E virus infection. *Nat. Rev. Dis. Primers* 3:17086. doi: 10.1038/nrdp.2017.86

Kenney, S. P., and Meng, X.-J. (2015). Identification and fine mapping of nuclear and nucleolar localization signals within the human ribosomal protein S17. *PLoS One* 10:e0124396. doi: 10.1371/journal.pone.0124396

Kenney, S. P., and Meng, X.-J. (2019). Hepatitis E Virus genome structure and replication strategy. *Cold Spring Harb. Perspect. Med.* 9:a031724. doi: 10.1101/cshperspect.a031724

Koonin, E. V., Gorbalenya, A. E., Purdy, M. A., Rozanov, M. N., Reyes, G. R., and Bradley, D. W. (1992). Computer-assisted assignment of functional domains in the nonstructural polyprotein of hepatitis E virus: delineation of an additional group of positive-strand RNA plant and animal viruses. *Proc. Natl. Acad. Sci. U.S.A.* 89, 8259–8263.

LeDesma, R., Nimgaonkar, I., and Ploss, A. (2019). Hepatitis E virus replication. *Viruses* 11:719. doi: 10.3390/v11080719

Lenggenhager, D., Gouttenoire, J., Malehmir, M., Bawohl, M., Honcharova-Biletska, H., Kreutzer, S., et al. (2017). Visualization of hepatitis E virus RNA and proteins in the human liver. *J. Hepatol.* 67, 471–479. doi: 10.1016/j.jhep.2017.04.002

Lhomme, S., Abravanel, F., Dubois, M., Sandres-Saune, K., Mansuy, J.-M., Rostaing, L., et al. (2014). Characterization of the polyproline region of the hepatitis E virus in immunocompromised patients. *J. Virol.* 88, 12017–12025. doi: 10.1128/jvi.01625-14

Lhomme, S., Marion, O., Abravanel, F., Izopet, J., and Kamar, N. (2020). Clinical manifestations, pathogenesis and treatment of Hepatitis E virus infections. *J. Clin. Med.* 9:331. doi: 10.3390/jcm9020331

Liao, W., Li, X., Mancini, M., and Chan, L. (2006). Proteasome inhibition induces differential heat shock protein response but not unfolded protein response in HepG2 cells. *J. Cell Biochem.* 99, 1085–1095. doi: 10.1002/jcb.20996

Liu, D., Tedbury, P. R., Lan, S., Huber, A. D., Puray-Chavez, M. N., Ji, J., et al. (2019). Visualization of positive and negative sense viral RNA for probing the mechanism of direct-acting antivirals against Hepatitis C Virus. *Viruses* 11:1039. doi: 10.3390/v11111039

Montpellier, C., Wychowski, C., Sayed, I. M., Meunier, J.-C., Saliou, J.-M., Ankavay, M., et al. (2018). Hepatitis E virus lifecycle and identification of 3 forms of the ORF2 capsid protein. *Gastroenterology* 154, 211–223.e8. doi: 10.1053/j.gastro.2017.09.020

Muñoz-Chimeno, M., Cenalmor, A., Garcia-Lugo, M. A., Hernandez, M., Rodriguez-Lazaro, D., and Avellon, A. (2020). Proline-rich hypervariable region of Hepatitis E Virus: arranging the disorder. *Microorganisms* 8:1417. doi: 10.3390/microorganisms8091417

Nair, V. P., Anang, S., Subramani, C., Madhvi, A., Bakshi, K., Srivastava, A., et al. (2016). Endoplasmic reticulum stress induced synthesis of a novel viral factor mediates efficient replication of genotype-1 Hepatitis E virus. *PLoS Pathog.* 12:e1005521. doi: 10.1371/journal.ppat.1005521

Nguyen, H. T., Torian, U., Faulk, K., Mather, K., Engle, R. E., Thompson, E., et al. (2012). A naturally occurring human/hepatitis E recombinant virus predominates in serum but not in faeces of a chronic hepatitis E patient and has a growth advantage in cell culture. *J. Gen. Virol.* 93, 526–530. doi: 10.1099/vir.0.037259-0

Nimgaonkar, I., Ding, Q., Schwartz, R. E., and Ploss, A. (2018). Hepatitis E virus: advances and challenges. *Nat. Publ. Group* 15, 96–110. doi: 10.1038/nrgastro.2017.150

Oren, R., Takahashi, S., Doss, C., Levy, R., and Levy, S. (1990). TAPA-1, the target of an antiproliferative antibody, defines a new family of transmembrane proteins. *Mol. Cell Biol.* 10, 4007–4015. doi: 10.1128/mcb.10.8.4007

Pérez-Gracia, M. T., Suay-García, B., and Mateos-Lindemann, M. L. (2017). Hepatitis E and pregnancy: current state. *Rev. Med. Virol.* 27:e1929. doi: 10.1002/rmv.1929

Ploss, A., and Dubuisson, J. (2012). New advances in the molecular biology of hepatitis C virus infection: towards the identification of new treatment targets. *Gut* 61:i25. doi: 10.1136/gutjnl-2012-302048

Proudfoot, A., Hyrina, A., Holdorf, M., Frank, A. O., and Bussiere, D. (2019). First crystal structure of a nonstructural hepatitis e viral protein identifies a putative novel zinc-binding protein. *J. Virol.* 93:e00170-19. doi: 10.1128/jvi.00170-19

Rehman, S., Kapur, N., Durgapal, H., and Panda, S. K. (2008). Subcellular localization of hepatitis E virus (HEV) replicase. *Virology* 370, 77–92. doi: 10.1016/j.virol.2007.07.036

Romero-Brey, I., Merz, A., Chiramel, A., Lee, J.-Y., Chlanda, P., Haselman, U., et al. (2012). Three-dimensional architecture and biogenesis of membrane structures associated with hepatitis C virus replication. *PLoS Pathog.* 8:e1003056. doi: 10.1371/journal.ppat.1003056

Schofield, D. J., Glamann, J., Emerson, S. U., and Purcell, R. H. (2000). Identification by phage display and characterization of two neutralizing chimpanzee monoclonal antibodies to the hepatitis E virus capsid protein. *J. Virol.* 74, 5548–5555. doi: 10.1128/jvi.74.12.5548-5555.2000

Shiota, T., Li, T.-C., Yoshizaki, S., Kato, T., Wakita, T., and Ishii, K. (2013). The hepatitis E virus capsid C-terminal region is essential for the viral life cycle: implication for viral genome encapsidation and particle stabilization. *J. Virol.* 87, 6031–6036. doi: 10.1128/jvi.00444-13

Shukla, P., Nguyen, H. T., Faulk, K., Mather, K., Torian, U., Engle, R. E., et al. (2012). Adaptation of a genotype 3 Hepatitis E virus to efficient growth in cell culture depends on an inserted human gene segment acquired by recombination. *J. Virol.* 86, 5697–5707. doi: 10.1128/jvi.00146-12

Shukla, P., Nguyen, H. T., Torian, U., Engle, R. E., Faulk, K., Dalton, H. R., et al. (2011). Cross-species infections of cultured cells by hepatitis E virus and discovery of an infectious virus-host recombinant. *Proc. Natl. Acad. Sci. U.S.A.* 108, 2438–2443. doi: 10.1073/pnas.1018878108

Smith, D. B., and Simmonds, P. (2018). Classification and genomic diversity of enterically transmitted hepatitis viruses. *Cold Spring Harb. Perspect. Med.* 8:a031880. doi: 10.1101/cshperspect.a031880

Szkolnicka, D., Pollán, A., Silva, N. D., Oechslin, N., Gouttenoire, J., and Moradpour, D. (2019). Recombinant hepatitis E viruses harboring tags in the ORF1 protein. *J. Virol.* 93:e00459-19. doi: 10.1128/jvi.00459-19

V'kovski, P., Kratzel, A., Steiner, S., Stalder, H., and Thiel, V. (2021). Coronavirus biology and replication: implications for SARS-CoV-2. *Nat. Rev. Microbiol.* 19, 155–170. doi: 10.1038/s41579-020-00468-6

Wang, B., and Meng, X.-J. (2021). Structural and molecular biology of Hepatitis E virus. *Comput. Struct. Biotechnol. J.* 19, 1907–1916. doi: 10.1016/j.csbj.2021.03.038

Wang, F., Flanagan, J., Su, N., Wang, L.-C., Bui, S., Nielson, A., et al. (2012). RNAscope a novel in situ RNA analysis platform for formalin-fixed, paraffin-embedded tissues. *J. Mol. Diagnostics* 14, 22–29. doi: 10.1016/j.jmoldx.2011.08.002

Webb, G. W., and Dalton, H. R. (2020). Hepatitis E: an expanding epidemic with a range of complications. *Clin. Microbiol. Infect.* 26, 828–832. doi: 10.1016/j.cmi.2020.03.039

Welsch, S., Miller, S., Romero-Brey, I., Merz, A., Bleck, C. K. E., Walther, P., et al. (2009). Composition and three-dimensional architecture of the dengue virus replication and assembly sites. *Cell Host Microbe* 5, 365–375. doi: 10.1016/j.chom.2009.03.007

WHO (2021). *Hepatitis E: Fact Sheet*. Available online at: https://www.who.int/news-room/fact-sheets/detail/hepatitis-e (accessed July 27, 2021)

Yadav, K. K., Boley, P. A., Fritts, Z., and Kenney, S. P. (2021). Ectopic expression of genotype 1 Hepatitis E virus ORF4 increases genotype 3 HEV viral replication in cell culture. *Viruses* 13:75. doi: 10.3390/v13010075

Yin, X., Li, X., Ambardekar, C., Hu, Z., Lhomme, S., and Feng, Z. (2017). Hepatitis E virus persists in the presence of a type III interferon response. *PLoS Pathog.* 13:e1006417. doi: 10.1371/journal.ppat.1006417

Young, J. T. F., and Heikkila, J. J. (2010). Proteasome inhibition induces hsp30 and hsp70 gene expression as well as the acquisition of thermotolerance in Xenopus laevis A6 cells. *Cell Stress Chaperones* 15, 323–334. doi: 10.1007/s12192-009-0147-4

Conflict of Interest: The authors declare that the research was conducted in the absence of any commercial or financial relationships that could be construed as a potential conflict of interest.

Publisher's Note: All claims expressed in this article are solely those of the authors and do not necessarily represent those of their affiliated organizations, or those of the publisher, the editors and the reviewers. Any product that may be evaluated in this article, or claim that may be made by its manufacturer, is not guaranteed or endorsed by the publisher.